NEW NITRIC OXIDE RELEASING MATERIALS

Alistair Craig McKinlay

A Thesis Submitted for the Degree of PhD
at the
University of St. Andrews

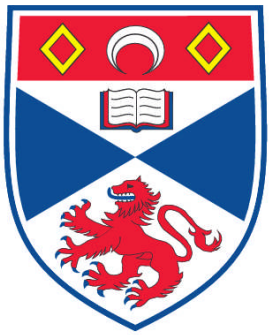

2010

New Nitric Oxide Releasing Materials

A thesis submitted in application for the title of Ph.D. by

Alistair Craig McKinlay B.Sc.

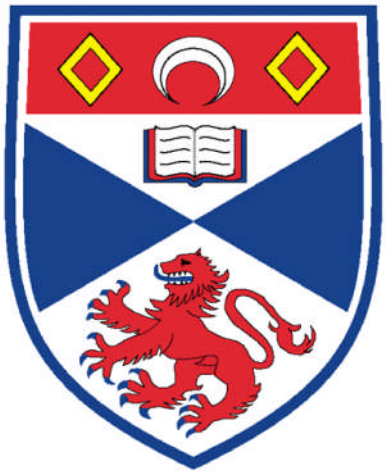

University of St Andrews

March 2010

Declaration

I, Alistair Craig McKinlay, hereby certify that this thesis, which is approximately 45000 words in length, has been written by me, that it is the record of work carried out by me and that it has not been submitted in any previous application for a higher degree. I was admitted as a research student in September 2006 and as a candidate for the degree of Ph.D. in September 2007; the higher study for which this is a record was carried out in the University of St Andrews between 2006 and 2010.

Date Signature of candidate

I hereby certify that the candidate has fulfilled the conditions of the Resolution and Regulations appropriate for the degree of Ph.D. in the University of St Andrews and that the candidate is qualified to submit this thesis in application for that degree.

Date Signature of supervisor

In submitting this thesis to the University of St Andrews we understand that we are giving permission for it to be made available for use in accordance with the regulations of the University Library for the time being in force, subject to any copyright vested in the work not being affected thereby. We also understand that the title and the abstract will be published, and that a copy of the work may be made and

supplied to any bona fide library or research worker, that my thesis will be electronically accessible for personal or research use unless exempt by award of an embargo as requested below, and that the library has the right to migrate my thesis into new electronic forms as required to ensure continued access to the thesis. We have obtained any third-party copyright permissions that may be required in order to allow such access and migration, or have requested the appropriate embargo below.

The following is an agreed request by candidate and supervisor regarding the electronic publication of this thesis:
Access to Printed copy and electronic publication of thesis through the University of St Andrews.

Date Signature of candidate

Signature of supervisor

Courses Attended

The School of Chemistry at the University of St. Andrews requires that a postgraduate attend a number of taught courses. The courses attended were:

Fundamentals in solid state NMR:	Dr. S. Ashbrook
Crystallography:	Dr. P. Lightfoot
Main Group / Synthetic Chemistry:	Prof. G. Bertrand / Prof. H. Roesky
Advanced Coordination Chemistry:	Dr. C. Glidewell

Publications

Exceptional Behaviour over the Whole Adsorption-Storage-Delivery Cycle for NO in Porous Metal Organic Frameworks.

Alistair C. McKinlay, Bo Xiao, David S. Wragg, Paul S. Wheatley, Ian L. Megson and Russell E. Morris *J. Am. Chem. Soc.* **2008**, *130*, 10440.

A comparison of zeolites and Metal Organic Frameworks as storage and delivery vehicles for biologically active nitric oxide

Paul S. Wheatley, **Alistair C. McKinlay** and Russell E. Morris *Stud. Surf. Sci. Catal.*; Elsevier: 2008; Vol. Volume 174, Part 1, p 441.

Metal organic frameworks as NO delivery materials for biological applications.

Nathan J. Hinks, **Alistair C. McKinlay**, Bo Xiao, Paul S. Wheatley and Russell E. Morris *Micropor. Mesopor. Mater.* **2010**, *129*, 330.

The BioMOF concept – Metal organic frameworks for biological and medical applications.

Alistair C. Mckinlay, Russell E. Morris, Patricia Horcajada, Gerard Férey and Christian Serre *Angew. Chem., Int. Ed.* **2010**, *accepted*

Nitric oxide adsorption and delivery in Fe MIL-88 metal organic frameworks

Alistair C. McKinlay, Bo Xiao, Paul S. Wheatley, Patricia Horcajada, Christian Serre and Russell E. Morris *Script in preparation.*

Acknowledgements

I would firstly like to thank Professor Russell Morris for his excellent supervision and guidance throughout the entirety of this PhD project. I would also like to thank the Morris group members past and present, in particular, Dr Paul Wheatley, Dr Bo Xiao and Dr David Wragg for all their helpful suggestions along the way and for answering all my questions. Thanks are also due to our collaborators in France, Jarrod Eubank, Patricia Horcajada and Christian Serre. Many thanks to the people in Pascal Dietzel's group in Norway and the Long group in the United States for giving me some samples. Thanks must also go to the technical staff at the University of St Andrews, in particular Mrs S. Williamson for help with N_2 surface area analysis, TGA measurements, atomic adsorption analysis and CHN analysis. Thanks are also due to Mrs. M. Smith (NMR) and Mr. R. Blackley (PXRD).

I would also like to thank both of my parents Neill and Sue and my younger brother Ross for putting up with me during my PhD studies and my mum in particular for proof reading my thesis.

Similarly, to my friends and in particular my girlfriend, Valentina, for helping me through the many years of study that I have enjoyed here at the University of St Andrews.

Finally I would also like to thank the EPSRC for funding this project.

Abstract

The aim of this thesis was to examine the ability of metal organic frameworks (MOFs) to store and controllably release biologically significant amounts of nitric oxide (NO). Initial work involved the synthesis of a series of isostructural MOFs, known as M-CPO-27, which display coordinatively unsaturated metal sites (CUSs) when fully activated (guest solvent molecules both coordinated and uncoordinated to the metal atom are removed). Two of these frameworks (Ni and Co CPO-27) displayed exceptional performance over the entire cycle of activation, storage and delivery showing the largest storage and release of NO of any known porous material (up to 7 $mmolg^{-1}$). These frameworks would therefore be considered for initial research into the formulation of MOFs, for possible use in medical applications. It was shown that they still release large amounts of NO even when placed inside porous paper bags, creams or hydrocolloids. The other versions of M-CPO-27 also displayed significant adsorption of NO however they show poor total NO release. It was also shown that it is possible to synthesise both Ni and Co CPO-27 using microwave synthesis without any detrimental effect to the porous structure.

Several iron-based MOFs were also investigated for NO storage and release. The results showed that Fe MIL-88 based structures adsorb good amounts of NO but only release a small amount of the irreversibly adsorbed NO. Two successfully amine grafted giant pore MOFs were then investigated to attempt to improve the NO adsorption and release. This result was not observed however, due to the poor total amine grafting coverage and pore blockage resulting from the amines. In-situ IR studies reveal that when exposed to NO, activated Fe MIL-100 forms a chemical bond

with the NO. The studies also displayed that when water is then allowed to attempt to replace the NO that only a small amount of NO is actually released, the majority of the NO either remains chemically bonded to the Fe atom or forms N_2O in conjunction with a Fe-OH group.

Other MOFs were also successfully synthesised and characterised for NO storage and release. Both Ni succinate and Ni STA-12 display good adsorption and excellent release of NO. This indicates that Ni based MOFs show the best results for NO adsorption and release.

In the conclusion of the thesis I am able to categorise the NO release ability of MOFs based on composition and formulate a theory as to why this happens.

Table of Contents

Abbreviations used throughout this thesis

MOF	metal-organic framework
HKUST	Hong Kong University of Science and Technology
UMCM	University of Michigan Crystalline Material
PTMTC	polychlorinated triphenylmethyl tricarboxylate
PAF	Porous Aromatic Framework
BTB	1,3,5-Tris(4-carboxyphenyl)benzene
SBU	Secondary building unit
MIL	Materials of Institut Lavoisier
NO	Nitric oxide
NOS	Nitric Oxide Synthase
CUS	Coordinatively unsaturated metal site
STP	Standard temperature and pressure
TGA	Thermogravimetric analysis
CPO	Coordination polymer of Oslo
XRD	X-ray diffraction
IR	Infrared
NMR	Nuclear Magnetic Resonance
THF	Tetrahydrofuran
DMF	Dimethylformamide
BET	Brunauer, Emmett and Teller
DHTP	2,5-dihydroxyterephthalic acid

1 Introduction

1.1 Metal-organic frameworks

1.1.1 Introduction

Over the last 15 years or so there has been an intensification of interest in the field of porous materials research after the discovery of a class of compounds known as metal-organic frameworks or MOFs[1-3]. Previously, porous materials research had been dominated by zeolites and activated carbons[4]. Since the late 1990s however, the emphasis has very much shifted towards MOFs. This can be easily seen in the number of publications produced per year (see figure 1.1). There are several names that have been used to describe these structures, including porous coordination polymers (PCP), however as the field grew the more general term MOFs was adopted. Even today there are derivations of the term MOF such as metal organic polyhedra (MOP), isoreticular MOF (IRMOF), zeolitic imidazolate framework (ZIF) and microporous metal-organic framework (MMOF). MOFs are constructed from metal ions which act as connectors, and these are combined with organic ligands which act as linkers. This combination leads to structures with ranging dimensionality (mostly 3D) but linked exclusively with strong bonds. One of the factors influencing the explosion in MOF research is the properties they have been shown to exhibit, including high surface area and permanent porosity.

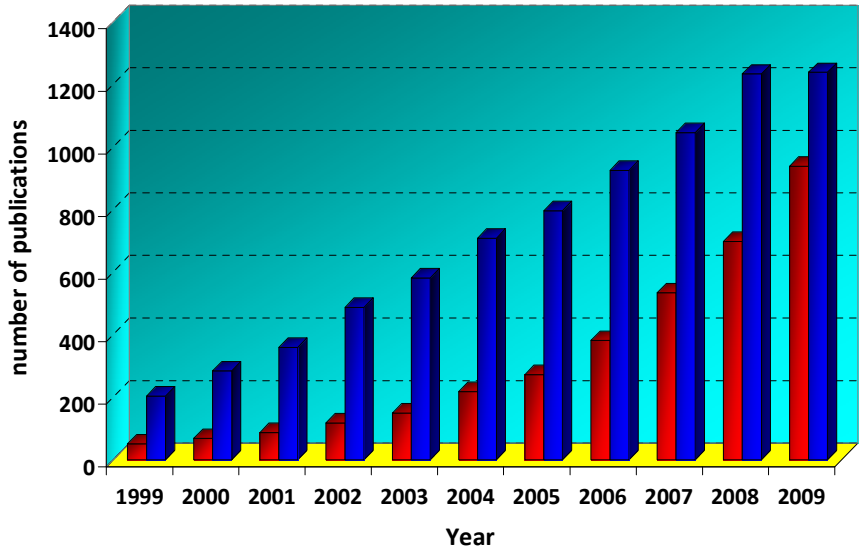

Figure 1.1 Chart showing the number of publications concerning metal-organic frameworks (red) and coordination polymers (blue) versus year.

In fact certain MOFs have shown extremely high surface areas; MOF-5[5], HKUST-1[6], MIL-101[7] and MOF-177[8] are prime examples. Indeed, until very recently a MOF known as UMCM-2 had the highest surface area of any known porous material[9] (Langmuir surface area of 6060 m^2g^{-1}). This has since been superseded by a porous aromatic framework[9] (PAF) which has a Langmuir surface area of 7100 m^2g^{-1}.

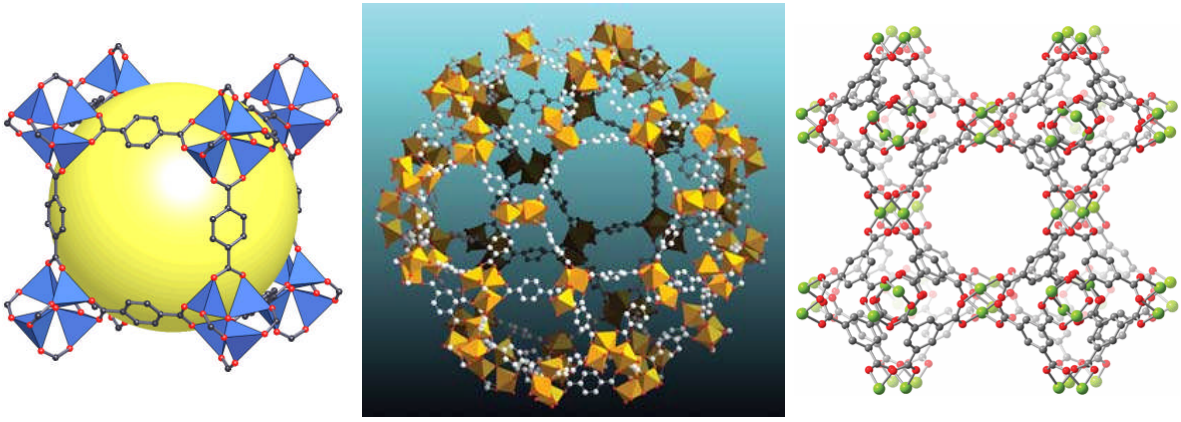

Figure 1.2 Examples of MOFs (from left to right), the world famous MOF-5, MIL-101 and HKUST-1 structures. Reproduced with kind permission from Nature and the Royal Society of Chemistry.

MOFs also have several advantages over zeolites. For example, during synthesis the solvent acts as the template for MOF formation with the result that the majority of MOFs are neutrally charged. This is not the case for zeolites where a charged template is required. However this can also be an advantage for zeolites as negatively charged frameworks present more functionality then neutral ones. The biggest advantage for MOFs however, is the almost limitless possibilities for structure types. Beginning with the cations, zeolites are for the most part, based on aluminium and silicon with a number of exceptions. MOFs can be constructed from almost any cation, certainly all the di, tri (including the rare-earth elements) and tetravalent transition metals. This represents an extremely large number of framework possibilities. This number is then increased vastly when the number of organic linkers which could be utilised is taken into account. Linkers fall primarily into two categories: O donors and N donors. The vast majority of O donor MOFs have been constructed using either mono or poly carboxylates. There have, however, also been many MOFs constructed using phosphonates and to a lesser extent sulfonates[10]. The most commonly used N donors are cyanides, pyridine and imidizoles, which attach directly to the cation. This leads to a huge number of possible frameworks. This number can be increased again as post synthetic modification can be carried out on MOFs to functionalise organic parts, tailoring them for specific applications[11]. However there are certain scientific constrictions which reduce this number. For example, certain metals form particular clusters that appear again and again. These are known as secondary building units (SBUs)[1,12]. Three of the most common examples of SBUs can be seen in figure 1.3.

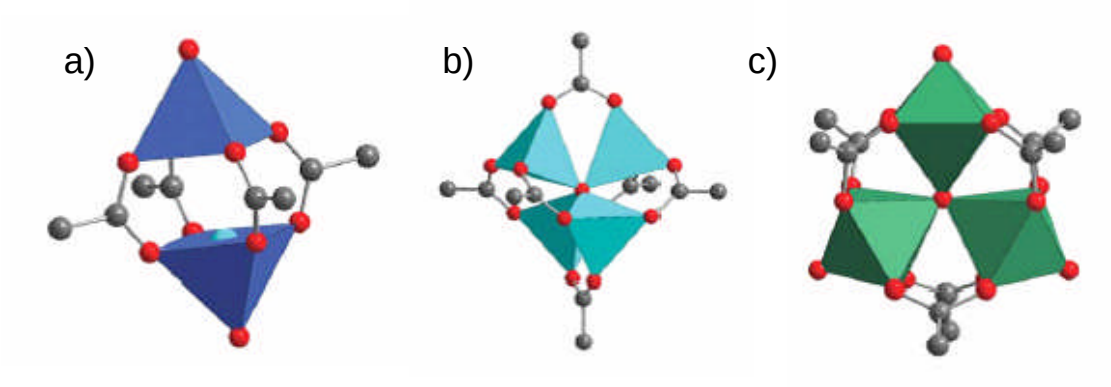

Figure 1.3 Three of the most common SBUs. (a) The paddlewheel MO_5 dimer. (b) The MO_4 tetrahedron and (c) The planer trimer containing MO_6 octahedra with a central oxygen atom.

Figure 1.3(a) shows the "paddlewheel" SBU which is produced by a number of metals, most notably Cu^{2+} but also others such as Zn^{2+} and Fe^{2+}. Figure 1.3(c) shows the trimer SBU, which can be produced by a number of metals including Fe^{3+} and Cr^{3+}. Using these SBUs an entire series of MOFs can be produced that have the same topology but utilise different linkers in synthesis. The best example of this is the isoreticular MOFs (IRMOFs) produced by Yaghi and co-workers. By using the same zinc SBU (figure 1.3(b)), but using different organic linkers, they were able to synthesise an entire range of MOFs (see figure 1.4) differing in surface area and functionality, but with the same cubic topology[13]. The most famous of this set is MOF-5 (figure 1.2)[5], which has been one of the most studied MOFs to date.

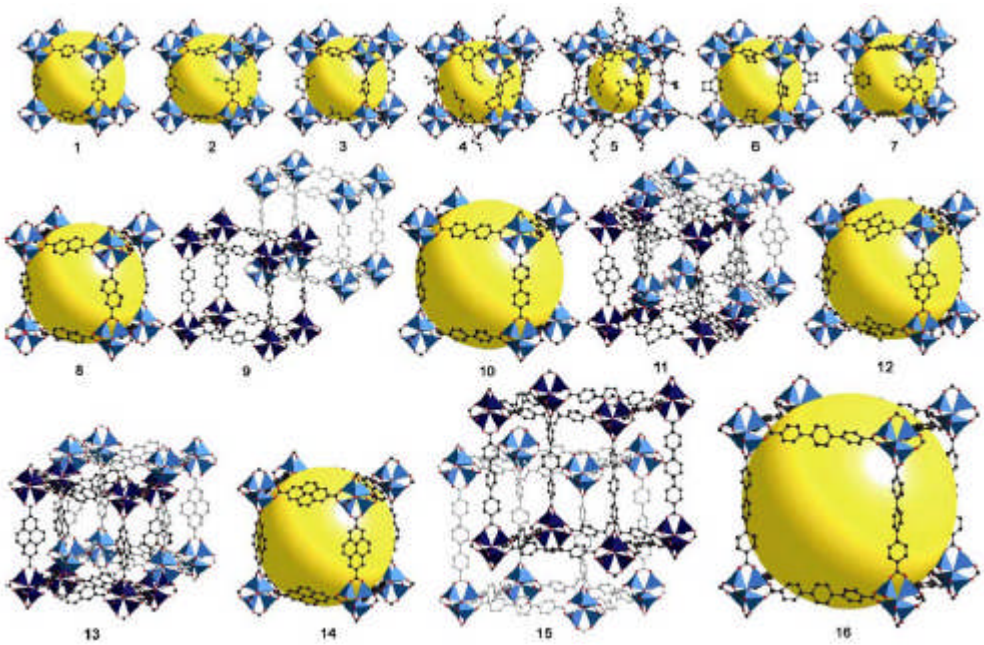

Figure 1.4 The series of iso-reticular MOFs produced by Yaghi and co-workers[14], showing the same SBU (cubic topology) but with differing linker length and functionality. (Reprinted from reference 14, Copyright (2004), with permission from Elsevier).

1.1.2 Synthesis of MOFs

The original method for producing MOFs involved slow coupling of the coordinating species. This method was time consuming and therefore other synthetic procedures were adopted. Solvothermal synthesis very quickly took over and has proved to be the dominant synthesis procedure used to produce MOFs. In a typical synthesis the precursor reactants are diluted into solutions using polar solvents such as water, alcohols, dialkyl formamides or less commonly acetone. These solutions are combined in a Teflon-lined autoclave (figure 1.5) and then heated to the required temperature (somewhere between room temperature and 250°C). Once the reaction has finished (ranging from a few hours to several days) the autoclave is removed

from the oven and cooled to room temperature. The resulting solid is filtered, washed with the parent solvent and then dried. The crystallinity of the sample produced is then checked using powder X-ray diffraction. The results can be compared with a database of known materials to see if the phase has been synthesised before or to confirm that your phase is exactly what is required.

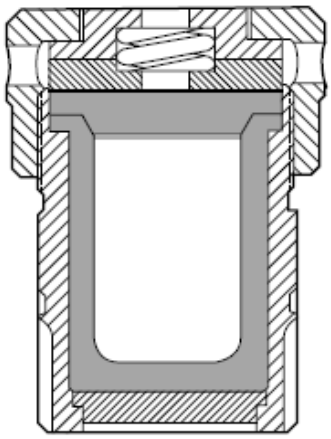

Figure 1.5 A diagram showing a Teflon lined Parr bomb[15] (autoclave) which relieves excess pressure safely.

1.1.3 New methods of producing MOFs

In recent years there have been numerous efforts at producing frameworks using different synthesis techniques. The first of these is so-called Ionothermal synthesis. This involves using an ionic liquid as both the solvent and template in the reaction. This method has been pioneered by Morris and co-workers[16-18]. They have shown that it is possible to make several types of frameworks using ionic liquids in the reaction. It is still a technique in its infancy, however, as there are only very few examples of frameworks being produced using ionic liquids.

The next technique being pioneered to produce MOFs involves using microwave synthesis. This method has already been used to form dense solids and seems very promising for the production of MOFs. The advantages of microwave synthesis are much shorter crystallisation times compared with conventional techniques and control over morphology. Indeed Chang and co-workers have shown recently that microwave synthesis is an extremely efficient way of producing certain MOFs. They have synthesised the giant pore structures of chromium trimesate and terephthalate (MIL-100 and MIL-101 respectively) in less than 1 hour[19] which is 60 times faster than the conventional hydrothermal route. Chang and co-workers have also produced the famous MOF-5 structure[20] and Choi and co-workers have synthesised MOF-5 and shown which factors are important for higher quality material to be produced[21]. Another example of efficient microwave heating is the Ni glutarate system. Whereas the conventional method takes many hours, the microwave method can produce both the original MIL-77 [$Ni_{20}(C_5H_6O_4)_{20}(H_2O)_8 \cdot 40H_2O$] and also the formation of a different phase, [$Ni_{22}(C_5H_6O_4)_{20}(OH)_4(H_2O)_{10}] \cdot 38H_2O$, within a few minutes[22]. Morris and co-workers have also shown that it is possible to synthesise MOFs using microwave ionothermal synthesis. Indeed they produced the same frameworks both ionothermally and using microwave synthesis and concluded that the microwave samples were purer and had higher crystallinity[23].

All these examples show that there are definite steps towards commercialisation in the production of MOFs. This commercialisation has already begun as it is now possible to purchase several MOF structures from Aldrich. These are produced by BASF and one of them uses the third of the new synthetic techniques. This involves

electrochemical production of MOFs[24]. The best and only example of this is the structure known as HKUST-1, which is a copper 1,3,5 benzenetricarboxylate MOF. BASF produce this MOF (see figure 1.3) using copper plates as both anode and cathode and have the organic linker dissolved in a solution of methanol. After 2 ½ hours (12-19V, 3A) of reaction time a greenish-blue precipitate is formed. The HKUST-1 formed from the electrochemical route has also proved to be of a higher quality[24] and give increased surface areas compared with the conventional solvothermal synthesis sample.

The final method now being employed for the creation of MOFs is the production through high throughput synthesis[25-31]. This method has four main stages: design of experiment, synthesis, characterisation and data evaluation. A tremendous amount of data can be produced in a very short space of time, but in order to be efficient it is the design of the experimental stage which is the most important. A typical experiment includes 48 mini autoclaves and so entire combinations and variance can be tested in only a few days. Bein, Stock and co-workers have pioneered this technique and have shown that it is possible to find new phases of materials[26]. They have proved that water content and pH play a very important role in reaction trends and they also have optimised the production of MOFs with this particular synthesis method[30-31].

1.1.4 Applications for MOFs

It is no surprise that given the surface areas and pore volumes available within MOFs that they have major potential for a large number of applications[32]. Due to the aforementioned properties it is in the areas of catalysis and the separation and storage of gases that have received the most attention for research. However, there are other areas of research for which MOFs are considered potential candidates for use including light-emission and magnetism. Finally, the area in which this thesis concentrates is in the emerging field of biomedical research using MOFs.

1.1.5 Catalysis using MOFs

MOFs have been looked at for possible catalytic applications[32-34], although hydrogen (H_2) and carbon dioxide (CO_2) storage remain the most heavily researched areas. For catalytic applications it is in the area of heterogeneous catalysis where nanoporous materials are of significant interest. This is not only due to the high surface areas available but also to the lack of "dead volume" (inaccessible volume) these materials possess. There are three main approaches to the utilisation of MOFs in catalysis, the first involves using the porous material as the carrier for the active mass. An example of a MOF being used for this process is MOF-5, and both silver and platinum are catalytically active when encapsulated by MOF-5[35-36]. A further example is produced by the Fischer group in Germany who have achieved different catalytic properties using MOF-5 loaded with gold, palladium and copper[37]. The second method involves fixing catalytically active species within the framework. This has been done by modifying previously known catalysts, so that they are capable of forming MOFs. Hupp and co-workers have shown that a MOF constructed using manganese salen

struts has only a slightly lower reaction rate for olefin epoxidations than the homogenous alternative,[38] proving that the reaction takes place inside the pores of the MOF. The final approach employed is the generation of coordinated species in the framework which are also stabilised by the framework. Two recent examples of such an approach are from Rosseinsky and co-workers[39] and Wenbin Lin's group[40]. The Rosseinsky group managed to protonate a chiral MOF and use it efficiently as a catalyst in the enantioselective methanolysis of *cis*-2,3-epoxybutane. The Lin group constructed a homochiral MOF which was extremely useful in forming chiral secondary alcohols via addition of diethylzinc to aromatic aldehydes. Finally the most recent method for producing catalytic MOFs used post-synthetic modification. The most noteworthy example of this class of approach is the modification of MIL-101 with ethylenediamine[41]. Hwang and co-workers have managed to achieve the Knoevenagel condensation of benzenealdehyde and ethyl cyanoacetate with a selectivity of 99.3% towards the product. This high selectivity has also been shown to be due to the MOF and the structural features contained within the framework.

1.1.6 Light emitting and magnetic MOFs

Light emission by MOFs has received a great deal of attention and there have been over 200 papers and several reviews published regarding the luminescent properties of MOF systems[42-45]. Indeed there is a comprehensive review of luminescence in MOFs published recently by Allendorf *et al*[46]. The reasons for utilising MOFs for light emission are threefold. Firstly, the organic linkers present in MOFs have their own inherent luminescent properties. Secondly, by combining these organics with metal clusters the thermal stability is greatly increased compared with the free

organic molecules, increasing the likelihood of applications. Finally this combination of metal and linker could improve the luminescent properties of the linkers. Examples of MOFs improving luminescent properties compared with the free organic linker are $Zn(C_6N_2O_2H_5)_2(H_2O)_{4.5}$ and $Cd(C_8O_4H_4)(py)$,where both show a vast improvement compared with the free linkers (urocanate and terephthalate)[47-48]. The urocanate ligand shows almost no luminescence at room temperature in the solid state but when placed in the MOF it displays an intense blue[47]. A similar effect is noted in the second structure where a 100 fold improvement in the blue fluorescence is seen[48]. The majority of light emitting MOFs are constructed using metals from the transition elements (especially the d^{10} configured cations Zn^{2+} and Cd^{2+}). However, the rare earth metals have also been used. Song and co-workers created some frameworks consisting of lanthanide oxalates with phosphate decoration which displayed blue, red and near IR luminescence[49]. The Férey group doped Eu, Tb and Dy into the $Y_{1-x}En_x(C_9O_6H_3)$ (x~0.024) complex which then showed blue, green and red emissions respectively[50].

Research has also been carried out into the magnetic properties of MOFs, and several reviews have now been written concerning this area[42,51-53]. The majority of magnetic MOFs contain paramagnetic metal centres such as those in the first row of the transition metal series (V, Cr, Mn, Fe, Co, Ni, and Cu). Using MOFs with magnetism could lead to new applications such as molecular sensors[42]. One of the major discoveries concerning magnetic MOFs are solvatomagnetic effects. That is changes in magnetic ordering, when a MOF has been desolvated or if the structure has collapsed. These effects were first reported by Ohkoshi and co-workers in their

$Co^{II}_{1.5}[Cr^{III}(CN)_6].7.5(H_2O)$ framework which when it was exposed to ethanol, it changed from peach coloured to blue. This effect was attributed to a change from 6 coordination to 4 coordination at the Co^{II} centre[54]. Another notable example of a magnetic MOF is the highly flexible nanoporous magnet $Cu_3(PTMTC)_2(py)_6(CH_3CH_2OH)_2(H_2O)$ produced by Veciana and co-workers[55]. This structure expands/shrinks by 30% depending on ethanol sorption and also displays subtle solvatomagnetic properties.

1.1.7 Gas adsorption, storage and release by MOFs

Due to the extremely large surface areas and porosities that MOFs possess, it is no surprise that the majority of application research has focused on gas storage or separation using MOFs[56]. Indeed in the current climate of trying to reduce carbon footprints and cut carbon emissions, it is energy and environmental applications which receive the largest amount of attention regarding gas storage. It could be either storing H_2 for a hydrogen fuelled car, or using MOFs to capture carbon dioxide (CO_2) to reduce greenhouse gases. However there is an emerging area of storage application which uses MOFs for medicinal applications.

1.1.8 Storage of gas for energy applications

Due to concerns regarding carbon dioxide emissions from the usage of petrol and diesel causing irreparable damage to the earth's eco-system, alternative fuels and energy sources are now required. Battery and fuel-cell powered modes of transport are likely candidates to replace petrol engines, as is utilising hydrogen as a fuel.

Hydrogen is attractive as a replacement fuel as it is abundantly available (from water) and is carbon free. The US Department of Energy (DOE) has produced stringent targets for the storage of H_2 for use in mobile applications. They are as follows: 6.0 wt% and 45 gL^{-1} of H_2 capacity, a refuelling time of less than 10 minutes, a lifetime of 1000 refuelling cycles and an ability to operate within -30°C and 50°C by 2010[57-58]. MOFs are attractive for the storage of hydrogen as they have extremely high surface areas and low densities. Therefore a vast amount of research has centred on hydrogen adsorption of different MOFs. The MOF with the highest volumetric storage density is MOF-5 which takes up 66g L^{-1}, corresponding to 10 wt% at 100 bar[59]. This is achieved with a sample which has been fully activated and not exposed to air (displaying an optimal BET surface area of 3800 m^2g^{-1}). It has also been demonstrated that MOF-5 can adsorb that amount of hydrogen within 2 minutes and can desorb and re-adsorb for at least 24 cycles without loss of capacity. Hydrogen storage performance on over 150 MOFs has now been carried out in an effort to increase and improve the results on MOF-5[60-62]. A MOF which has closely matched the results on MOF-5 is MOF-177 ($Zn_4O(BTB)_2$) which has equalled MOF-5 in terms of excess H_2 adsorption at 77K[8,63-64], however due to its larger pores, has a lower volumetric density. The best performing MOFs have been validated by BASF and have been compared with compressing hydrogen in an empty container. The results can be seen in figure 1.6.

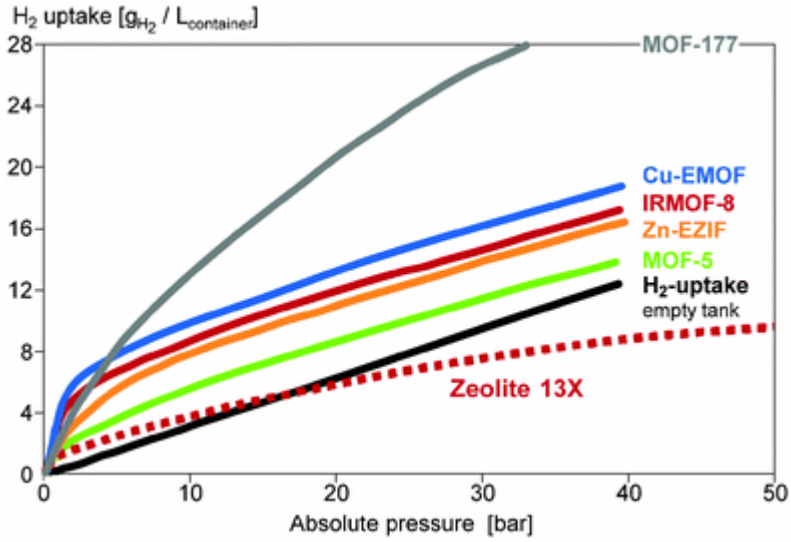

Figure 1.6. A graph displaying H_2 capacities for different MOFs and comparing them with a zeolite and an empty tank[32]. Reproduced with permission from the Royal Society of Chemistry.

One of the main strategies used to improve H_2 uptake in MOFs is using the coordinatively unsaturated sites (CUS) or open metal sites present in some frameworks. Many synthesised MOFs have exposed metal sites available for binding when guest molecules (solvents) have been thermally removed. Some good examples of such frameworks are the M-CPO-27 series (M_2(DHTP))[65-67] and HKUST-1 ($Cu(BTC)_2$)[68-69]. The concept of using open metal sites is that the H_2 will bind to the exposed site. Indeed HKUST-1 has been shown to bind H_2 at the metal site using both infrared spectroscopy and neutron powder difraction[70-71]. HKUST-1 has the common paddlewheel SBU and this allows one solvent molecule to be removed to leave an open metal site. HKUST-1 has been shown to have a hydrogen uptake of 2.27% at 77K and 1bar[72]. Other Cu paddlewheel based structures include the PCN series of MOFs from the Zhou group which have shown good uptakes of hydrogen notably PCN-11 which adsorbs 2.55% at 77K and 1bar[73]. The Long group have produced some very interesting research concerning hydrogen storage in MOFs and

have synthesised two MOFs with open metal sites, Mn BTT and Cu BTT ($M_3[(M_4Cl)_3(BTT)_8]_2$) which adsorb 2.25% and 2.42% of hydrogen at 77K and 900 torr respectively[74-75]. The M-CPO-27 series of MOFs has been tested and has proved to be of significant interest as comparisons between different metals and their binding energy with H_2 can be measured[76]. It was shown that Ni has the highest initial isosteric heat of adsorption, which means that the Ni version binds the H_2 strongest compared with the others. Several reviews have been written concerning the use of MOFs for hydrogen storage and the challenge of finding a material with the right set of properties is being widely undertaken[60-62]. Indeed there seems to be a consensus that surface area and the amount of hydrogen adsorbed are related[61]. This can be seen clearly in figure 1.7.

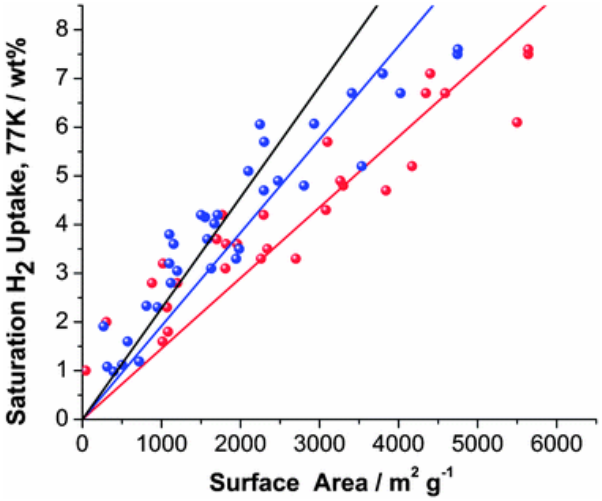

Figure 1.7. Graph showing the relationship between surface areas and hydrogen uptakes in MOFs[61] (red: Langmuir method, blue: BET method and black shows a theoretical carbon H_2 adsorption). Reproduced with kind permission from the Royal Society of Chemistry

Another potential alternative fuel is methane gas (CH_4) and unlike hydrogen it is easier to store at room temperature in appreciable amounts. For a MOF to be even considered a candidate for industrial methane storage it must compete with compressed natural gas (CNG) and exceed a DOE target which requires storage of about 35 wt% or 180 cm^3(STP)cm^3 at 298K and 35 bar[77]. There have been many studies carried out on MOFs for methane storage starting back in the late 1990s with the Kitagawa group. They produced a MOF ($\{[M_2(4,4'\text{-bpy})_3(NO_3)_4].xH_2O\}_n$) (M=Co, Ni and Zn) which showed a methane uptake of 2.3 mmol CH_4 per gram of MOF material at 30 atm[78]. Following this initial success many groups have matched and indeed improved on this result. The Yaghi group have run CH_4 adsorption on many of their MOFs and IRMOF-6 has shown an exceptionally high uptake of 155 cm^3 (STP)cm^3 CH_4 at room temperature and at 36 atm[13]. The most recent publications concerning methane storage in MOFs show great promise for industrial applications. Hong Cai Zhou's group have synthesised a MOF known as PCN-14 which illustrates extremely high CH_4 uptake[79], indeed it is 28% above the DOE target for methane storage. The M-CPO-27 series of frameworks have been investigated for methane storage[80] and it has been shown that methane binds initially at the open metal sites, followed by secondary binding again at the metal site. In addition it was shown that the nickel version of this MOF has the highest adsorption of CH_4 of this series (200 cm^3 (STP)/cm^3) and exceeds the DOE target (180 cm^3 (STP)/cm^3) at room temperature and 35 bar.

1.1.9 Storage of gas for environmental applications

The world is now very aware of some of the effects of climate change and almost everyone knows about "carbon footprints" and the effect that carbon dioxide (CO_2) has on our environment. Therefore there is much interest in trying to remove or separate CO_2 from industrial processes and also to try and cut down on the amount of CO_2 produced by vehicles. MOFs have the ability to be used as materials to capture environmentally toxic gases such as CO_2, sulphur dioxide (SO_2) and ammonia (NH_3). MOFs are also being used to separate CO_2 from flue gases to try and limit the amount of CO_2 released.

There have been numerous studies conducted on MOFs for both the storage (removal) of CO_2 and separation of CO_2 from other exhaust gases. The first MOF to be tested for CO_2 adsorption was MOF-2, a Zn paddlewheel based benzenedicarboxylate MOF[81]. It had a modest uptake of about 2 $mmolg^{-1}$ at 1 atm and 195K. Since then, Yaghi and co-workers have tested many MOFs for CO_2 adsorption and have had some outstanding results including MOF-177 which adsorbs 33.5 $mmolg^{-1}$ of CO_2[82] at room temperature and 42 bar. Again the M-CPO-27 series has been investigated for CO_2 storage and it was shown that the magnesium version adsorbs the largest amount of CO_2 (35 wt%) at 1 atm[83]. The nickel version has been thoroughly investigated and the CO_2 molecule has been shown to bind directly to the open metal site through an oxygen atom. Some of the most interesting results regarding CO_2 storage in MOFs are from the "breathing" MIL-*n* MOFs synthesised by Férey and co-workers[84]. The "breathing" phenomenon occurs in only a few examples such as MIL-53[85-86] and MIL-88[87-88] and is observed when guest molecules

are removed from the structure, altering the shape of the structure considerably and having a very pronounced effect on the adsorption/desorption properties of these materials. For example MIL-53, has a distinct adsorption isotherm for CO_2[89]. Initially it shows a modest uptake of CO_2 (3 $mmolg^{-1}$ at 5 bar), however under increased pressure it shows a step and adsorbs a large amount of CO_2 (8 $mmolg^{-1}$ at 20 bar), as can be seen in figure 1.8.

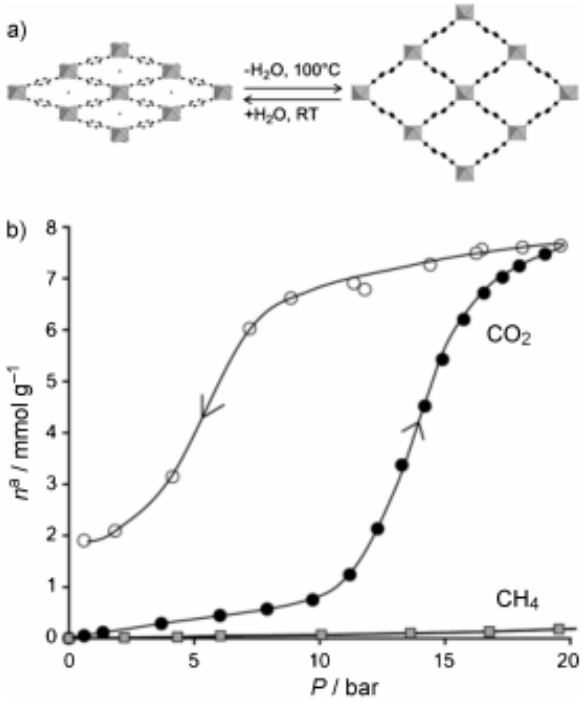

Figure 1.8 a) Structure of MIL-53 and its ability to breathe and b) the adsorption/desorption curve for CO_2 on hydrated MIL-53[56]. The methane adsorption isotherm is also included for comparison. (Reproduced with kind permission from Wiley Interscience)

Research into storage or removal of sulphur dioxide (SO_2) and ammonia (NH_3) is still in its infancy as far as MOFs are concerned, however there are a few publications highlighting MOFs as potential materials for the capture of these toxic gases. Yaghi and co-workers have released a paper showing the adsorption isotherms for six famous MOFs and their affinity towards eight harmful gases including SO_2 and NH_3[90]. These results showed that MOFs outperform a Calgon activated carbon material in the storage of most gases, therefore making MOFs very attractive for use as harmful gas adsorbers. The results also highlighted the importance of open metal sites or linker functionality and their impact on the adsorption of different gases.

1.1.10 Prospective biomedical applications of MOFs

An area of research concerning MOFs which up until recently, had remained unexplored, is the use of MOFs for medicinal applications and therapies. It is only in the last few years that papers have been published regarding applications for MOFs in biology or medicine. However, there are now a number of research groups within the porous materials community who are interested in the idea of using MOFs for biomedical applications. This area can be broadly split into two categories. The first concerns using MOFs themselves as active materials and the second involves utilising the properties of large surface area and open metal sites for the delivery of different therapeutic remedies based on the requirements of the individual patient.

The first category using MOFs as active materials in medicine has been pioneered by Wenbin Lin's group in the United States. They have produced MOFs that have been

shown to be useful as contrast agents in magnetic resonance imaging (MRI) scans. They first produced a Gd^{3+} based nanoscale MOF (nanoMOF) as Gd^{3+} is highly paramagnetic (a requirement for useful MRI contrast agents). Using this nanoMOF they were able to show large relaxivities orders of magnitude higher than those of other Gd^{3+} based MRI contrast agents[91-92]. However, the toxicity of the nanoMOF would be too large for clinical use. They then produced a Mn^{2+} based nanoMOF as Mn^{2+} is much less toxic than its Gd^{3+} counterpart[93]. The relaxivities observed this time were modest, but they proved that site-specific imaging would be a possibility using a silica based coating on nanoMOFs to delay the leaching of metal ions until they reached the specific site. They have also produced nanoMOFs that show potential as anti-cancer drug delivery vehicles via decomposition of the platinum based linker[94]. Finally their most recent research has yielded the first nanoscale production of MIL-101[95]. To achieve this they used post-synthetic modification to produce a nanoMOF with a fluorophore and an anti-cancer drug, which could be used for optical imaging and as an anti-cancer therapy respectively.

Meanwhile there has been a lot of initial research investigating the use of MOFs as storage and delivery vehicles for a number of different therapies. These include biologically active gases, such as nitric oxide (NO), carbon monoxide (CO), hydrogen sulphide (H_2S) and pharmaceuticals. Nitric oxide will be discussed in much greater detail in section 1.2. However, it is necessary to give a brief statement of why it is beneficial to store and release nitric oxide. Using nitric oxide as a therapy would enable wound-healing times on chronic wounds (such as diabetic ulcers) to be reduced by several days[96]. It could also be used to coat medical instruments to

prevent clotting after invasive surgery[97]. Other NO releasing therapies being investigated have their disadvantages[98-99], whereas there would be no side-effects from NO being released from porous materials as it would be in the form of pure NO gas. Morris *et al* began storing and releasing NO in zeolites[100-101]. Zeolite-A shows a good adsorption capacity of NO and this can be tailored depending on the metal ion present in the framework and the amount of exchanged metal present[100,102-103]. They also carried out thrombus studies proving that the NO-containing zeolite prevents aggregation of platelets (thrombus formation). Subsequent publications have shown that trials on human skin were successful and the NO-releasing zeolite causes no harm to the skin whereas the acidified cream (a competing NO-releasing therapy) actually causes quite severe damage to the skin[104]. Following NO storage in zeolites the Morris group then tried storing NO in HKUST-1[72]. Due to the larger surface area and big pores, HKUST-1 displays a higher uptake of NO compared with the zeolites previously investigated. However the release of NO from HKUST-1 is 2 orders of magnitude less than the amount actually adsorbed. Despite this, NO-loaded HKUST-1 completely inhibits platelet aggregation, showing that the small amount of NO released is still of biological significance. Included in this thesis are the most recent publications from the Morris group regarding NO storage in MOFs. The MOF family of M-CPO-27 (M = Ni, Co, Zn, Mn and Mg) are shown to be of interest in NO storage particularly the Ni and Co versions as they display almost perfect storage and release of NO[103,105-106]. Indeed M-CPO-27 (M=Ni and Co) has shown the highest reported uptakes of NO of any porous material. A comparison between MOFs and zeolites and their NO storage abilities can be seen in figure 1.9. Clearly toxicology could be a problem and that is addressed within this thesis also. Recent testing of

iron carboxylate MOFs (Fe MIL-88) could help as there are already therapies (though not NO related) on the market containing iron carboxylates, (Ferretts^{TM} has the same composition as Fe MIL-88-A). So their toxicology would not be problematical compared with those composed of Ni and Co CPO-27. The most recent publication regarding NO storage and release in MOFs comes from the Rosseinsky group[107]. They have carried out post-synthetic modification on the open copper sites of HKUST-1 with a secondary amine, which, when reacted with NO produces an *N*-diazeniumdiolate (NONOate) inside the pores of the framework. This should allow NO to be released upon exposure to moisture. Unfortunately the majority of the NO attached to the open copper sites that had not been successfully grafted with amine. However this route of grafting of amines to improve NO storage and release is of interest and will also be covered in this thesis.

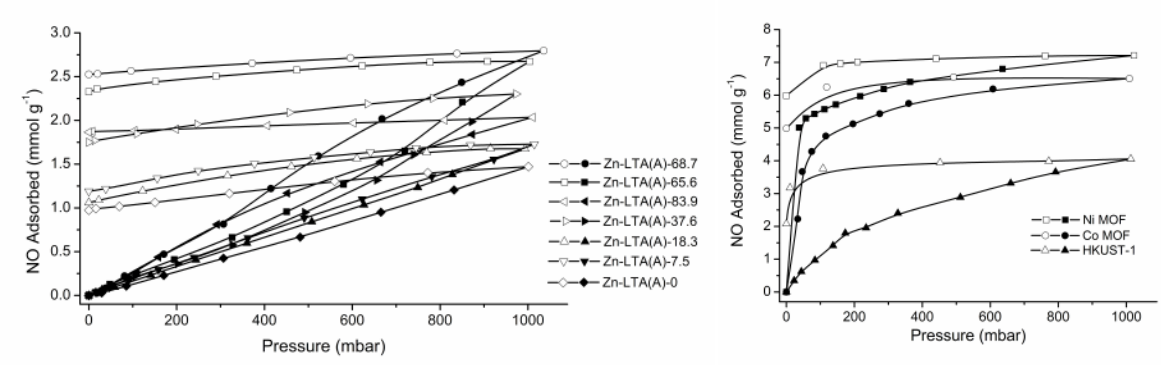

Figure 1.9 Graphs showing the comparison between zeolite Zn-LTA and 3 different MOFs (Ni, Co CPO-27 and HKUST-1) and their NO adsorption capacity, all conducted at 298K.

Carbon monoxide (CO), like NO, is mostly known for its toxicity, however it is also potentially useful in biological and medical applications. Indeed there is considerable literature regarding carbon monoxide releasing molecules (CORMs) and their ability

to release CO gas in a biological setting[108]. There is, however, very little research on CO storage in porous materials. The storage and delivery systems of CO gas will essentially be the same as for NO. There are a few papers that have looked into CO storage in MOFs, but not from a biological point of view[90,109]. They are more concerned with separation of CO from H_2, or as a trap from other systems[109]. Results for CO adsorption from a selection of MOFs proved that there is no improvement in adsorption when compared with the current technology of activated carbon[90]. However, these are just initial results and the lack of research in this area might be partially due to the discovery of CO as a signalling molecule after NO and therefore biological studies on CO are still fifteen years behind those of NO.

Hydrogen sulfide (H_2S) has also been identified as a potential therapeutic agent as it has been linked with several biological functions and its targeted release could be beneficial in numerous areas including vasodilation[110] and neuroprotection[111]. In addition it is capable of producing a suspended animation type state in mice[112]. A theory has been put forward that suggests organ preservation could be improved with its use and it could also have benefits during surgical procedures[113-114]. There is only one example of MOFs being used to adsorb H_2S so far and this came from the Férey group[115]. Their main aim was to purify natural gas, however the adsorption results are obviously still of interest. It showed that MILs 101,100, 53 and 47 can certainly be used for the storage of H_2S, however, selecting the correct metal and structure type is very important as H_2S can destroy some structures and be irreversibly adsorbed in others.

Of course MOFs are not just being used to store gases which could be used for therapies. The Férey group have investigated the storage and release of ibuprofen[116-117] using several of their MOFs. Great efforts are being employed in finding new methods for storing and controlling the release of drugs. Using MOFs is a suggested solution as they contain large porosity and organic groups within their frameworks which could hold the key to both high storage capacity and controlled release of drugs. The MOFs studied so far for ibuprofen storage and delivery are MIL-53 and the giant-pore MIL-100 and MIL-101. Initial testing was carried out on MIL-100 and MIL-101[116]. The results were extremely encouraging as MIL-101 showed four times the capacity for ibuprofen compared with MCM-41. It also took 6 days to completely release its store of the drug. Following these initial results, ibuprofen loading was carried out on Fe MIL-53[117]. The MIL-53 structure is of significant interest as it "breathes" (undergoes a reversible cell expansion) when dehydrated. MIL-53 delivers about the same amount of ibuprofen as MCM-41, however it is delivered over a period of 20 days compared to just 2 for MCM-41. A graph showing these release values can be seen in figure 1.10. Very recently the Férey group have studied many of their iron-based MOFs for the storage and delivery of both anti-cancer and anti-AIDS based therapies[118]. They have shown that several of their MOFs exhibit storage and release capacities that greatly exceed the current technology for delivery of these pharmaceuticals. Further to these results they have also proved that these MOFs are non-toxic *in vivo* and would present no problem for use as nanocarriers of drugs. These initial results show great potential in using MOFs as delivery vehicles for medical therapies both internally and externally.

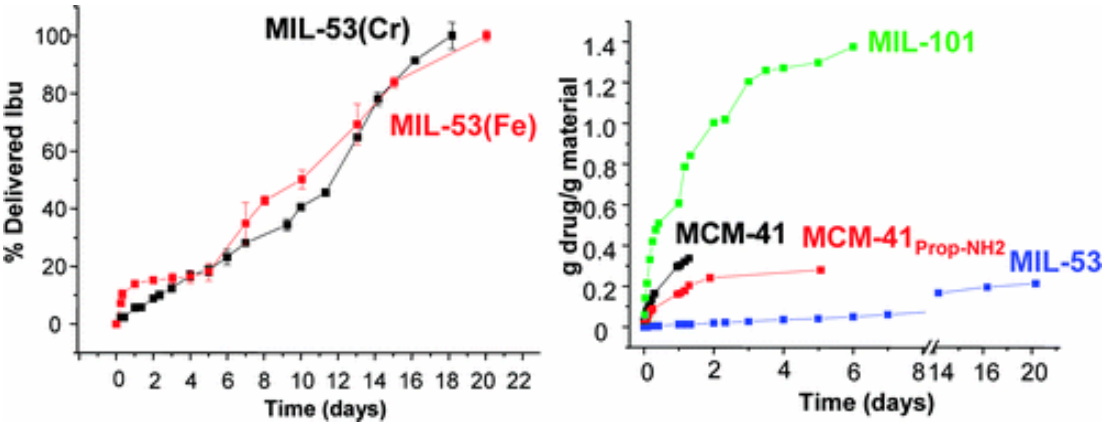

Figure 1.10 Graphs displaying the ibuprofen release from a selection of frameworks.

(Reprinted from reference 117, Copyright (2008), with permission from ACS journals)

1.2 Nitric oxide

1.2.1 Background

The gaseous diatomic nitric oxide (NO) molecule was until 1986 perceived only as one of the toxic gases produced from car exhausts. Its chemistry was fully explored by the oil companies in an effort to reduce NO levels produced from the internal combustion engine. Since 1986, this small free radical has been named 'molecule of the year' in 1992 in science[119]. Subsequently in 1998 three American scientists (F. Murad, R. Furchgott and L. Ignarro) won the Nobel Prize in physiology for discovering its uses in the human body and in particular its action as a muscle relaxant. A family of enzymes are now known to produce NO in the body, collectively called Nitric Oxide Synthase (NOS). The chemistry of this interesting molecule, its reactivity, its roles in the body and prospective applications of NO will all be examined.

1.2.2 Nomenclature, structure, properties and reactions of NO

Nitric oxide is the common name for the molecule that is being introduced however, IUPAC gives it the name nitrogen monoxide. NO has an unpaired electron in its valence shell and this means it is classed as a radical. For this reason it is a reactive species. The molecular orbital diagram of NO shown in figure 1.11 illustrates this unpaired electron and its position in the π^* (anti-bonding) orbital. As can be seen NO contains eleven valence electrons, five come from the nitrogen atom and six from the oxygen atom. This means that there are three electrons in anti-bonding orbitals and eight in bonding orbitals. Consequently, there is an excess of five bonding electrons (2.5 bonding pairs or bond order) and this gives the bond a partially double, partially

triple nature[120]. As a result, the bond length in NO is 1.15Å, which is in between the triply bonded NO^+ (1.06Å) and the length of an O_2 double bond (1.2Å). As already explained due to its unpaired electron NO is a radical and would normally be expected to dimerise. This would eliminate the unpaired electrons by forming a N-N bond, however this process involves a loss of entropy and does not occur. However, it should be noted that in its liquid and solid state dimerisation does occur, although they are joined side on rather than end to end. It has been shown that the unpaired electron is only near the nitrogen atom 60% of the time and this delocalisation contributes to the lack of reactivity in NO.

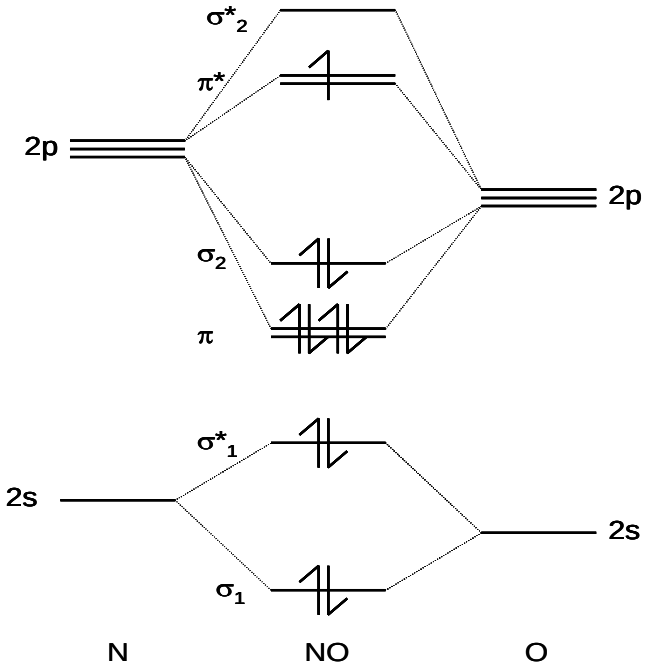

Figure 1.11 Ground state molecular orbital diagram of NO.

This lower than expected reactivity does not, however, mean that NO does not spontaneously react. For example, the Gibbs free energy of the decomposition reactions of NO are all negative. This does not take into account the activation

energy which is high and the rate of reaction which is slow for these reactions and therefore a cylinder of NO could stand alone for weeks before any of these reactions would occur. However, if left for long enough contamination with N_2, O_2, N_2O and NO_2 would result.

1.2.3 The oxides of nitrogen and chemical reactivity

NO reacts readily with oxygen to form the brown gas known as nitrogen dioxide (NO_2). This means that when NO forms in the atmosphere it is a mixture of NO and NO_2. The formation of NO in our environment occurs mostly from combustion engines, but also a small percentage comes from lightning strikes. From these sources a mixture is produced (mentioned above) known as NO_x. It is this mixture which is directly responsible for the photochemical smog that famously appeared above Los Angeles in the 1950s. Measures were then taken to remove the NO_x emissions from exhausts using catalytic converters. Another problem caused by the NO_x mixture occurs when it reacts with water in the atmosphere to form nitrous and nitric acids which contribute to the “acid” rain that damages buildings and can harm the wildlife in lakes and rivers. There is a whole series of oxides defined by the increasing valency of the nitrogen. These vary from the well known N_2O (also known as laughing gas) used in anaesthetics, to the unstable NO_3 (or N_2O_6). Some of these oxides react with water to form acids (the oxides are the anhydrides of acids) i.e. N_2O_5 is the anhydride of nitric acid and N_2O_3 is the anhydride of the weaker nitrous acid. Thus it would be sensible to assume an acid – anhydride relationship for NO. It was thought that NO might be the anhydride of the weak acid $H_2N_2O_3$, however no relationship exists. This relationship was also thought to exist with the

rare hydronitrous acid (H_2NO_2) because, in theory it could be formed from the reaction of NO and water. Studies have shown, however, that nitric oxide undergoes no hydrolysis in an aqueous environment. This lack of reaction with water is essential for the use of NO in the body. It can be generated in a cell, released into the aqueous environment between the cells and diffuse unchanged until it reaches a cell membrane, provided there is no oxygen present. Membranes of cells are constructed from non-polar lipids which allow the small hydrophobic NO molecule through to interact with the enzymes in a neighbouring cell. The sparing solubility of NO in water (1.7×10^{-3} mol L^{-1} in normal conditions) is comparable with that of oxygen and nitrogen as they do not have the large dipole moment required for solution in a polar substrate like water. In an aqueous environment, NO readily reacts with oxygen to form nitrites, which are then easily oxidised to nitrates. One of the reasons why NO is so useful is its ability to be both easily oxidised and easily reduced. For example, if its unpaired electron is removed the nitrosonium ion (NO^+) is formed. NO^+ is isoelectronic with carbon monoxide (CO) and also involves the same strong triple bond that is present in CO. The nitrosonium ion is useful in forming ionic salts like $NO^+BF_4^-$, which in water are rapidly hydrolysed to form nitrous acid. A more interesting use for the nitrosonium ion is in biologically important reactions involving the transfer of an NO^+ group from a nitrosothiol to a secondary thiol (see equation 1.1).

$$RSNO + R'S^- \rightarrow RS^- + R'SNO \qquad (1.1)$$

Where R and R' are organic groups.

A single electron reduction of NO gives the nitroxide ion NO^-. Studies have shown that there is yet no known biological role for the nitroxide ion in the body. However, it is used in reactions that seem to be biologically significant, for example in altering thiols and also binding to iron in haemoglobin. NO very rapidly reacts with natural compounds which make detecting it in aqueous biological media very difficult. For example, our immune system produces both NO and superoxide (O_2^-). These two molecules react together to give peroxynitrites (equation 1.2) which are toxic and can lead to cell death and this is how NO kills bacteria. Other examples include NO binding to metal centres in complexes etc (i.e. the iron in the sodium nitroprusside complex $Na_2[Fe(CN)_5NO]$ which is useful in the treatment of cardiovascular dysfunction[121]). As mentioned previously, it can form nitrosothiols from thiols and these can be used as a storage facility for NO in the body. They may also be used in drugs specifically for the production of NO in the body for patients whose own natural production is low[122-124]. However, research for this is still in the preliminary stages.

$$NO + O_2^- \rightarrow O{=}N{-}O{-}O^- \qquad (1.2)$$

The natural production of NO in mammals involves the conversion of L-arginine to L-citrulline using enzymes known as Nitric Oxide Synthase (NOS).

1.2.4 NO in the body and NOS

Enzymes are responsible for nearly all chemical reactions occurring in living things. They are used to increase the rate of reaction to a significant level, however in general they only ever catalyse one reaction and their substrate selectivity is very high. As stated above the family of enzymes responsible for the natural production of NO in the body are the NOSs. The production of NO requires two substrates. The nitrogen providing substrate is L-arginine (a natural amino acid) and the oxygen donating substrate is oxygen gas. An overview of the reaction is shown in figure 1.12. A more detailed mechanism will be illustrated later in this chapter. There are three main family members of NOS, which are eNOS, iNOS and nNOS: again more detail of each synthase will be given later. It is noticeable though that the enzymes are self sufficient as they do not need any other enzymes to be able to produce NO.

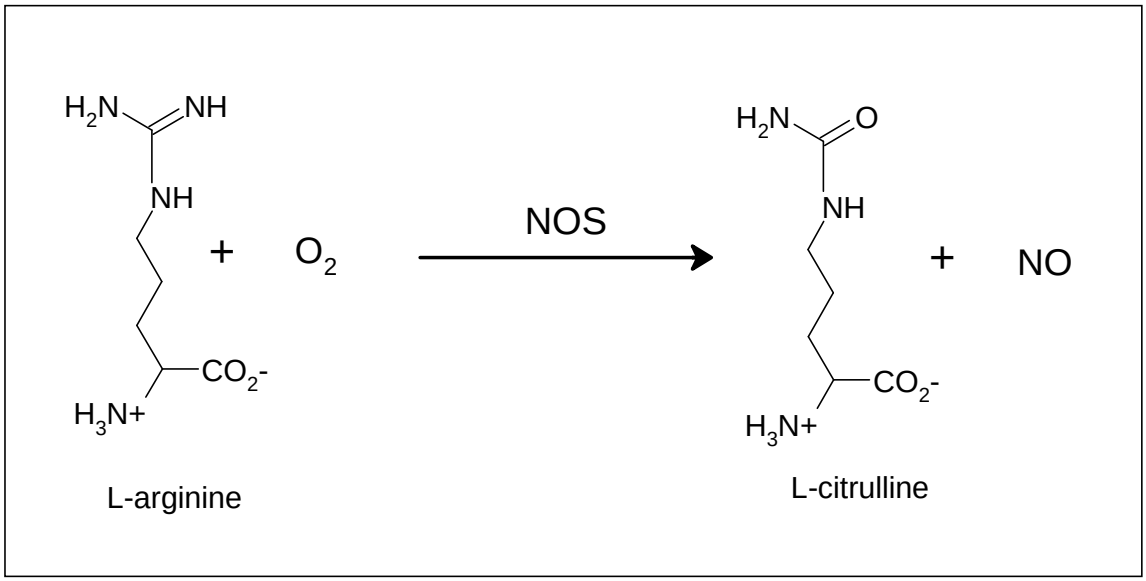

Figure 1.12 An overview of the production of NO from arginine and oxygen

The conversion of L-arginine to L-citrulline is a complex one and requires the use of several cofactors, Nicotinamide Adenine Dinucleotide Phosphate (NADPH), Flavin Mononucleotide (FMN), Flavin Adenine Dinucleotide (FAD) and tetrahydrobiopterin (BH_4). An understanding of the structure of NOS is required before a more detailed look at the mechanism of the conversion is undertaken. The NOS enzyme is split into two domains. The oxygenase domain contains the cofactors BH_4 and an iron protoporphyrin IX (PPIX, haem) and receives the electrons to permit the change of arginine and oxygen into citrulline and NO. The reductase domain contains the other cofactors FMN and FAD. Once electrons have been donated from the transformation of NADPH into $NADP^+$ and H^+, they then are passed on to the haem cofactor in the oxygenase domain. The domains are linked via a sequence involving Calmodulin (Ca^{2+}), which allows the transport of electrons between them and also FAD and FMN without which it would be impossible to produce NO in the body[125]. The NOS structure has been compared to a baseball catcher's glove[126] with the iron haem component being the part where your palm sits. The hydrophobic regions are folded which creates a tunnel through which the BH_4 can access and bind to the haem part of the oxygenase domain.

Following discussion of the structure of NOS, it is easier to describe the mechanism in which NO is produced from L-arginine. When required, NO is produced in the following way. NADPH found in the reductase domain of NOS is oxidised to form $NADP^+$ and H^+. This means that there are two free electrons which react with the flavins (FMN and FAD). The responsibility of these flavins is to separate the two electrons for transfer to the oxygenase domain at the appropriate time. This is where

the Calmodulin (CaM) is used to improve the flow of these electrons. As there is a flow of electrons from one NOS monomer in one domain to another NOS monomer in the other domain there is a requirement for dimerization of the enzyme to ensure full NOS activity[127]. One of these free electrons then reacts with the iron haem centre, which causes a valence charge on the iron cation. Following this, molecular oxygen reacts with the ferrous haem centre. Another electron then attacks, and the combination of these two attacks leaves a very reactive species which then itself attacks the L-arginine. This produces hydroxyarginine and a molecule of water leaving the iron centre ferric again and thus completing the first of two monooxygenations[128] required to produce NO. For the second monooxygenation, another electron attacks the ferric centre and molecular oxygen to form a tetrahedral intermediate which is unstable and quickly collapses to form the L-citrulline and produces NO and water. BH_4 is required for this second step in order to maintain the dimer structure. A more detailed mechanism is shown in figure 1.13.

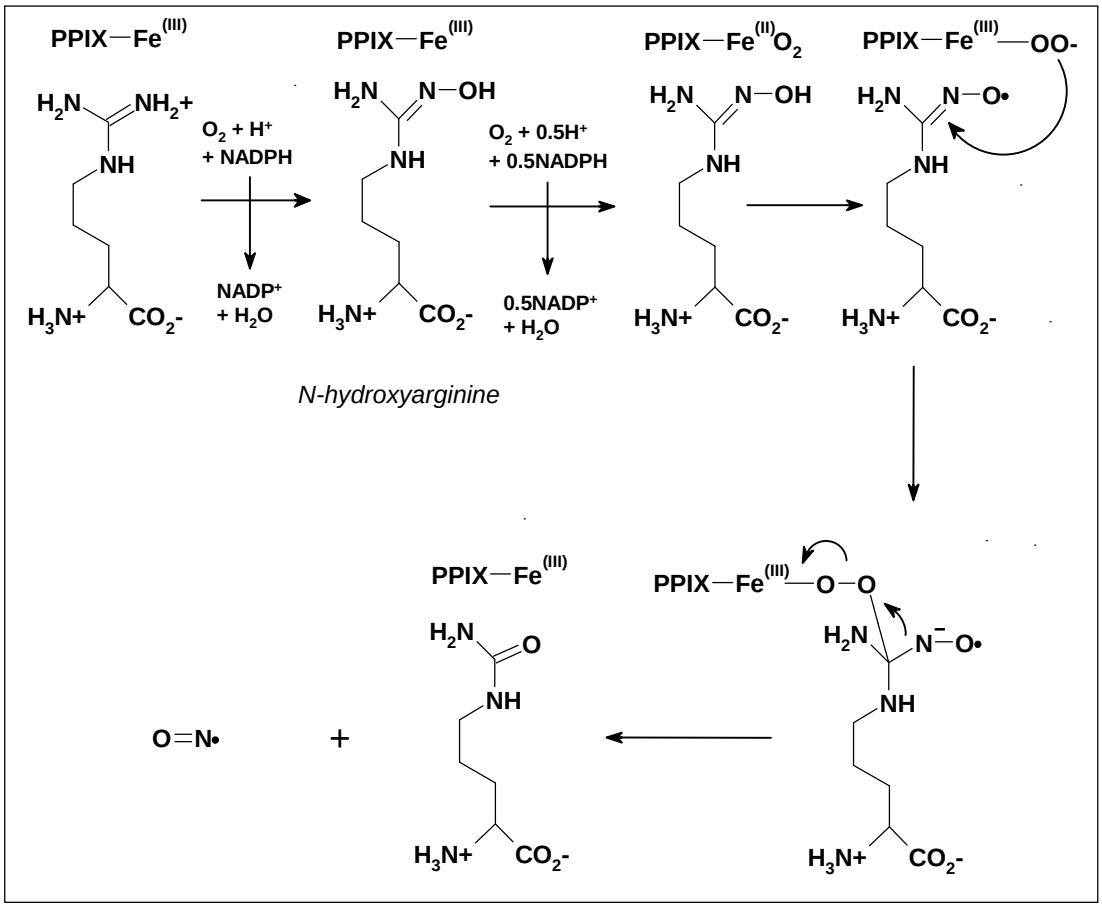

Figure 1.13 A more detailed look at the mechanism for the conversion of L-arginine into L-citrulline and NO[9].

1.2.5 Different types of NOS

As mentioned previously, there are three different types of NOS. These are detailed below, the name refers to where they are most commonly found in the body.

- eNOS (endothelial NOS) is responsible for generating NO in the endothelium. The endothelium is the layer of cells which line the walls of blood vessels. eNOS can however also be found in the kidneys, heart and brain. It is the principle NOS used for regulating the vascular function.
- iNOS (inducible NOS) is part of macrophage cells (scavenger cells that make up part of the immune system, and guard against unfriendly microbes). It is also found in the cardiovascular system.
- nNOS (neural NOS) is found in brain cell responsible for cell communication and has a role in forming memory and learning. There is also an nNOS variant called mitochondrial NOS (mtNOS) which is calcium dependent and has been identified to play an important role in respiration function.

As mentioned before, the structures of all three synthases are very similar. The main differences are in their responses to the concentration of calcium ions (Ca^{2+}) within the cell. eNOS and nNOS differ from iNOS in that when calcium ion levels rise nNOS and eNOS are activated. iNOS appears to be insensitive to calcium levels. Calmodulin is associated with all three forms of NOS and is a calcium binding protein, linking both domains in the NOS and allowing the flow of electrons between the two. A calcium ion rise allows the Ca^{2+}/calmodulin complex to bind strongly to eNOS and nNOS, activates the enzyme and so NO is produced. However, in iNOS,

the calmodulin complex is already strongly bound and therefore does not depend on the calcium ion levels for activation. The activation for iNOS occurs when an unfriendly agent invades the body and NO is required to eliminate any threat. The gene for the production of iNOS is activated and once the agents are destroyed the iNOS disappears. This is different to eNOS and nNOS again, as at any point in time there is a large quantity of each lying dormant in the endothelial and neuronal tissue respectively, whereas there is very little iNOS until it is required.

1.2.6 An overview of the biological roles of NO in the body

As NO is a very small highly reactive species, it can diffuse very easily in the body. Its impact on the body is therefore dependent upon the concentration of NO produced and where its production occurs. It is also true to say that the NO requirement is a delicate balance as too little or too much can lead to life threatening diseases and can even be fatal. A table illustrating some of these diseases relative to the NO concentration can be seen in figure 1.14.

NO Concentration	
Too Low	**Too High**
Hypertension	Septic Shock
Atheriosclerosis	Hypotension
Parkinsons disease	Excessive bleeding
Fibrosis	Meningitis
Sexual Impotence	Rheumatoid Arthritis
	Ischemia
	Cancer
	Diabetes
	Asthma

Figure 1.14 Diseases related to insufficient or excess NO in the body.

NO is very useful in the brain as it helps in memory function[129], however too much is very dangerous. A stroke occurs when there is a restriction in blood flow to the brain, possibly due to a blood clot or atherosclerosis (when arteries fur up). Initial damage to the brain is caused by the release of excessive amounts of glutamate (a neurotransmitter) and not by oxygen starvation. This excess results in over stimulation of NDMA and produces a large flow of calcium ions into the postsynaptic neurone, and as already stated, calcium ions stimulate the arginine conversion into citrulline producing NO. Oxygen will finally arrive again in the brain once the blockage has been removed, however this leads to the production of radicals such as superoxide which is readily oxidised to destructive peroxynitrite. This means neural damage can result from both a stroke and reoxygeneration.

1.2.7 The role of NO in the cardiovascular system.

Before discussing the skin and NO it is necessary to give an overview of blood vessels. The vessels that carry blood around the body have the ability to enlarge or contract, depending on how much blood is required for different tissues or organs. Blood vessels have three main parts. (figure 1.15). The lumen is where the blood flows, on the inside of the lumen is a layer of cells known as the endothelium and finally the wall of the vessel consists mainly of smooth muscle. When the smooth muscle relaxes the lumen enlarges and allows more blood to flow and vice versa.

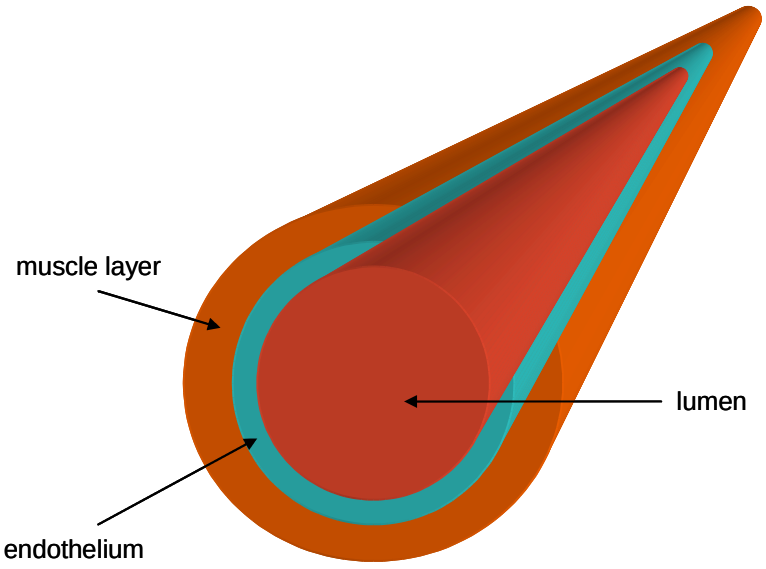

Figure 1.15 Diagram illustrating the main components of a human blood vessel.

When a blood vessel is damaged there is an extremely efficient repair mechanism in place to help and if it were not for this a person would simply bleed to death. The mechanism employed depends on the size of the vessel that is affected. A very small arterial wound is readily dealt with using a sheath of smooth muscle to close the lumen and restrict blood flow to the affected area. This results in opposing

endothelial surfaces being pressed together and sticking to each other sealing off the vessel permanently. Obviously with larger vessels permanent closure is not viable and loss of blood is stopped with a mechanism involving platelets. Platelets are fragments of cells that circulate around in blood, they are 2 μm in diameter and in healthy blood there are ≈250 million platelets in each millilitre. When the endothelium is damaged these blood platelets adhere to the exposed surface and facilitate the production of more platelets and this process (termed platelet aggregation) continues until a platelet plug is formed. This obviously prevents bleeding, however if platelet aggregation were to continue then a clot or thrombus would form. This can be dangerous and sometimes fatal and so there is a chemical agent called prostaglandin I_2 (PGI_2) responsible for removing the plug. The first part of the NO story was its discovery as the EDRF (endothelium-derived relaxing factor)[130] which allows the vascular muscle to relax permitting arterial dilation and preventing platelet aggregation. NO prevents platelet aggregation in a similar way to smooth muscle relaxation as platelets contain guanylate cyclase and NO activates this enzyme to form cGMP from GTP which inhibits platelet aggregation. Therefore if a clot or thrombus occurs when it is not required, new drugs containing NO may be administered. When the endothelium is damaged macrophages also move to the affected site and die after ingesting the oxidised lipids available. A lipid core is then left on the inside of the lumen. This is one step in the complex process called stenosis which, if it continues, can cause a severe narrowing of the artery. NO also prevents stenosis by removing oxygen based radicals, forming nitrates instead, and also prevents macrophages adhering to the affected site. Nonetheless, stenosis does occur mostly in the arteries close to the heart and one treatment is the use of a stent which

enlarges the artery, but can sometimes damage the endothelium resulting in thrombus formation. There is currently research into coating stents and other medical devices with NO releasing materials to prevent thrombus formation. More will be discussed about this below.

1.2.8 NO in the skin

The skin is the largest organ in the human body. It gives protection from extremes of temperature along with UV radiation from the sun and is the first defence against germs. It consists of two layers; the outer dermis and the inner dermis (figure 1.16). Keratinocytes form at the base of the epidermis and gradually make their way to the surface over two weeks before becoming dehydrated and flattened, and eventually shed altogether. Also located at the base of the epidermis are the melanocytes which produce the pigment melanin which protects the keratinocytes. Also, part of the dermis, although not shown in figure 1.16, are fibroblasts, structural protein (collagen), blood vessels, nerves, sweat glands, hair roots and muscles. When stimulated, keratinocytes produce NO and hydrogen peroxide. Both are useful in limiting the numbers of bacteria present on the skin's surface and trying to enter the body via a cut or abrasion. It should come as no surprise that the skin protects as it contains sources of NO. The skin could really be considered part of the immune system and therefore when attacked it is iNOS that produces the required NO.

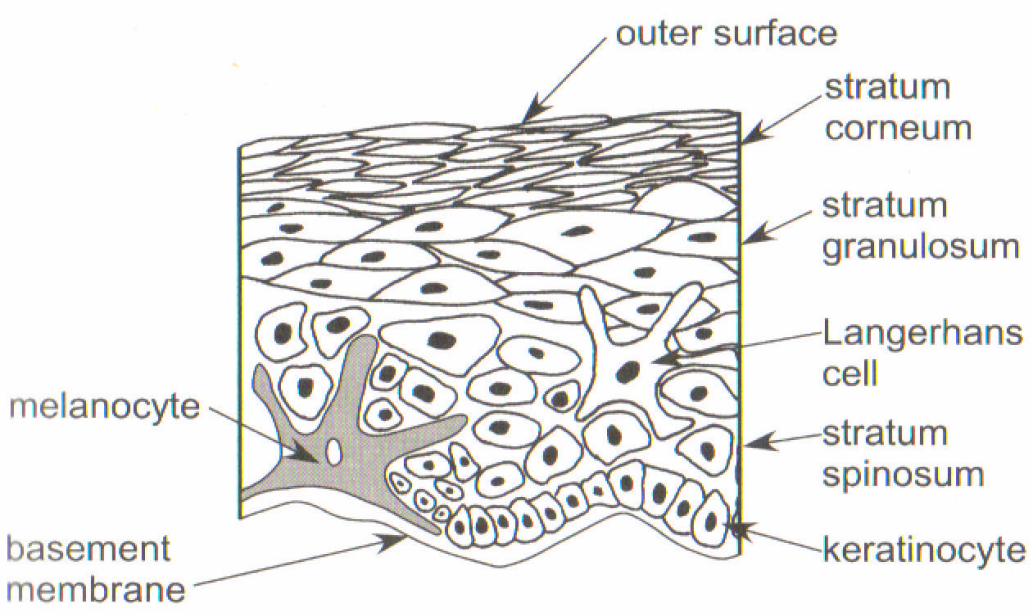

Figure 1.16 A section of the epidermis in human skin[3].

1.2.9 Drugs and therapies that utilise NO

Doctors have been prescribing drugs that utilise nitric oxide for years, although it was not until 1987 when NO's full biological significance was discovered. The best example still remains glyceryl trinitrate (GTN, figure 1.17). The use of GTN as a treatment for the symptoms of angina pectoris was finally confirmed by William Murrell in 1879[131], however people had already experienced the effects of GTN before this. Indeed GTN is still to this day the most effective treatment of angina. The mechanism for the production of NO from GTN is still unclear but it involves an enzyme metabolism. GTN also has uses in treating thrombosis. This class of organic-nitrates do however have their drawbacks and side-effects reported include headaches and dizziness[132].

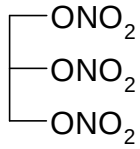

Figure 1.17 Glyceryl trinitrate.

There are also therapies available that spontaneously produce NO in the body. The use of NO gas is still used only rarely because of the obvious danger of its toxicity. It does however have use in the treatment of infants with respiratory failure, though with mixed and contradictory results[133-135]. A family of compounds known as diazeniumdiolates also produce NO spontaneously[97,136-138]. Also called NONOates because of their structure ($R^1R^2NN(O)=NOR^3$), they are produced using secondary amines. There are a number of ways in which diazeniumdiolates can be used to release NO. All of which involve the use of polymers to encase the diazeniumdiolate and allow them to release NO without also releasing dangerous precursors that can lead to carcinogens being formed in the body. NONOates can be used as vascular grafts, clinical sensors or even have use in the procedure known as Extracorpeal membrane oxygenation circuits (ECMO). This is where the patient's lungs are not functioning properly and their blood has to be pumped through an oxygenation chamber.

S-nitrosothiols when used as NO donor drugs break down to form NO and, depending on the nature of the S-nitrosothiol, a disulphide may also result (see equation 1.3)[138]. Some nitrosothiols occur naturally in the body while others have been made in the laboratory. It is believed that S-nitrosothiols in the body act as a

storage facility for NO and allow it to be released when necessary. However, it is still not known how S-nitrosothiols are formed *in vivo* (as the reaction of NO with a thiol doesn't produce a S-nitrosothiol) or how NO is released when necessary.

$$2RSNO \rightarrow RSSR + 2NO \qquad (1.3)$$

It is the presence of copper that decomposes S-nitrosothiols, especially the use of Cu^{+} ions which are formed by the reduction of Cu^{2+} ions by thiols. There are two other methods used to release NO from S-nitrosothiols, firstly using an ascorbate with the nitrosothiol to release NO. The other method involves the use of light in a homolytic reaction to remove NO. S-nitrosothiols are potentially useful as medical coatings to aid in the prevention of restenosis and angioplasty along with the inhibition of platelet aggregation. Research into the use of medical coatings involved the use of both diazemiumdiolates and nitrosothiols being inserted into polymers[139-143].

1.2.10 Wound healing and current research involving NO

After an injury wound healing is required to keep the integrity of the body intact. It is a complicated process involving a sequential number of events. Figure 1.18 shows the concentration of NO in the area affected by the injury over time[144]. In the early part of wound healing iNOS is synthesised by inflammatory cells (macrophages). NO (released through iNOS) regulates the formation of collagen and wound contraction and therefore is essential in wound repair.

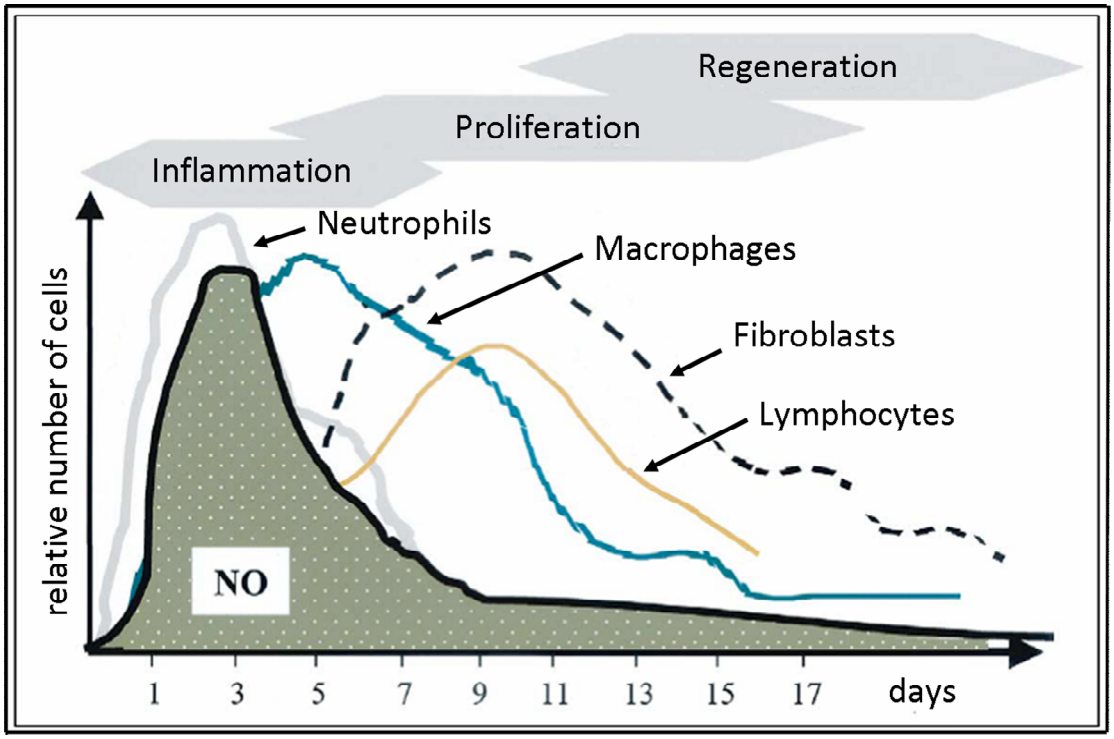

Figure 1.18 Concentration of NO in affected area over time, showing the huge increase in NO after initial clotting to ensure no infection occurs. Image adapted from reference 141.

It has also been shown that NO has a functional role in wound healing. For example, feeding humans on an arginine (the precursor to NO) enriched diet improves wound healing (measured by collagen deposition) and when rats are fed an arginine free diet

their wound repair is impaired[145-147]. Therefore, there is current research into utilising NO releasing materials to aid in wound healing. This takes a several forms and one idea is using NO gas topically applied to the skin. Another is to use NO releasing creams on the skin, and the final idea is to use dressings or plasters that will release NO in a controlled manner. Before discussing new NO releasing materials, mention must be made of other current wound healing promoters. The best example is the recent use of silver compounds in dressing which have improved wound repair times. Wright, Lam and Burrel[148] have reported the use of silver in a variety of delivery methods and found that the use of silver in dressings reduces the number of wound impairing bacteria on the skin during wound repair. However, the effects of silver on wounds are disputed and have been shown to cause delayed wound healing and even harm by Burd *et al*[149].

Using NO gas topically applied to the body is an idea used by Miller *et al*[150] in treating non-healing leg ulcers with success in their case study, though they admit more research is required. Also the use of gaseous NO has been applied to wounds on rats by Shekter *et al*[96]. Indeed "Plason" gas has been used to good effect in the treatment of many different types of wounds[96,151]. However, as with gaseous NO in the treatment of infants care must be taken to ensure the gas is extremely pure otherwise NO_2 could be administered instead. Another drawback is the difficulty in handling gaseous NO.

The second method of NO delivery to wounds is by using a cream. Weller *et al*[152] have demonstrated the use of an acidified nitrate cream in the treatment of tinea

pedis with success and again Weller and Finnen have demonstrated that an acidified nitrate cream improves wound healing time in normal and diabetic mice[153]. However, there is also evidence available which shows that using acified nitrate creams produces inflammation and scarring. Omerod *et al*[99] have shown that the use of such creams increases cytotoxic effects along with producing inflammation of the skin.

The final method of delivery of NO to an exposed wound is by using dressings or plasters within which a framework containing NO is present. There are many such frameworks that are currently being investigated. As mentioned previously, Wheatley *et al*[100] have successfully synthesised zeolite-A and investigated its NO storage capacity and its release. MOFs have already been found to give pores large enough to accommodate NO. Xiao *et al*[72] have investigated both the NO and hydrogen storage and releaseability of HKUST-1, a copper benzene tricarboxylate MOF. The area of storage and release of NO from MOFs is of significant interest for a number of possible applications.

1.3 References

(1) Eddaoudi, M.; Moler, D. B.; Li, H.; Chen, B.; Reineke, T. M.; O'Keeffe, M.; Yaghi, O. M. *Acc. Chem. Res.* **2001**, *34*, 319.

(2) Kitagawa, S.; Kitaura, R.; Noro, S.-i. *Angew. Chem., Int. Ed.* **2004**, *43*, 2334.

(3) Férey, G. *Chem. Soc. Rev.* **2008**, *37*, 191.

(4) Lee, J.; Kim, J.; Hyeon, T. *Adv Mater* **2006**, *18*, 2073.

(5) Li, H.; Eddaoudi, M.; O'Keeffe, M.; Yaghi, O. M. *Nature* **1999**, *402*, 276.

(6) Chui, S. S.-Y.; Lo, S. M.-F.; Charmant, J. P.; H.; Orpen, A. G.; Williams, I. D. *Science* **1999**, *283*, 1148.

(7) Férey, G.; Mellot-Draznieks, C.; Serre, C.; Millange, F.; Dutour, J.; Surble, S.; Margiolaki, I. *Science* **2005**, *309*, 2040.

(8) Wong-Foy, A. G.; Matzger, A. J.; Yaghi, O. M. *J. Am. Chem. Soc.* **2006**, *128*, 3494.

(9) Ben, T.; Ren, H.; Ma, S.; Cao, D.; Lan, J.; Jing, X.; Wang, W.; Xu, J.; Deng, F.; Simmons, J. M.; Qiu, S.; Zhu, G. *Angew. Chem., Int. Ed.* **2009**, NA.

(10) Shimizu, G. K. H.; Vaidhyanathan, R.; Taylor, J. M. *Chem. Soc. Rev.* **2009**, *38*, 1430.

(11) Wang, Z.; Cohen, S. M. *Chem. Soc. Rev.* **2009**, *38*, 1315.

(12) Tranchemontagne, D. J.; Mendoza-Cortes, J. L.; O'Keeffe, M.; Yaghi, O. M. *Chem. Soc. Rev.* **2009**, *38*, 1257.

(13) Eddaoudi, M.; Kim, J.; Rosi, N.; Vodak, D.; Wachter, J.; O'Keeffe, M.; Yaghi, O. M. *Science* **2002**, *295*, 469.

(14) Rowsell, J. L. C.; Yaghi, O. M. *Micropor. Mesopor. Mater.* **2004**, *73*, 3.

(15) http://www.parrinst.com/doc_library/members/4700-Sample_Prep_Bulletin.pdf.

(16) Cooper, E. R.; Andrews, C. D.; Wheatley, P. S.; Webb, P. B.; Wormald, P.; Morris, R. E. *Nature* **2004**, *430*, 1012.

(17) Parnham, E. R.; Morris, R. E. *Acc. Chem. Res.* **2007**, *40*, 1005.

(18) Parnham, E. R.; Morris, R. E. *J. Am. Chem. Soc.* **2006**, *128*, 2204.

(19) Jhung, S. H.; Lee, J. H.; Chang, J. S. *Bull. Korean Chem. Soc.* **2005**, *26*, 880.

(20) Choi, J. Y.; Kim, J.; Jhung, S. H.; Kim, H. K.; Chang, J. S.; Chae, H. K. *Bull. Korean Chem. Soc.* **2006**, *27*, 1523.

(21) Choi, J.-S.; Son, W.-J.; Kim, J.; Ahn, W.-S. *Micropor. Mesopor. Mater.* **2008**, *116*, 727.

(22) Jhung, S. H.; Lee, J.-H.; Forster, P. M.; Férey, G.; Cheetham, A. K.; Chang, J.-S. *Chem. -Eur. J.* **2006**, *12*, 7899.

(23) Lin, Z.; Wragg, D. S.; Morris, R. E. *Chem. Commun.* **2006**, 2021.

(24) Mueller, U.; Schubert, M.; Teich, F.; Puetter, H.; Schierle-Arndt, K.; Pastre, J. *J. Mater. Chem.* **2006**, *16*, 626.

(25) Stock, N.; Bein, T. *Solid State Sci.* **2003**, *5*, 1207.

(26) Stock, N.; Bein, T. *Angew. Chem., Int. Ed.* **2004**, *43*, 749.

(27) Bauer, S.; Bein, T.; Stock, N. *Inorg. Chem.* **2005**, *44*, 5882.

(28) Forster, P. M.; Burbank, A. R.; O'Sullivan, M. C.; Guillou, N.; Livage, C.; Férey, G.; Stock, N.; Cheetham, A. K. *Solid State Sci.* **2005**, *7*, 1549.

(29) Serre, C.; Groves, J. A.; Lightfoot, P.; Slawin, A. M. Z.; Wright, P. A.; Stock, N.; Bein, T.; Haouas, M.; Taulelle, F.; Férey, G. *Chem. Mater.* **2006**, *18*, 1451.

(30) Bauer, S.; Serre, C.; Devic, T.; Horcajada, P.; Marrot, J. R. M.; Férey, G.; Stock, N. *Inorg. Chem.* **2008**, *47*, 7568.

(31) Biemmi, E.; Christian, S.; Stock, N.; Bein, T. *Micropor. Mesopor. Mater.* **2009**, *117*, 111.

(32) Czaja, A. U.; Trukhan, N.; Mueller, U. *Chem. Soc. Rev.* **2009**, *38*, 1284.

(33) Lee, J.; Farha, O. K.; Roberts, J.; Scheidt, K. A.; Nguyen, S. T.; Hupp, J. T. *Chem. Soc. Rev.* **2009**, *38*, 1450.

(34) Ma, L.; Abney, C.; Lin, W. *Chem. Soc. Rev.* **2009**, *38*, 1248.

(35) U. Mueller, O. M., H. Junicke, T. Butz and O. M. Yaghi *Patent* **2004**, *US 2004/081611*.

(36) U. Mueller, L. L., M. Hesse, O. M. Yaghi and M. Eddaoudi *Patent* **2003**, *WO 03/101975*.

(37) Hermes, S.; Schröter, M.-K.; Schmid, R.; Khodeir, L.; Muhler, M.; Tissler, A.; Fischer, R. W.; Fischer, R. A. *Angew. Chem., Int. Ed.* **2005**, *44*, 6237.

(38) Cho, S.-H.; Ma, B.; Nguyen, S. T.; Hupp, J. T.; Albrecht-Schmitt, T. E. *Chem. Commun.* **2006**, 2563.

(39) Ingleson, M. J.; Barrio, J. P.; Bacsa, J.; Dickinson, C.; Park, H.; Rosseinsky, M. J. *Chem. Commun.* **2008**, 1287.

(40) Wu, C.-D.; Hu, A.; Zhang, L.; Lin, W. *J. Am. Chem. Soc.* **2005**, *127*, 8940.

(41) Hwang, Young K.; Hong, D.-Y.; Chang, J.-S.; Jhung, Sung H.; Seo, Y.-K.; Kim, J.; Vimont, A.; Daturi, M.; Serre, C.; Férey, G. *Angew. Chem, Int. Ed.* **2008**, *120*, 4212.

(42) Maspoch, D.; Ruiz-Molina, D.; Veciana, J. *Chem. Soc. Rev.* **2007**, *36*, 770.

(43) Suh, M. P.; Cheon, Y. E.; Lee, E. Y. *Coord. Chem. Rev.* **2008**, *252*, 1007.

(44) Cahill, C. L.; Lill, D. T. D.; Frisch, M. *CrystEngComm* **2007**, *9*, 15.

(45) Janiak, C. *Dalton Trans.* **2003**, 2781.

(46) Allendorf, M. D.; Bauer, C. A.; Bhakta, R. K.; Houk, R. J. T. *Chem. Soc. Rev.* **2009**, *38*, 1330.

(47) Zou, R.-Q.; Yamada, Y.; Xu, Q. *Micropor. Mesopor. Mater.* **2006**, *91*, 233.

(48) Fun, H. K.; Raj, S. S. S.; Xiong, R. G.; Zuo, J. L.; Yu, Z.; You, X. Z. *J. Chem. Soc.-Dalton Trans.* **1999**, 1915.

(49) Song, J.-L.; Mao, J.-G. *Chem. -Eur. J.* **2005**, *11*, 1417.

(50) Serre, C.; Millange, F.; Thouvenot, C.; Gardant, N.; Pelle, F.; Férey, G. *J. Mater. Chem.* **2004**, *14*, 1540.

(51) Kurmoo, M. *Chem. Soc. Rev.* **2009**, *38*, 1353.

(52) Rao, C. N. R.; Cheetham, A. K.; Thirumurugan, A. *J. Phys.-Condes. Matter* **2008**, *20*.

(53) Underhill, A. E., Day, P. *Spec. Pub - Royal. Soc. Chem.* **2000**, *252*.

(54) Sato, Y.; Ohkoshi, S.-i.; Arai, K.-i.; Tozawa, M.; Hashimoto, K. *J. Am. Chem. Soc.* **2003**, *125*, 14590.

(55) Maspoch, D.; Ruiz-Molina, D.; Wurst, K.; Domingo, N.; Cavallini, M.; Biscarini, F.; Tejada, J.; Rovira, C.; Veciana, J. *Nat. Mater.* **2003**, *2*, 190.

(56) Morris, R. E.; Wheatley, P. S. *Angew. Chem., Int. Ed.* **2008**, *47*, 4966.

(57) DoE Office of Energy Efficiency and Renewable Energy Hydrogen, Fuel Cells & Infrastructure Technologies Program, Grand Challenge for Basic and Applied Research in Hydrogen Storage Solicitation, available at: http://www.eere.energy.gov/hydrogenandfuelcells/2003_storage_solicitation.html.

(58) DoE Office of Energy Efficiency and Renewable Energy Hydrogen, Fuel Cells & Infrastructure Technologies Program Multi-Year Research, Development and Demonstration Plan, available at: http://www.eere.energy.gov/hydrogenandfuelcells/mypp.

(59) Kaye, S. S.; Dailly, A.; Yaghi, O. M.; Long, J. R. *J. Am. Chem. Soc.* **2007**, *129*, 14176.

(60) Murray, L. J.; Dinca, M.; Long, J. R. *Chem. Soc. Rev.* **2009**, *38*, 1294.

(61) Zhao, D.; Yuan, D.; Zhou, H.-C. *Energy Environ. Sci.* **2008**, *1*, 222.

(62) Collins, D. J.; Zhou, H.-C. *J. Mater. Chem.* **2007**, *17*, 3154.

(63) Rowsell, J. L. C.; Millward, A. R.; Park, K. S.; Yaghi, O. M. *J. Am. Chem. Soc.* **2004**, *126*, 5666.

(64) Furukawa, H.; Miller, M. A.; Yaghi, O. M. *J. Mater. Chem.* **2007**, *17*, 3197.

(65) Dietzel, P. D. C.; Morita, Y.; Blom, R.; Fjellvag, H. *Angew. Chem., Int. Ed.* **2005**, *44*, 6354.

(66) Dietzel, P. D. C.; Panella, B.; Hirscher, M.; Blom, R.; Fjellvag, H. *Chem. Commun.* **2006**, 959.

(67) Rowsell, J. L. C.; Yaghi, O. M. *J. Am. Chem. Soc.* **2006**, *128*, 1304.

(68) Chui, S. S.-Y.; Lo, S. M.-F.; Charmant, J. P. H.; Orpen, A. G.; Williams, I. D. *Science* **1999**, *283*, 1148.

(69) Prestipino, C.; Regli, L.; Vitillo, J. G.; Bonino, F.; Damin, A.; Lamberti, C.; Zecchina, A.; Solari, P. L.; Kongshaug, K. O.; Bordiga, S. *Chem. Mater.* **2006**, *18*, 1337.

(70) Bordiga, S.; Regli, L.; Bonino, F.; Groppo, E.; Lamberti, C.; Xiao, B.; Wheatley, P. S.; Morris, R. E.; Zecchina, A. *Phys. Chem. Chem. Phys.* **2007**, *9*, 2676.

(71) Peterson, V. K.; Liu, Y.; Brown, C. M.; Kepert, C. J. *J. Am. Chem. Soc.* **2006**, *128*, 15578.

(72) Xiao, B.; Wheatley, P. S.; Zhao, X. B.; Fletcher, A. J.; Fox, S.; Rossi, A. G.; Megson, I. L.; Bordiga, S.; Regli, L.; Thomas, K. M.; Morris, R. E. *J. Am. Chem. Soc.* **2007**, *129*, 1203.

(73) Wang, X.-S.; Ma, S.; Rauch, K.; Simmons, J. M.; Yuan, D.; Wang, X.; Yildirim, T.; Cole, W. C.; López, J. J.; Meijere, A. d.; Zhou, H.-C. *Chem. Mater.* **2008**, *20*, 3145.

(74) Dinca, M.; Dailly, A.; Liu, Y.; Brown, C. M.; Neumann, D. A.; Long, J. R. *J. Am. Chem. Soc.* **2006**, *128*, 16876.

(75) Dinca, M.; Han, Won S.; Liu, Y.; Dailly, A.; Brown, C. M.; Long, J. R. *Angew. Chem., Int. Ed.* **2007**, *46*, 1419.

(76) Zhou, W.; Wu, H.; Yildirim, T. *J. Am. Chem. Soc.* **2008**, *130*, 15268.

(77) Burchell, T. *SAE Tech. Pap. Ser* **2000**, 2001.

(78) Kondo, M.; Yoshitomi, T.; Matsuzaka, H.; Kitagawa, S.; Seki, K. *Angew. Chem., Int. Ed.* **1997**, *36*, 1725.

(79) Ma, S.; Sun, D.; Simmons, J. M.; Collier, C. D.; Yuan, D.; Zhou, H.-C. *J. Am. Chem. Soc.* **2007**, *130*, 1012.

(80) Wu, H.; Zhou, W.; Yildirim, T. *J. Am. Chem. Soc.* **2009**, *131*, 4995.

(81) Li, H.; Eddaoudi, M.; Groy, T. L.; Yaghi, O. M. *J. Am. Chem. Soc.* **1998**, *120*, 8571.

(82) Millward, A. R.; Yaghi, O. M. *J. Am. Chem. Soc.* **2005**, *127*, 17998.

(83) Caskey, S. R.; Wong-Foy, A. G.; Matzger, A. J. *J. Am. Chem. Soc.* **2008**, *130*, 10870.

(84) Férey, G.; Serre, C. *Chem. Soc. Rev.* **2009**, *38*, 1380.

(85) Serre, C.; Millange, F.; Thouvenot, C.; Nogues, M.; Marsolier, G.; Louer, D.; Férey, G. *J. Am. Chem. Soc.* **2002**, *124*, 13519.

(86) Loiseau, T.; Serre, C.; Huguenard, C.; Fink, G.; Taulelle, F.; Henry, M.; Bataille, T.; Férey, G. *Chem.-Eur. J.* **2004**, *10*, 1373.

(87) Serre, C.; Mellot-Draznieks, C.; Surble, S.; Audebrand, N.; Filinchuk, Y.; Férey, G. *Science* **2007**, *315*, 1828.

(88) Serre, C.; Millange, F.; Surblé, S.; Férey, G. *Angew. Chem., Int. Ed.* **2004**, *43*, 6285.

(89) Bourrelly, S.; Llewellyn, P. L.; Serre, C.; Millange, F.; Loiseau, T.; Férey, G. *J. Am. Chem. Soc.* **2005**, *127*, 13519.

(90) Britt, D.; Tranchemontagne, D.; Yaghi, O. M. *Proc. Natl. Acad. Sci. U. S. A.* **2008**, *105*, 11623.

(91) Rieter, W. J.; Taylor, K. M. L.; An, H.; Lin, W.; Lin, W. *J. Am. Chem. Soc.* **2006**, *128*, 9024.

(92) Taylor, K. M. L.; Jin, A.; Lin, W. *Angew. Chem., Int. Ed.* **2008**, *47*, 7722.

(93) Taylor, K. M. L.; Rieter, W. J.; Lin, W. *J. Am. Chem. Soc.* **2008**, *130*, 14358.

(94) Rieter, W. J.; Pott, K. M.; Taylor, K. M. L.; Lin, W. *J. Am. Chem. Soc.* **2008**, *130*, 11584.

(95) Taylor-Pashow, K. M. L.; Rocca, J. D.; Xie, Z.; Tran, S.; Lin, W. *J. Am. Chem. Soc.* **2009**, *131*, 14261.

(96) Shekhter, A. B.; Serezhenkov, V. A.; Rudenko, T. G.; Pekshev, A. V.; Vanin, A. F. *Nitric Oxide* **2005**, *12*, 210.

(97) Keefer, L. K. *Nat. Mater.* **2003**, *2*, 357.

(98) Mowbray, M.; Tan, X.; Wheatley, P. S.; Morris, R. E.; Weller, R. B. *J. Invest. Dermatol.* **2007**, *128*, 352.

(99) Ormerod, A. D.; Copeland, P.; Hay, I.; Husain, A.; Ewen, S. W. B. *J. Invest. Dermatol.* **1999**, *113*, 392.

(100) Wheatley, P. S.; Butler, A. R.; Crane, M. S.; Fox, S.; Xiao, B.; Rossi, A. G.; Megson, I. L.; Morris, R. E. *J. Am. Chem. Soc.* **2006**, *128*, 502.

(101) Wheatley, P. S.; Butler, A. R.; Crane, M. S.; Rossi, A. G.; Megson, I. L.; Morris, R. E. *Molecular Sieves: From Basic Research to Industrial Applications, Pts a and B* **2005**, *158*, 2033.

(102) Xiao, B.; Wheatley, P. S.; Morris, R. E. In *Stud. Surf. Sci. Catal.*; Elsevier: 2007; Vol. Volume 170, Part 1, p 902.

(103) Wheatley, P. S.; McKinlay, A. C.; Morris, R. E.; Antoine Gédéon, P. M.; Florence, B. In *Stud. Surf. Sci. Catal.*; Elsevier: 2008; Vol. Volume 174, Part 1, p 441.

(104) Mowbray, M.; Tan, X.; Wheatley, P. S.; Morris, R. E.; Weller, R. B. *J. Invest. Dermatol.* **2007**, *128*, 352.

(105) McKinlay, A. C.; Xiao, B.; Wragg, D. S.; Wheatley, P. S.; Megson, I. L.; Morris, R. E. *J. Am. Chem. Soc.* **2008**, *130*, 10440.

(106) Hinks, N. J.; McKinlay, A. C.; Xiao, B.; Wheatley, P. S.; Morris, R. E. *Micropor. Mesopor. Mater.* **2010**, *doi:10.1016/j.micromeso.2009.04.031*

(107) Ingleson, M. J.; Heck, R.; Gould, J. A.; Rosseinsky, M. J. *Inorg. Chem.* **2009**, *48*, 9986.

(108) Mann, B. E.; Motterlini, R. *Chem. Commun.* **2007**, 4197.

(109) Chavan, S.; Vitillo, J. G.; Groppo, E.; Bonino, F.; Lamberti, C.; Dietzel, P. D. C.; Bordiga, S. *J. Phys. Chem. C* **2009**, *113*, 3292.

(110) Bhatia, M. *IUBMB Life* **2005**, *57*, 603.

(111) Kimura, H.; Nagai, Y.; Umemura, K.; Kimura, Y. *Antioxid. Redox Signaling* **2005**, *7*, 795.

(112) Blackstone, E.; Morrison, M.; Roth, M. B. *Science* **2005**, *308*, 518.

(113) Drew, K. L.; Rice, M. E.; Kuhn, T. B.; Smith, M. A. *Free Radic. Biol. Med.* **2001**, *31*, 563.

(114) Carey, H. V.; Andrews, M. T.; Martin, S. L. *Physiol. Rev.* **2003**, *83*, 1153.

(115) Hamon, L.; Serre, C.; Devic, T.; Loiseau, T.; Millange, F.; Férey, G.; De Weireld, G. *J. Am. Chem. Soc.* **2009**, *131*, 8775.

(116) Horcajada, P.; Serre, C.; Vallet-Regí, M.; Sebban, M.; Taulelle, F.; Férey, G. *Angew. Chem., Int. Ed.* **2006**, *45*, 5974.

(117) Horcajada, P.; Serre, C.; Maurin, G.; Ramsahye, N. A.; Balas, F.; Vallet-Regi, M.; Sebban, M.; Taulelle, F.; Férey, G. *J. Am. Chem. Soc.* **2008**, *130*, 6774.

(118) Horcajada, P.; Chalati, T.; Serre, C.; Gillet, B.; Sebrie, C.; Baati, T.; Eubank, J. F.; Heurtaux, D.; Clayette, P.; Kreuz, C.; Chang, J.-S.; Hwang, Y. K.; Marsaud, V.; Bories, P.-N.; Cynober, L.; Gil, S.; Férey, G.; Couvreur, P.; Gref, R. *Nat. Mater.* **2010**, *9*, 172.

(119) Koshland, D.E. *Science* **1992**, *258*, 1861.

(120) Butler, A; Nicholson, R. *Life, Death and Nitric Oxide, RSC paperbacks* **2003**.

(121) Heitzer, T.; Schlinzig, T.; Krohn, K.; Meinertz, T.; Munzel, T. *Circulation* **2001**, *104*, 2673.

(122) Napoli, C.; Ignarro, L. J. *Annu. Rev. Pharmacol. Toxicol.* **2003**, *43*, 97.

(123) Martelli, A.; Rapposelli, S.; Calderone, V. *Curr. Med. Chem.* **2006**, *13*, 609.

(124) Al-Sa'doni, H. H.; Ferro, A. *Mini-Rev. Med. Chem.* **2005**, *5*, 247.

(125) Dudzinski, D. M.; Igarashi, J.; Greif, D.; Michel, T. *Annu. Rev. Pharmacol. Toxicol.* **2006**, *46*, 235.

(126) Crane, B. R.; Arvai, A. S.; Ghosh, D. K.; Wu, C.; Getzoff, E. D.; Stuehr, D. J.; Tainer, J. A. *Science* **1998**, *279*, 2121.

(127) Siddhanta, U.; Presta, A.; Fan, B. C.; Wolan, D.; Rousseau, D. L.; Stuehr, D. J. *J. Biol. Chem.* **1998**, *273*, 18950.

(128) Adams, D.R, Brochwicz-Lewinski, M., Butler, A.R. *Progress in the Chemistry of Organic Natural Products* **1999**, *Springer Chemistry*

(129) Roskams, A. J.; Bredt, D. S.; Dawson, T. M.; Ronnett, G. V. *Neuron* **1994**, *13*, 289.

(130) Palmer, R. M. J.; Ferrige, A. G.; Moncada, S. *Nature* **1987**, *327*, 524.

(131) Murrell, W. *The Lancet* **1879**, *113*, 80.

(132) Williams, D. L. H. *Org. Biomol. Chem.* **2003**, *1*, 441.

(133) Roberts, J. D.; Polaner, D. M.; Lang, P.; Zapol, W. M. *Lancet* **1992**, *340*, 818.

(134) Field, D.; Elbourne, D.; Truesdale, A.; Grieve, R.; Hardy, P.; Fenton, A. C.; Subhedar, N.; Ahluwalia, J.; Halliday, H. L.; Stocks, J.; Tomlin, K.; Normand, C.; Grp, I. T. C. *Pediatrics* **2005**, *115*, 926.

(135) Van Meurs, K. P.; Wright, L. L.; Ehrenkranz, R. A.; Lemons, J. A.; Ball, M. B.; Poole, W. K.; Perritt, R.; Higgins, R. D.; Oh, W.; Hudak, M. L.; Laptook, A. R.; Shankaran, S.; Finer, N. N.; Carlo, W. A.; Kennedy, K. A.; Fridriksson, J. H.; Steinhorn, R. H.; Sokol, G. M.; Konduri, G. G.; Aschner, J. L.; Stoll, B. J.; D'Angio, C. T.; Stevenson, D. K.; Hensman, A.; Gingras, D.; Jain, L.; Hale, E.; Seabrook, I.; Sokol, G.; Lorant, D.; Appel, D. D.; Miller, L.; Chriscinske, D.; Attwood, J.; Steinhorn, R.; Sautel, M.; Van Meurs, K.; Ball, B.; Proud, D.; Cosby, S. S.; Johnson, R. B.; Fridriksson, J.; Warner, B.; Mersmann, M.; Alexander, B.; Shively, J.; Mincey, H.; Hoover, M.; Sapienz, S.; Stephenson, E.; Rasmussen, M. R.; Henderson, C.; Demetrio, C.; Rich, W.; Joseph, C.; Hudak, M.; Osbeck, S.; Case, E.; Kellum, A.; Hogans, L.; Reubens, L.; Hutton, G.; Laptook, A.; Madison, S.; Hensley, G.; Miller, N.; Metoyer, G.; Kennedy, K.; McDavid, G.; Emerson, D.; Konduri, G.; Paquette, M.; Wong, S.; Aschner, J.; O'Shea, T. M.; Peters, N.; Hansell, B. J.; Griffin, J.; Adams, C.; Bara, R. A.; Muran, G.; Weekfall, W.; Gettner, P.; Caldwell, A.; Fanaroff, A. A.; Goldberg, R. N.; Donovan, E. F.; Duara, S.; Phelps, D. L.; Tyson, J. E.; Jobe, A.; Hastings, B.; Petrie, C.; McClure, E.; Bulas, D.; Mertens, D.; Slovis, T.; Avery, G.; D'Alton, M.; Fletcher, J. C. *N. Engl. J. Med.* **2005**, *353*, 13.

(136) DeRosa, F.; Kibbe, M. R.; Najjar, S. F.; Citro, M. L.; Keefer, L. K.; Hrabie, J. A. *J. Am. Chem. Soc.* **2007**, *129*, 3786.

(137) Keefer, L. K. *Annu. Rev. Pharmacol. Toxicol.* **2003**, *43*, 585.

(138) Miller, M. R.; Megson, I. L. *Br. J. Pharmacol.* **2007**, *151*, 305.

(139) Pulfer, S. K.; Ott, D.; Smith, D. J. *J. Biomed. Mater. Res.* **1997**, *37*, 182.

(140) Smith, D. J.; Simmons, M. L. *J. Controlled Release* **1998**, *51*, 153.

(141) Bohl, K. S.; West, J. L. *Biomaterials* **2000**, *21*, 2273.

(142) Duan, X.; Lewis, R. S. *Biomaterials* **2002**, *23*, 1197.

(143) Oh, B. K.; Meyerhoff, M. E. *Biomaterials* **2004**, *25*, 283.

(144) Maria, B. W.; Adrian, B. *Am. J. Surg.* **2002**, *183*, 406.

(145) Barbul, A.; Fishel, R. S.; Shimazu, S.; Wasserkrug, H. L.; Yoshimura, N. N.; Tao, R. C.; Efron, G. *J. Surg. Res.* **1985**, *38*, 328.

(146) Barbul, A.; Lazarou, S. A.; Efron, D. T.; Wasserkrug, H. L.; Efron, G. *Surgery* **1990**, *108*, 331.

(147) Bulgrin, J. P.; Shabani, M.; Smith, D. J. *J. Nutr. Biochem.* **1993**, *4*, 588.

(148) Wright, J. B.; Kan, L.; Robert, E. B. *Am. J. Infect. Control* **1998**, *26*, 572.

(149) Burd, A.; Kwok, C. H.; Hung, S. C.; Chan, H. S.; Gu, H.; Lam, W. K.; Huang, L. *Wound Repair Regen.* **2007**, *15*, 94.

(150) Miller, C. C.; Miller, M. K.; Ghaffari, A.; Kunimoto, B. *Journal of Cutaneous Medicine and Surgery: Incorporating Medical and Surgical Dermatology* **2004**, *8*, 233.

(151) I.V. Reshetov, R. K. K., A.B. Shekhter, A.V. Pekshev, *Annals of Plastic, Reconstructive and Anesthetic Surgery (Moscow)* **2000**, *4*, 24.

(152) Weller, R.; Ormerod, A. D.; Hobson, R., P.; Benjamin, N., J. *J. Am. Acad. Dermatol.* **1998**, *38*, 559.

(153) Weller, R.; Finnen, M. J. *Nitric Oxide* **2006**, *15*, 395.

2 Aims of this Project

The overall objective of this thesis was to investigate the storage and release of nitric oxide (NO) from a series of porous materials known as metal-organic frameworks (MOFs). As NO has been shown to play a significant role in the human anatomy, in particular its beneficial effects in wound healing were of interest[1-7]. Currently there are no known NO donor materials that controllably release pure NO when triggered except the recently developed NO releasing zeolites[8-11]. The aim of this project was to synthesise MOFs which could store and release biologically significant amounts of NO for possible use in medicinal applications.

The first major objective was the synthesis of MOF materials containing coordinatively unsaturated metal sites (CUSs) once activated. Following successful synthesis, characterisation techniques would be employed to show that the material produced matched the expected MOF.

The next major objective was to study the amount of NO that different MOFs can adsorb, and more importantly, controllably release with time. MOFs were chosen on the basis that comparisons could be made between different metals and their affinity for NO. Also different structure types were investigated to see if surface area has a bearing on NO adsorption. Further experiments were carried out using samples kindly donated from different sources, including some that contained diamines which had been grafted onto the CUSs present in the framework hoping to achieve higher adsorption and release of NO.

Finally, the MOFs that did show promise for NO adsorption and release were tested in a variety of formulations for potential use in medicinal applications. If a good NO donor MOF has been found, it would be considered for commercialisation.

2.1 References

(1) Maria, B. W.; Adrian, B. *Am. J. Surg.* **2002**, *183*, 406.

(2) Weller, R. *Clin. Sci.* **2003**, *105*, 533.

(3) Zhu, H.; Wei, X.; Bian, K.; Murad, F. *J. Burn Care Res.* **2008**, *29*, 804.

(4) Shekhter, A. B.; Serezhenkov, V. A.; Rudenko, T. G.; Pekshev, A. V.; Vanin, A. F. *Nitric Oxide* **2005**, *12*, 210.

(5) Weller, R.; Finnen, M. J. *Nitric Oxide* **2006**, *15*, 395.

(6) Barbul, A.; Lazarou, S. A.; Efron, D. T.; Wasserkrug, H. L.; Efron, G. *Surgery* **1990**, *108*, 331.

(7) Zhu, H.; Ka, B.; Murad, F. *World J. Surg.* **2007**, *31*, 624.

(8) Mowbray, M.; Tan, X.; Wheatley, P. S.; Morris, R. E.; Weller, R. B. *J. Invest. Dermatol.* **2007**, *128*, 352.

(9) Wheatley, P. S.; Butler, A. R.; Crane, M. S.; Fox, S.; Xiao, B.; Rossi, A. G.; Megson, I. L.; Morris, R. E. *J. Am. Chem. Soc.* **2006**, *128*, 502.

(10) Wheatley, P. S.; Butler, A. R.; Crane, M. S.; Rossi, A. G.; Megson, I. L.; Morris, R. E. *Molecular Sieves: From Basic Research to Industrial Applications, Pts a and B* **2005**, *158*, 2033.

(11) Xiao, B.; Wheatley, P. S.; Morris, R. E. In *Stud. Surf. Sci. Catal.*; Elsevier: 2007; Vol. Volume 170, Part 1, p 902.

3 Experimental Techniques

3.1 Hydrothermal Synthesis

The vast majority of MOFs are synthesised using hydrothermal synthesis. This technique involves calculated amounts of reactants being combined with appropriate solvents and homogenised. This reaction mixture is then placed in a polytetrafluoroethylene (Teflon) lined acid digestion bomb (autoclave) and heated for a pre-determined period of time. The product is then recovered from the liner, vacuum filtered and washed with parent solvent before being dried. The nature of the material obtained can depend on many variables such as concentration, solvent, temperature and even the reaction vessel itself. Indeed it is sometimes difficult to reproduce products and high throughput studies are required to show what the conditions required for production of certain phases are, even although these methods can suffer from inconsistent results[1-2].

3.2 Microwave Synthesis

Microwave-assisted synthesis is a field of synthesis which has only really come to the fore in the last 20 years or so. It allows reactions that would normally take hours or even days to be run in a matter of minutes or seconds. The first reported use of microwave assisted synthesis was in 1986[3-4]. However since then there have been huge advances in the field and as of 2007 there are now well over 3500 publications describing the use of microwave synthesis. The majority of these publications concern organic synthesis and the term microwave assisted organic synthesis (MAOS) is now well known. However, in recent years there have been a number of

publications concerning the microwave production of MOFs[5-11]. Most of these publications report shortened reaction times for the production of MOFs, synthesis of more crystalline versions of MOFs or in some cases the production of entirely new phases. Reactions can also be optimised by using microwave initiators which are now fitted with the ability to control the many variables of a reaction, such as time, temperature and pressure. So both yields and reaction conditions can be optimised as well as the ability to scale reactions up. Microwave synthesis can also remove unwanted side effects that are sometimes observed with conventional solvothermal synthesis, with uncertainty over exact reaction temperature and pressure. Factors which, as already stated can be easily controlled by modern initiators, such as the Biotage Initiator Eight[12] pictured (figure 3.1) and used in all microwave experiments reported in this thesis.

Figure 3.1 The Biotage Initiator Eight[12] used for all microwave experiments mentioned.

3.3 X-ray Diffraction

3.3.1 Background and theory

In a perfect crystalline solid, identical motifs are arranged in repeating units which produce a highly ordered structure. The regular repeating motif present in such systems is known as the unit cell of the structure. When X-ray diffraction is employed it allows chemists to understand the structural properties of the material in question. For example, inter and intra molecular distances and the arrangement of atoms in the unit cell can be deduced as well as the unit cell parameters. Diffraction of the X-rays by the crystal only takes place if the radiation wavelength is of the same magnitude as the object separation. This means that X-rays are well suited for the investigation of atom positions as the wavelength of X-rays (~1Å) and the interatomic distances are very similar. This diffraction is described by Bragg's Law (3.1).

$$n\lambda = 2d\sin\theta \tag{3.1}$$

This law gives the conditions by which a diffracted beam can be observed. Bragg's law can be easily derived using figure 3.2.

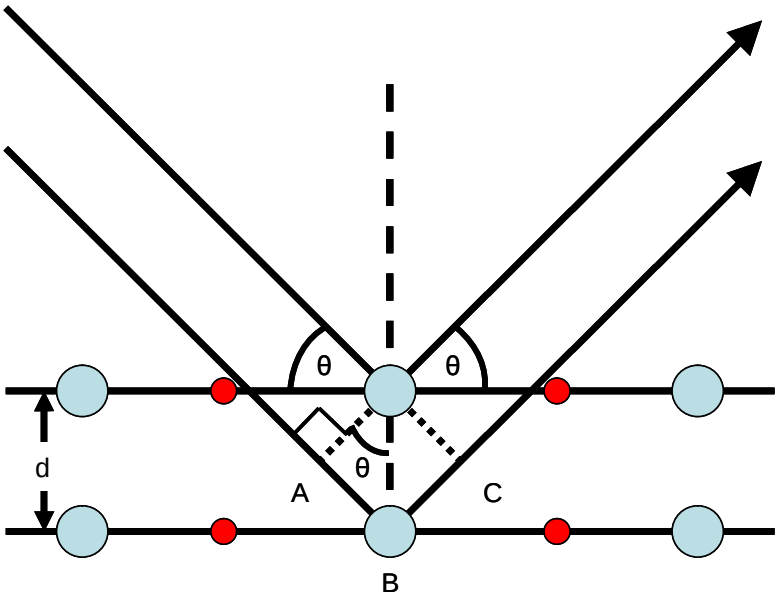

Figure 3.2 Derivation of Bragg's law showing the reflection of X-rays from two lattice planes.

When the in-phase X-rays strike the top layer, the top beam is diffracted by the atom on the top layer, the second beam continues through to the bottom layer and is diffracted by the atom on the bottom layer. The second beam has travelled the extra distance AB+BC = $2d\sin\theta$ if the two beams are to continue travelling in parallel. This extra distance is known as the path difference. The path difference must be equal to an integral multiple (n) of the wavelength (λ) for both beams to be the same. This results in Bragg's law being satisfied for constructive interference. When X-rays enter the crystal the lattice planes diffract the incoming X-rays only producing constructive interference if Bragg's law is satisfied. These planes can be described by Miller indices (or planes) and are represented by three integers (hkl). Examples of Miller planes can be seen in figure 3.3.

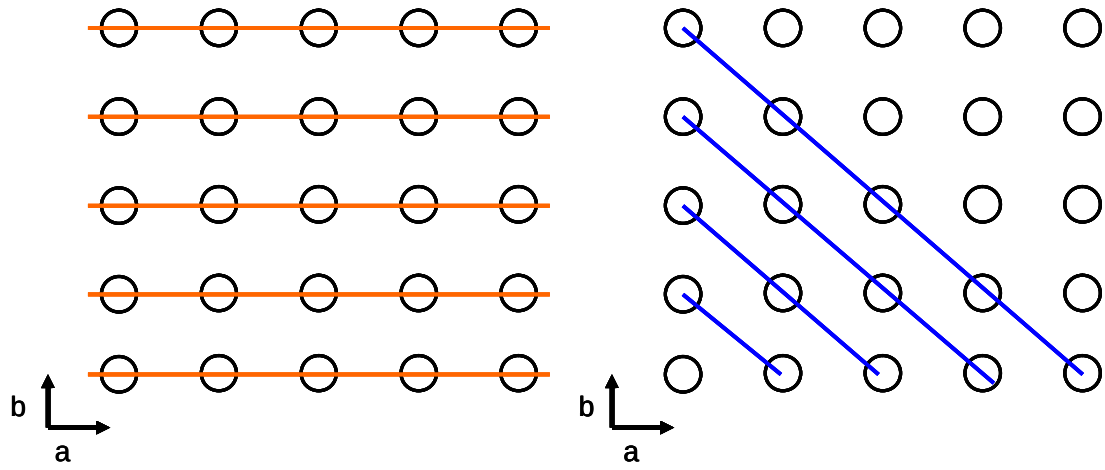

Figure 3.3 Examples of Miller planes. The orange line represents the (010) plane where the b axis is intercepted once but both the a and c axis are never crossed. The blue line represents the (110) plane where the a and b axis are intercepted once but never intercepts the c axis.

3.3.2 Powder X-ray diffraction

Powder X-ray diffraction is a very powerful tool in the characterisation of solids. It examines the bulk material and can be used to very quickly establish the crystallinity of a sample. Where single crystal X-ray diffraction gives single diffraction spots, powder X-ray diffraction gives thousands of diffraction spots forming a ring as can be seen in figure 3.3. This is due to the varying orientations of the crystals in the bulk sample being examined. The blue line through the circle represents what would be observed in a powder X-ray diffraction pattern, where the detector cuts through the rings as shown.

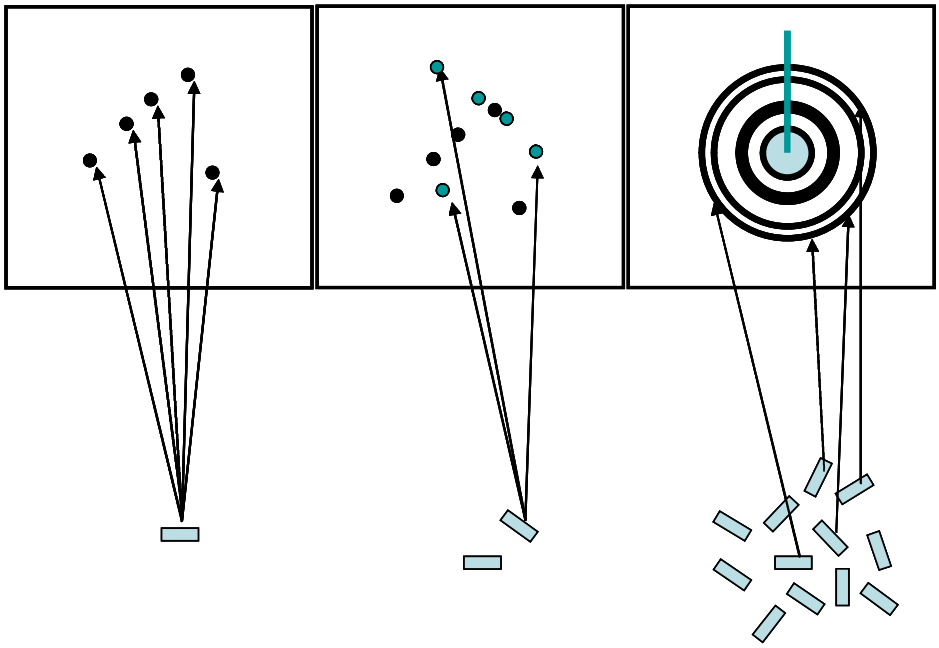

Figure 3.3 Examples showing the difference between single crystal (left) and powder X-ray diffraction (right). The large number of random orientations form rings and a normal experimental X-ray powder diffraction can be viewed by slicing the rings (blue line). 2θ is increasing from the centre of the rings outwards.

3.3.3 Phase identification using X-ray diffraction

In this work powder X-ray diffraction has been used as a characterisation tool for checking that the materials produced match those already published in the literature. This has been carried out by comparing the X-ray powder diffraction patterns with theoretical patterns produced using the Diamond 3 crystal visualisation software[13]. The unit cell parameters, space group and atomic coordinates of the published structure are input into the program which then produces a theoretical pattern which can then be compared with the experimental data. This process can also be carried out using an existing cif file as an input. An example can be seen below for Co CPO-27.

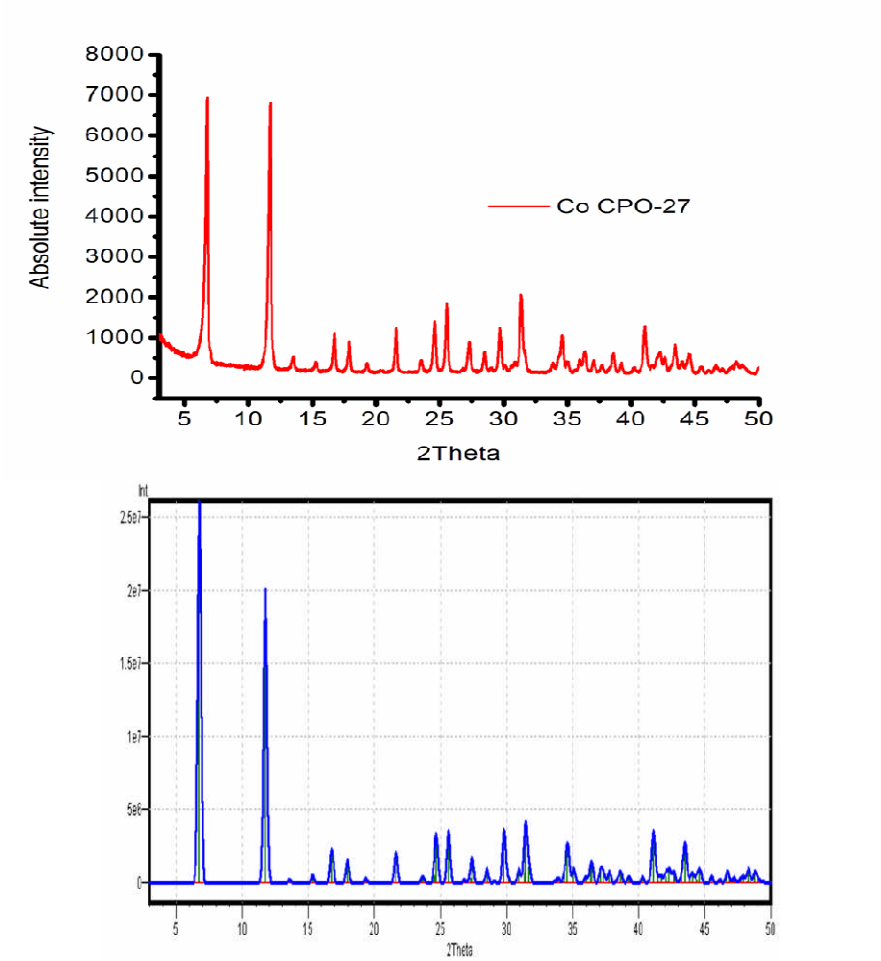

Figure 3.4 Experimental X-ray powder pattern (top) compared with the theoretical one (bottom) for Co CPO-27.

3.3.4 Equipment used for powder X-ray diffraction

In this thesis powder X-ray measurements were carried out using either a STOE STADIP diffractometer using monochromated Cu $K_{\alpha 1}$ radiation or on a Phillips XPERT data collector. Although both produce very similar outputs the machinery works in a different manner. The STOE diffractometer consists of an X-ray source, a moveable sample platform, an X-ray detector and associated computer software and electronics. A sample is placed in a sample holder (a sample can either be in a capillary that is spun or can be in a pre-prepared disc). The sample holder is then spun to ensure that all orientations of the crystals in the powder are examined. The beam of X-rays is fixed and the platform rotates at an angle theta with respect to the beam. The detector rotates at twice the rate of the sample being analysed and therefore is at an angle of 2θ with respect to the X-ray beam. This is known as transmission mode. The Phillips diffractometer works in reflection mode and has the sample on a plate with the detector on a moving arm and the plate remaining stationary. The X-rays are reflected off the surface. Photos of the powder X-ray equipment can be seen below (figure 3.5).

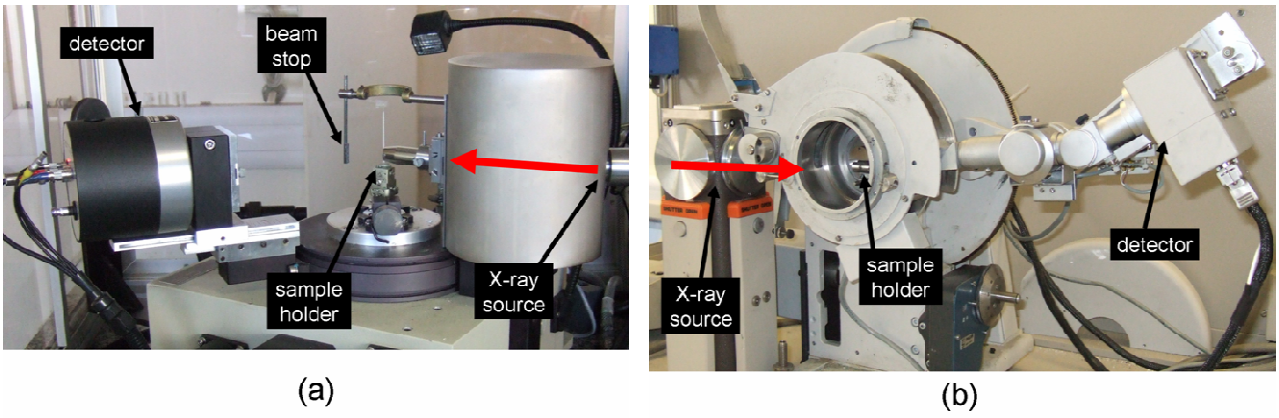

Figure 3.5 The powder X-ray diffractometer setups used in this work; (a) shows the capillary (transmission) setup with appropriate labels and (b) displays the flat plate (reflection) setup with appropriate labels. The red arrow in each case illustrates the direction of the X-ray beam.

3.3.5 Rietveld refinements

As a structural model for all of the MOFs synthesised in this thesis is available, it is possible to refine a structural model against an observed experimental powder pattern using a Rietveld refinement. The refining process uses the GSAS program suite[14]. The refinement is carried out by minimising the residual R_{wp} using a least squares procedure, where y_{io} and y_{ic} are the observed and calculated intensities and setting w_i is set to be equal to a suitable weight at the ith step giving equation 3.2.

$$R_{wp} = \sum w_i \left| y_{io} - y_{ic} \right|^2 \qquad (3.2)$$

Using this least squares method, the difference between y_{obs} and y_{calc} is minimised. Firstly the diffractometer zero point, background shape and peak shape are refined.

Once a reasonable model is established then other parameters are refined such as the unit cell, x,y,z coordinates and site occupancies. The quality of the refinement model can then be seen from the use of weighted residual factors R_{wp} (3.3) and goodness of fit χ^2 (3.4). A powder pattern is then expressed in terms of y_{obs} and the intensity is compared with y_{calc} at a set 2θ.

$$R_{wp} = \left\{ \frac{\sum_i w_i \left[y_i(obs) - y_i(calc) \right]^2}{\sum_i w_i \left[y_i(obs) \right]^2} \right\} \tag{3.3}$$

$$\chi^2 = \frac{R_{wp}}{R_{\exp}} \tag{3.4}$$

The quality of the data can be measured and is represented by R_{exp} using equation (3.5) which uses the number of profile points (N) and refined parameters (P).

$$R_{\exp} = \left\{ \frac{(N-P)}{\sum_{i=1}^{n} w_i y_i^{\,2}} \right\}^{\frac{1}{2}} \tag{3.5}$$

If a good refinement has been carried out the value of R_{wp} should approach that of R_{exp} and this can be seen from the goodness of fit value represented by χ^2.

Rietveld refinements have been used on powder diffraction data in this thesis to establish the exact location of the NO molecule in the pores of M-CPO-27. An example of the output from GSAS can be seen in figure 3.6.

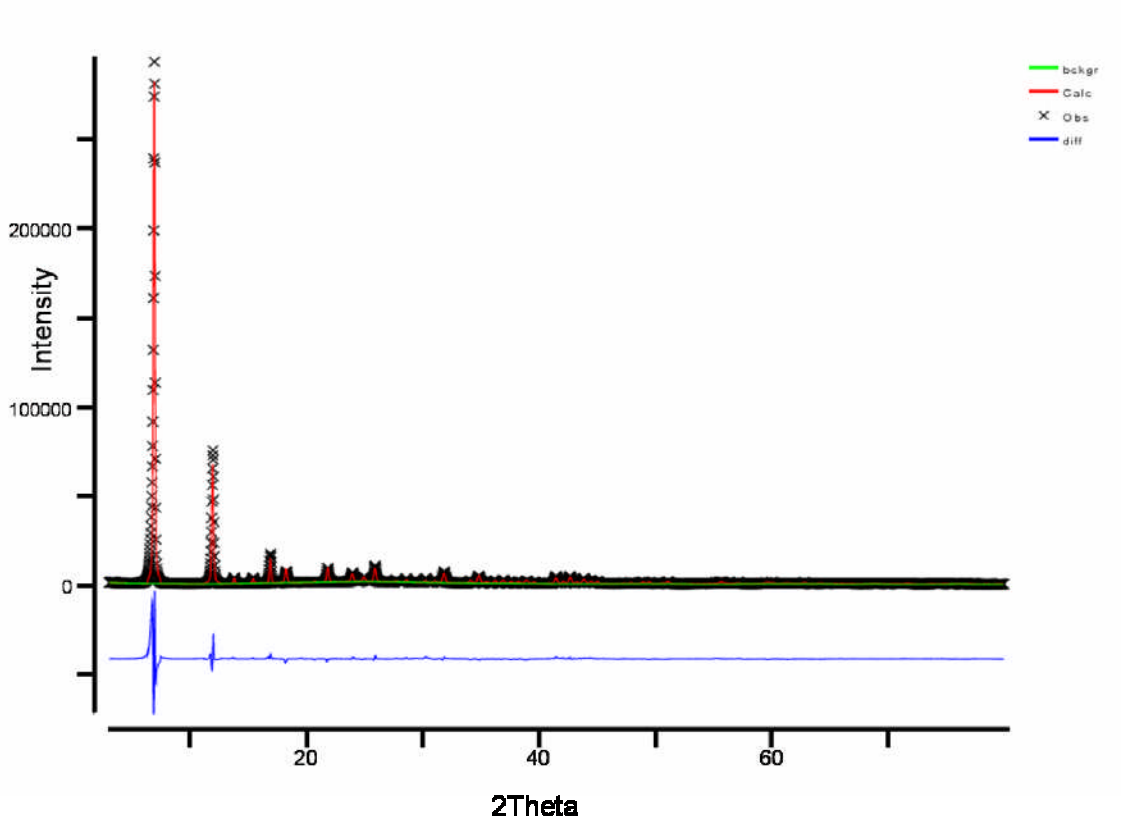

Figure 3.6 An example GSAS output illustrating the differences between the calculated pattern and the experimental one. The red graph shows the measured pattern, the black graph is the calculated pattern and the blue line shows the differences between the two (R_{wp}).

3.4 Surface area and porosity measurements

3.3.1 Introduction

One of the most crucial parts in the characterisation of MOFs is surface area analysis. This technique has been thrust into the limelight in recent years due to the increasing advancement of MOFs, and indeed MOFs have recently been synthesised with surface areas exceeding 6000 m^2g^{-1}. Gas adsorption in all porous solids is a very complex phenomenon. It involves mass and energy interaction and possible phase changes. There are many theories concerned with describing the behaviour of interactions between gas and solid and the most commonly used theories will be discussed later in this section. It is now common practice to measure the surface area of any newly produced MOF (or any porous material). Not only can surface areas of porous materials be measured, it is also possible to calculate pore volume and pore size distribution. Gas adsorption is always carried out at a constant temperature with the pressure being variable. There are two methods by which gas adsorption isotherms are measured. The first involves volumetric adsorption. Pressure measurements are taken before and after the data point in question. The difference forms the adsorption isotherm. This method is used in all N_2 adsorption isotherms. The second type of adsorption is gravimetric adsorption. In this type the sample's mass is constantly monitored and the adsorbate pressure is gradually increased, with increases in mass being used to form the adsorption isotherm of sample mass versus pressure. This is the method used in the NO adsorption isotherms as discussed later in this chapter.

Adsorption isotherms are plotted as an equivalent volume at standard pressure (either as a true volume, mass or moles per gram of material) against the equilibrium pressure (P/P_0) at constant temperature. There are six types of adsorption isotherm that are known for porous materials (see figure 3.7) from IUPAC definitions. Types 1 to 5 were originally assigned by Brunauer[15], whereas type 6 is a relatively recent addition[16].

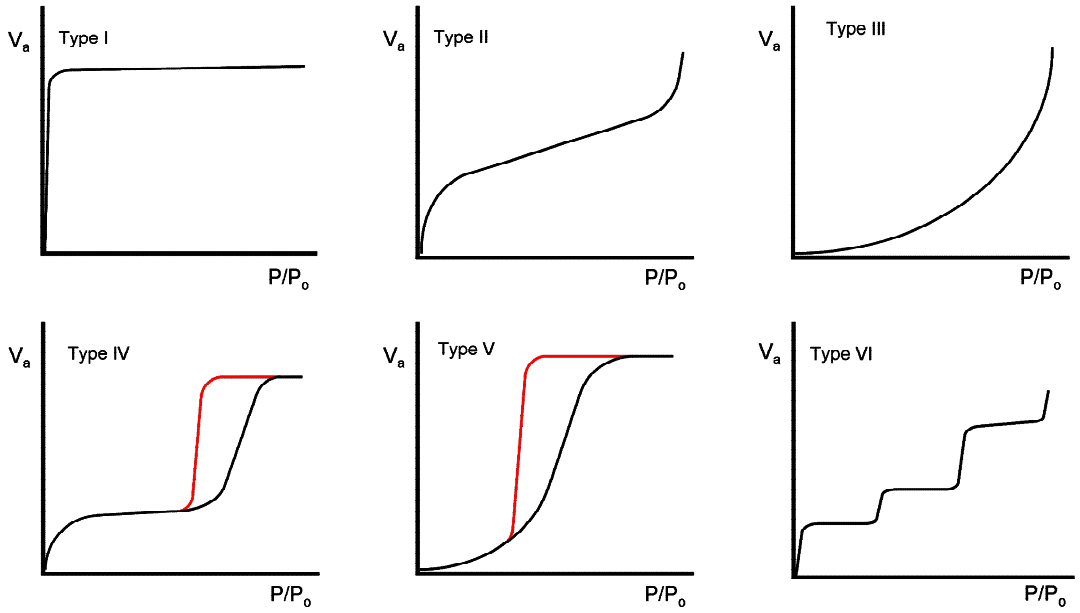

Figure 3.7 The six basic types of adsorption according to the Brunauer classification. The red lines indicate the desorption arm of the isotherm.

Type I isotherms (also known as Langmuir isotherms) are typically seen with microporous solids and are noted for the rapid rise in the volume adsorbed at low pressure. This initial rise indicates monolayer deposition of molecules in the pores. The long plateau section is governed by the total pore volume and is interpreted as gradual filling of the micropores. Occasionally there is a rise at high partial pressure,

which can be attributed to multilayer coverage of the external surface of the pores (see figure 3.8).

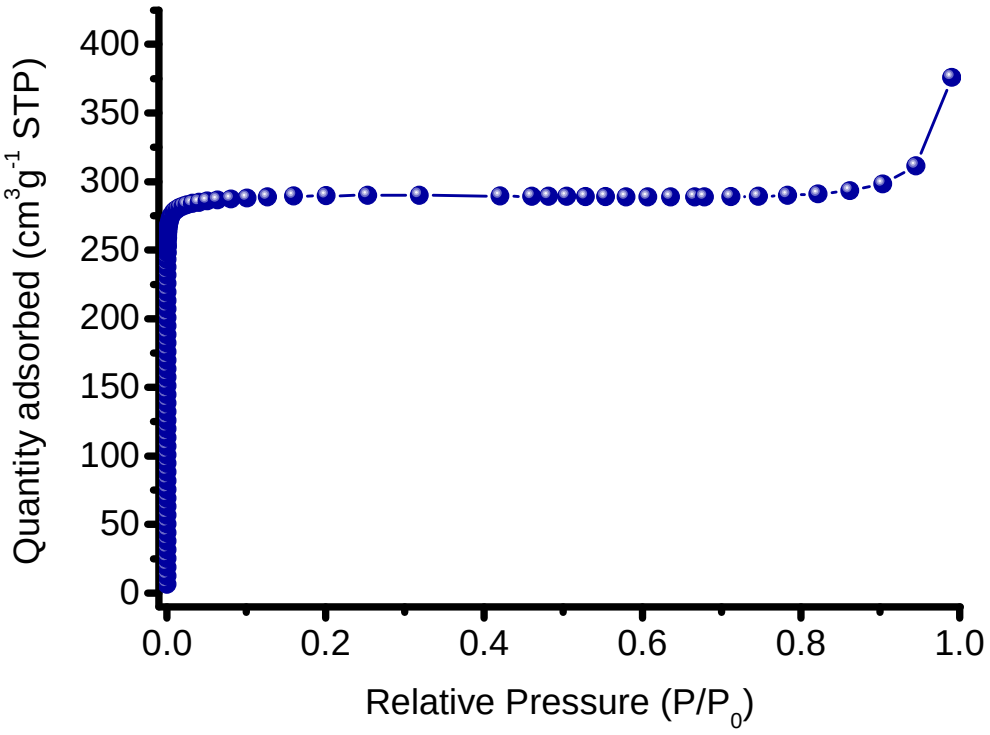

Figure 3.8 - Experimental N_2 adsorption isotherm carried out at 77K for Ni CPO-27 (a microporous MOF), showing type I isotherm shape and a second rise indicative of multilayer coverage of external surfaces.

Type II and IV isotherms are characteristic of either nonporous materials or porous materials with relatively large pores (a good example is mesoporous materials). Type III and V isotherms arise when the adsorptive molecules have more affinity for each other than they do for the solid. Type VI isotherms are encountered very rarely and indicate a nonporous material with an almost completely uniform surface[16-17].

3.3.2 Determination of surface area and porosity

There are now several theories which can be used to determine the surface area of a material. For microporous materials, the two most commonly used are the BET equation and the Langmuir equation.

3.3.2.1 Langmuir Theory

Langmuir developed his theory of adsorption and surface area between 1916 and 1918[18-20]. It should be stated that the Langmuir theory more correctly applies to chemisorption situations and not physical adsorption, due to the fact that its first assumption states that gases will only form one monolayer on a material. The collision of a gas molecule with the surface is assumed to be inelastic (meaning that the gas molecule remains in contact with the surface for a time before returning to the gas phase). It is this delay in time which is responsible for adsorption. The initial equation (3.6) relates the rate at which molecules strike the surface to the rate at which they leave.

$$V_a = \frac{V_m bP}{1+bP} \tag{3.6}$$

Here V_a is the quantity of gas adsorbed at a pressure P. V_m is the quantity of gas adsorbed to produce monolayer coverage of the solid and b is a constant. If this equation is re-arranged to the linear form (see equation 3.7) and values of P/V_a are plotted against P, a straight line should be observed. In fact when using liquid nitrogen temperatures and using nitrogen as the gas to be adsorbed, some sets of data

plot straight lines only in certain regions. This still allows *b* and V_m to be calculated from the slope and intercept.

$$\frac{P}{V_a} = \frac{1}{V_m b} + \frac{P}{V_m} \tag{3.7}$$

Therefore the specific surface area *s* of the material (the area contained in 1g) can be calculated from V_m using equation 3.8.

$$s = \frac{V_m \sigma N_A}{m V_o} \tag{3.8}$$

Here σ is the surface area occupied by a single adsorbed gas molecule (for nitrogen σ = 16.2 $Å^2$ or 16.2 x 10^{-20} m^2), N_A is the Avogadro constant (6.023 x 10^{23} molecules/mole), m is the mass of the adsorbing sample and V_o the molar volume of the gas (22414 cm^3). As all the surface measurements used N_2 as the adsorptive gas the surface area can be calculated using equation 3.8 arranged as follows.

$$s(m^2/g) = \frac{4.35 V_m (cm^3 at STP)}{m(g)} \tag{3.9}$$

3.3.2.2 BET Theory

Brunauer, Emmett and Teller produced an improved version of Langmuir's theory by incorporating the concept of multilayer adsorption. It is now known as the BET theory taken from the surnames of the founders[21]. The main assumption is that the forces responsible for the condensation of gases are also active in the binding energy in multimolecular adsorption. Therefore by equating the rate of the condensation of gas onto an already covered surface to the rate of evaporation from that layer and then summing for an infinite number of layers, equation 3.10 can be derived.

$$V_a = \frac{V_m C P}{(P_0 - P)\left[1 + (C-1)\frac{P}{P_0}\right]} \tag{3.10}$$

Here C is a constant, P_0 is the saturation pressure of the gas and all the other terms are the same as stated previously. The value of the constant C is as follows:

$$C \propto \exp \frac{q_1 - q_L}{RT} \tag{3.11}$$

Where q_1 is the heat of adsorption of the first layer of gas molecules, q_L is the heat of the liquefaction of N_2, R represents the gas constant and T the absolute temperature. Again, equation 3.10 can be re-arranged into the linear form to give 3.12.

$$\frac{P}{V_a(P_0 - P)} = \frac{1}{V_m C} + \frac{C-1}{V_m C}\left(\frac{P}{P_0}\right) \tag{3.12}$$

From this it should be possible to plot $P/[V_a (P_0-P)]$ vs. P/P_0. A straight line should be observed with intercept $1/V_mC$ and slope $(C-1)/V_mC$. The values of V_m and C can then be calculated. Following calculation of the volume, the surface area may now be calculated using the area occupied by a single adsorbed molecule. This can be determined from an assumption of close packing at the surface given by the following formula:

$$\sigma = (4)(0.866)\left[\frac{M}{4(2N_A\rho)^{1/2}}\right]^{2/3} \tag{3.13}$$

σ is the mean area per molecule, M is the molecular weight, N_A is Avogadro's number and ρ is the density of the liquid adsorbate.

This model is best applied to multilayer adsorption in Type II adsorption isotherms and low pressure regions of type IV isotherms. However due to the high number of assumptions, it has been shown that BET theory is not the best at estimating surface areas in microporous materials. For example, there are no lateral interactions between the adsorbed species and the heats of adsorption are the same for all the layers adsorbed. Indeed these assumptions lead the BET equation away from the ideal Langmuir adsorption isotherm.

3.3.2.3 Chemical adsorption (Chemisorption)

There is a distinction to be made between physical adsorption (physisorption) and chemisorption. Physical adsorption is the result of a relatively weak interaction between a material and the gas, and usually such interactions are formed from weak van der Waals forces and have low heats of adsorption (not exceeding 80 kJ/mole). During the desorption part of an experiment usually all the gas (and therefore the interaction) is removed by vacuum. Chemisorption is a much stronger interaction, sometimes with extremely high heats of adsorption. During the adsorption process the adsorbing molecule forms a chemical bond with the adsorption site (in the case of dehydrated MOFs the coordinatively unsaturated metal site (CUS)). This bond involves the sharing of electrons and it is therefore very difficult to reverse the desorption under vacuum. However, it is not uncommon for both chemisorption and physisorption to occur at the same time. It is possible that once all of the available metal sites have been used that a layer of physisorbed molecules may form on top, or may occur at the non-active sites present in the material. Indeed as will be shown later, in order to be useful for the stated applications, NO requires an active metal site to bind to, otherwise poor adsorption is observed at room temperature.

3.3.2.4 Equipment used for surface area determinations

For all nitrogen adsorption experiments (physical adsorption) a Micromeritics ASAP 2020 surface area and porosity analyser was used (see figure 3.9). Samples of mass ~100 mg were placed into pre-weighed glass sample tubes and sealed using a seal-frit, a piece of equipment that prevents exposure to the atmosphere between the degas and analysis steps. The sample tube is then inserted into the degas port of the analyser, and the sample is degassed (under vacuum and exposure to temperatures varying between 120 and 250°C for a certain time period). Once fully desolvated the sample tube is transferred to the analysis port and the analysis part of the experiment can begin. All experiments are carried out at 77K using a liquid nitrogen bath.

Figure 3.9 A Micromeritics ASAP 2020 Surface Area and Porosity Analyser. Degas ports are on the left complete with heating manifolds. The analysis port is on the right with a liquid N_2 bath directly below.

3.4 NO gas adsorption and desorption measurements

3.4.1 Adsorption/desorption experiments

Much of the research in this thesis involved the adsorption and desorption of NO. The adsorption of NO gas was an integral part of this work and was carried out using a gravimetric adsorption system (see figure 3.10). A CI instruments microbalance was thermally stabilized to eliminate the effect from the external environment. The microbalance has a sensitivity of 0.1 μg and a reproducibility of 0.01% of the load. The pressure of the adsorption system was monitored by two BOC Edwards Active gauges in the ranges of 1×10^{-8} to 1×10^{-2} and 1×10^{-4} to 1×10^{3} mbar, respectively. The sample (~30 mg) was initially degassed at the required temperature (depending on the sample's activation temperature and stability) under 1×10^{-4} mbar, until no further weight loss was observed. The sample temperature was then decreased to 25°C and kept constant by a circulation water bath with temperature accuracy ±0.02 K. The counterbalance temperature was kept the same as that of the sample to minimize the influence of temperature difference on weight readings. The sample temperature was monitored using a K type of thermocouple, located close to the sample bucket (<5 mm). The variation in sample temperature was minimal (<0.1 K) throughout the experiment. NO gas was introduced into the adsorption system until the desired pressure was achieved, and the mass uptake of the sample was measured as a function of time until the adsorption equilibrium was achieved. In this manner an adsorption isotherm was collected by incrementally increasing the pressure and noting the mass gain of the sample after equilibrium was reached. The desorption of the NO gas adsorbed in the samples was performed by gradually decreasing the system pressure to a desired value (until 2×10^{-2} mbar).

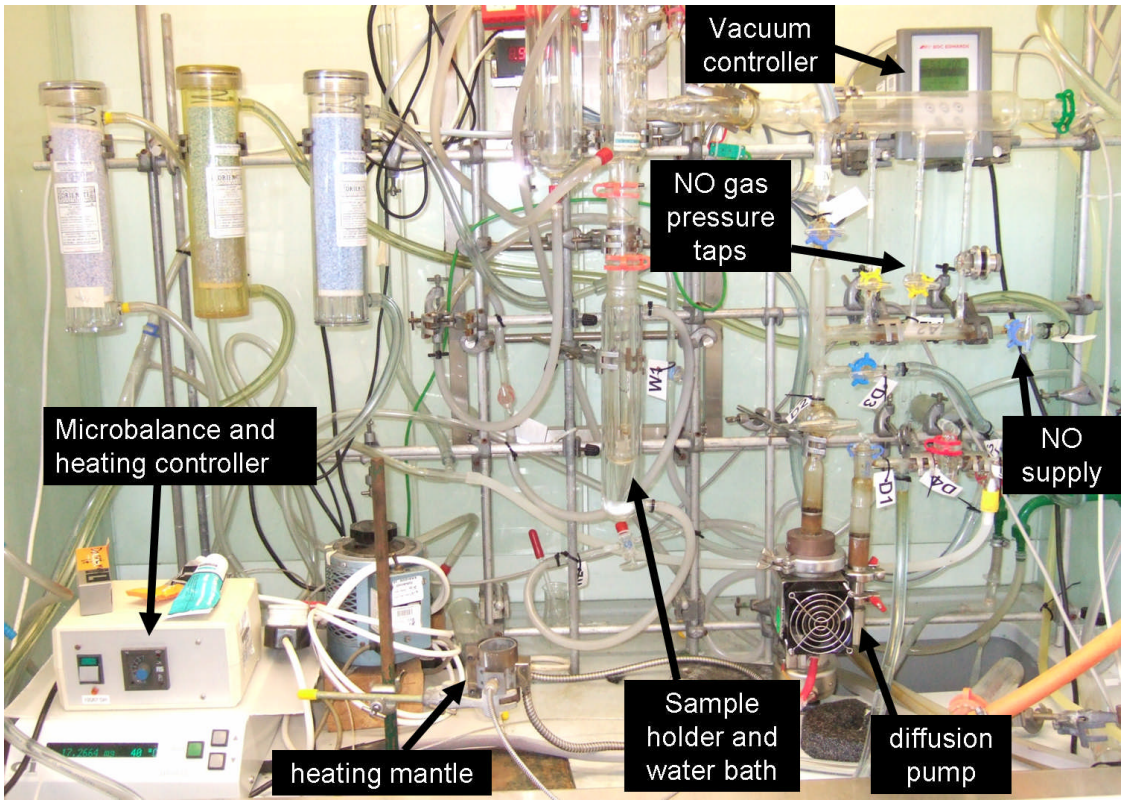

Figure 3.10 Photograph showing the NO gravimetric adsorption system. Relevant parts of the system are labelled appropriately.

3.4.2 Measurement of NO release by chemiluminescence

It is possible to see from the adsorption experiments how much NO various MOFs would adsorb both physically and chemically. However to quantify the amount of NO that could be recovered from samples, a NO analyser was used (see figure 3.11). The Sievers NOA 280i chemiluminescence Nitric Oxide Analyser uses a high-sensitivity detector for measuring NO based on a gas-phase chemiluminescent reaction between NO and ozone (O_3) (see equations 1 and 2).

$$NO + O_3 \rightarrow NO_2^* + O_2 \quad (1)$$

$$NO_2^* \rightarrow NO_2 + h\nu \quad (2)$$

The emission from the excited nitrogen dioxide is in the near-infrared end of the spectrum and is detected by a red-sensitive photomultiplier tube. The instrument was calibrated by first passing air through a zero filter (Sievers, <1 ppb NO) and then 89.48 parts per million (PPM) NO gas (Air Products, balance nitrogen). The flow rate was set to 200 mL/min with a cell pressure of 8.5 torr and an oxygen pressure of 6.1 psig. To measure NO release from different samples, nitrogen gas of known humidity was passed over the powders. The resultant gas was directed into the analyser and the concentration of NO in PPM or parts per billion (PPB) was recorded. For the liquid-based experiments a sample vial was connected to the instrument using tubes with needles and with the sample already inside, a pre-determined amount of liquid was then injected into the vial and the sample stirred to ensure good mixing.

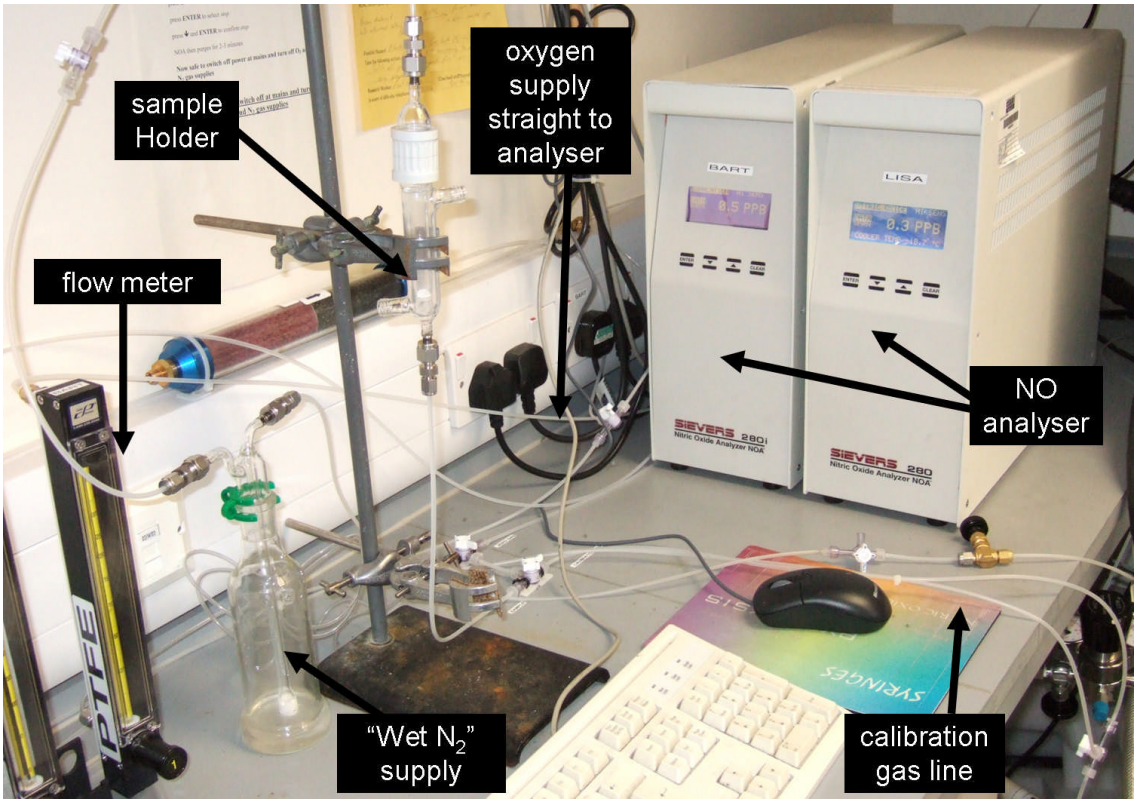

Figure 3.11 The Sievers NOA 280i chemiluminescence Nitric Oxide Analyser. Picture showing the sample holder and the output from the analyser. Relevant parts are labelled appropriately

3.5 Thermogravimetric analysis

Thermogravimetric analysis (TGA) is useful as it quantifies the loss of mass in microporous materials with increasing temperature. The procedure involves pre-weighing and zeroing an alumina crucible, before a small sample of material is transferred into the crucible, which is then re-weighed. The experiment involves heating the crucible in a controlled manner under a gaseous atmosphere (usually nitrogen or laser air). The changes in mass are recorded and can be used to give information about the stability of the material at certain temperatures and also when guest solvent molecules are lost. It can also give clues about molecular formula. All samples were analysed using a Netzsch TG 209 analyser under an air atmosphere. An example of an experimental TGA curve can be seen in figure 3.12.

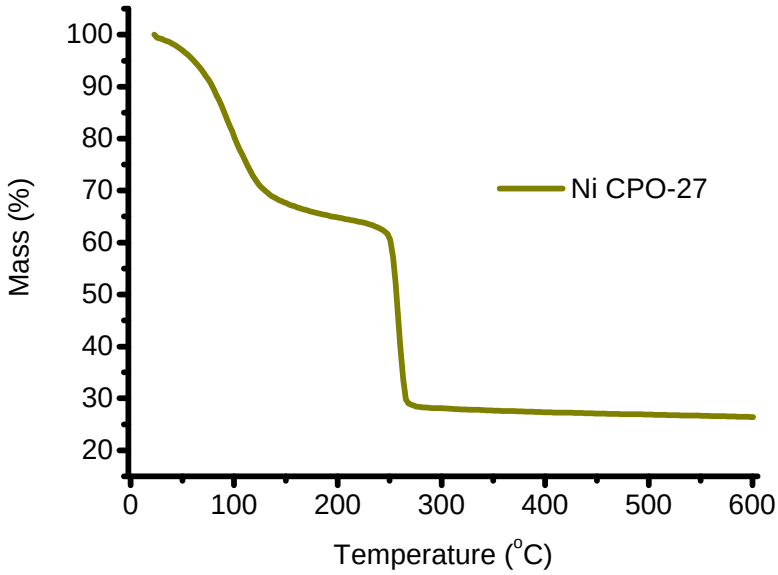

Figure 3.12 Experimental TGA curve for Ni CPO-27 (a metal organic framework) showing two distinct mass losses. The first (50-175°C) can be attributed to solvent in the pores (in this case water) and the second (~250°C) signals the collapse of the framework as the organic linker decomposes.

3.6 Elemental analysis

C,H,N elemental analysis gives the percentage amount of each of the aforementioned elements found in the sample. It can yield useful data regarding organic molecules present within frameworks. It can also be used to quantify successful solvent exchange in a MOF. Elemental analysis was carried out using a Carlo Erba 1106 CHN elemental analyser.

3.7 References

(1) Bauer, S.; Serre, C.; Devic, T.; Horcajada, P.; Marrot, J. R. M.; Férey, G.; Stock, N. *Inorg. Chem.* **2008**, *47*, 7568.

(2) Biemmi, E.; Christian, S.; Stock, N.; Bein, T. *Micropor. Mesopor. Mater.* **2009**, *117*, 111.

(3) Gedye, R.; Smith, F.; Westaway, K.; Ali, H.; Baldisera, L.; Laberge, L.; Rousell, J. *Tetrahedron Lett.* **1986**, *27*, 279.

(4) Giguere, R. J.; Bray, T. L.; Duncan, S. M.; Majetich, G. *Tetrahedron Lett.* **1986**, *27*, 4945.

(5) Choi, J.-S.; Son, W.-J.; Kim, J.; Ahn, W.-S. *Micropor. Mesopor. Mater.* **2008**, *116*, 727.

(6) Choi, J. Y.; Kim, J.; Jhung, S. H.; Kim, H. K.; Chang, J. S.; Chae, H. K. *Bull. Korean Chem. Soc.* **2006**, *27*, 1523.

(7) Hong, D.-Y.; Hwang, Y. K.; Serre, C.; Férey, G.; Chang, J.-S. *Adv. Funct. Mater.* **2009**, *19*, 1537.

(8) Jhung, S. H.; Lee, J. H.; Chang, J. S. *Bull. Korean Chem. Soc.* **2005**, *26*, 880.

(9) Jhung, S. H.; Lee, J.-H.; Forster, P. M.; Férey, G.; Cheetham, A. K.; Chang, J.-S. *Chem. -Eur. J.* **2006**, *12*, 7899.

(10) Lin, Z.; Wragg, D. S.; Morris, R. E. *Chem. Commun.* **2006**, 2021.

(11) Taylor-Pashow, K. M. L.; Rocca, J. D.; Xie, Z.; Tran, S.; Lin, W. *J. Am. Chem. Soc.* **2009**.

(12) http://www.biotage.com/DynPage.aspx?id=22045.

(13) Diamond 3 Crystal and Molecular Structure Visualisation, Crystal Impact.

(14) Bruker AXS ltd, TOPAS V3.0: General Profile and Structure Analysis Software for Powder Diffraction Data. 2004.

(15) Brunauer, S. *The Adsorption of Gases and Vapors vol 1, Physical Adsorption* **1943**, *Princeton University Press, Princeton, N.J.*

(16) Sing, K. S. W. *Pure Appl. Chem.* **1985**, *57*, 603.

(17) Krätschmer, W.; Rathouský, J.; Zukal, A. *Carbon* **1999**, *37*, 301.

(18) Langmuir, I. *J. Am. Chem. Soc.* **1916**, *38*, 2221.

(19) Langmuir, I. *Physical Review* **1916**, *8*, 149.

(20) Langmuir, I. *J. Am. Chem. Soc.* **1918**, *40*, 1361.

(21) Brunauer, S.; Emmett, P. H.; Teller, E. *J. Am. Chem. Soc.* **1938**, *60*, 309.

4 M-CPO-27: an isostructural series of MOFs

4.1 Background

In 2005 Dietzel and co-workers synthesised a highly crystalline MOF[1] with the formula $[Co_2(C_8H_2O_6)(H_2O)_2]\cdot 8H_2O$. Dietzel was interested in running in-situ single crystal X-ray diffraction to see if the long range order in such frameworks is maintained even after guest solvent molecules are removed (activation). This phenomenon is known as permanent porosity and is key for porous materials to be useful for gas storage. The in-situ single crystal X-ray diffraction experiments showed that the dehydrated form of this compound has an open metal site which originally had a solvent molecule bound to it. Since this initial discovery, several isostructural analogues have been produced including Ni[2], Zn[3-5], Mg[6-7], Mn[8] and very recently Fe[9]. This MOF is also known as MOF-74 which was originally designated to the zinc version by Yaghi and co-workers who first synthesised it. However, to avoid confusion throughout this thesis the name M-CPO-27 will be adopted.

4.2 Aims of chapter 4

The main aim in this chapter was to synthesise an isostructural set of MOFs which contain coordinatively unsaturated metal sites (when activated), which it is believed are a key requirement in the storage and delivery of significant quantities of NO. Following successful synthesis and characterisation of the materials, NO storage and release measurements would be undertaken. M-CPO-27 was chosen to be

synthesised due to the isostructural nature of the frameworks, allowing comparisons to be made between different metals and their affinity for NO.

4.3 Synthesis of M-CPO-27

In order for a complete investigation to be carried out and for comparative purposes all the analogues of this MOF were produced for NO investigation using the literature based synthetic methods[1-2,4,6-8,10]. However, an iron analogue of this structure was produced very recently and therefore is not covered in this thesis[9]. M-CPO-27 is produced in autoclaves using hydrothermal synthesis, however individual versions use slightly different procedures. Figure 4.1 displays the various methods which can be employed to successfully synthesise the isostructural frameworks. The linker utilised in each case is 2,5-dihydroxyterephthalic acid (DHTP). Dietzel and co-workers have produced almost all of the compounds using the solvent tetrahydrofuran (THF) combined with some water. Once the heating of the autoclaves is finished they are cooled and the resulting powder is filtered and washed with the parent solvent and air dried. For certain analogues, solvent exchange is required to allow enhanced activation. In the reactions involving dimethylformamide (DMF) and ethanol, the DMF is solvent-exchanged with a solvent which has a lower boiling point, such as methanol to allow the framework to be evacuated fully and without destroying the pores.

Ref	MOF	Metal source	Solvent used	Additional reagents	Temp (°C)	Time (hours)
1	Co CPO-27	$Co(CH_3COO)_2 \cdot 4H_2O$	water/THF	n/a	110°C	72
2	Ni CPO-27	$Ni(CH_3COO)_2 \cdot 4H_2O$	water/THF	n/a	110°C	72
4	Zn CPO-27	$Zn(NO_3)_2 \cdot 6\ H_2O$	DMF/water	n/a	100°C	24
5	Zn CPO-27	$Zn(NO_3)_2 \cdot 6\ H_2O$	water/THF	1mol NaOH	110°C	72
6	Mg CPO-27	$Mg(NO_3)_2 \cdot 6H_2O$	water/THF	1mol NaOH	110°C	72
7	Mg CPO-27	$Mg(NO_3)_2 \cdot 6H_2O$	DMF/ethanol/water	n/a	125°C	24
8	Mn CPO-27	$MnCl_2 \cdot 4H_2O$	DMF/ethanol/water	n/a	135°C	24

Figure 4.1 Table showing the various synthetic procedures employed to form M-CPO-27.

4.4 Structure of M-CPO-27

The structure of M-CPO-27 is three dimensional and consists of one dimensional channels, giving a honeycomb-like appearance (see figure 4.2). The metal atom is coordinated by six oxygen atoms in a distorted octahedron. Five of the atoms originate from the fully deprotonated organic linker and the one remaining oxygen atom comes from a solvent molecule. In the Co, Ni, Zn and Mg versions produced by Dietzel and co-workers this is a water molecule.

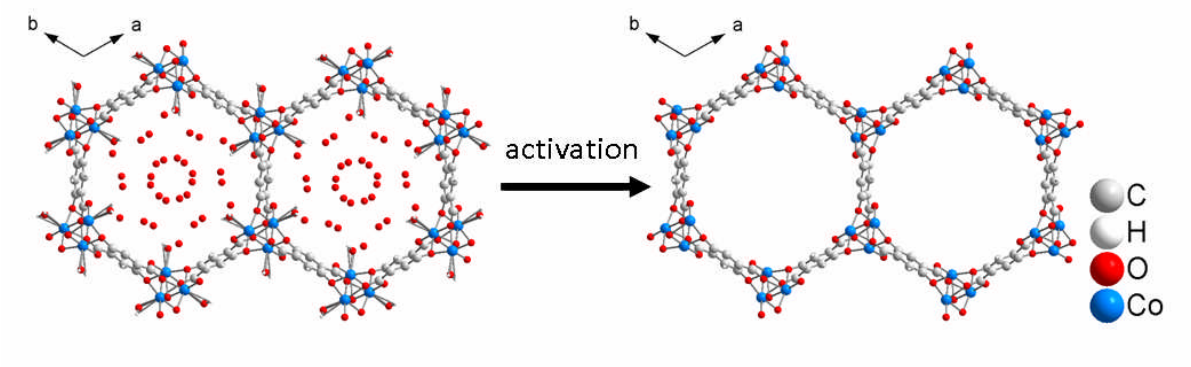

Figure 4.2 A diagram of a section of M-CPO-27 viewed down the c-axis showing the honeycomb appearance. It also illustrates the vacant pores and the coordinatively unsaturated metal sites (CUSs) available once the MOF is activated.

The pores of M-CPO-27 are ~11Å wide and are filled with guest solvent molecules (in the Co and Ni versions it is water, in others it can be a mixture of water, DMF and ethanol). However, activation of these frameworks can yield a fully evacuated MOF with accessible metal sites to which gases can bind. This activation process again is different for the various analogues as some of the structures are less thermally robust compared with the others. Figure 4.3 shows a table listing the activation conditions used for each of the versions of M-CPO-27. The empty channels of the partially dehydrated structure occupy 49% of the total structure. This figure rises to 60% once all coordinated solvent molecules are also removed. The coordination environment around the metal atom changes from a distorted octahedron to a coordinatively unsaturated square pyramid.

Ref	Compound	Activation conditions	Reported Langmuir surface area (m^2g^{-1})
1	Co CPO-27	vacuum + 150°C	not reported
2	Ni CPO-27	vacuum + 150°C	1083
3, 4	Zn CPO-27	solvent exchange then vacuum + 270°C	245, 1132
5	Zn CPO-27	solvent exchange then vacuum + 250°C	not reported
6	Mg CPO-27	vacuum + 250°C	varying 150 - 1030
7	Mg CPO-27	solvent exchange then vacuum + 250°C	1905
8, 16	Mn CPO-27	solvent exchange then vacuum + 250°C	1102 (BET)

Figure 4.3 A table showing the procedures required for full activation of the different analogues of M-CPO-27.

4.5 Characterisation of Co and Ni CPO-27

The Co and Ni versions were the first to be synthesised for this chapter. Powder X-ray diffraction was used initially to characterise these materials and to check for phase purity. The Phillips diffractometer was used for this process. It also allowed the Co version to be examined using Cu radiation. On the STOE diffractometer a large fluorescence was observed due to the differing mode of collection (reflection versus transmission). Figure 4.4 shows the experimental powder X-ray patterns for both Ni and Co versions of M-CPO-27. As can be observed they match very well to each other and also the XRD patterns found in the literature. Importantly they also match the theoretical powder X-ray pattern produced using the Co CPO-27 cif file and Diamond 3.0 software package (see figure 4.5).

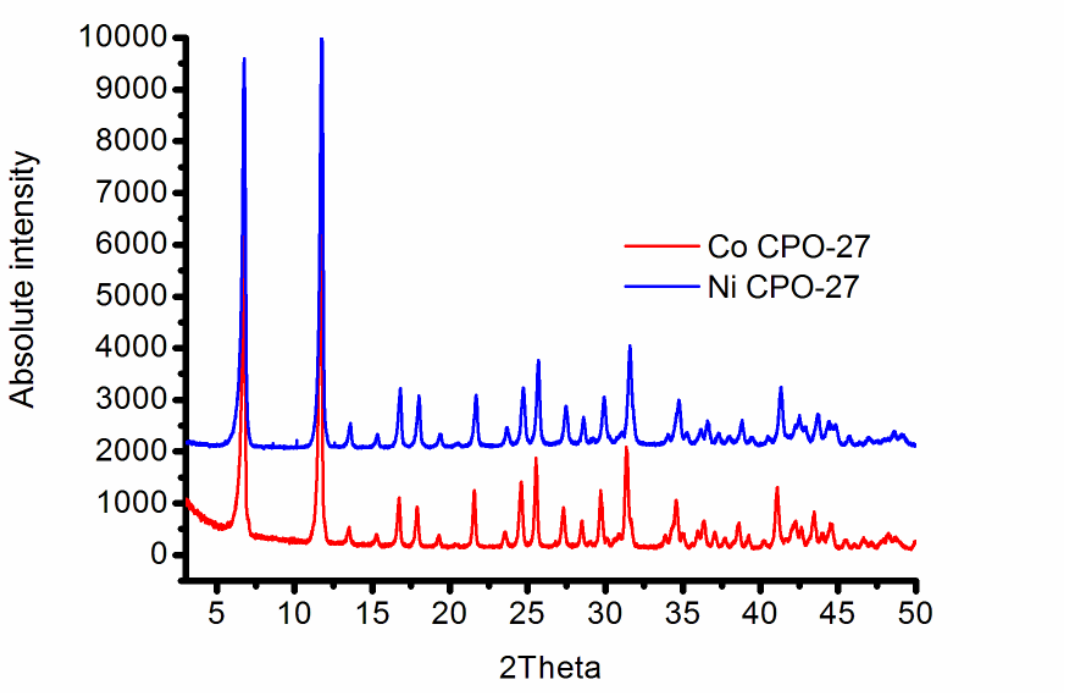

Figure 4.4 An experimental powder X-ray diffraction pattern for both Co and Ni CPO-27.

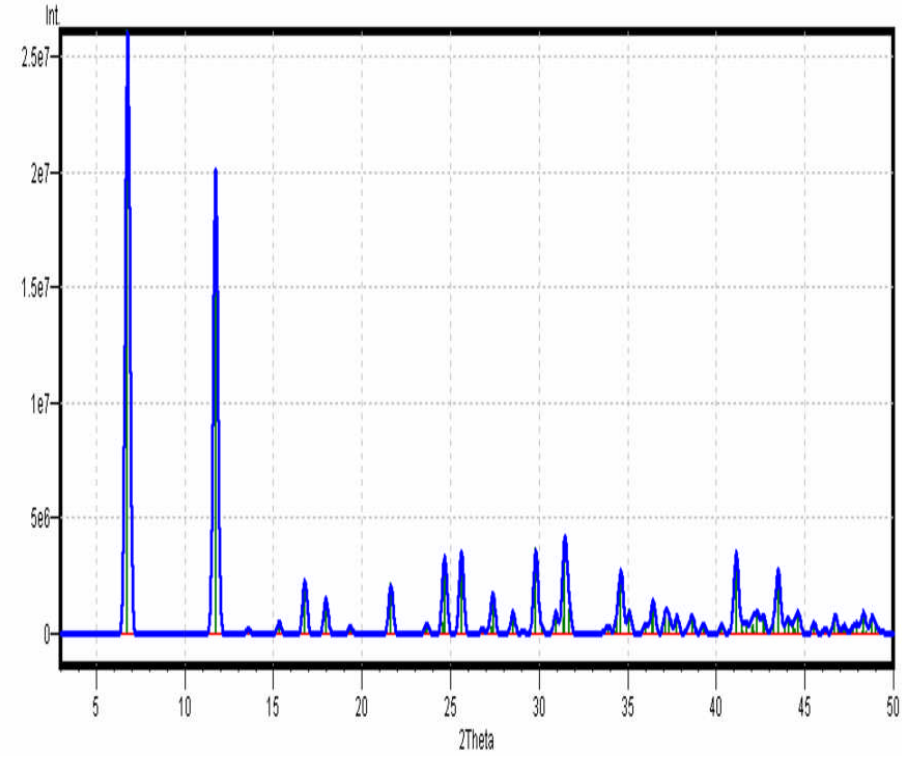

Figure 4.5 The theoretical powder XRD pattern for Co CPO-27, produced using the Diamond 3.0 software package.

Following successful powder X-ray diffraction studies, thermogravimetric (TGA) experiments were run on both Ni and Co CPO-27. The TGA curves matched the appropriate literature very well (figure 4.6). The drop in mass observed initially between 50 and 150°C is indicative of the removal of both the water trapped in the pores and also the water coordinated to the metal and matches very well to the expected value of 36% (29% uncoordinated and 7% coordinated water). This leaves the fully dehydrated porous structure. Decomposition then occurs at 250°C.

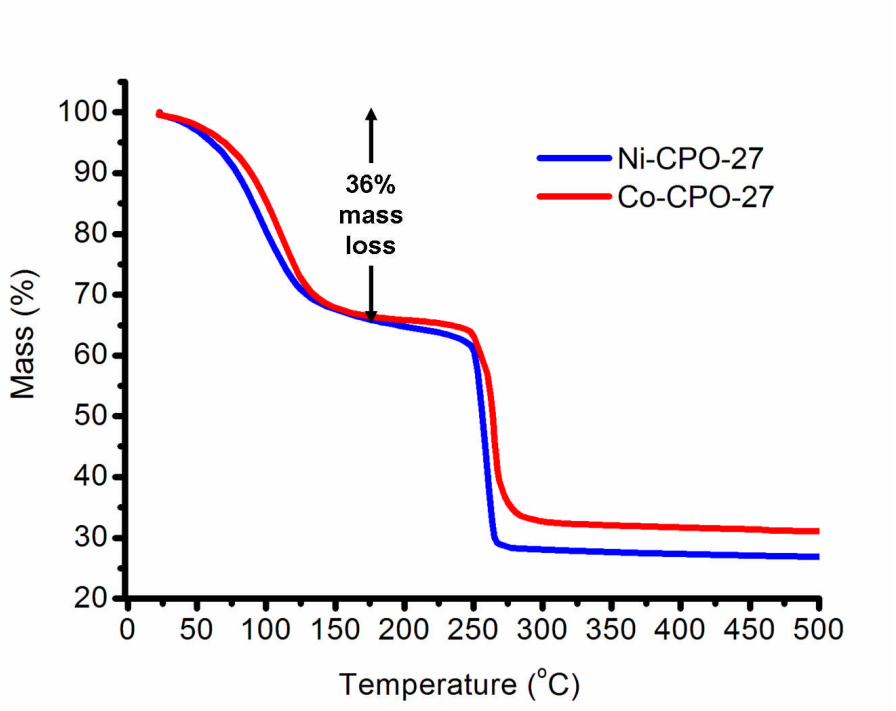

Figure 4.6 Experimental TGA curve showing mass losses for both Co and Ni CPO-27. Both samples lose all water trapped in the pores and attached to the metal, after heating to 150°C.

One of the fundamental characterisation techniques of MOFs is nitrogen (N_2) physisorption, as it is used to determine the porosity. This includes both surface area measurements and determination of pore volume. There have been many publications concerning M-CPO-27 and its gas storage properties[2,7-8,11-15]. The

characterisation of the series in each case has led to differing surface area measurement values. Ni and Co CPO-27 presented no problems with regard to their activation and their adsorption isotherms are comparable with those stated in the literature[1-2]. As can be seen in figure 4.7 both show almost ideal Langmuir behaviour at 77K. Co CPO-27 showed a measured Langmuir surface area of 1060 m^2g^{-1} and a pore volume of 0.39 cm^3g^{-1}, while Ni CPO-27 showed a Langmuir surface area measurement of 1055 m^2g^{-1} and a pore volume of 0.40 cm^3g^{-1}. In the original paper,[2] Dietzel stated that Ni CPO-27 shows a Langmuir surface area of 1083 m^2g^{-1} and a pore volume of 0.41 cm^3g^{-1}. These values match extremely well to the synthesised compounds.

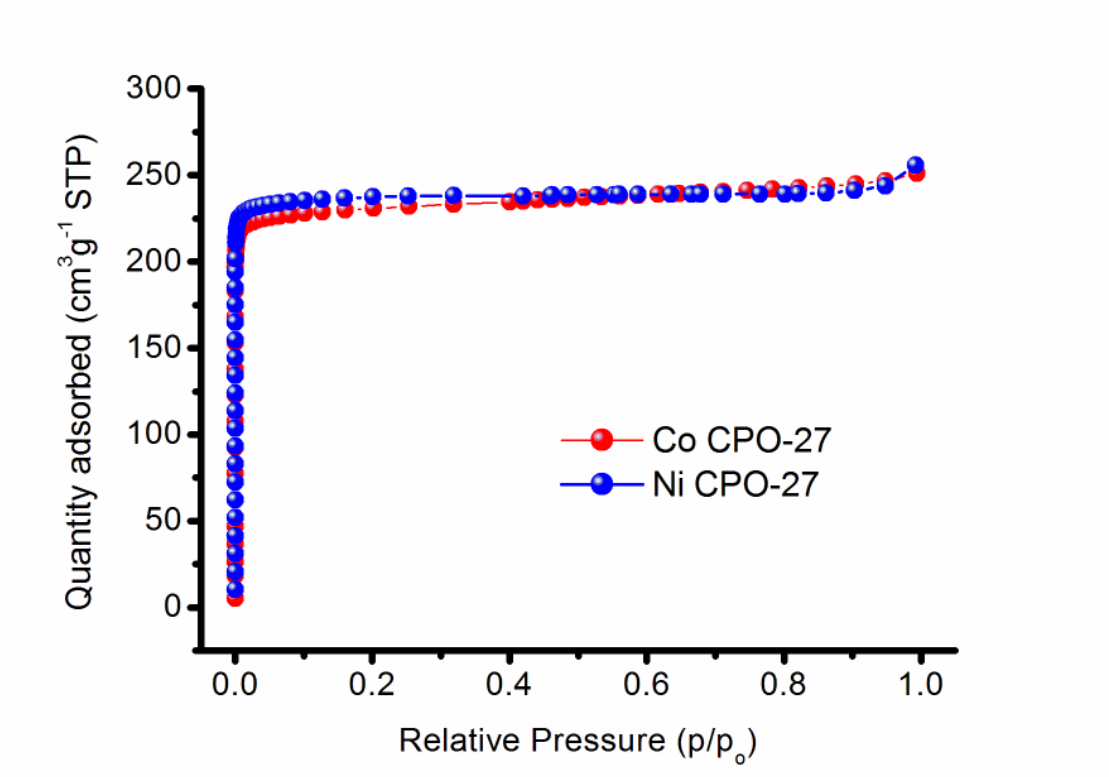

Figure 4.7 Experimental N_2 adsorption isotherm at 77K for Co and Ni CPO-27. Both samples show almost identical Langmuir (Type I) isotherm profiles.

Using the above mentioned characterisation methods it can be deduced that high quality Ni and Co CPO-27 have been successfully synthesised.

4.6 NO adsorption and release using Co and Ni CPO-27

Since originally synthesised, the CPO-27 series of MOFs have attracted significant interest for gas storage not only due to the CUSs available when the framework is activated but also due to their isostructural nature[2,7-8,11-15]. This allows comparisons to be made between different metals and their affinity towards certain gases. As stated in chapter 2, the main goal of this project is to investigate the affinity which MOFs have for NO and their ability to store and release biologically significant amounts of this gas for possible use in medical applications. Using the NO adsorption apparatus available, several NO adsorption isotherms were measured. The MOFs were activated, initially under high vacuum, then using a thermal treatment at 150°C. The initial vacuum activation step removes the guest molecules in the pores, which account for a mass loss of ~29%. The thermal treatment subsequently removes two water molecules per formula unit (a further 7% mass loss) leaving a theoretical 0.0064 mol CUSs per gram of activated material. During this activation process, there is a noticeable and distinct colour change observable for these materials (both turn much darker colours). The materials were then cooled to room temperature and a water bath was used to maintain a constant temperature of 25°C. The activated MOF sample was then exposed to NO. The results for Ni and Co CPO-27 were remarkable. Previous NO studies on MOFs had shown HKUST-1[16] (a porous benzenetricarboxylate-based MOF with open copper sites upon activation) had a NO uptake of 3 $mmolg^{-1}$. Both Ni and Co CPO-27 show NO capacities of between 6 and

7 mmol per gram of activated MOF. This is twice as much as the previous MOF studied and ~5 times greater than the best performing zeolite[17-19]. As can also be seen from the isotherm, the desorption arm shows a very distinct hysteresis, which is indicative of the NO binding strongly to the CUSs. The amount of NO adsorbed is ~1 NO molecule per available CUS. Therefore the maximum adsorption capacity should be 6.4 $mmolg^{-1}$ of NO, however there are extra NO molecules weakly adsorbed (physisorbed) onto the pore walls of the MOF. The actual amount of NO chemisorbed is 4.99 $mmolg^{-1}$ for Co CPO-27 and 5.99 $mmolg^{-1}$ for Ni CPO-27 which is very close to the theoretical maximum of 6.4 $mmolg^{-1}$.

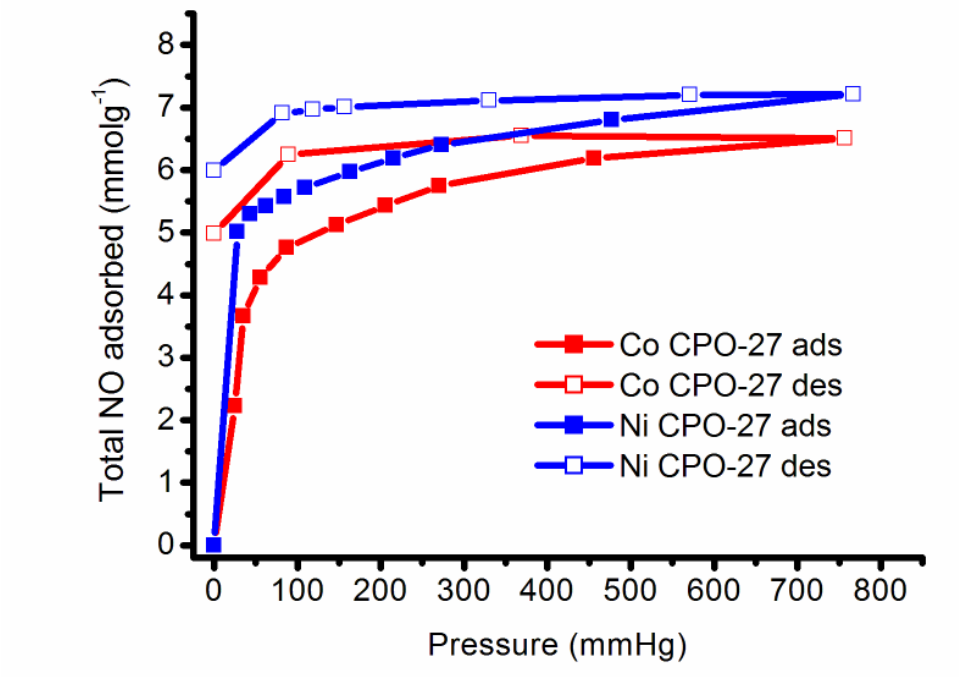

Figure 4.8 NO adsorption/desorption isotherm for Ni and Co CPO-27 at 298K showing the exceptional NO uptake of these MOFs.

This large capacity of NO storage is extremely significant, however it is only useful for potential applications if the gas which has been stored can be recovered. In this

case a very simple trigger is used to start the release of NO from the samples. Water or moisture has a greater affinity for the metal in the MOF and therefore when triggered, the NO gas should be released from the metal and replaced with water molecules.

To investigate the releaseability of NO from pre-loaded MOFs a NO analyser was used. The Ni and Co CPO-27 samples were placed into sealable vials, before being activated in the same manner as mentioned above. This time a Schlenk line and Buchi glass oven were used to produce the necessary vacuum and thermal treatments required to fully activate the compounds. Once activated the samples were cooled to room temperature before being exposed to 2 atmospheres (atms) of NO gas. The activated materials show a distinct colour change when exposed to the NO. The Co CPO-27 (already a much darker colour from the activation step) turns almost black and Ni CPO-27 turns from yellow to a very dark green. In figure 4.9 these colour changes can be seen. This colour change is indicative of the NO interacting with the available CUSs.

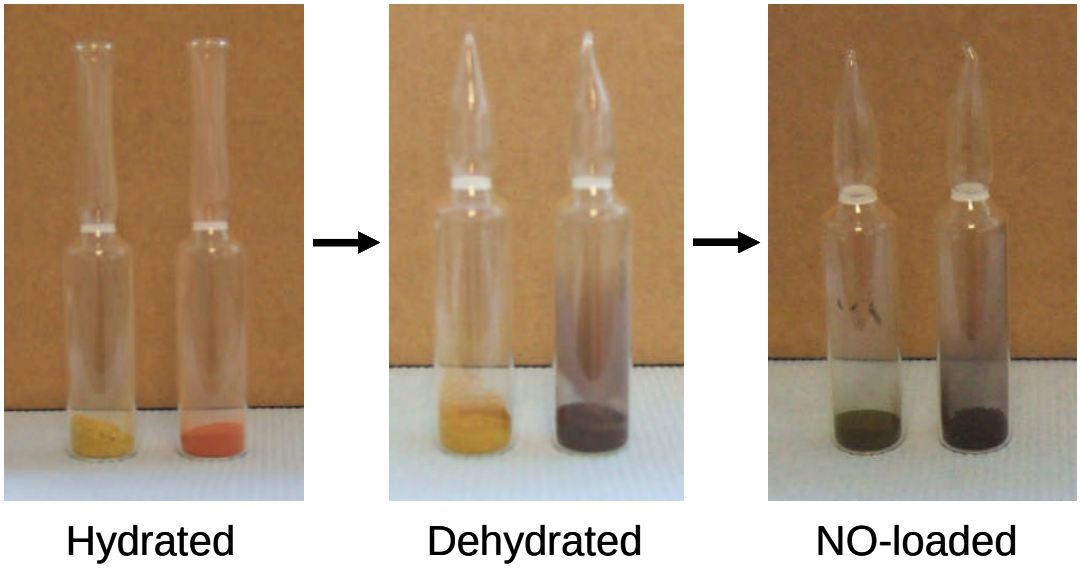

Figure 4.9 Photos of Ni CPO-27 (always on left) and Co CPO-27 (always on right) showing the colour changes when samples are dehydrated and NO-loaded.

Once loaded the vials containing the NO-loaded samples are then flame sealed under an argon atmosphere to ensure no contamination occurs. The experimental set-up for the NO analyser has already been explained in chapter 3. Samples were exposed to a "wet nitrogen" atmosphere (11% relative humidity) and the amount of NO released was recorded. Release profiles for both Ni and Co CPO-27 can be seen in figure 4.10. As shown below the total amount of NO released is ~7 $mmolg^{-1}$, indicating that the entire store of NO has been released. This occurs over ~20 hours. This observation is further evidenced by the fact that the samples placed in the analyser sample holder gradually returned to their original hydrated colours (red for Co CPO-27 and yellow for Ni CPO-27). This release behaviour is in complete contrast to that which occurs in HKUST-1 where only 2 $\mu molg^{-1}$ is released[16].

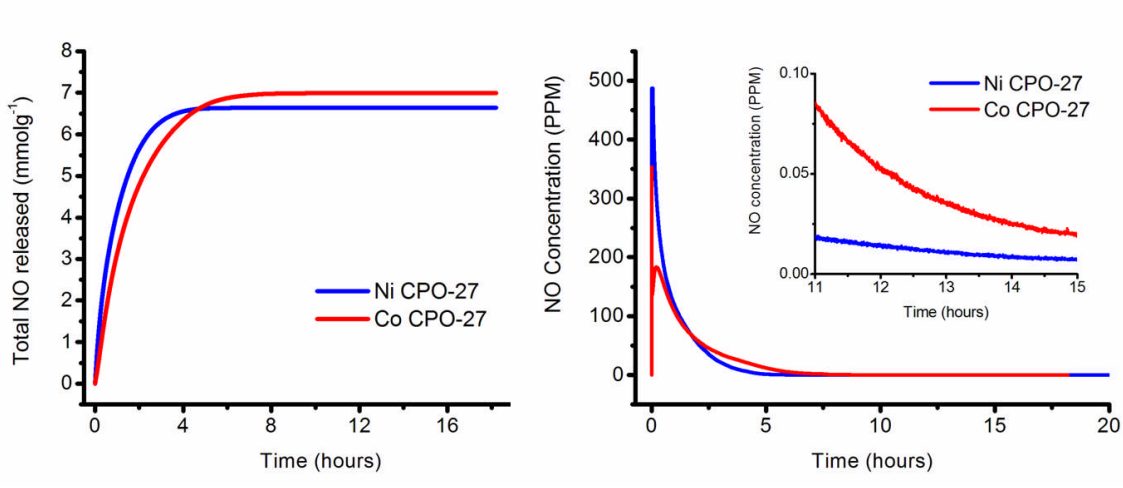

Figure 4.10 Graphs showing the amount of NO released by Ni and Co CPO-27 and the time taken.

The amount of NO released from these materials did not diminish over storage time. Figure 4.11 shows NO release profiles for Co and Ni CPO-27 over several weeks. In each case the amount of NO released is still between 5.75 and 7 $mmolg^{-1}$. In addition to this it is also possible to re-cycle the samples and load them again with NO. This means there is a complete cycle of activation, storage and delivery (see figure 4.12). This is essential for a successful gas storage material. The storage and release of NO from Co and Ni CPO-27 is extremely significant and represents a milestone for the use of MOFs as possible delivery vehicles of biologically active gases for medicinal applications.

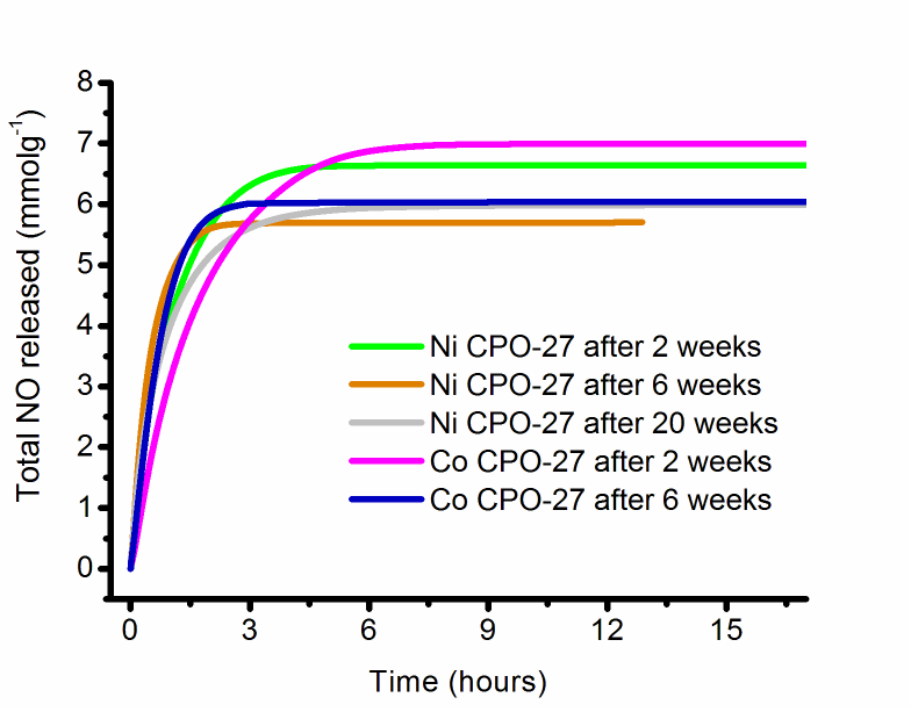

Figure 4.11 Graph showing the release profiles of NO over several weeks of storage for Ni and Co CPO-27.

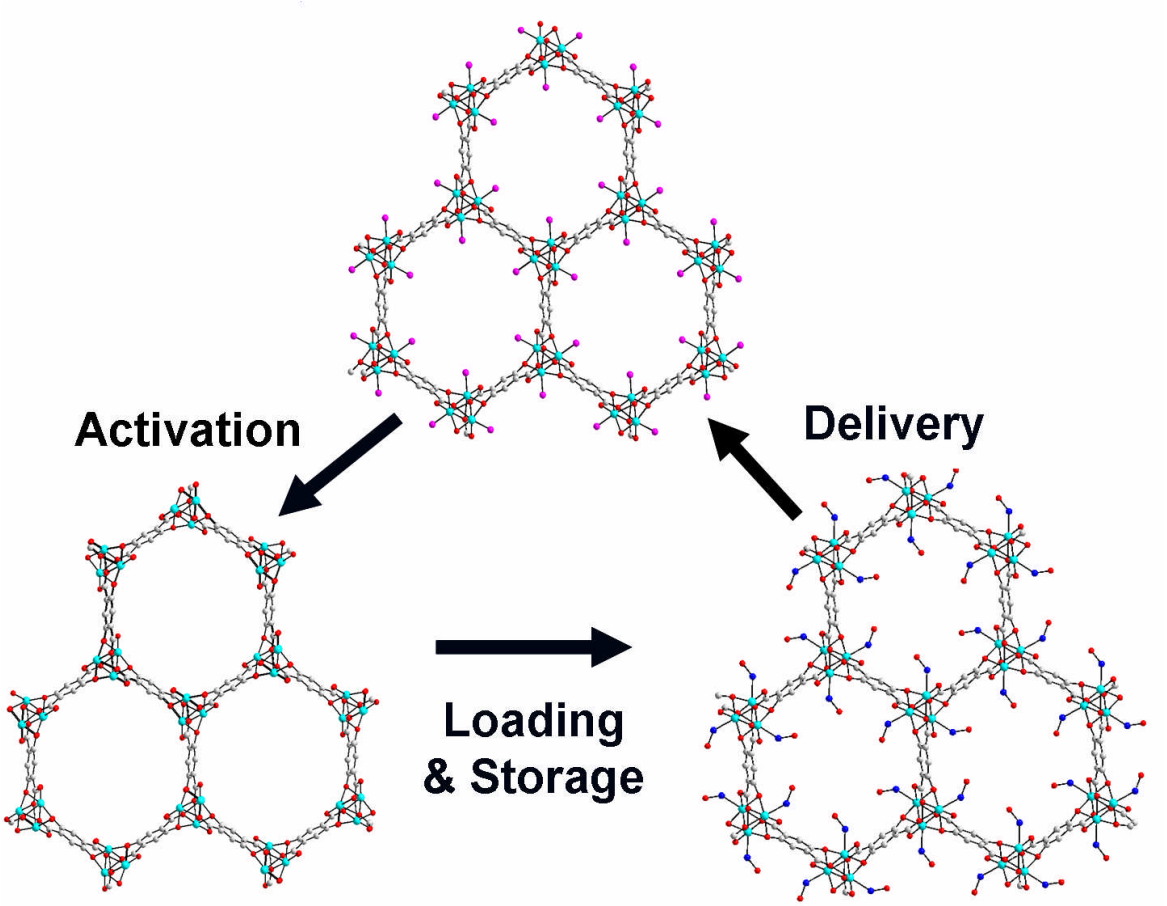

Figure 4.12 The required cycle of activation, loading, storage and delivery for a prospective candidate material suitable for gas storage. The activation stage is extremely important as great care must be taken to ensure all guest solvent molecules are removed to allow all CUSs available for NO binding. Colour key: cyan, Ni/Co; red, oxygen; grey, carbon; pink, oxygen of coordinated water molecules. The hydrogen atoms and uncoordinated water molecules have been omitted for clarity.

4.7 Rietveld refinement of NO-loaded M-CPO-27

In order to confirm that the NO gas was indeed chemically binding to the free metal site, powder X-ray diffraction was carried out on the as-synthesised (hydrated), dehydrated and NO-loaded Ni CPO-27. Confirmation of the NO binding to the available metal site has also been confirmed using in-situ IR studies[20]. Initially, the Co CPO-27 analogue crystal structure had been solved by Dr David Wragg using the dehydrated structure as a base model[14]. The NO atoms were located using Fourier maps and included in the refinement. The final refinement converged to R_{wp} = 0.0784, R_p = 0.0582 and $R(F^2)$ = 0.2166. Figure 4.13 shows a pore with the NO loaded onto the cobalt atom. The atom positions, bond lengths and the NO binding to the Co atoms can be seen in the enlarged view on the right. The NO is bound in a bent fashion, a phenomenon which has already been observed in NO-loaded cobalt zeolites[21].

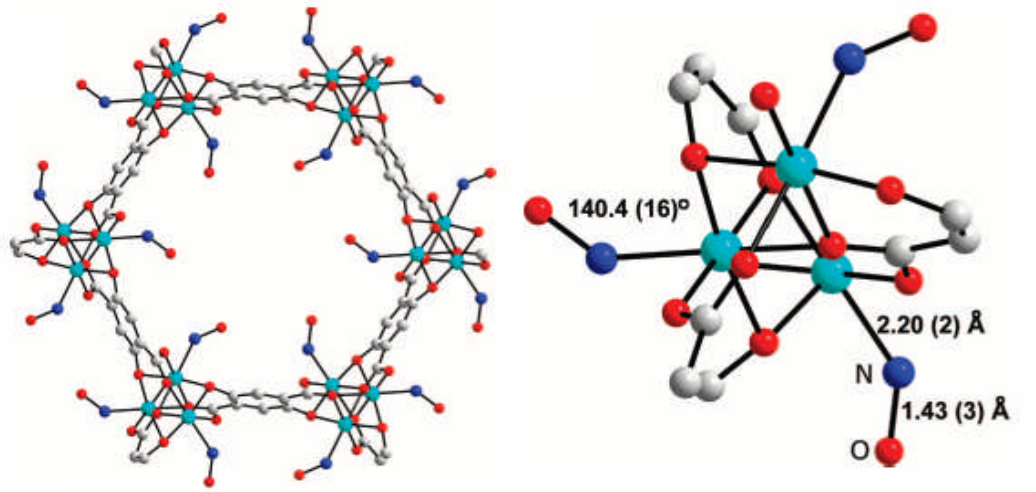

Figure 4.13 A view of the pore of Co CPO-27 with the NO loaded onto the free Co CUSs. On the right is an enlarged view showing the bent nature of the NO molecule together with the bond angle and lengths.

Using the NO-loaded Co CPO-27 model, further calculations were carried out on Ni CPO-27 to prove that the NO binds in a bent fashion to the nickel atom of this framework. The NO-loaded version of Ni CPO-27 was sealed in a capillary and run overnight on the STOE diffractometer. Following a successful run, the pattern produced was used in the refinement process and compared with the Co analogue result. The atom positions were kept fixed and the final refinement pattern can be seen in figure 4.14. The NO-loaded version had values of R_{wp} = 0.2199, $R(F^2)$ = 0.1944 and R_p = 0.1573. The final parameters can be viewed in figure 4.15. These values are consistent with the NO molecule binding to the open metal site in a bent fashion as already noted in Co zeolites[21] and Co-CPO-27[14] and this can be seen in figure 4.16. The quality of the diffraction is not the highest and further work is required using a synchrotron source (single crystal diffraction) to be more definitive. To show that the NO binds in a bent fashion, the oxygen atom was moved to form a linear M-NO bond and the final values were as follows R_{wp} = 0.2759, $R(F^2)$ = 0.2815 and R_p = 0.1920 showing that the bent NO binding is most likely. To fully confirm this, the refinement was carried out without the NO atoms and the final values were R_{wp} = 0.3717, $R(F^2)$ = 0.4121 and R_p = 0.2863.

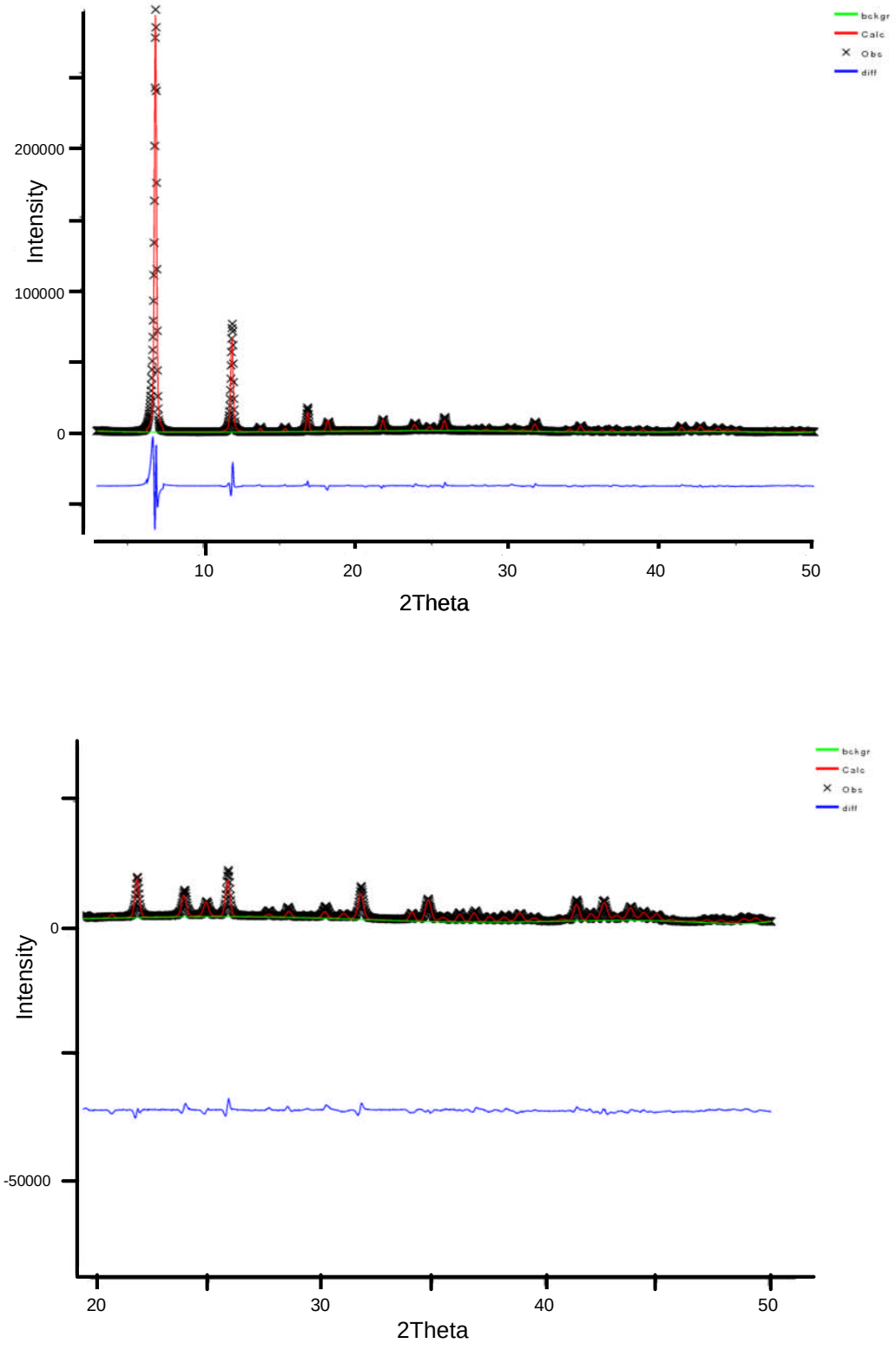

Figure 4.14 The final Rietveld patterns for the NO-loaded version of Ni CPO-27. Top shows the overall pattern. Bottom figure shows an enlargement of the 20° to 50° degree region.

space group: R-3			
a = b = 25.8063 (19)		c = 6.7188 (13)	
α = β = 90°		γ = 120°	
	Fractional coordinates		
atom	x	y	z
Ni1	0.36687	0.04968	1.01840
C1	0.24600	-0.07060	1.07670
C2	0.20720	-0.11990	1.21360
C3	0.22180	-0.12260	1.41560
C4	0.15350	-0.16390	1.13840
H3	0.14520	-0.16180	1.00490
O1	0.29400	-0.02700	1.14750
O2	0.22830	-0.06510	0.91810
O3	0.27620	-0.08820	1.50230
N1	0.44530	0.13430	0.93000
O1N	0.50740	0.15880	0.88610

Figure 4.15 Table of final parameters for the NO-loaded Ni CPO-27.

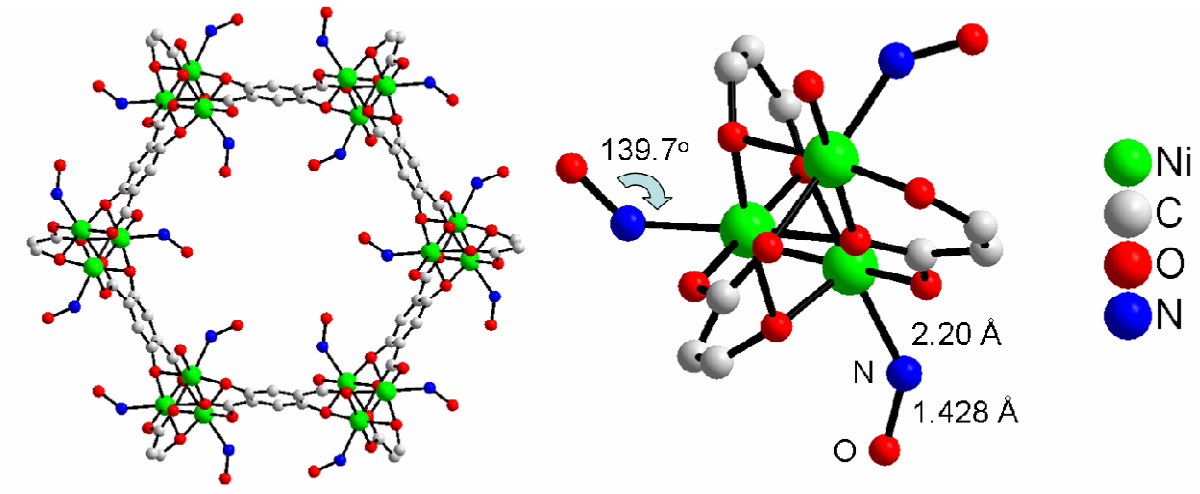

Figure 4.16 A view of the Ni CPO-27 pore. On the right is an enlarged view of the coordination of the NO to the Ni metal which is the same as in the Co version.

4.8 Results on Zn, Mg and Mn CPO-27

Following the significant results obtained from Ni and Co CPO-27 showing their exceptional storage and release properties for NO, other versions of M-CPO-27 were subsequently synthesised. This was particularly prompted as one of the major drawbacks of Ni and Co CPO-27 for use as delivery vehicles is that cobalt and nickel toxicology is well known and not beneficial. However, Zn, Mg and even Mn are much less toxic metals for humans and so a MOF composed of such metals would be of great interest if they could perform to the same standard. The materials were synthesised according to the methods described in the literature. In the case of Zn and Mg CPO-27, two hydrothermal methods were used for each[4-7]. One required solvent exchange of the materials prior to any porosity experiments being carried out[4,7] but the second did not require this step[5,6]. The materials were successfully synthesised and characterised using powder XRD, TGA, N_2 and NO adsorption and release measurements. All XRD patterns were carried out on the STOE diffractometer with the exception of Mn CPO-27 which displayed a large fluorescence. In this case the Phillips diffractometer was employed.

4.8.1 Zn CPO-27

Zn CPO-27 was originally synthesised by Yaghi and co-workers using dimethylformamide (DMF) as the solvent in the reaction[3-4]. It was then solvent exchanged with methanol (a solvent with a lower boiling point) to aid in the activation process. Dietzel and co-workers managed to synthesise this phase, using a similar method to that utilised in the formation of the Co and Ni analogues, only adding base (NaOH 1 molL^{-1}) to ensure deprotonation of the linker. A sample of this was kindly donated by the Sintef group in Norway for investigation. Figure 4.17 shows the XRD patterns for the solvent exchanged Zn CPO-27 and as-synthesised Sintef Zn CPO-27 (Dietzel's sample).

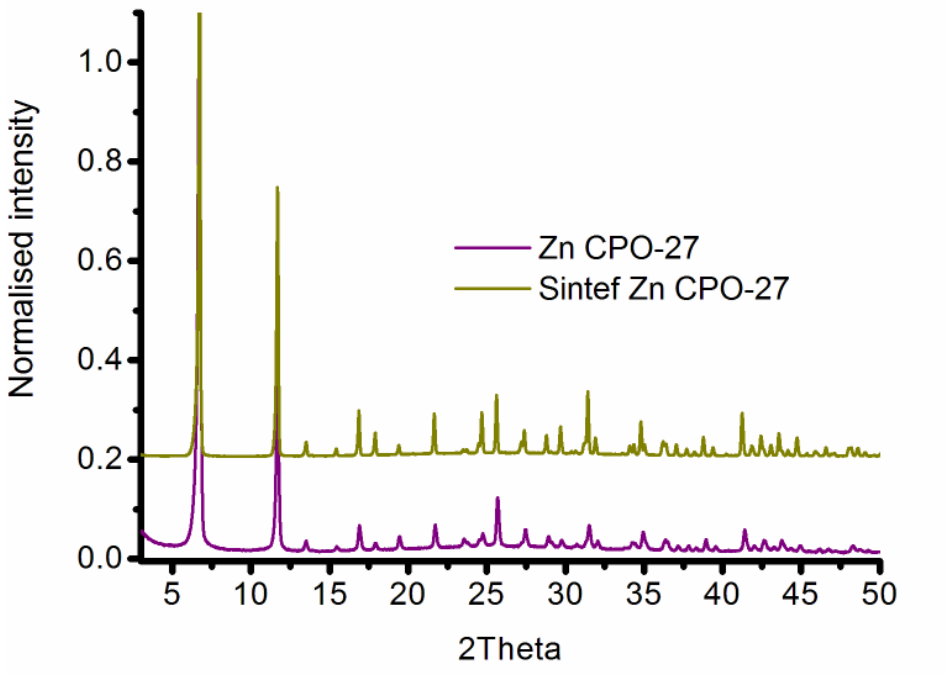

Figure 4.17 Powder XRD patterns of solvent-exchanged Zn CPO-27 and as-synthesised Sintef Zn CPO-27.

However the TGA curves for the Zn CPO-27 samples show distinct differences (figure 4.18). With the Sintef sample the solvent located in the pores is water, whereas with the Zn CPO-27 it is initially DMF. This explains why the TGA curve shows only a small drop in mass between 50 and 150°C.

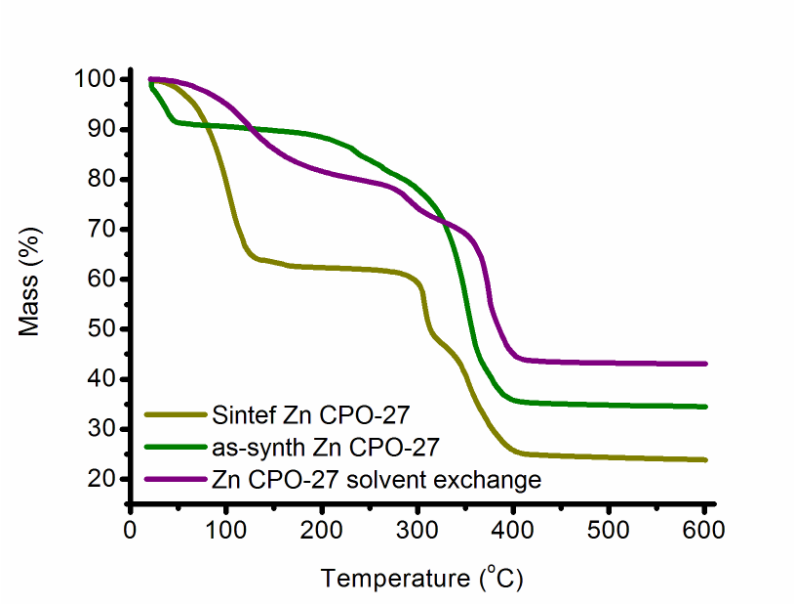

Figure 4.18 TGA curves for the various versions of Zn CPO-27. The DMF version shows no large initial drop in mass and even after solvent exchange it still does not lose the appropriate mass of solvent.

Even after solvent exchange procedures have been carried out using methanol, it still only shows a small drop in mass at the appropriate region. This shows that the Zn CPO-27 sample is extremely difficult to fully solvent exchange and even harder to activate. This was highlighted by Yaghi in his initial paper concerning Zn CPO-27[3]. The Sintef version of Zn CPO-27 has also been shown to have problems with activation as it goes through several structural transformations before being fully evacuated[5] and this puts great strain on the structure. Therefore, it is not unexpected that the N_2 adsorption results were much lower than the theoretical surface areas. The surface area obtained by Yaghi initially, when solvent exchanging with water[3], was

245 m^2g^{-1}. This was subsequently improved to 1132 m^2g^{-1} using methanol and a higher temperature for activation[4]. The N_2 results obtained on the samples showed varied and low surface areas. Surface area measurements were carried out on the solvent exchanged Zn CPO-27 only. One batch produced a Langmuir surface area of 379 m^2g^{-1} and another 548 m^2g^{-1}. There are obviously problems with the activation of this compound in the N_2 adsorption equipment.

Despite these problems, NO measurements were still taken. Figure 4.19 shows the NO adsorption isotherms for both solvent-exchanged Zn CPO-27 and Sintef Zn CPO-27. As can be observed, there is no sharp initial uptake as seen with the Ni and Co versions, however both still show remarkable NO capacity, particularly the solvent-exchanged Zn CPO-27 which displays an uptake of ~6 $mmolg^{-1}$. Both samples still exhibit a large hysteresis indicating that CUSs were available to bind to and so the materials must have been at least partially activated.

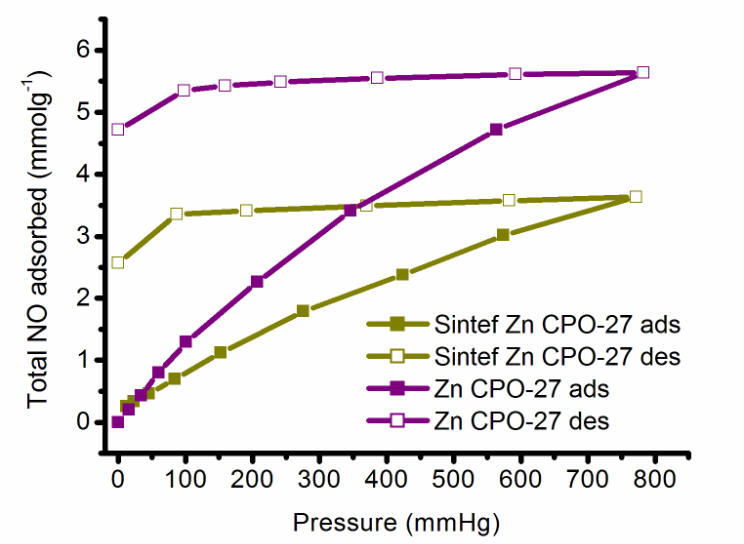

Figure 4.19 NO adsorption isotherm at 298K for both samples of Zn CPO-27. There is obviously still chemisorption occurring, however they do not show the huge initial uptake behaviour exhibited by Ni and Co CPO-27.

The next logical step was to carry out release measurements on both samples of Zn CPO-27. The total release of NO from both zinc compounds is poor in comparison with the Ni and Co versions. The amount released from the Sintef Zn CPO-27 only averaged 0.12 $mmolg^{-1}$ and the Zn CPO-27 only averaged 0.18 $mmolg^{-1}$ (both averaged over 4 samples). These results can be seen in figure 4.20.

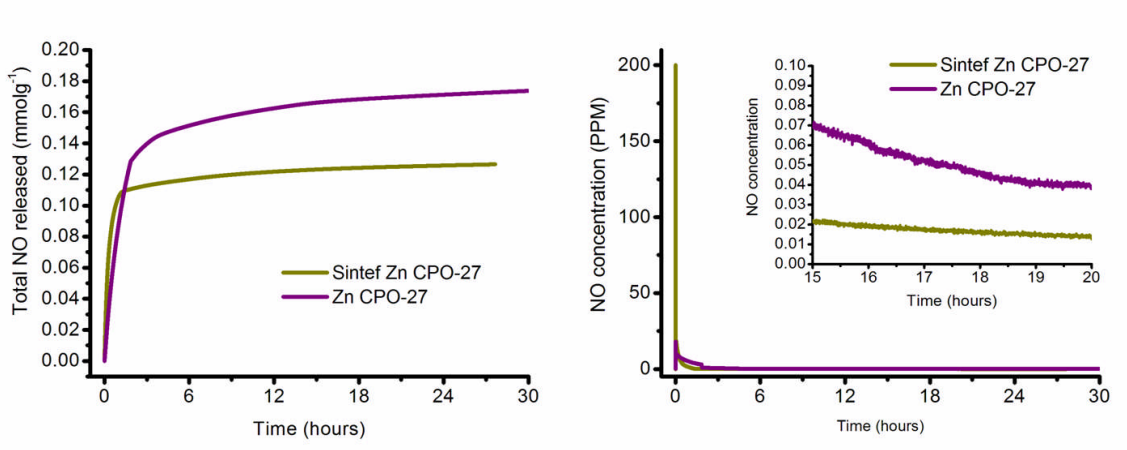

Figure 4.20 NO release curves for both samples of Zn CPO-27 showing that only a small amount of the total NO adsorbed is released.

Both samples however, are still releasing biologically significant amounts of NO up to 20 hours after starting the experiment. The amount of NO required to be considered biologically significant varies depending upon which application and indeed which organ of the body is to be targeted. Indeed, HKUST-1 only releases 2 $\mu molg^{-1}$, but this is still considered to be of biological significance, as it was shown that platelet aggregation is prevented using only this small amount of NO[16].

Due to the low NO release values obtained, methods were used to try and improve the total NO released by Zn CPO-27. It was thought that an increase in temperature would result in more of the adsorbed NO being released. Therefore a water circulator system was used in combination with a sample holder utilising a water bath function. Two elevated temperatures were adopted (50°C and 80°C), as well as a comparison with the room temperature release.

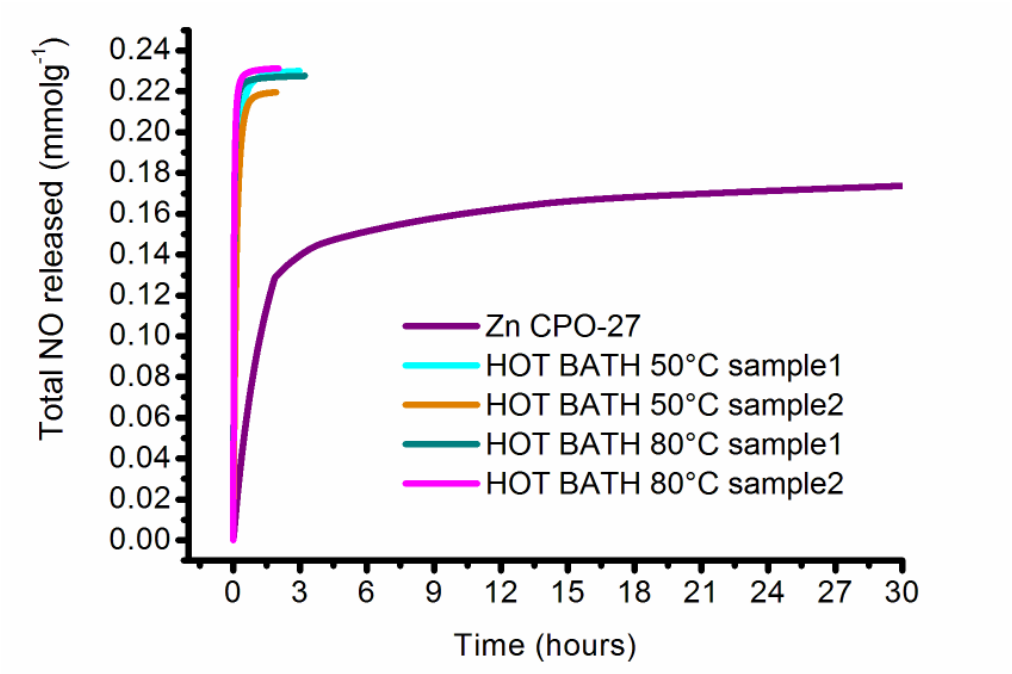

Figure 4.21 Comparison of the hot water bath experiments with the room temperature release of NO from Zn CPO-27.

As can be seen, there is a slight increase in total NO released, however all the experiments run to completion after about 4 hours. This is not unexpected, as an increase in temperature should promote the replacement of NO with water quicker than at room temperature. Another method employed involved using a UV lamp pointed directly at the sample holder during the experiment. It was thought that UV

light might act as a catalyst for cleaving the M-NO bond. However there was no noticeable difference in the release data acquired. The results demonstrate that Zn CPO-27 does not act in the almost ideal fashion that Ni and Co CPO-27 perform. However, due to the minimal toxicological effects of Zn compared to the two aforementioned metals, it is still of interest for potential biological applications.

4.8.2 Mg CPO-27

The Mg form of CPO-27 was also synthesised in two different ways. For comparative purposes both Mg versions were synthesised. To clarify, Sintef Mg CPO-27 is the version made using Dietzel's method[6] and Mg CPO-27 is produced using the method of Caskey and co-workers[7]. The first method (from the work of Sintef[6]) was similar to those used for the Ni and Co versions (utilising THF as the solvent and 110°C as the reaction temperature). Some base was added to ensure full deprotonation of the linker[6]. The second procedure combined a solvent mixture of DMF, ethanol, and water in a 15:1:1 ratio and a reaction temperature of 125°C. Following initial synthesis, solvent exchange procedures were then used to exchange the DMF molecules for methanol[7]. Powder XRD patterns for both versions (Sintef and the solvent-exchanged Mg CPO-27) can be seen in figure 4.22 and show that both match the theoretical XRD pattern extremely well.

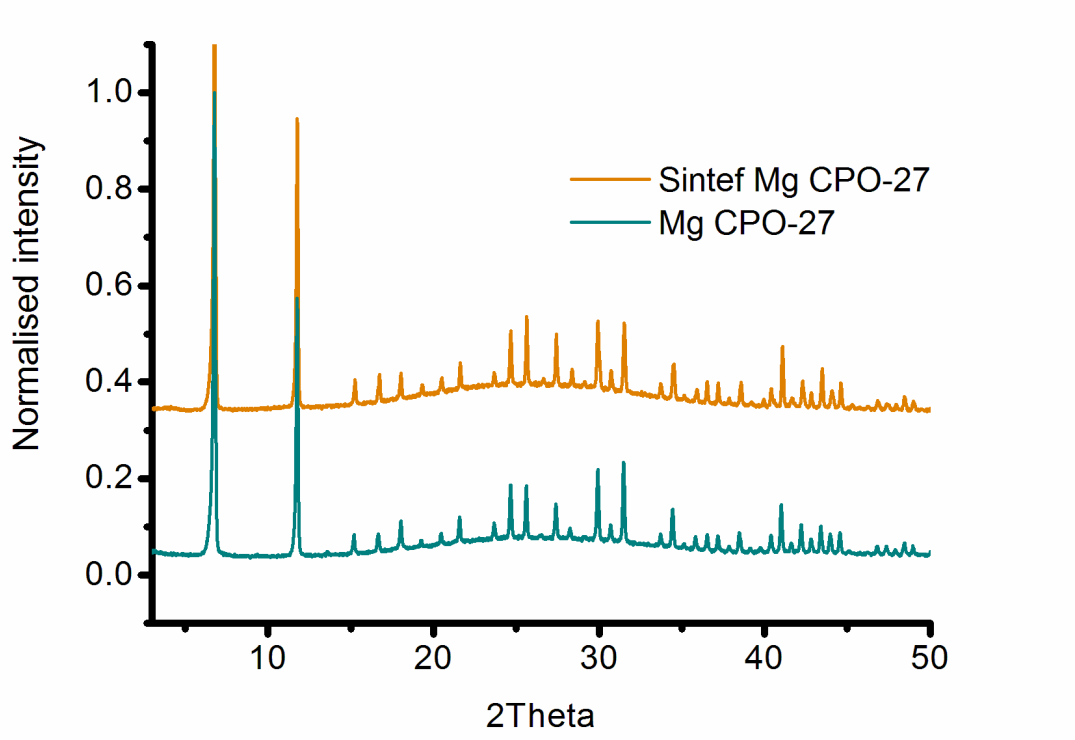

Figure 4.22 Normalised powder XRD pattern for both synthesised samples of Mg CPO-27.

Observation shows that they are almost identical, indicating that both synthetic methods produce highly crystalline Mg CPO-27. Following the solvent exchange process TGA measurements were taken on both the Sintef Mg CPO-27 and the solvent exchanged Mg CPO-27. Figure 4.23 shows the TGA curves for both samples. Interestingly both of the graphs are very similar indicating that the solvent exchange process was much more successful compared with that on Zn CPO-27. Both show large drops in mass (~30%) up to the activation temperature for this version (250°C)

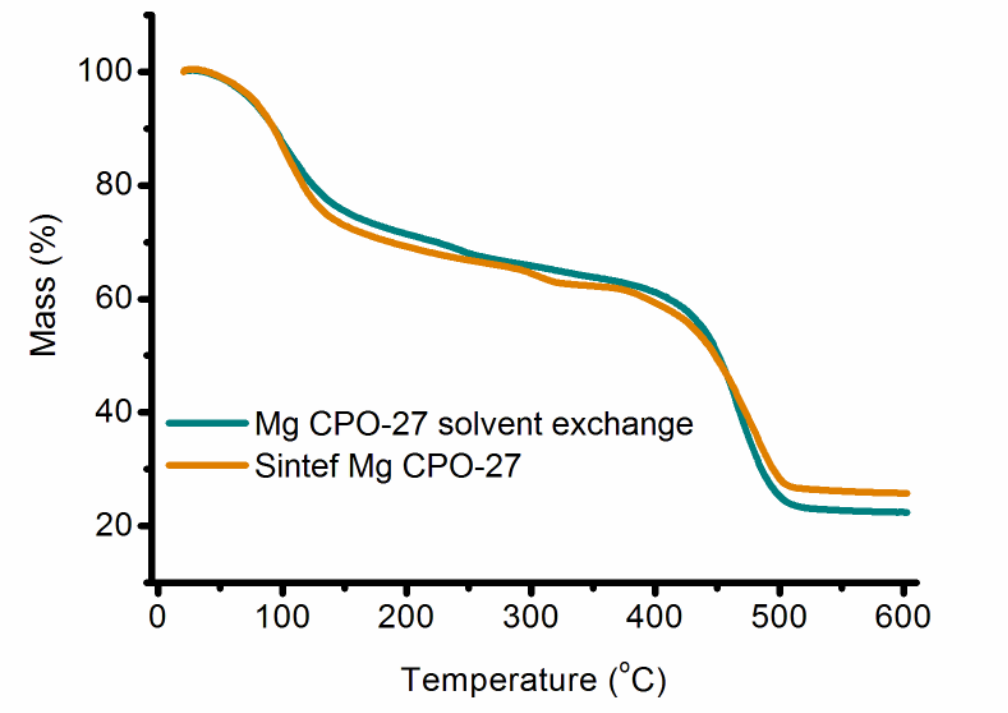

Figure 4.23 TGA curves of both types of Mg CPO-27 including the pre and post solvent exchanged samples.

Once again there are problems with regard to full activation of these MOFs. Dietzel and co-workers obtained Langmuir surface areas ranging from 150-1030 m^2g^{-1}. They tried a series of different pre-treatments and activation temperatures and could only make some generalisations regarding the activation of the material. These were firstly that a higher activation temperature is required for the Mg analogue compared with the Ni and Co versions (up to 250°C compared with just 110-150°C for the Ni and Co structures). Secondly that pre-treatment of this compound is required to give even mediocre surface areas. In the case of the Caskey synthesis, no mention is made of problems regarding activation of their Mg CPO-27, although solvent exchange methods have already been shown to be unreliable[3]. N_2 adsorption isotherms were carried out on both versions of Mg CPO-27. Mg CPO-27 shows a Langmuir surface

area of 203 m^2g^{-1}, which is much lower than the reported 1905 m^2g^{-1}. The Sintef Mg CPO-27 showed a surface area of only 138 m^2g^{-1}. Both these values are very low compared with those published. However, in the paper the Sintef version which performed best had to be kept under an inert atmosphere for two weeks and included a solvent exchange before the measurements were carried out. It is believed that the ineffective activation of these compounds is responsible for the resulting low surface areas. However in the NO adsorption apparatus, the results were much more promising.

The theoretical adsorption of NO by the Mg version of CPO-27 is 8.2 $mmolg^{-1}$, assuming that one NO molecule attaches to one available CUS. The results for NO adsorption of both versions of Mg CPO-27 can be viewed in figure 4.24.

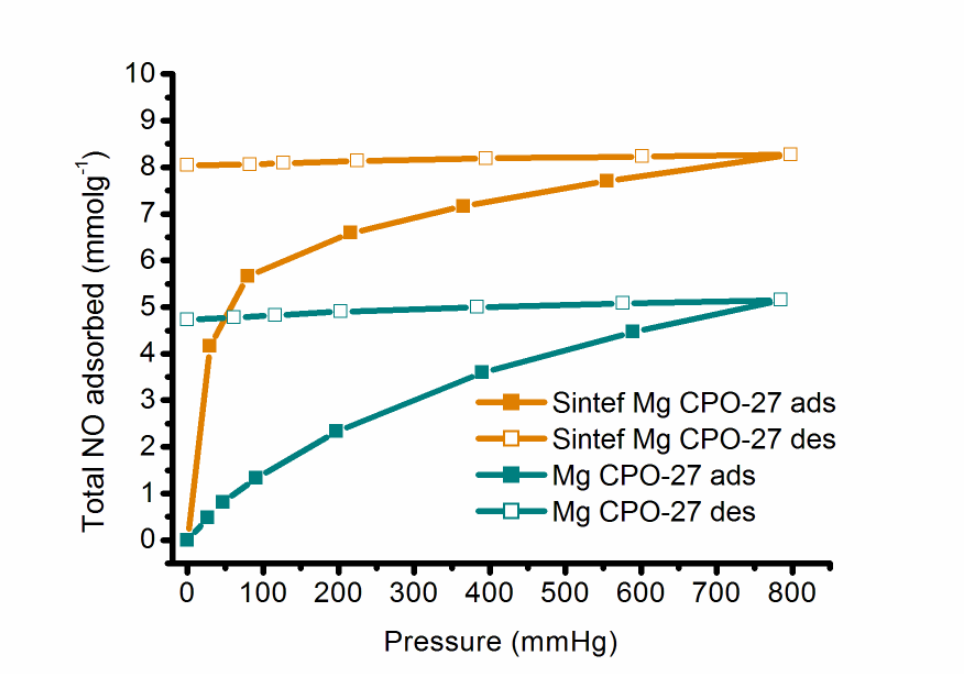

Figure 4.24 NO adsorption isotherm for different versions of the Mg CPO-27 analogue carried out at 298K. The Sintef version almost reaches the theoretical adsorption for NO.

It is noteworthy that the Sintef Mg CPO-27 almost reaches the theoretical amount, indicating that the vast majority of the CUSs must have been available to bind to. It also displays a much higher uptake at low pressures of NO compared with the Zn CPO-27 versions mentioned previously. These high NO adsorption results are in contrast with the low N_2 adsorption results which showed poor adsorption. The Caskey synthesised Mg CPO-27 adsorbs ~5 $mmolg^{-1}$ of NO which, is less than theoretically expected. This could be explained by ineffective solvent exchange or improper activation procedures. Nonetheless the Sintef Mg CPO-27 shows the highest NO adsorption of any porous material tested to date. The NO release results were comparable with those of the Zn analogues, whereby only a fraction of the NO adsorbed was actually quantifiably released. The release curves can be seen in figure 4.25.

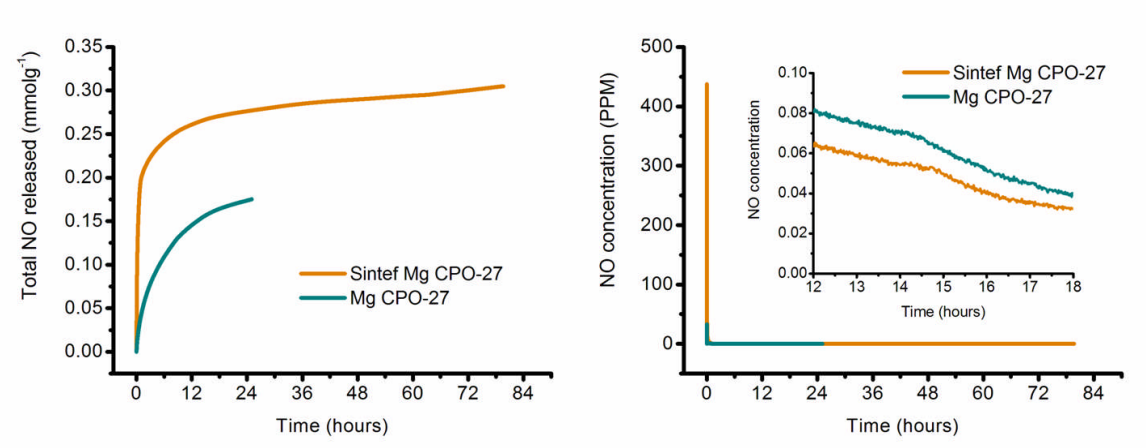

Figure 4.25 NO release curves for both versions of the Mg CPO-27 analogue. Both show much lower amounts released than initially adsorbed.

The Sintef analogue showed a much more promising total NO release compared with the Mg CPO-27, however both were still releasing significant amounts of NO up to 20 hours after the experiment began.

4.8.3 Mn CPO-27

The final analogue synthesised was the Mn version. So far there has only been one synthetic procedure published for creating this analogue of the CPO-27 series. It follows a similar method to the Mg CPO-27, utilising a 15:1:1 ratio of DMF, ethanol and water and a slightly higher reaction temperature of 135°C. Once again, solvent exchange with methanol is required to enable this MOF to be used for porosity measurements. The MOF was successfully synthesised and characterised using powder XRD and TGA measurements. Figure 4.26 shows both the experimental XRD pattern and TGA curve obtained for Mn CPO-27.

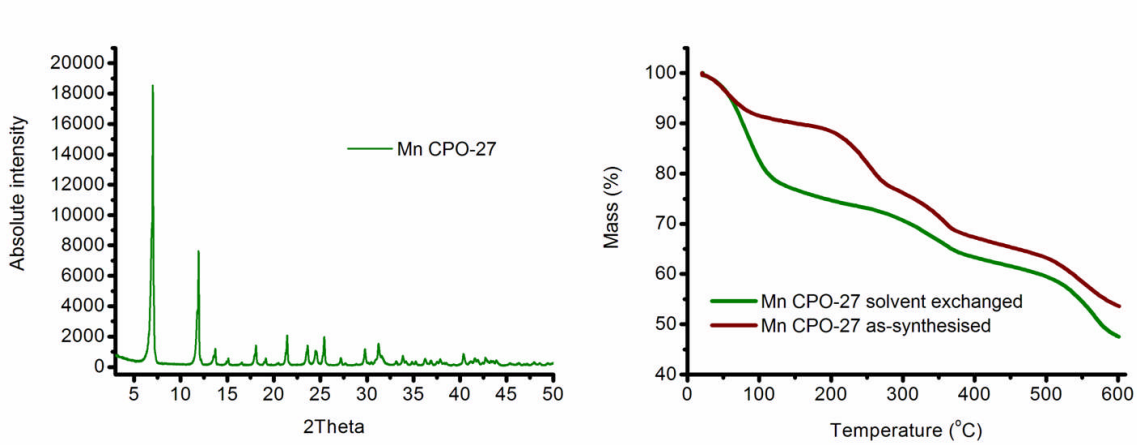

Figure 4.26 Experimental powder XRD and TGA curves for Mn CPO-27. The XRD pattern matches very well with the literature based synthesis. Note the difference between the TGA curves before and after solvent exchange with methanol.

The TGA curves show distinct differences. This can be attributed to the solvent exchange process. DMF molecules are exchanged with methanol over the course of several days, with the removal and addition of fresh methanol every day. Methanol has a lower boiling point and therefore is removed very easily from the pores

compared with DMF. The main difference is noticeable in the first mass drop between 50 and 200°C, where the solvent exchanged sample shows a mass loss of 25% compared with just 12% for the as-synthesised sample.

Despite the encouraging results from the TGA curve, the Mn CPO-27 illustrates no noticeable adsorption of N_2 which again is in contrast with the results stated in the literature[16]. This apparent lack of available porosity can be attributed to the solvent exchange process. It could be possible that during the exchange process, some of the pore walls are destroyed by the removal of DMF and the insertion of methanol.

Finally the NO results were once again undertaken despite the lack of apparent surface area. Figure 4.27 shows the NO adsorption isotherm for Mn CPO-27.

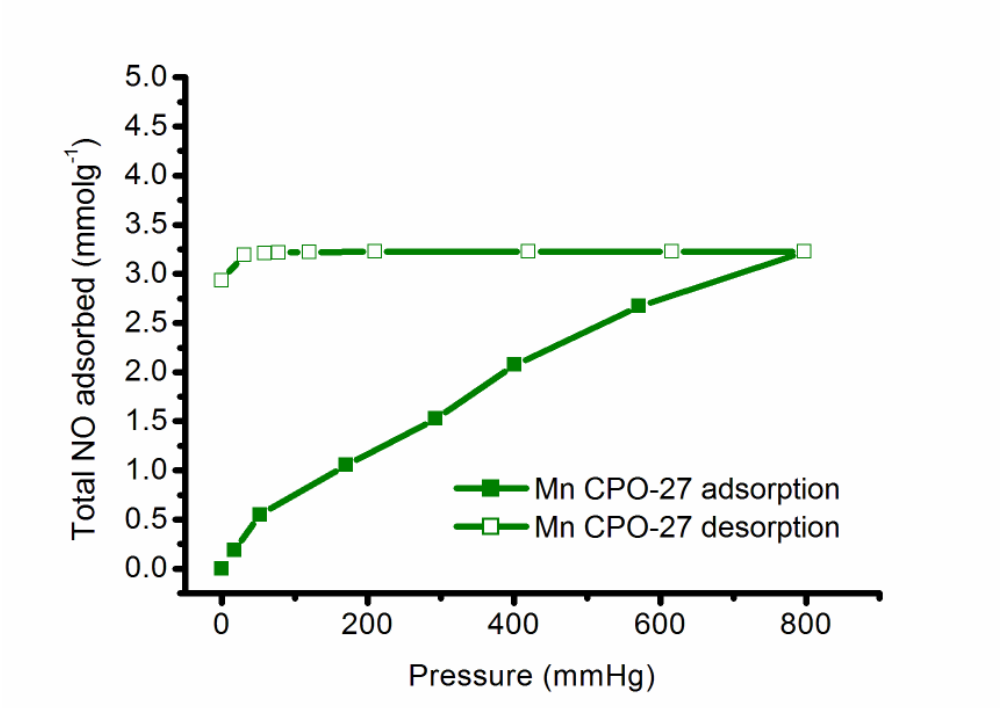

Figure 4.27 NO adsorption isotherm for Mn CPO-27 carried out at 298K.

This is very similar to the Zn CPO-27 graphs where there is no immediate uptake of NO and the amount adsorbed is not as high as the Ni and Co analogues. However, over 3 $mmolg^{-1}$ is adsorbed and again is a significant amount and comparable with that of HKUST-1[17]. The NO release profiles once again follow the same pattern as the Zn and Mg analogues where only a small percentage of the amount of NO actually adsorbed is fully released. Figure 4.28 displays the release profiles for Mn CPO-27.

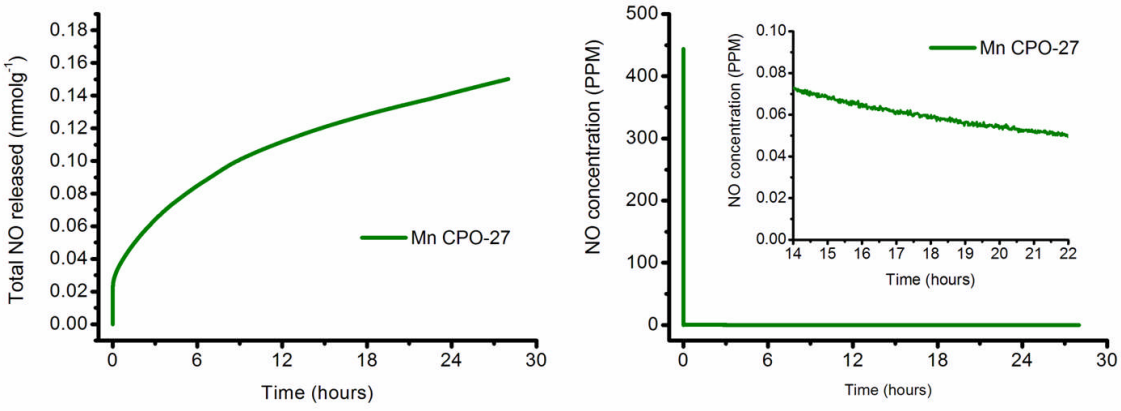

Figure 4.28 NO release profiles for Mn CPO-27. Biologically significant amounts of NO are still being released after 20 hours, but the total released is only a fraction of the amount actually adsorbed.

4.9 Alternative synthetic routes to produce M-CPO-27

Following the important results shown by the M-CPO-27 series and their NO adsorption and release, efforts were made at alternative synthetic methods to produce these frameworks. For any application, a synthesis which requires 72 hours heating time in an oven before usage is inefficient. As explained in chapter 1 microwave synthesis has recently come to the forefront as a method of creating MOF phases in exceedingly quick times and has even been shown to produce materials that are more crystalline than their solvothermal counterparts[22]. Further to this, being able to produce MOFs at room temperature by simply mixing reactants together and stirring would be much easier and less harmful to the environment, depending on the solvents employed.

4.9.1 Microwave synthesis of Ni and Co CPO-27

The utilisation of microwave synthesis has so far yielded several world famous MOFs including MOF-5[23-24] and MILs-100 and 101[25-27]. The method employed here was to use the existing reagent concentrations, but instead of solvothermally heating for 72 hours, microwaves would be employed. The table shown in figure 4.29 details the concentrations of the various reagents and the conditions used in the microwave synthesis.

MOF	Vial size	M acetate used (g)	DHTP used (g)	Metal:ligand ratio	pretreatment	main reaction
Ni CPO-27 1 min	6ml	0.3733	0.149	2:1	5 mins at 60°C	1 min at 110°C
Ni CPO-27 1 hour	6ml	0.3733	0.149	2:1	10 mins at 60°C	1 hour at 110°C
Co CPO-27	6ml	0.384	0.149	2:1	10 mins at 60°C	1 hour at 110°C

Figure 4.29 Table detailing the reaction conditions used in the microwave synthesis of Ni and Co CPO-27.

The procedure from the most recent synthesis of Ni CPO-27 was utilised[11]. Using calculated amounts of reactants each phase formed with no impurities. This is the first time that this framework has been formed using microwave synthesis. Initial experiments lasted 1 hour and the powder XRD patterns proved that both Ni and Co CPO-27 were successfully synthesised. Following this initial success, it was decided to see how quickly the Ni CPO-27 compound could be produced. The results were very impressive. It is possible to form the Ni CPO-27 framework after only 1 minute of microwave heating at 110°C. Figure 4.30 shows the 1 hour micro Ni CPO-27 and the 1 min micro Ni CPO-27 experimental powder XRD patterns. The TGA curves for each MOF are also shown. These match extremely well to the hydrothermally synthesised versions. A comparison is also made with the hydrothermally produced version. It is noticeable from the XRD results, however, that the full width at half maximum (FWHM) value is much larger for the microwave synthesised compounds indicating that the particle size is smaller. Using the Scherrer equation[28] (4.1) the particle size (τ) for each Ni CPO-27 version was estimated.

$$\tau = \frac{K\lambda}{\beta \cos\theta} \tag{4.1}$$

The particle size is calculated using a constant K, wavelength (λ) and uses the full width at half maximum (β) and the Bragg angle (θ) in radians. Using this equation the particle size for the hydrothermally synthesised version was estimated to be at least 1123 nm and 353 nm for the microwave synthesised version.

This result is not unexpected as it has been observed before in microwave synthesised MOFs[25]. Following this, scanning electron microscopy (SEM) images were taken of both the hydrothermally synthesised Ni CPO-27 and the microwave synthesised version. From these it can be seen that the hydrothermal synthesis gives particle sizes of about 4μm whereas the microwave synthesis yields particles of about 1μm. The SEM images are shown in figure 4.31.

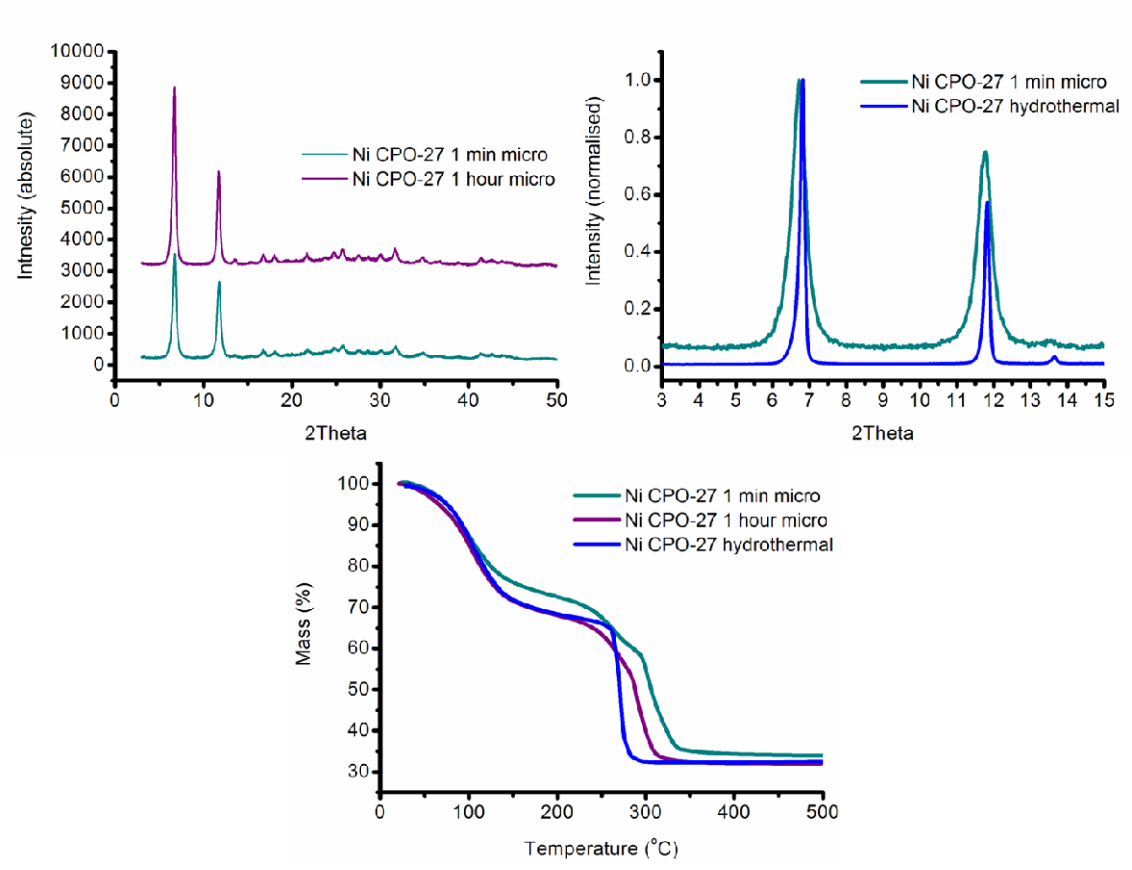

Figure 4.30 Top left, experimental XRD curves for both microwave synthesised versions of Ni CPO-27. Top right, a comparison with the hydrothermally produced Ni CPO-27 shows broader peaks indicative of smaller particle size. Bottom picture shows the TGA curves of both microwave versions and a comparison with the hydrothermally produced Ni CPO-27.

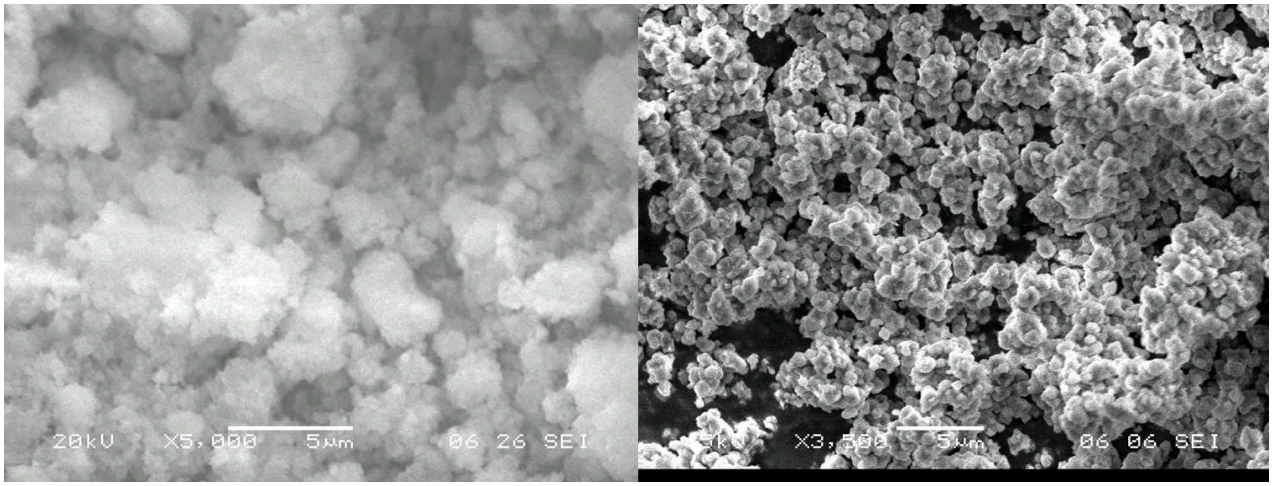

Figure 4.31 SEM images of both versions of Ni CPO-27. On the left is the hydrothermal version showing a particle size of ~4µm and the right shows the 1 min micro version with particle size of ~1µm.

Comparisons between the hydrothermally produced MOF and the microwave synthesised framework were then made. Initially the N_2 adsorption capacity and surface area measurements for each Ni version were taken. Figure 4.32 shows the adsorption isotherms for each of the three materials; the hydrothermal Ni CPO-27, the 1 hour microwave synthesised Ni CPO-27 and the 1 minute microwave synthesised Ni CPO-27.

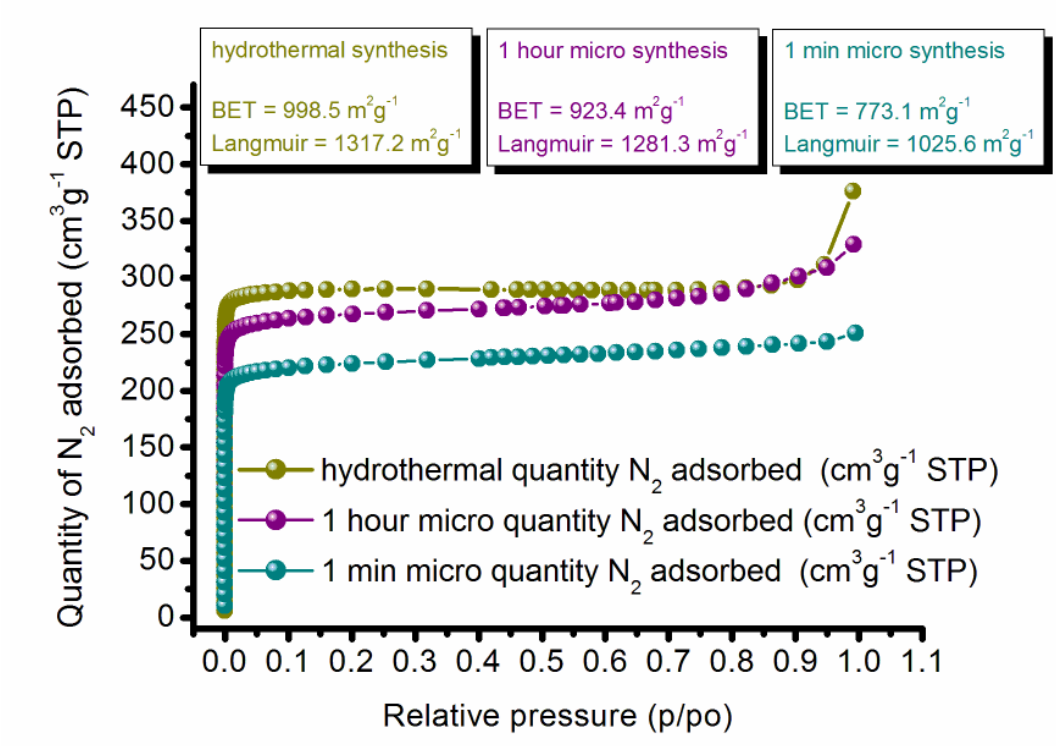

Figure 4.32 N_2 adsorption isotherms comparing the microwave synthesised Ni CPO-27 with the traditional hydrothermally produced Ni CPO-27. All experiments were carried out at 77K.

As can be seen there are slight differences between the microwave synthesised samples and the hydrothermally produced Ni CPO-27 although the microwave samples still show high Langmuir surface areas. This proves that the porosity of the framework is of the same standard as that produced using hydrothermal methods. There is a slight drop in surface area in the 1 min micro Ni-CPO-27 sample, which could be due to poorly formed pores. The difference is minimal and the surface area measurement matches that of the originally synthesised Ni CPO-27[2]. To further confirm this, NO adsorption investigations were carried out and compared with the hydrothermal sample. The results can be seen in figure 4.33.

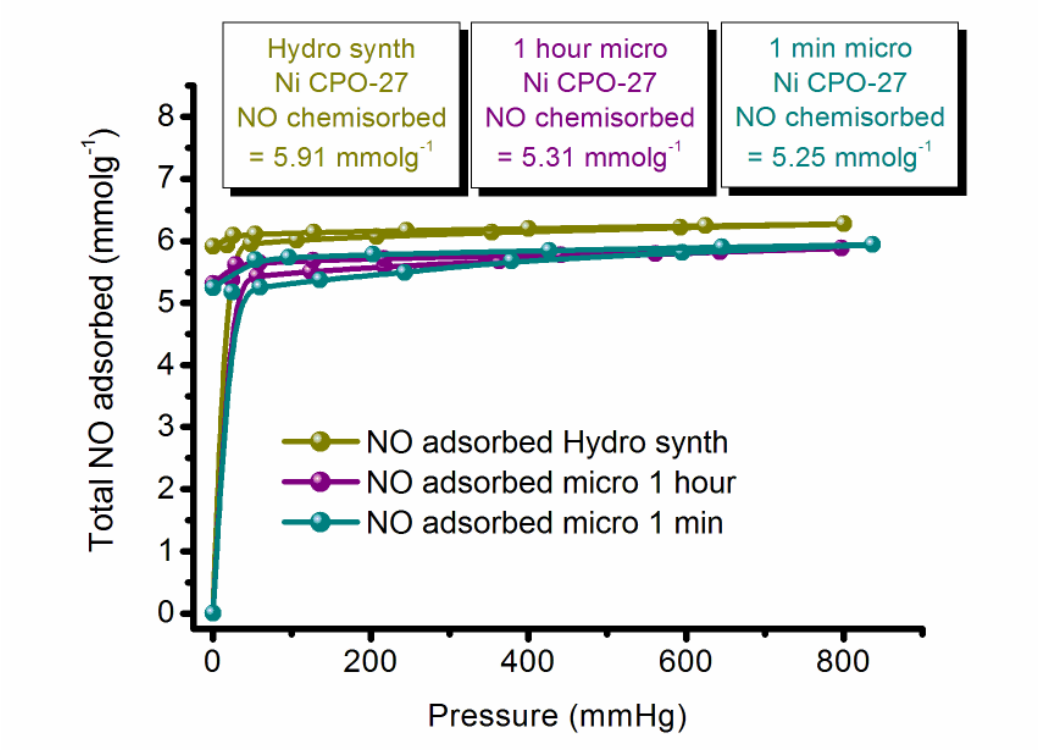

Figure 4.33 NO adsorption isotherms for the three different samples of Ni CPO-27. All three experiments were carried out at 298K.

As shown the variations in the amount of NO actually adsorbed are very low. There is a slightly lower amount of NO actually chemisorbed by the microwave samples. However, it is still storing an extremely large amount of NO. Finally, to see if the samples still have the exceptional performance over the storage and delivery cycle, NO release measurements were also carried out. The results can be seen in figure 4.34.

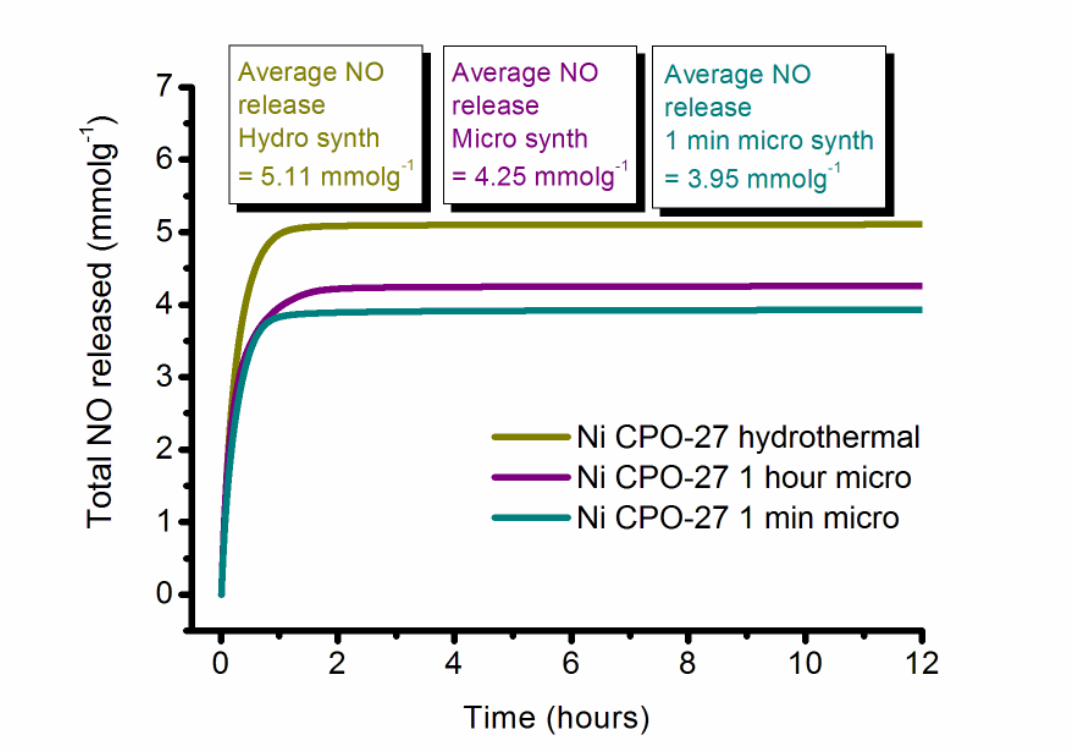

Figure 4.34 Total NO released by the 3 different types of Ni CPO-27.

As can be seen the amount of NO released by the microwave synthesised samples is a little lower than for the standard hydrothermally-produced Ni CPO-27. This might arise from the slightly lower surface areas measured by N_2 adsorption. However, the microwave samples are still releasing the NO in the same controlled manner as the hydrothermal version and the total NO released is still remarkably high. The microwave synthesised Co analogue was also tested for NO adsorption and the results can be seen in figure 4.35.

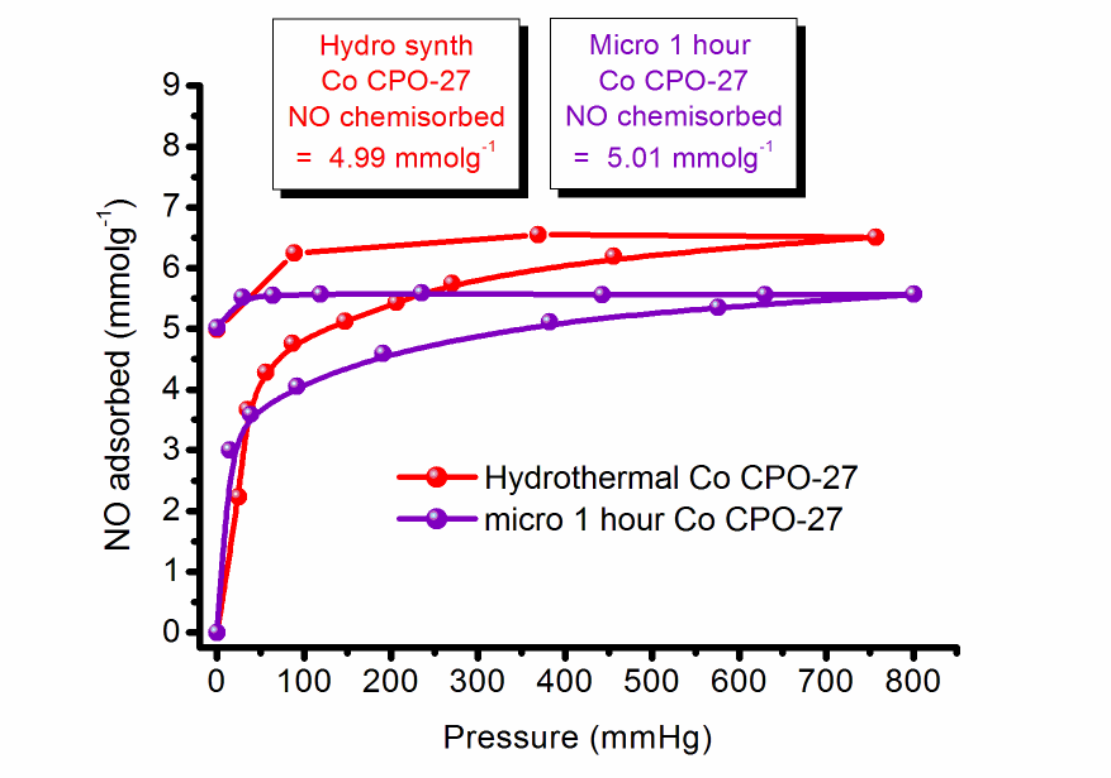

Figure 4.35 NO adsorption graphs carried out at 298K, comparing the microwave synthesised Co CPO-27 with the hydrothermal Co CPO-27.

As can be observed, there is almost no difference in the total NO that is chemisorbed onto the CUS in the pores of both Co CPO-27 samples. However, the total NO adsorbed including the physisorbed NO shows a small difference. These results are extremely encouraging. This means that bulk quantities of these materials can be produced in minutes compared with the 72 hours required for the hydrothermally produced M-CPO-27. The materials obtained match very well to those produced using hydrothermal synthesis with only slight differences in the total NO release properties.

4.9.2 Room temperature synthesis of Zn CPO-27

A recent paper from Yaghi and co-workers illustrated the possibility of synthesising several famous MOFs at room temperature[29], one of which is Zn CPO-27. To compare this with the hydrothermally synthesised Zn CPO-27, the experimental procedure from the literature was followed and the room temperature version of Zn CPO-27 was successfully produced. Initially zinc acetate and DHTP are dissolved in two separate portions of DMF (20ml). The dissolved acid solution is then added drop wise over 10 minutes to the dissolved metal salt while stirring. The mixture is then left stirring overnight. The next day the resulting powder is separated from the parent solvent by centrifugation. The powder is then solvent exchanged by immersion in methanol for three days, replacing the methanol everyday after centrifugation. Powder XRD and TGA curves match very well to the theoretical patterns found in the literature (figure 4.36).

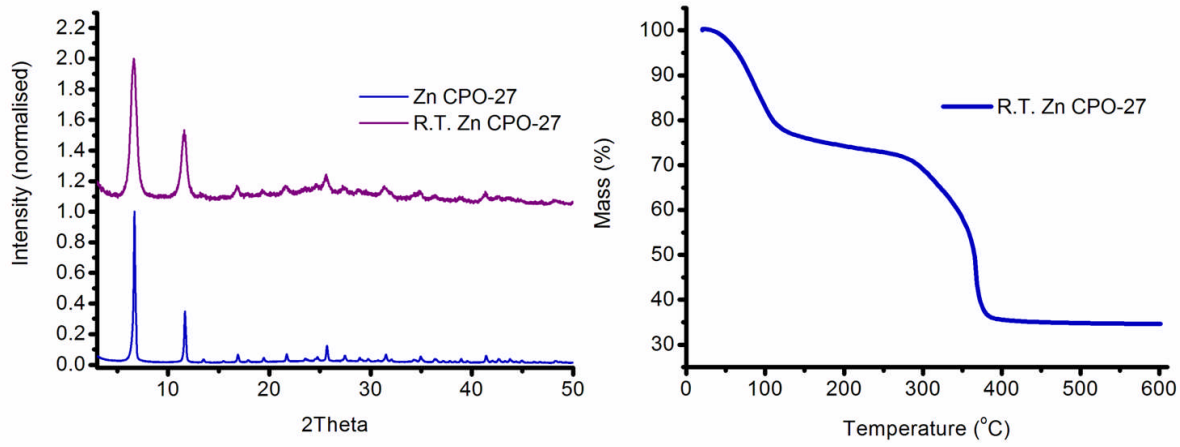

Figure 4.36 XRD and TGA patterns for room temperature synthesised Zn CPO-27.

The RT Zn CPO-27 (room temperature Zn CPO-27) is then activated at elevated temperature (250°C), under vacuum. Once again, however, the N_2 adsorption isotherm was not an ideal match with the surface area described in the literature. A Langmuir surface area of 860 m^2g^{-1} was found and this is slightly lower than the 1187 m^2g^{-1} for the RT Zn CPO-27 mentioned in the paper. However it is a significant improvement on the surface area measured for the hydrothermal Zn CPO-27 discussed earlier. The discrepancy in these values can be attributed to either incomplete activation or ineffective solvent exchange.

The NO adsorption results, however, compare well with the Zn CPO-27 already described. Indeed there are actually improvements noted in the uptake of NO. Figure 4.37 shows both NO isotherms.

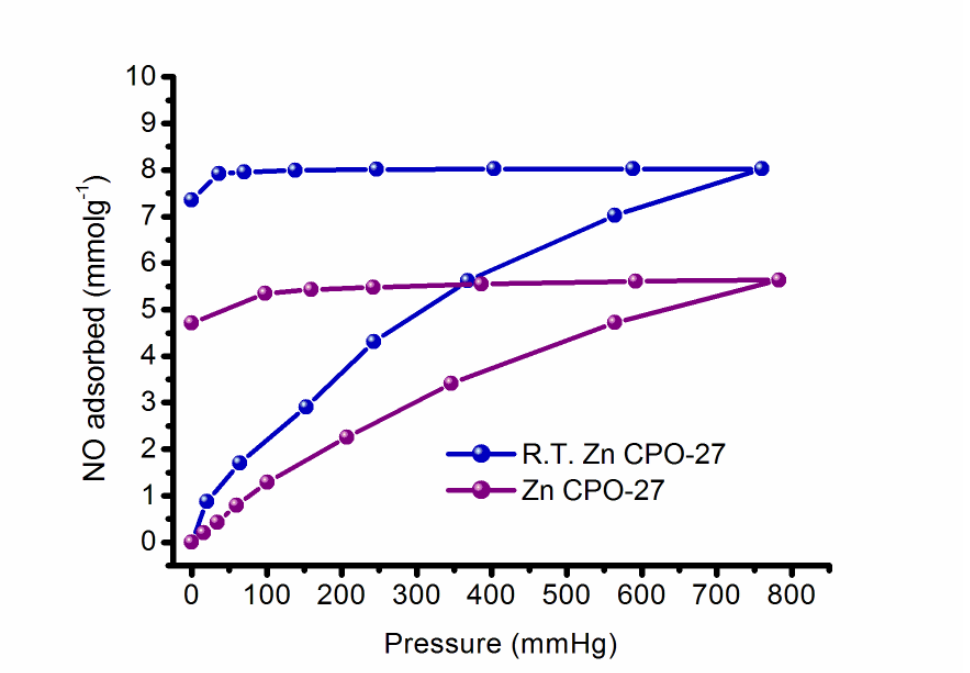

Figure 4.37 NO adsorption at 298K of RT Zn CPO-27 compared with that of the hydrothermally produced Zn CPO-27.

There is a pronounced difference in total NO adsorbed, and indeed in the actual amount of NO chemisorbed. The RT Zn CPO-27 has chemisorbed 7.36 $mmolg^{-1}$, whereas the hydrothermally produced Zn CPO-27 has only 4.72 $mmolg^{-1}$ attached to the CUSs after desorption. It would be expected that an increase in the amount of NO released by this MOF would be observed when these samples are exposed to the "wet nitrogen" of the NO analyser. As can be seen from figure 4.38 there is no increase noticeable from the RT Zn CPO-27.

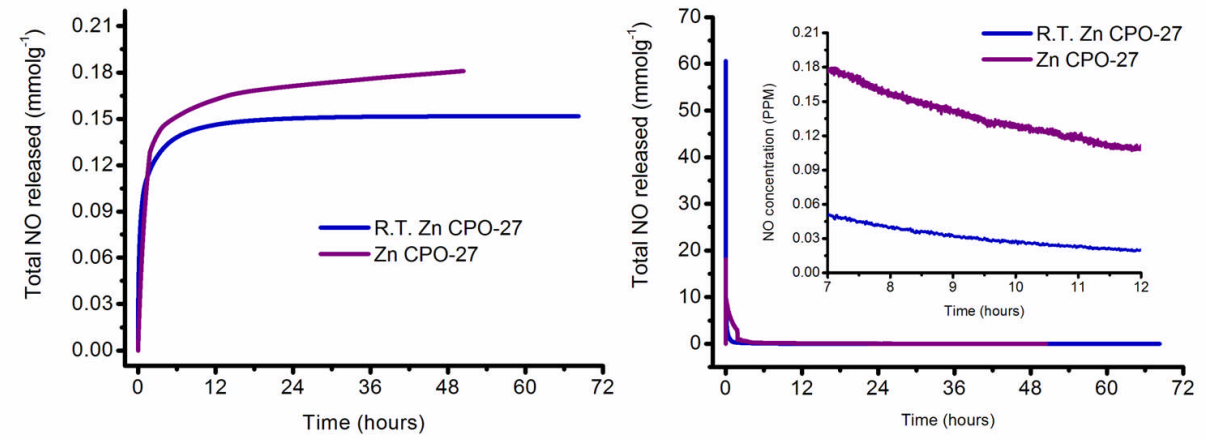

Figure 4.38 NO release curves for the two versions of Zn CPO-27. Even though the RT Zn CPO-27 adsorbs more NO, it releases marginally less than the hydrothermally produced Zn CPO-27.

RT Zn CPO-27 releases marginally less than its hydrothermally produced analogue. From the inset in the concentration curve one can see that it has released almost all the biologically significant NO after only 10 hours, which is in much less time than the hydrothermally produced samples took.

4.10 Summary and discussions from chapter 4

It has been shown that MOFs can store and release large amounts of NO. In particular the M-CPO-27 series have shown a remarkable affinity for NO gas. The Ni and Co versions display an exceptional activation, loading and delivery cycle and as such have shown important potential for investigation into various biological applications. The other versions however, have problems possibly arising from poor activation or due to the fact they have to be synthesised with DMF and then solvent-exchanged prior to use. Even though some still show excellent adsorption isotherms for NO, the amount released is poor in comparison, although still enough for many biological applications. Figure 4.39 shows the theoretical chemical adsorption compared with the actual chemical adsorption of NO. It also details the total NO released and the percentage of NO released compared with the amount originally chemisorbed.

MOF	Theoretical NO ads ($mmolg^{-1}$)	Total amount of NO adsorbed ($mmolg^{-1}$)	Actual NO chemisorbed ($mmolg^{-1}$)	NO released ($mmolg^{-1}$)	% of NO chemisorbed which is released
Co CPO-27	6.412	6.507	5	7	140.00%
Ni CPO-27	6.423	7.211	5.91	6.64	112.35%
Sintef Zn CPO-27	6.158	3.645	2.57	0.127	4.94%
Zn CPO-27	6.158	5.636	4.71	0.181	3.84%
RT Zn CPO-27	6.158	8.024	7.35	0.152	2.07%
Sintef Mg CPO-27	8.243	8.267	8.05	0.305	3.79%
Mg CPO-27	8.243	5.152	4.73	0.175	3.70%
Mn CPO-27	6.581	3.226	2.93	0.15	5.12%

Figure 4.39 Table displaying theoretical adsorption of NO compared with actual experimental results. Also shown is the percentage of NO released compared with the amount adsorbed.

The values for Ni and Co CPO-27 show almost perfect releaseablity. The reason for the release percentage being over 100 is due to the aforementioned physisorbed NO, which is not accounted for in the calculations. This value can vary due to the unknown amount of NO which is physisorbed. The physisorbed NO is also the first to be released as it is not chemically bonded to the metal. This discrepancy in the percentages may also be due to the NO-loading procedure being carried out under slightly different conditions to the adsorption measurement. It is interesting to note that the release percentages from all the other analogues of CPO-27 are all between 2 and 5%. There are several reasons that could explain this. Several processes occur during the activation, loading and release steps and careful analysis of these steps might yield an answer as to why several of the analogues show good adsorption but poor release of NO. The steps involved in the various processes can be seen in figure 4.40. The stability of the dehydrated structure will determine whether or not the NO-loaded MOF will transfer back to the hydrated state. The reaction that occurs during the replacement of NO with H_2O (NO release) will involve a reaction mechanism, and here are two possible mechanistic processes. These are illustrated in figure 4.40. Mechanism 1 would suggest that the incoming water molecule and the exiting NO molecule are both attached to the metal before the NO departs. Mechanism 2 suggests that the NO dissociates from the metal before the water reattaches itself suggesting that there is an intermediate of similar structure to the dehydrated MOF. Mechanism 2 would be the most logical as mechanism 1 would be sterically hindered as the combination of both a water molecule and an NO molecule would be too bulky around the one metal atom. Indeed a seven coordinated metal is unlikely to form is such a constrained space. In the Ni and Co versions the dehydrated structure clearly

must display good stability as it is much easier to activate these materials compared with the others. If the dehydrated structure is easy to form, then changing the species attached to the activated version should also be straightforward. It therefore follows that if it is difficult to achieve the fully activated structure, then replacing any species attached to the activated structure will be very difficult.

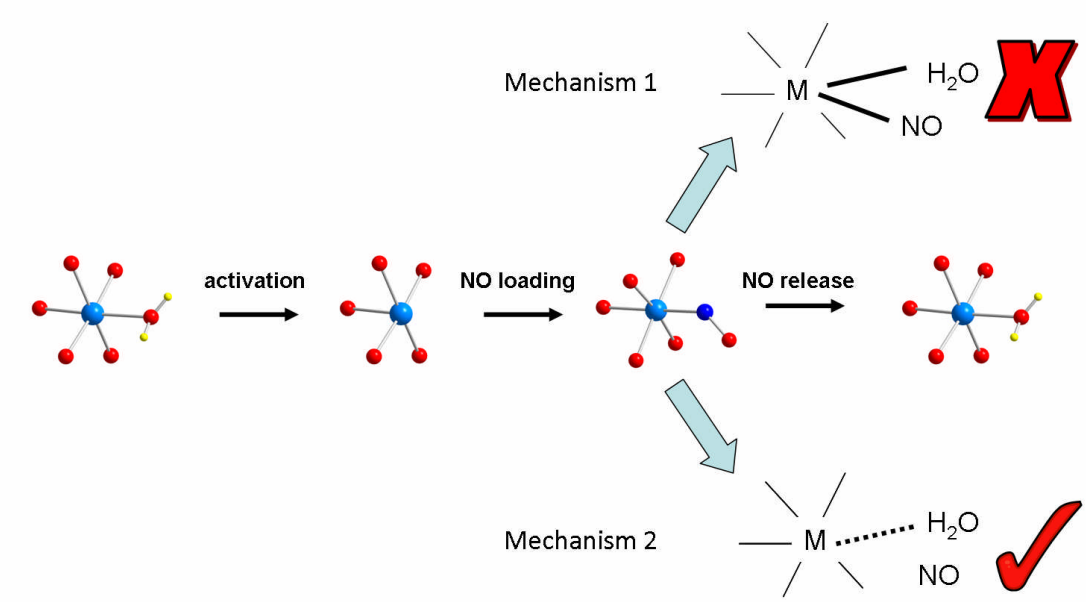

Figure 4.40 Diagram depicting the reactions involved at the metal in the activation and loading and release of NO in MOFs. Also illustrated are the 2 possible mechanisms for NO release from a loaded MOF. Mechanism 2 is the most likely process as steric hindrance would prevent mechanism 1 from occurring. Metal atoms are shown in light blue, oxygen in red, hydrogen in yellow and nitrogen in dark blue.

Therefore in the Zn, Mg and Mn analogues, the dehydrated structure must not be as stable and this might lead to the NO not being replaced by the water molecule. This situation would lead to the NO-loaded structure being more favourable compared

with the dehydrated intermediate, which is required before the water can attach itself back to the metal. Another factor influencing the NO release is the strength of the M-NO bond that is formed when the activated material is exposed to NO. It is possible that the M-NO bond is much stronger for Zn, Mg and Mn than Ni and Co. This would explain why such low NO release percentages are found. Microcalorimetry experiments could be carried out to investigate this further. The IR measurements carried out in the next chapter give an explanation of what is occurring at an iron atom in MIL-100 during NO loading and release. Obviously different MOFs will react differently with NO, however some of the main points may offer another reason as to why the NO release is poor for certain analogues of M-CPO-27.

In conclusion it has been shown that there is significant potential in using the M-CPO-27 MOFs to store and release NO for medicinal applications. The initial results of which can be found in chapter 7.

4.11 References

(1) Dietzel, P. D. C.; Morita, Y.; Blom, R.; Fjellvag, H. *Angew. Chem., Int. Ed.* **2005**, *44*, 6354.

(2) Dietzel, P. D. C.; Panella, B.; Hirscher, M.; Blom, R.; Fjellvag, H. *Chem. Commun.* **2006**, 959.

(3) Rosi, N. L.; Kim, J.; Eddaoudi, M.; Chen, B.; O'Keeffe, M.; Yaghi, O. M. *J. Am. Chem. Soc.* **2005**, *127*, 1504.

(4) Rowsell, J. L. C.; Yaghi, O. M. *J. Am. Chem. Soc.* **2006**, *128*, 1304.

(5) Dietzel, P. D. C.; Johnsen, R. E.; Blom, R.; Fjellvag, H. *Chem.--Eur. J.* **2008**, *14*, 2389.

(6) Dietzel, P. D. C.; Blom, R.; Fjellvåg, H. *Eur. J. Inorg. Chem.* **2008**, *2008*, 3624.

(7) Caskey, S. R.; Wong-Foy, A. G.; Matzger, A. J. *J. Am. Chem. Soc.* **2008**, *130*, 10870.

(8) Zhou, W.; Wu, H.; Yildirim, T. *J. Am. Chem. Soc.* **2008**, *130*, 15268.

(9) Bhattacharjee, S.; Choi, J.-S.; Yang, S.-T.; Choi, S. B.; Kim, J.; Ahn, W.-S. *J. Nanosci. Nanotechnol.* **2010**, *10*, 135.

(10) Dietzel, P. D. C.; Besikiotis, V.; Blom, R. *J. Mater. Chem.* **2009**, *19*, 7362.

(11) Chavan, S.; Bonino, F.; Vitillo, J. G.; Groppo, E.; Lamberti, C.; Dietzel, P. D. C.; Zecchina, A.; Bordiga, S. *Phys. Chem. Chem. Phys.* **2009**, *11*, 9811.

(12) Chavan, S.; Vitillo, J. G.; Groppo, E.; Bonino, F.; Lamberti, C.; Dietzel, P. D. C.; Bordiga, S. *J. Phys. Chem. C* **2009**, *113*, 3292.

(13) Dietzel, P. D. C.; Johnsen, R. E.; Fjellvag, H.; Bordiga, S.; Groppo, E.; Chavan, S.; Blom, R. *Chem. Commun.* **2008**, 5125.

(14) McKinlay, A. C.; Xiao, B.; Wragg, D. S.; Wheatley, P. S.; Megson, I. L.; Morris, R. E. *J. Am. Chem. Soc.* **2008**, *130*, 10440.

(15) Wu, H.; Zhou, W.; Yildirim, T. *J. Am. Chem. Soc.* **2009**, *131*, 4995.

(16) Xiao, B.; Wheatley, P. S.; Zhao, X. B.; Fletcher, A. J.; Fox, S.; Rossi, A. G.; Megson, I. L.; Bordiga, S.; Regli, L.; Thomas, K. M.; Morris, R. E. *J. Am. Chem. Soc.* **2007**, *129*, 1203.

(17) Wheatley, P. S.; Butler, A. R.; Crane, M. S.; Fox, S.; Xiao, B.; Rossi, A. G.; Megson, I. L.; Morris, R. E. *J. Am. Chem. Soc.* **2006**, *128*, 502.

(18) Wheatley, P. S.; Butler, A. R.; Crane, M. S.; Rossi, A. G.; Megson, I. L.; Morris, R. E. *Molecular Sieves: From Basic Research to Industrial Applications, Pts a and B* **2005**, *158*, 2033.

(19) Wheatley, P. S.; McKinlay, A. C.; Morris, R. E.; Gédéon, P. M.; Florence, B. In *Stud. Surf. Sci. Catal.*; Elsevier: 2008; Vol. Volume 174, Part 1, p 441.

(20) Bonino, F.; Chavan, S.; Vitillo, J. G.; Groppo, E.; Agostini, G.; Lamberti, C.; Dietzel, P. D. C.; Prestipino, C.; Bordiga, S. *Chem. Mater.* **2008**, *20*, 4957.

(21) Mowbray, M.; Tan, X.; Wheatley, P. S.; Morris, R. E.; Weller, R. B. *J. Invest. Dermatol.* **2007**, *128*, 352.

(22) Lin, Z.; Wragg, D. S.; Morris, R. E. *Chem. Commun.* **2006**, 2021.

(23) Choi, J.-S.; Son, W.-J.; Kim, J.; Ahn, W.-S. *Micropor. Mesopor. Mater.* **2008**, *116*, 727.

(24) Choi, J. Y.; Kim, J.; Jhung, S. H.; Kim, H. K.; Chang, J. S.; Chae, H. K. *Bull. Korean Chem. Soc.* **2006**, *27*, 1523.

(25) Hong, D.-Y.; Hwang, Y. K.; Serre, C.; Férey, G.; Chang, J.-S. *Adv. Funct. Mater.* **2009**, *19*, 1537.

(26) Jhung, S. H.; Lee, J. H.; Chang, J. S. *Bull. Korean Chem. Soc.* **2005**, *26*, 880.

(27) Taylor-Pashow, K. M. L.; Rocca, J. D.; Xie, Z.; Tran, S.; Lin, W. *J. Am. Chem. Soc.* **2009**.

(28) J. I. Langford, J. C. W. *J. Appl. Crystallogr.* **1978**, *11*, 102.

(29) Tranchemontagne, D. J.; Hunt, J. R.; Yaghi, O. M. *Tetrahedron* **2008**, *64*, 8553.

5 NO storage and release from various MIL frameworks

5.1 Background

One of the most prominent research teams in the area of MOF chemistry has been the Férey group based in France. They have synthesised many of the most famous MOF structures and have written a large number of high profile publications. As mentioned in chapter 1, MOF structures have evolved several acronyms. Here at the University of St Andrews two examples are STA (St Andrews porous material) and STAM (St Andrews MOF). One of the most used acronyms is MIL, meaning Materials of Institut Lavoisier, and any framework with a MIL name was originally synthesised by this group. Over recent times they have synthesised MOFs with wide-ranging properties, including MILs 100, and 101 which have some of the largest surface areas of any MOFs and MILs 53 and 88 which show a fascinating breathing phenomenon. The Russell Morris group work closely with the Férey group and part of this project was to investigate the NO adsorption and release properties of several of the MILs synthesised in France.

5.2 Aims of chapter 5

The main aim in chapter 5 is to investigate a variety of iron-based carboxylate MOFs for NO storage and release. An investigation into structures with similar morphology but using different linkers is presented. Another comparison was made between MOFs which are amine grafted and those with CUSs present to bind NO. Finally in

collaboration with the Férey group based in France, an in-situ IR investigation is presented. This gives interesting results, which explain the adsorption and release results for NO in Fe based frameworks.

5.3 NO adsorption and release from MIL-88 structures

Following synthesis in France several samples of MIL-88 based structures were sent over to the University of St Andrews where NO adsorption and release experiments were carried out.

5.3.1 Introduction to the structures investigated

In 2002 Serre and co-workers synthesised MIL-53 using terephthalic acid and chromium metal[1-2]. The structure displayed a remarkable breathing effect upon dehydration, whereby the structure expanded and the pore size was greatly increased. This discovery was then followed by the creation of another breathing framework MIL-88[3-5]. They successfully used Fe^{3+} together with differing linkers to produce a set of structures which were very similar with variation in the linker, comparable with the isoreticular series of MOFs created by Yaghi[6]. Their approach uses a "Controlled Secondary Binding unit (SBU)", which means that the metal cluster is formed before being introduced into the reaction with the organic species to form the MOF. In this case the trimeric iron acetate is prepared and then added to various organic moieties (see figure 5.1). Fe MIL-88-A and Fe MIL-88-B have already been reported in the literature[3-5], however samples of two new forms of Fe MIL-88-B were also donated very kindly by the Férey group for NO investigation. Using nitroterephthalic acid and 2,5-dihydroxyterephthalic acid (DHTP) as linkers,

structures similar to Fe MIL-88-B are formed with extra functional groups present on the aromatic ring. Fe MIL-88-A is a three dimensional framework constructed from iron (III) trimers and fumaric acid with the formula $Fe^{III}_3O(CH_3OH)_3\{-O_2C-C_2H_2-CO_2-\}_3\cdot\{-O_2C-CH_3\}\cdot 4.5CH_3OH$ (see figure 5.2(a)). The framework is made up of cages together with channels running along the c-axis. Fe MIL-88-B is of the same topology as Fe MIL-88-A, however the fumaric acid has been replaced by terephthalic acid (figure 5.2(b)). The material is unique in that its cell volume undergoes a reversible expansion from the closed (dehydrated) to the open (fully hydrated) form. This increase (85% for Fe MIL-88-A) is the largest known for any MOF and is completed without any phase transition or bond breaking.

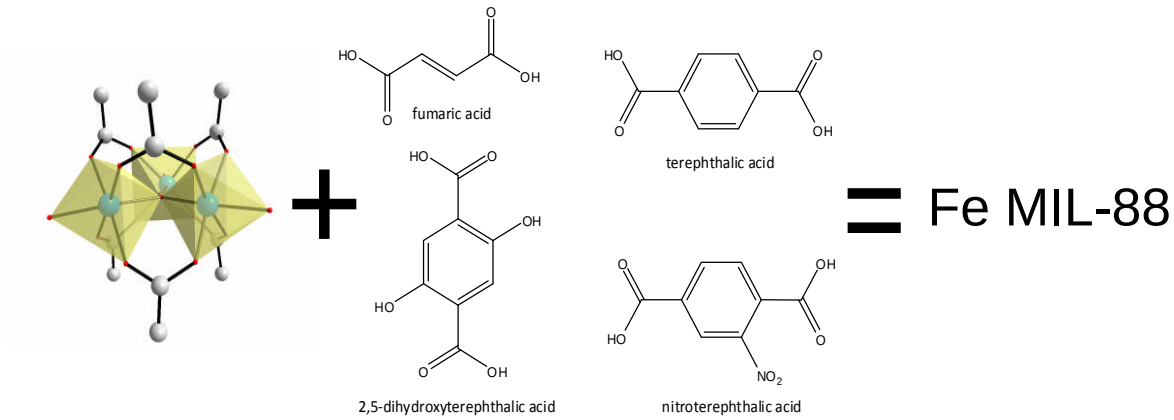

Figure 5.1 A scheme showing the iron acetate trimer and the various different linkers used in forming the set of Fe MIL-88 structures.

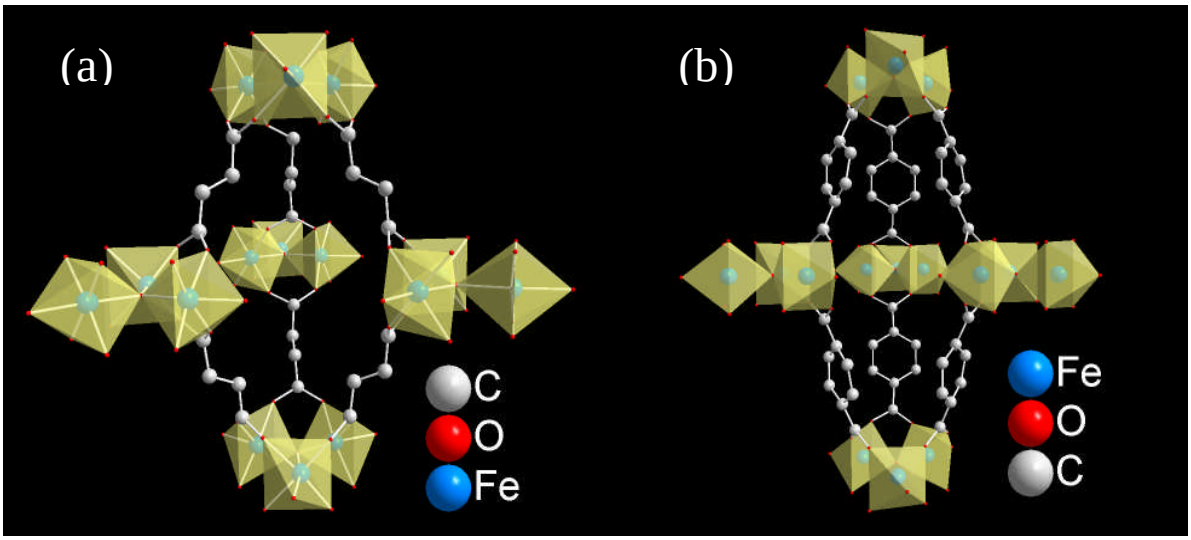

Figure 5.2 (a) Cage of Fe MIL-88-A, clearly showing the iron trimer connected to the fumaric acid linker and (b) similar view of the cage structure in Fe MIL-88-B except using terephthalic acid as the organic linker.

As mentioned in chapter 1, MOFs have great potential for use in healthcare applications. Indeed initial toxicology studies have already been carried out on iron carboxylate based MOFs resulting in no detrimental effects observed from acute and semi-chronic exposure[7]. Further to this, iron carboxylates (including MIL-88) have recently been shown to be of great interest for drug delivery and imaging[7]. The compositions of the Fe MIL-88 structures are very favourable in terms of toxicology as they contain iron as the metal source, which is substantially less toxic when compared with the other metals in MOFs studied for NO applications so far (Ni, Co and Cu)[8-9]. Indeed some current prescribed medicines have the same chemical composition as MOFs and have been approved for medical use. For example, iron fumarate (same composition as Fe MIL-88-A) has been approved as an oral iron supplement[10] (trade name Ferretts^{TM}).

5.3.2 NO adsorption results on Fe MIL-88

Figure 5.2 clearly shows the cage structure of both Fe MIL-88-A and Fe MIL-88-B (excluding guest solvent molecules). The iron trimer can be clearly seen and it is at the iron atoms that the NO would be expected to attach during NO adsorption studies. Thermal activation at 150°C (with the exception of Fe MIL-88-B-2OH for which 80°C was used) removed guest water molecules and the coordinated water leaving the dehydrated structure and coordinatively unsaturated metal sites (CUSs) which the NO can bind to. The Fe MIL-88 compounds were first subjected to gravimetric adsorption measurements. Fe MIL-88-A shows a 20% drop in mass after thermal activation before exposure to NO, which correlates well with the thermogravimetric analysis (TGA) carried out (figure 5.3), indicating that all guest solvent molecules (including bound ones) are removed. All the other Fe MIL-88 compounds show similar behaviour indicating that all solvent molecules were removed prior to NO adsorption.

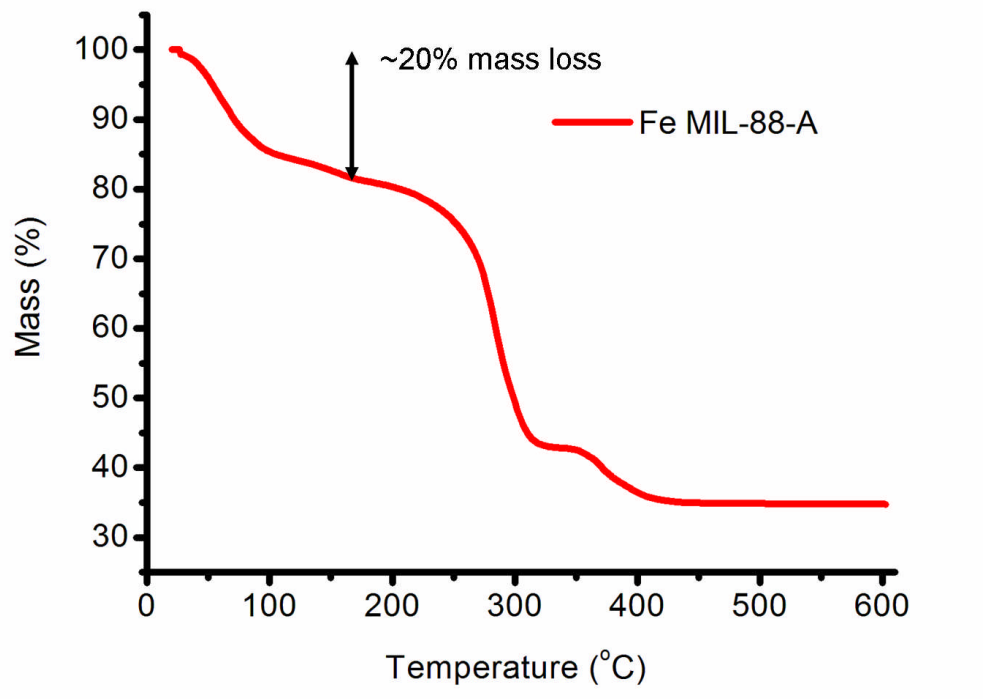

Figure 5.3 TGA curve for Fe MIL-88-A.

NO adsorption isotherms can be seen in figure 5.4. Fe MIL-88-A adsorbed the largest amount of NO, 2.5 $mmolg^{-1}$. The desorption curve showed some irreversible adsorption with 1.61 $mmolg^{-1}$ of NO probably chemically bonded to the iron atoms. Fe MIL-88-B showed an uptake of 1.8 $mmolg^{-1}$ with 1.31 $mmolg^{-1}$ irreversibly adsorbed. The other Fe MIL-88s both exhibited smaller uptakes of NO (~1 $mmolg^{-1}$) with Fe MIL-88-B-NO_2 irreversibly adsorbing 0.84 $mmolg^{-1}$ and the 2OH version just 0.66 $mmolg^{-1}$.

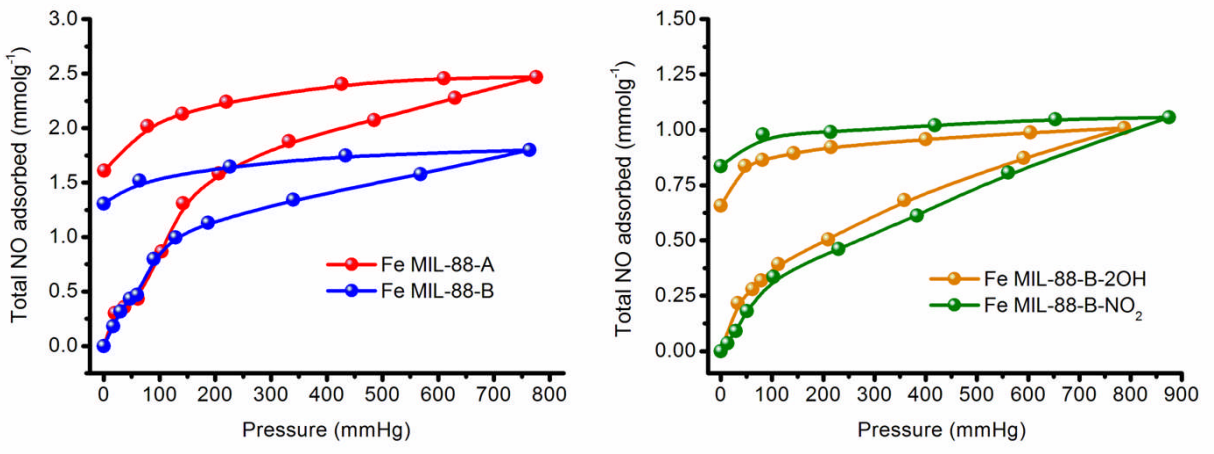

Figure 5.4 The NO isotherms for all Fe MIL-88 structures investigated. Fe MIL-88-A shows the highest uptake with the Fe MIL-88-B structures displaying similar uptakes of about 1 mmolg^{-1}. All results obtained at 298K.

However, all the adsorption values are significantly lower when compared with the theoretical values of adsorption (see figure 5.5). Assuming that all three of the iron atoms in the trimer are unsaturated prior to NO exposure, Fe MIL-88-A should chemisorb 5.7 mmolg^{-1} of NO. This value is unrealistic however, as removal of so many oxygen atoms would put too much strain on the iron trimer. It is therefore more likely that only one of the iron centres is coordinatively unsaturated and therefore available for chemical binding.

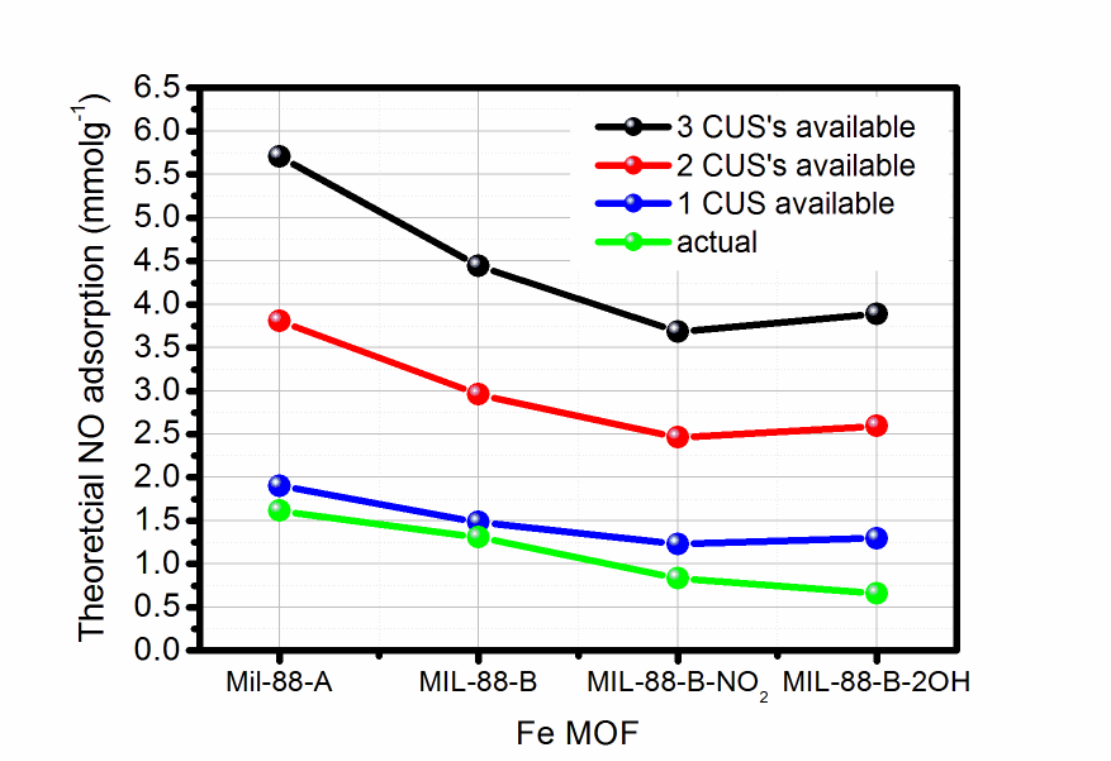

Figure 5.5 Graph displaying the theoretical adsorption of each Fe MIL-88 depending on the number of sites available on each trimer and comparing it with the actual NO adsorption observed.

From figure 5.5 it is clear that there is less than one site available per Fe trimer for adsorbing NO molecules. This corresponds well with the assumption that there could only be one of the three possible sites available. Additionally all of the adsorption isotherms show compounds that are not fully saturated with NO (the equipment only measures to two atmospheres of NO for safety reasons), which would also explain why the actual adsorption values are lower than the theoretical ones. These two effects explain the lower than expected adsorption of NO for all the Fe MIL-88 materials. In the curves for MIL-88-A and B a step can be observed between 50 and 100 mmHg. This could be due to a "gate opening" effect[11] which has been observed before in other MOFs. Initially the structure is in the closed form when dehydrated

and as NO is adsorbed into the structure it expands into the open form and thereby allows more NO into the pores. Mention must also be made of the fact that a very small amount of weakly adsorbed (physisorbed) NO will also be present in the pores of the framework at 298K, however upon desorption this should be removed. The desorption arm of the isotherm shows a large hysteresis which is consistent with previous NO studies and shows that the NO has bound to open iron sites. The amount of NO adsorbed is less than that of the exceptional storage and release capacity of the CPO-27 materials[8], however, it is still comparable with that of Zn zeolite-A which adsorbs ~ 1.5 $mmolg^{-1}$ of NO[12]. The extra functional groups added to the MIL-88-B could be responsible for lowering the amount of NO adsorbed as they will partially block access to the open metal sites located within the pores. This would explain the lower values of NO adsorption for the newer Fe MIL-88-B structures.

5.3.3 NO release measurements on Fe MIL-88 structures

As mentioned in the previous chapter the amount of gas adsorbed is vital for particular biological applications relating to NO. However of much greater importance is the amount of NO released and over what period of time which will determine if individual MOFs are suitable for further investigation. Release experiments were carried out on the Fe MIL-88 compounds to see if the NO stored in the framework could all be released using moisture as a trigger as demonstrated previously. Following the same activation procedure the NO-loaded samples were stored under a dry atmosphere before being placed in the sample holder. Once exposed to the “flowing wet gas” of the apparatus the water molecule should replace

the NO on the Fe atom. The NO should then be released and quantifiably calculated using the intensity of chemiluminescence on reaction of NO with ozone. The concentration release profile and the total amount of NO released from the Fe MIL-88 compounds can be seen in figure 5.6.

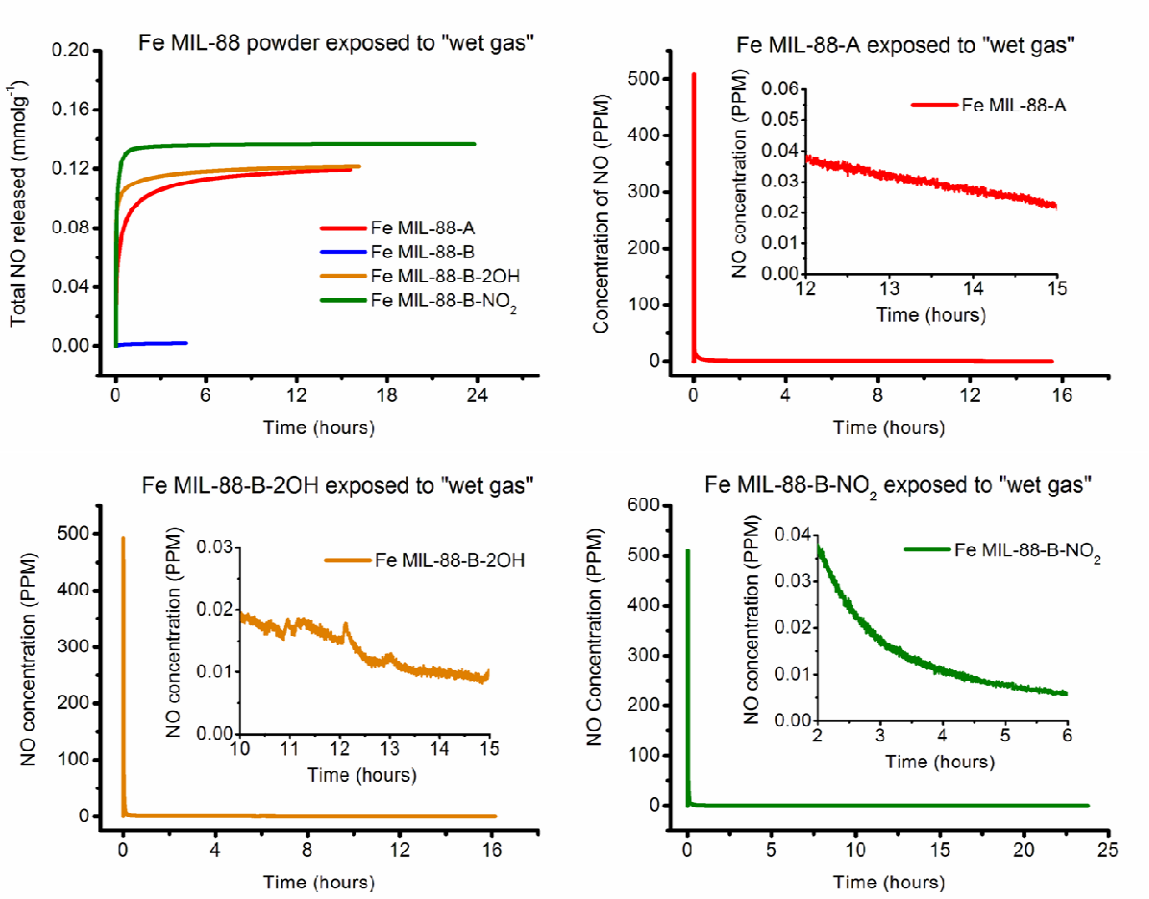

Figure 5.6 NO release profiles for the Fe MIL-88 structures. Top left shows the total amount released. The concentration curves for three of the structures are also shown. Fe MIL-88-B is omitted due to the extremely poor NO quantity released.

These graphs illustrate that the vast majority of the total NO released is liberated within the first hour of the experiment for most of the compounds. However, this is

not a major concern as the compounds are still releasing biologically significant quantities of NO (10 parts per billion (PPB)) up to 16 hours after starting the experiment, as in the case of Fe MIL-88-A. As noted, the compounds are releasing values of NO which are significantly less than the amount initially adsorbed. Fe MIL-88-A releases only about 5% of the total amount adsorbed, Fe MIL-88-B-NO_2 and Fe MIL-88-B-2OH both release about 14% of the total they adsorbed. This behaviour has been observed before in the previous chapter with Zn, Mg and Mn CPO-27 and in the literature with HKUST-1 (a Cu-based MOF) which adsorbed 3 $mmolg^{-1}$ of NO but only released 2 $\mu molg^{-1}$ of NO [9].

Overall the NO adsorption and release from the Fe MIL-88 structures is similar to the release from the Zn, Mg and Mn CPO-27 compounds. Again the release percentages from these compounds are not as high as would be expected and further discussions regarding these results can be found later in this chapter. Further investigation of how many CUSs are available following activation and the bond strength between iron and NO is required to fully understand the poor release of NO from these compounds. Nonetheless the amount of NO produced is still significant and merits further investigation for possible biological applications.

5.4 NO adsorption and release from MIL-101 and MIL-100 based structures

5.4.1 Introduction to structures

In 2005, Férey and co-workers synthesised structures known as MIL-100 and MIL-101[13-14]. They once again used the metal trimer, with two different carboxylic acids (trimesic and terephthalic acid). However, the structures produced had some of the largest unit cells ever reported for MOFs and huge surface areas. The MIL-101 structure used terephthalic acid and MIL-100 used trimesic acid in combination with Cr metal initially, however since then the Fe version of MIL-100 has been reported[15]. The structures are built from supertetrahedra which then form two different types of cages and can be seen in figure 5.7. By using the metal trimer in the synthesis it allows both structures to have CUSs upon desolvation of the framework. This combined with the huge available surface areas has led to many investigations into their gas storage properties[16-17]. Indeed drug storage and release has also been performed on these frameworks[18]. In 2008, however, there was a paper published which demonstrated the use of grafting amines onto the CUSs available in MIL-101 to improve certain catalytic reactions[19]. The MIL-101 structure was first dehydrated then the amine was successfully grafted onto the available CUS. It was thought that by using samples of amine grafted MIL-101 it would be possible to improve the amount of NO that the structure could adsorb. The reason for this is based on another set of NO releasing compounds known as diazeniumdiolates (NONOates)[20-21].

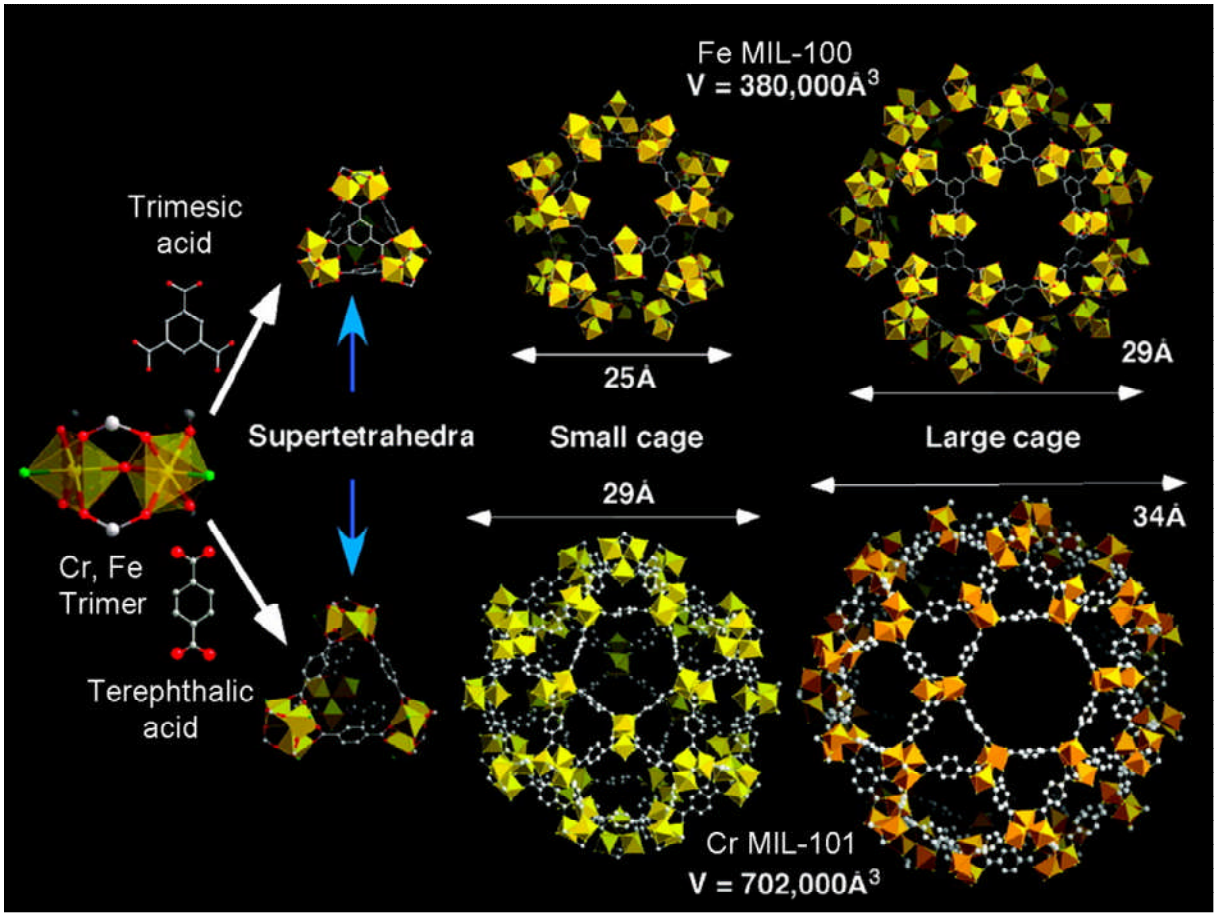

Figure 5.7 Structures of MIL-100 and MIL-101. (Left) A trimer of Cr octahedra and linkers (trimesic acid for MIL-100 and terephthalic acid for MIL-101). (Centre) Hybrid supertetrahedra. (Right) Cages of MIL- 100 and MIL-101. Picture adapted from reference 17.

As mentioned briefly in the introductory chapter, NONOates have the general structure illustrated in figure 5.8. Also shown is the spontaneous release of NO from this family of compounds when placed in aqueous media.

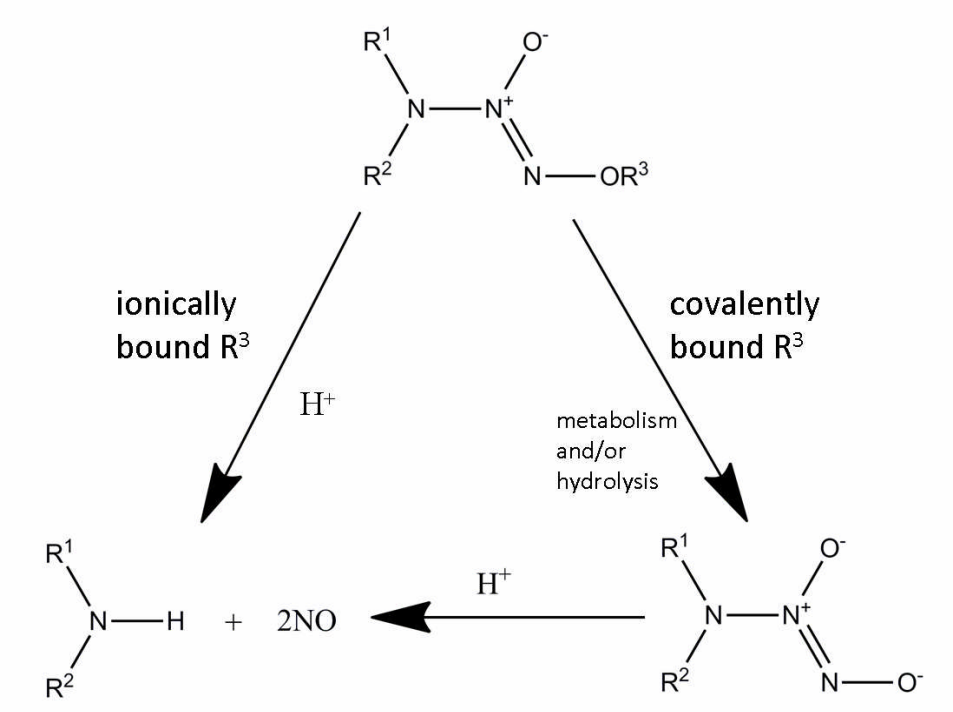

Figure 5.8 NO release from NONOates adapted from reference 20.

As can be observed, 2 molar equivalents of NO are released from the structure upon decomposition. By grafting an amine onto a CUS in a MOF, the possibility for creating the NONOate group is realised. Following successful grafting and subsequent activation (insuring that the secondary amine is not removed or decomposed) NO could be attached to the N atom creating the NONOate group. When exposed to the moisture from the wet gas the decomposition of the NONOate inside the pores should lead to 2 molar equivalents of NO being released from each metal site. On the other hand, if it is simply the open metal site that is chemically binding to NO only 1 molar equivalent of NO will be released. The two proposed mechanisms can be seen in figure 5.9 (using *N*-methylethylenediamine as an example). The use of amine grafting offers the possibility of doubling the NO adsorption capacity and release values for individual MOFs. This approach to the

loading and release of NO has been successfully shown in the HKUST-1 framework by Rosseinsky and co-workers[22]. Using the unsaturated Cu sites available after activation, they successfully grafted 4-(methylamino)pyridine and exposed this to NO gas. This formed the diazeniumdiolate group which, when triggered with water, released the 2 molecules of NO bound to the amine. The one major drawback to this technique, however, is firstly the assumption that all the metal centres are fully activated before grafting of the amine. Secondly it is assumed that the amine grafts successfully to the all the metal sites available. This second assumption was proven to be problematic, as when the amine-grafted samples of HKUST-1 were exposed to NO some of the NO bound directly to the Cu CUSs, indicating that full amine grafting is not guaranteed[22].

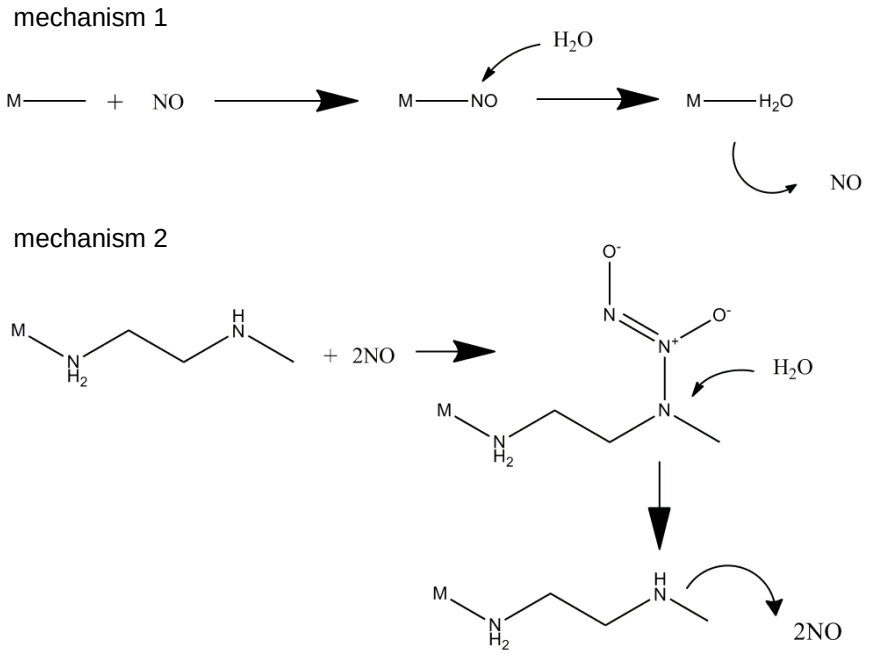

Figure 5.9 Two proposed mechanisms for NO-loading and release. Mechanism 1 shows the standard method of activation followed by exposure to NO, and before the NO is released via moisture. Mechanism 2 utilises the amine-grafted MOFs. Here the amine can bind 2 molar equivalents of NO forming a NONOate before releasing the NO in the same manner as above.

The NO adsorption isotherms for Fe MIL-100 and Cr MIL-101 have previously been carried out by another member of the Russell Morris group. The Férey group in France again kindly provided two samples of amine grafted MOFs for initial NO experimentation. One was a sample of Cr MIL-101 with *N*-methylethylenediamine grafted onto the metal (see figure 5.8). The other sample was Fe MIL-100 with a semicarbazide attached to the Fe atoms (see figure 5.8).

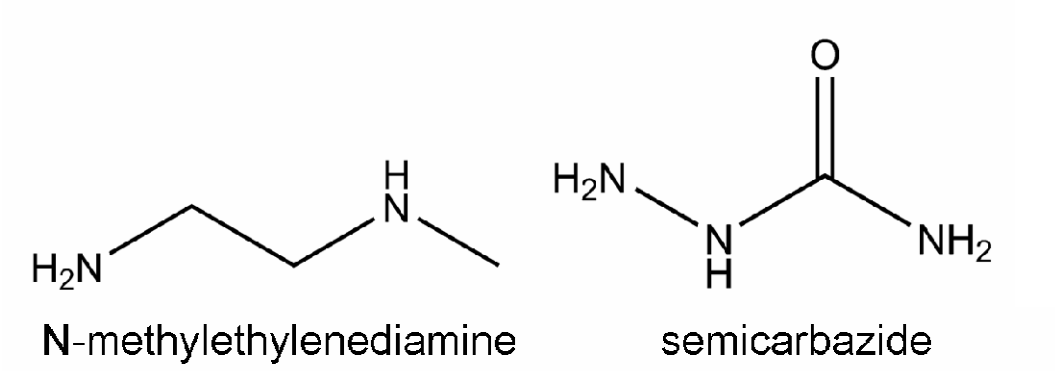

Figure 5.8 The diamine molecules grafted onto the metal sites to improve NO storage in Cr MIL-101 and Fe MIL-100.

5.4.2 NO results from amine grafted MIL frameworks

NO adsorption isotherms were undertaken for both amine grafted samples and then compared with the results of the bare frameworks (kindly provided by Dr Paul Wheatley and Dr Bo Xiao). The activation temperature used for each framework was 150°C which is the same as was used for the bare frameworks (except for the MIL-100 sample which is degassed at 250°C). Figure 5.9 shows the NO adsorption graph for the amine grafted MIL-101. MEDA stands for *N*-methylethylenediamine.

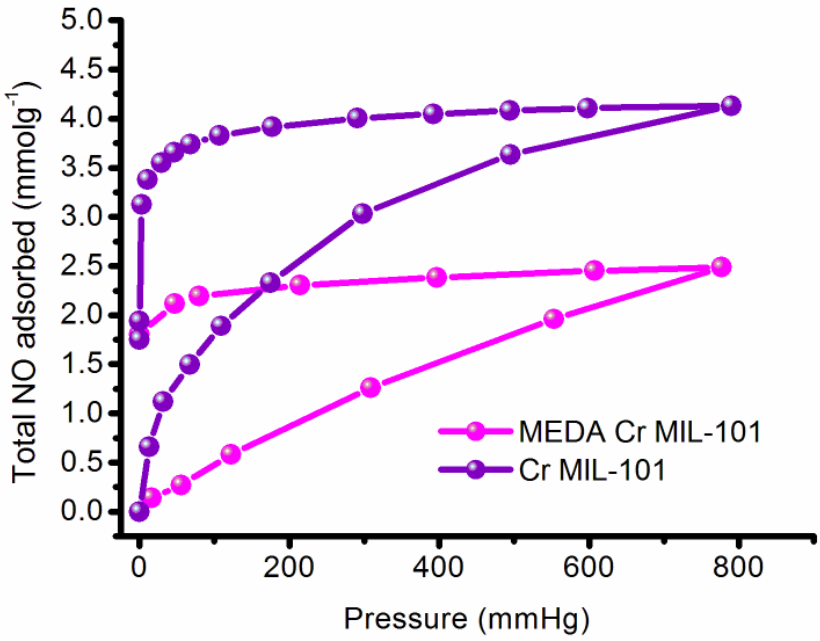

Figure 5.9 NO adsorption isotherm carried out at 298K comparing the amine grafted Cr MIL-101 with the bare Cr MIL-101 framework.

The amount of NO chemisorbed by the two samples is very similar, both showing chemical adsorption of 1.75 mmolg^{-1} of NO. However, there is significantly more NO adsorbed by the bare framework of Cr MIL-101. The adsorption of NO by the Fe

MIL-100 samples can be viewed in figure 5.10. The sample designated Fe MIL-100 250°C was activated at 250°C instead of the standard 150°C. This was carried out at the suggestion of the Férey group. It can be seen that the Fe MIL-100 activated at 150°C adsorbs much less NO than when activated at 250°C, suggesting that not all the solvent molecules are removed by activation at 150°C. In the case of the semicarbazide Fe MIL-100, it is not possible to heat beyond 150°C as the semicarbazide molecule would be destroyed. This proves that despite only being treated at 150°C prior to the experiment the semicarbazide grafted sample shows a much higher uptake of NO compared with the standard bare framework degassed at 150°C. This suggests that the NO is binding to the amine group in the expected way.

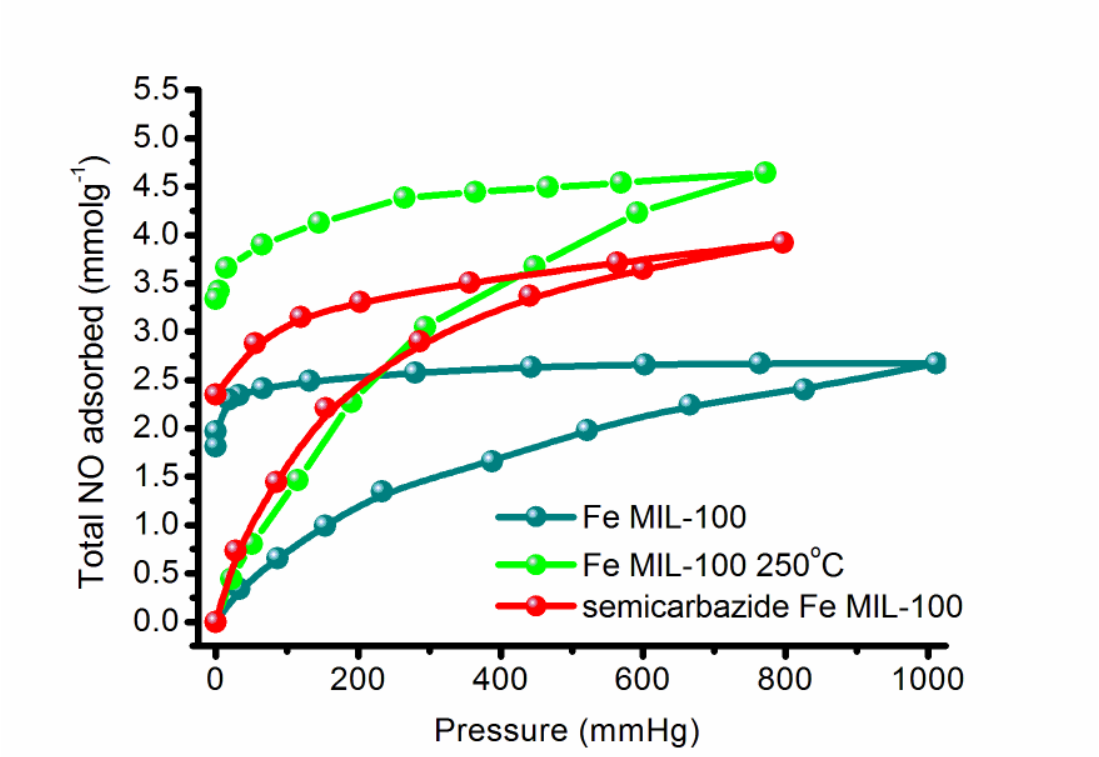

Figure 5.10 Comparison of Fe MIL-100 structures obtained at 298K. The graphs show that activation conditions play an important role in determining the NO adsorption of a material.

Comparing the amounts of NO adsorbed with the theoretical amount shows that in theory the bare framework should chemically adsorb 4.17 $mmolg^{-1}$ of NO. However, once again because the framework utilises the metal acetate trimer, this theoretical value is based on all three CUSs being available. This is unrealistic as if all three sites were unsaturated it would cause a great strain to the structure. Figure 5.11 details the theoretical amounts of NO that should be adsorbed depending on the number of available metal sites per trimer. It is then compared with the actual amount of NO chemisorbed using the gravimetric adsorption equipment.

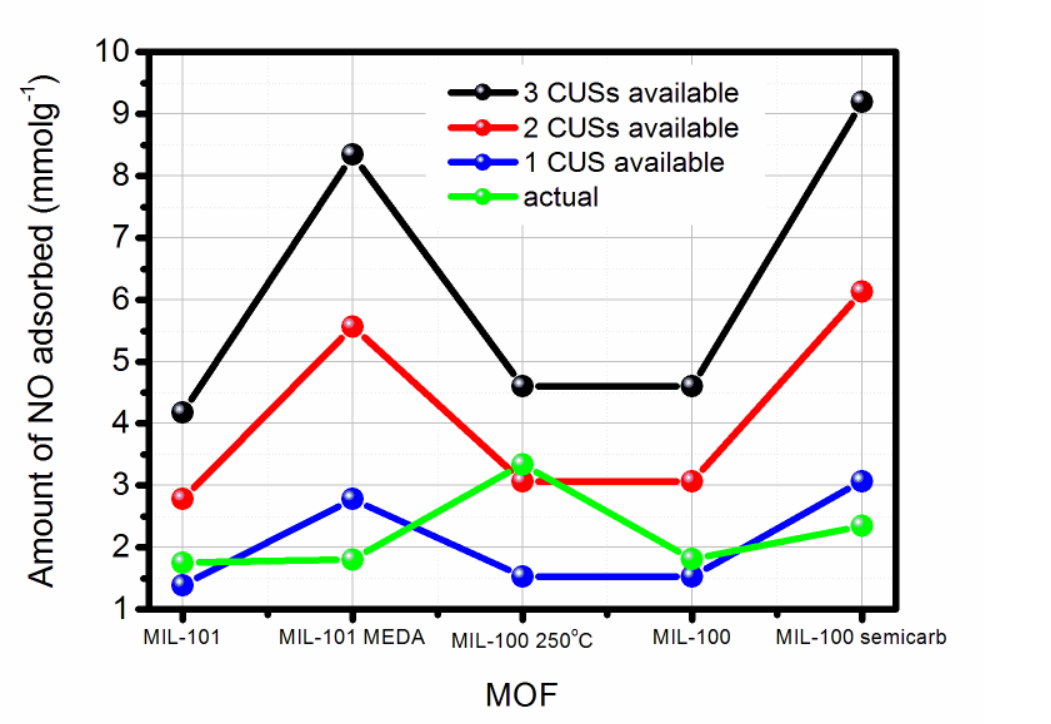

Figure 5.11 Graph showing the theoretical adsorption values for the bare frameworks of MILs 101 and 100 and the amine-grafted versions. These are compared with the actual amount of NO chemisorbed.

In the case of MIL-100 using the elevated thermal activation temperature brings the actual amount of NO adsorbed to almost 3.5 $mmolg^{-1}$, which shows that more than 2 CUSs per trimer are available for binding. This also indicates that the framework is evacuated to a better degree than if treated at 150°C. Thermal activation at 150°C gives adsorption values indicative of having 1 available CUS per metal trimer and this is evident in both Cr MIL-101 and Fe MIL-100.

Due to the larger theoretical NO adsorption value for the amine-grafted MOFs, It would then be anticipated that the amount of NO released from the amine-grafted samples should be greater than for the bare framework. The results can be seen in figure 5.12 together with a table in figure 5.13 summarising the NO release measurements for the bare frameworks and the amine grafted ones. The NO release results for the bare frameworks were once again kindly provided by Dr Paul Wheatley.

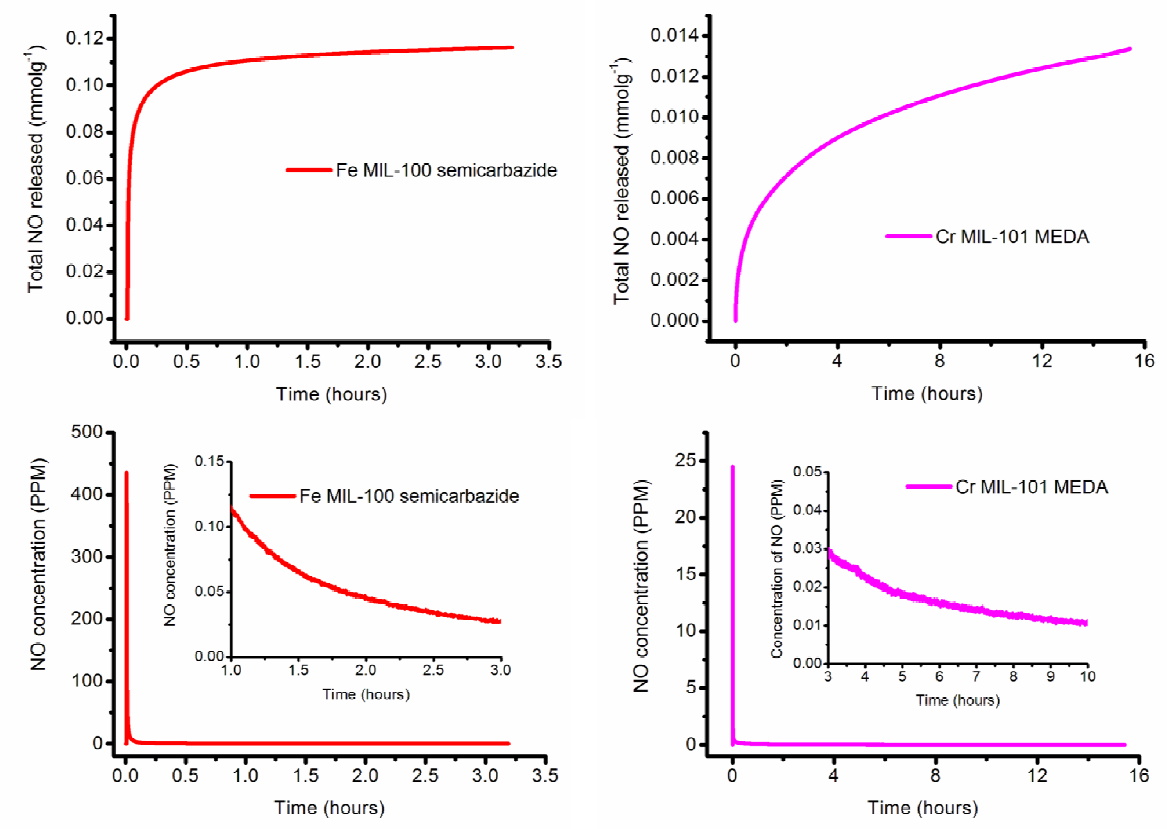

Figure 5.12 NO release curves for the amine-grafted samples of Fe MIL-100 and Cr MIL-101.

MOF	Total NO ads ($mmolg^{-1}$)	NO chemisorbed ($mmolg^{-1}$)	NO delivered gas flow ($mmolg^{-1}$)	% of total NO chemisorbed
Cr MIL-101	4.13	1.75	0.3	17.14%
Cr MIL-101 MEDA	2.49	1.8	0.013	0.722%
Fe MIL-100	2.67	1.81	0.365	20.17%
Fe MIL-100 (250°C)	4.64	3.34	0.6	17.96%
Fe MIL-100 semicarbazide	3.92	2.35	0.12	5.11%

Figure 5.13 Table summarising the NO adsorption and release from all forms of MIL-101 and MIL-100.

From figures 5.12 and 5.13 it is clear that neither of the amine-grafted MILs show higher NO release values than the parent framework. Indeed the values from the MEDA grafted MIL-101 are particularly low. Further analysis reveals that the poorly activated Fe MIL-100 shows a higher release of NO than the semicarbazide loaded version. As mentioned previously, it is very difficult to fully load the CUSs available with secondary amine. This result has been shown already[22]. An explanation might be that only a certain number of the metal sites are bound with amine. The loading of the amine onto the metal sites blocks the pores slightly and therefore when exposed to NO only a certain percentage of NO can access the pores and attach either directly to the metal or to the amine (forming the NONOate). When this is then exposed to moisture the NO adsorbed is released, however as seen previously only a small percentage of the NO bound to the metal will actually be released. Therefore smaller total NO release values are obtained.

5.5 In-situ IR investigation of NO on Fe MIL-100

As mentioned previously the Morris group collaborate closely with the Férey group in France on certain aspects of MOF chemistry and in particular the NO adsorption and release from various MIL frameworks. Initial results from iron carboxylate-based MOFs show lower than expected release of NO. In-situ IR measurements were then carried out on Fe MIL-100 to try to understand the processes involved in loading and release of NO from the framework. These experiments were all carried out at the in-situ IR facility located in Caen France. Several experiments were undertaken and the results give an insight as to why the release of NO is lower than expected.

5.5.1 Fe MIL-100 exposed to NO

Fe MIL-100 was activated at 250°C for 12 hours. An IR spectrum was taken of the activated MOF and used as a comparison with the NO-loaded spectra. Before being exposed to NO there are peaks observable at 1913 cm^{-1} and 1896 cm^{-1} which are most likely due to C-H stretches associated with the para-substituted benzene ring present in Fe MIL-100. When exposed to NO, an immediate change is noticeable in the IR spectra. Peaks appear at 1822 cm^{-1} and 1809 cm^{-1} which correspond to NO adsorbing at Fe^{2+} sites ($Fe^{II}(NO)$). These changes can be seen in figure 5.14. What can be seen from this result is the definite interaction between Fe^{2+} and NO, and that there is little interaction observed between Fe^{3+} and NO although there may be unsaturated Fe^{3+} sites in the framework. The hydrated structure contains only Fe^{3+} iron and so it is strange that interactions with are more prevalent with Fe^{2+}. This "self-reduction" of Fe^{3+} to Fe^{2+} has been explained (in the case of zeolites) as a

hypothetical hydrolysis reaction[23-24] (5.1). There are observable interactions between Fe^{3+} and NO at low temperatures (77K) where a sharp peak appears at 1895 cm^{-1} signifying this interaction and indeed showing that there are unsaturated Fe^{3+} sites even after activation. However as the temperature is increased this peak disappears indicating that the interaction between Fe^{3+} and NO is weak and more likely to be physisorbing than chemisorbing. The peak also appears at high loadings of NO however as we are interested in the chemisorbed NO, small loadings of NO were used (~10 torr) for all further experiments, so the Fe^{3+}-NO peak is generally absent.

$$2[Fe^{3+}OH^{-}] = 2[Fe^{2+}] + H_2O + \tfrac{1}{2}O_2 \qquad (5.1)$$

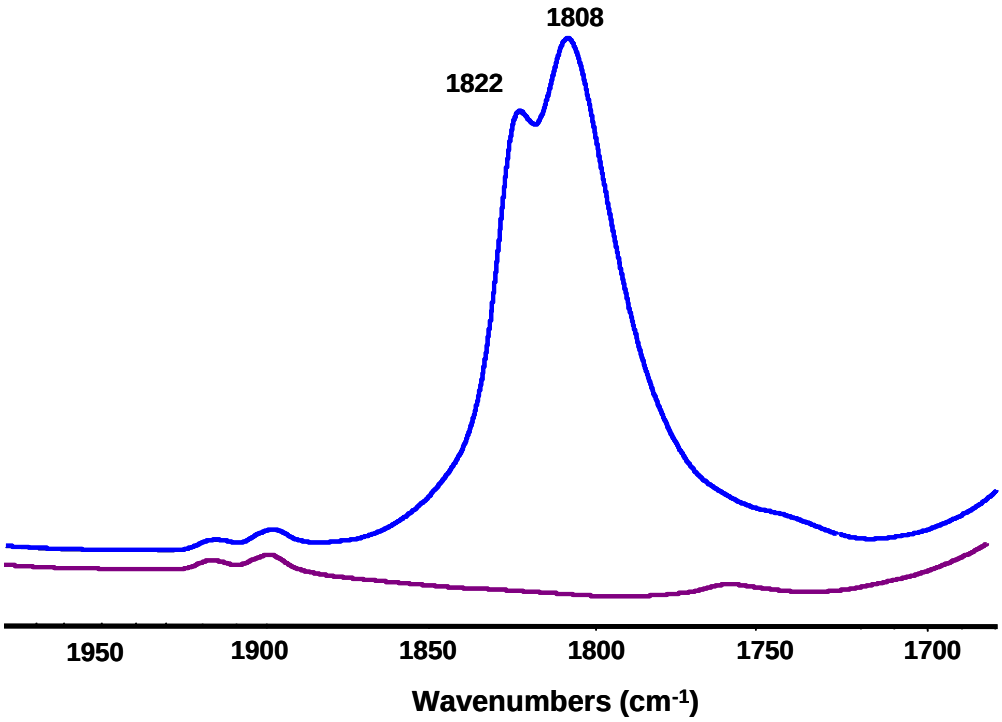

Figure 5.14. IR spectra of Fe MIL-100 activated at 250°C/12h upon exposure to NO at RT. The purple line shows Fe MIL-100 under vacuum after activation at 250°C for 12 h. The blue line shows Fe MIL-100 upon initial exposure to NO. Peaks are observable for Fe^{II}(NO).

5.5.2 Fe MIL-100 under prolonged exposure to NO

In order to study the stability of NO on the Fe^{2+} sites, a sample of Fe MIL-100 was exposed to 10 torr of NO for a prolonged period of time (~14 hours). During this time IR measurements were taken. As can be seen in figure 5.15 it appears that the NO peaks associated with Fe^{II}(NO) decrease in intensity. Indeed the peak that appears at 1822 cm^{-1}, when first exposed to NO almost disappears completely. In combination with this loss of the Fe^{II}(NO) peak intensity there is an increase of water observed. This could be due to the evolution of water as a result of an interaction between NO and the Fe-OH groups[25]. The peak at 3674 cm^{-1} may indicate the presence of Fe^{3+}-OH groups. This peak can be seen in figure 5.16.

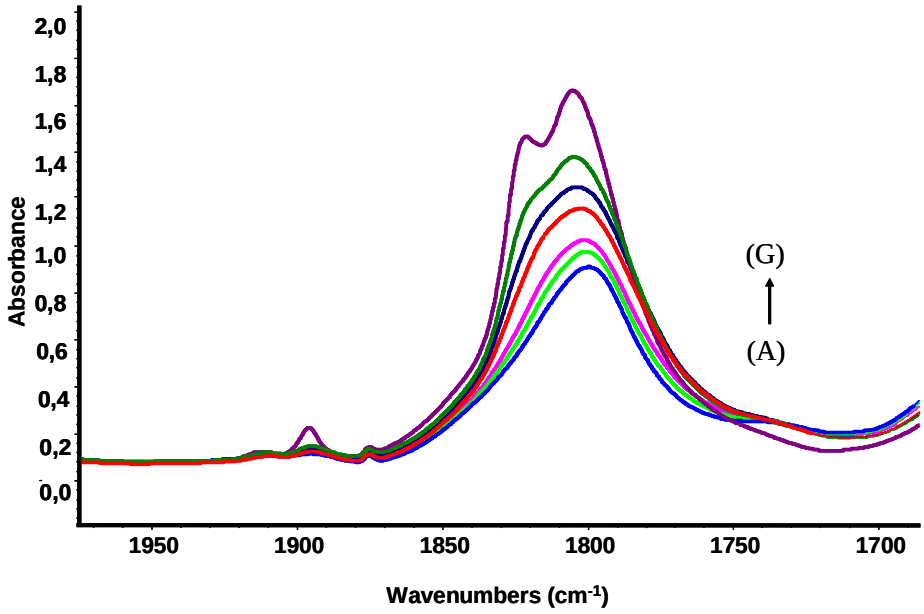

Figure 5.15. IR spectra of Fe MIL-100 comparing NO adsorption on Fe^{II} sites under prolonged exposure to NO, spectra taken at 298K: (A) 816 min; shoulder at 1822 cm^{-1} has almost completely disappeared, and peak at 1805 cm^{-1} has shifted to 1799. (B) 722 min. (C) 628 min. (D) 440 min. (E) 346 min. (F) 227 min; peak at 1897 cm^{-1} disappears, and peak at 1822 cm^{-1} becomes shoulder. (G) 31 min; peaks at 1897, 1876 (NO gas), 1822, and 1805 cm^{-1}.

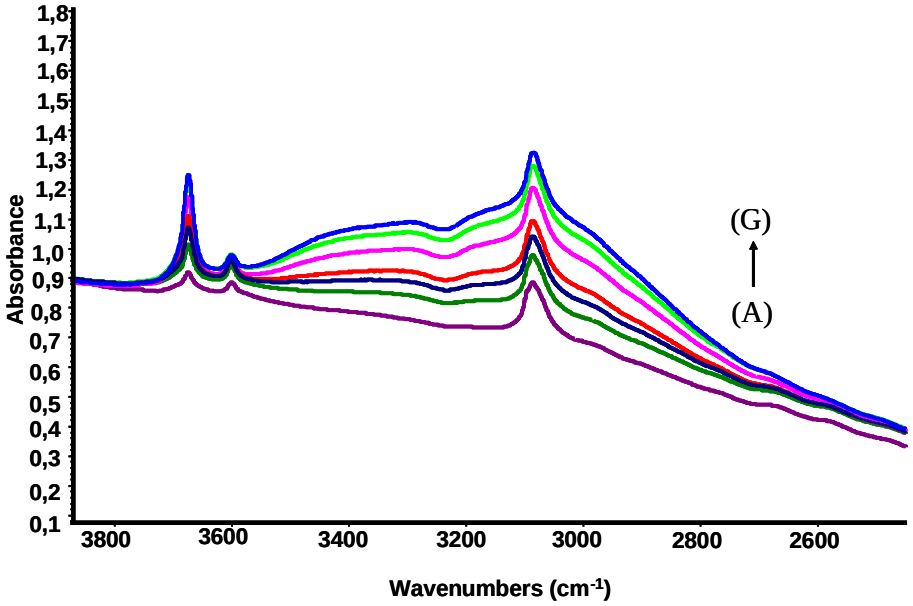

Figure 5.16. IR spectra of Fe MIL-100 comparing NO adsorption on Fe^{II} sites under prolonged exposure to NO, spectra taken at 298K: (A) 31 min; peaks observable at 3676, 3601, and 3087 cm^{-1}. (B) 227 min. (C) 346 min. (D) 440 min. (E) 628 min. (F) 722 min. (G) 816 min; peaks at 3676, 3601, and 3087 cm^{-1} have continued to increase in intensity, along with a broad background intensity increase.

This result suggests that unless completely sealed off, the amount of NO available for release will gradually decrease and the amount of water present in the framework will increase.

5.5.3 Spectra of NO-loaded Fe MIL-100 exposed to water

In the release experiments the NO is replaced with water. However the Fe MIL frameworks display minimal release of NO and therefore presumably water does not displace NO. To understand the competitive effect of H_2O and NO at the Fe^{2+} centre, experiments were carried out exposing an NO-loaded sample of Fe MIL-100 to water

vapour. Figure 5.17 shows the changes in the IR spectra for Fe MIL-100 at different stages. Initially no peaks are observed as this is the dehydrated sample prior to NO exposure. However, when NO is allowed into the sample the expected peaks at 1822 and 1809 cm^{-1} appear. The NO is then evacuated and the $Fe^{II}(NO)$ peaks remain, indicating that a chemical bond has formed between the iron atoms and the NO molecules. This is perfectly consistent with the conclusions regarding chemisorption from the adsorption isotherms. Following this, water vapour is then fed into the sample. An immediate reduction in the peak located at 1822 cm^{-1} is seen. It very quickly disappears and a new peak at 1770 cm^{-1} is observed. This peak also disappears over time (90 minutes). Scans were also taken of the gas phase during this experiment and an interesting result was that the peak associated with N_2O species (2224 cm^{-1}) increased over time with the addition of water vapour. It is therefore theorised that the peak at 1770 cm^{-1} is the result of the introduction of water either causing the formation of a dinitrosyl species at the Fe^{2+}, NO dimerisation or possibly as the result of an interaction between H_2O and NO (for example hydrogen bonding). It is thought that the probable explanation for this is the formation of a dimer at the Fe^{2+} site, with the antisymmetric NONO dimer [υ(-O=N)] on the Fe^{2+} centres. This peak should be observed at 1778 cm^{-1} and correlates well with the observed IR spectra[26]. This could lead to the formation of N_2O as has been observed before[27]. This theory is reinforced by the fact that after exposure to H_2O, the gas phase shows the peak attributed to N_2O increasing (see figure 5.18 and 5.19). Further evidenced by the fact that the amount of N_2O does not increase when placed in an empty cell, meaning that the Fe^{2+} site is required to produce the N_2O.

A number of conclusions from this initial result can be drawn. It is clear that after evacuation the $Fe^{II}(NO)$ remain, and this is a strong indication of a chemical bond being formed between the Fe^{2+} and the NO molecule. Another observation is that when initially exposed to water vapour the peak at 1822 cm^{-1} disappears, indicating that some of the bound NO has been liberated. The released NO will be the less strongly bound NO and could be liberated depending on the coordination environment of the surrounding trimer. In one case the $Fe^{II}(NO)$ might be surrounded by two Fe^{III}-OH environments or it might have another $Fe^{II}(NO)$ and one Fe^{III}-OH. Although as can also be seen the water does not displace all the NO indicating that some of the NO remains bound to the iron metal. This explains why there is poor release of NO observed from Fe-based frameworks. Finally the introduction of a new peak at 1770 cm^{-1} combined with the increase in N_2O is consistent with the formation of a NONO dimer at the Fe^{2+} leading to the evolution of N_2O gas[25-26].

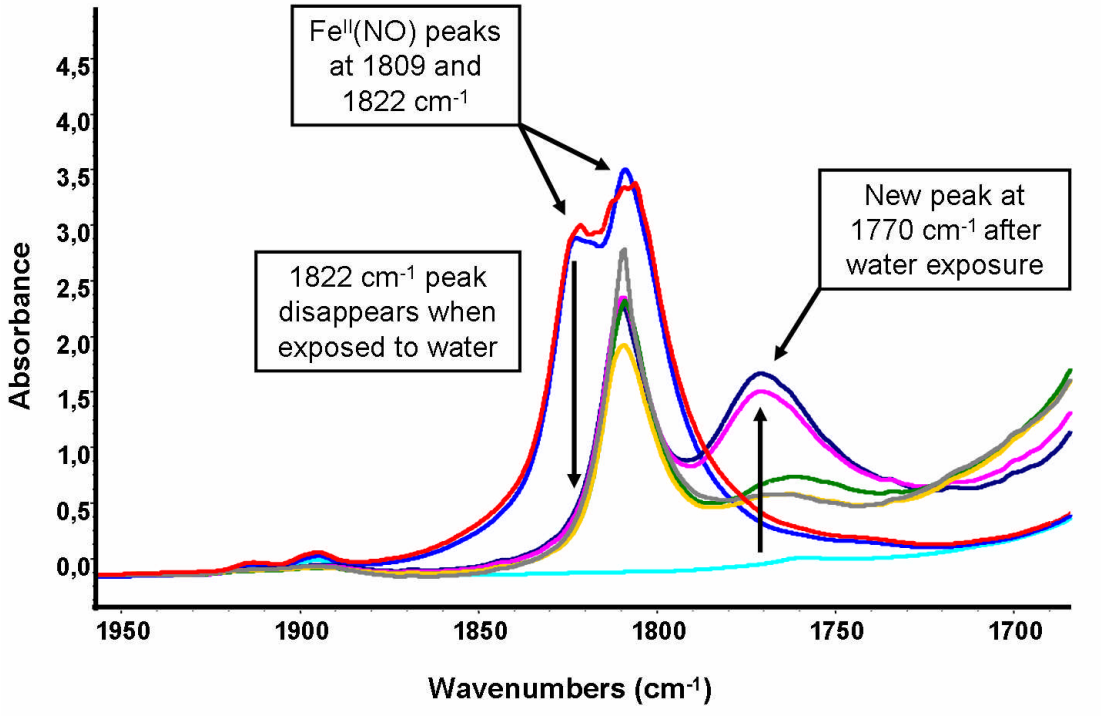

Figure 5.17. Fe MIL-100 activated at 250°C/12h upon exposure to NO followed by H_2O, spectra taken at 298K: IR spectra: cyan sample prior to NO; peaks observable at 1913 and 1896 cm^{-1}. Red line shows initial NO exposure and new peaks appear at 1822 and 1809 cm^{-1}. Blue line after rapid evacuation peaks at 1822 and 1809 cm^{-1} remain showing chemisorption of NO. Dark blue line, after initial H_2O exposure peak at 1822 cm^{-1} disappears, peak at 1809 cm^{-1} decreases in intensity and a new peak emerges at 1770 cm^{-1}. Pink line shows peak at 1770 cm^{-1} decreasing in intensity. Green line shows peak at 1770 cm^{-1} decreasing drastically. Gold line shows peak at 1770 cm^{-1} is practically gone and peak at 1809 cm^{-1} has decreased significantly. Finally grey line shows peak at 1809 cm^{-1} beginning to intensify.

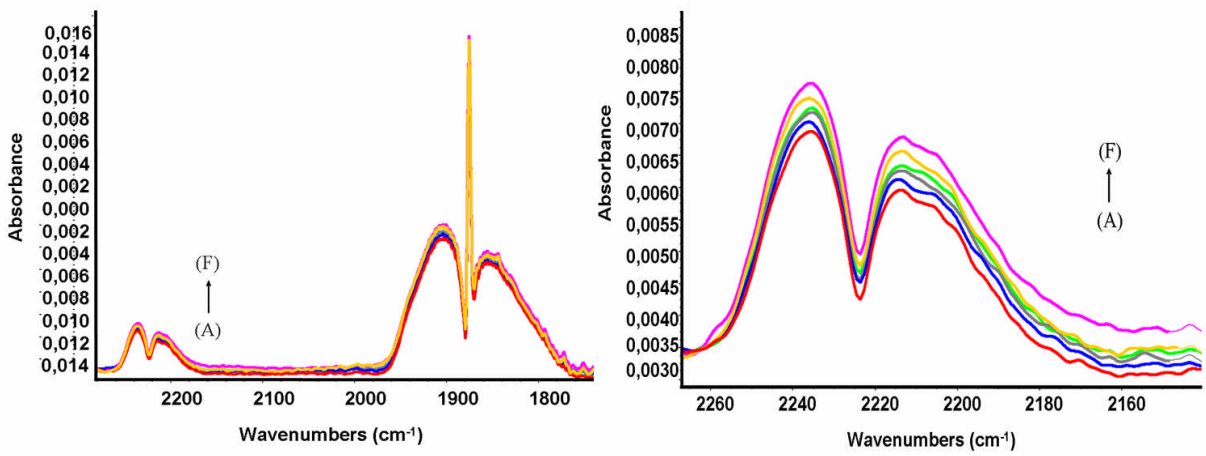

Figure 5.18. Left, IR spectra of gas phase of Fe MIL-100 activated at 250°C/12h upon exposure to NO followed by H_2O, spectra taken at 298K: Spectra showing the evolution of gas phase N_2O (2224 cm^{-1}) and gas phase NO (1876 cm^{-1}) peaks over time. (A) 99 min; peaks are observed at 2236, 2216, and 2203 cm^{-1} (centred at 2224 cm^{-1}). (B) 133 min. (C) 159 min. (D) 361 min. (E) 410 min. Right shows a close up of the N_2O peak region.

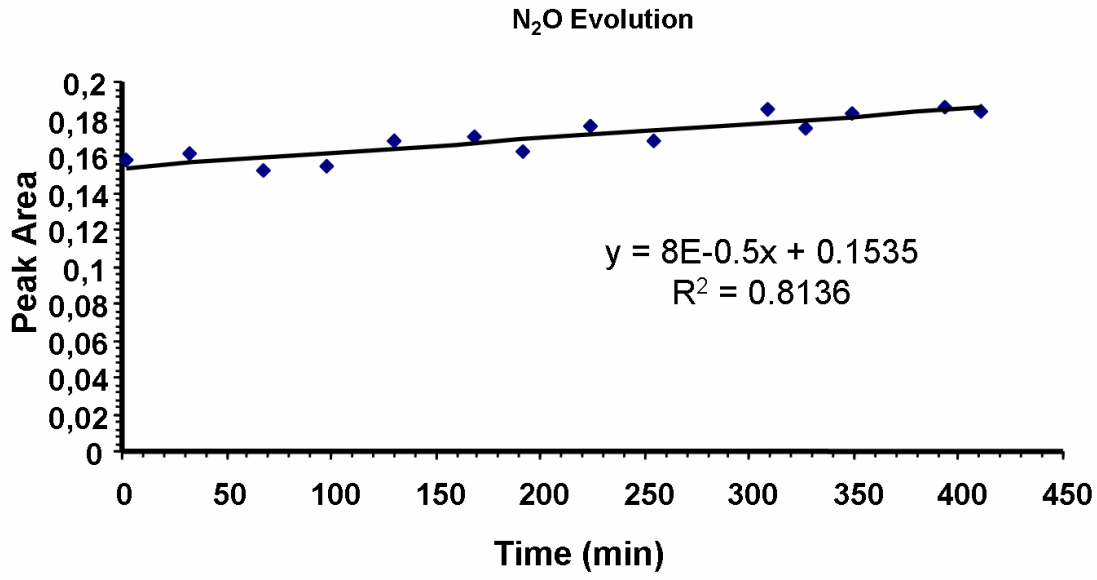

Figure 5.19. Graph of N_2O evolution in the gas phase of Fe MIL-100 activated at 250°C/12h upon exposure to NO followed by H_2O, spectra taken at 298K: There is a general increasing trend in the N_2O peak area over time.

These results show that certain MOFs (certainly those containing iron) do not exhibit the perfect activation, storage and release of NO that has been observed for Ni and Co CPO-27. Indeed once loaded it seems difficult to retrieve all the NO from the iron CUSs. This explains why the release results from the iron-based MOFs are so poor when compared with the amount of NO adsorbed. This could also explain some of the poor release results from certain versions of M-CPO-27, although further experiments would have to be carried out to prove this. It is clear from these results that there is an extremely complex process occurring when activating and loading MOFs with NO. The results shown here correlate well with the theory put forward in chapter 4, explaining that the stability of the dehydrated structure will determine how well the NO-loaded material will release its store of NO when exposed to water vapour.

5.6 Summary of chapter 5

As has been shown, MIL frameworks adsorb and deliver amounts of NO which are considered to be of interest for possible biological applications. The fact that the majority of these frameworks contain iron as the metal source is a significant advantage over other frameworks as iron has limited toxicity for humans. Unfortunately the iron frameworks (whether amine-grafted or not) do not show the almost ideal NO release behaviour associated with Ni and Co CPO-27. This has been explained using in-situ IR experiments and the results have shown the complex process which occurs in iron based MOFs when loading and releasing NO. These results give an insight into the key factors required when considering MOFs for NO storage and the results that can be obtained from them. Despite the relatively poor release of NO obtained from certain Fe MOFs studied here, there is still great potential for the storage and release of NO for medical applications using Fe-based MOFs.

5.7 References

(1) Millange, F.; Serre, C.; Férey, G. *Chem. Commun.* **2002**, 822.

(2) Serre, C.; Millange, F.; Thouvenot, C.; Nogues, M.; Marsolier, G.; Louer, D.; Férey, G. *J. Am. Chem. Soc.* **2002**, *124*, 13519.

(3) Mellot-Draznieks, C.; Serre, C.; Surble, S.; Audebrand, N.; Férey, G. *J. Am. Chem. Soc.* **2005**, *127*, 16273.

(4) Serre, C.; Millange, F.; Surblé, S.; Férey, G. *Angew. Chem., Int. Ed.* **2004**, *43*, 6285.

(5) Surble, S.; Serre, C.; Mellot-Draznieks, C.; Millange, F.; Férey, G. *Chem. Commun.* **2006**, 284.

(6) Eddaoudi, M.; Kim, J.; Rosi, N.; Vodak, D.; Wachter, J.; O'Keeffe, M.; Yaghi, O. M. *Science* **2002**, *295*, 469.

(7) Horcajada, P.; Chalati, T.; Serre, C.; Gillet, B.; Sebrie, C.; Baati, T.; Eubank, J. F.; Heurtaux, D.; Clayette, P.; Kreuz, C.; Chang, J.-S.; Hwang, Y. K.; Marsaud, V.; Bories, P.-N.; Cynober, L.; Gil, S.; Férey, G.; Couvreur, P.; Gref, R. *Nat. Mater.* **2010**, *9*, 172.

(8) McKinlay, A. C.; Xiao, B.; Wragg, D. S.; Wheatley, P. S.; Megson, I. L.; Morris, R. E. *J. Am. Chem. Soc.* **2008**, *130*, 10440.

(9) Xiao, B.; Wheatley, P. S.; Zhao, X. B.; Fletcher, A. J.; Fox, S.; Rossi, A. G.; Megson, I. L.; Bordiga, S.; Regli, L.; Thomas, K. M.; Morris, R. E. *J. Am. Chem. Soc.* **2007**, *129*, 1203.

(10) http://www.pharmics.com/ferretts.htm.

(11) Kitaura, R.; Seki, K.; Akiyama, G.; Kitagawa, S. *Angew. Chem., Int. Ed.* **2003**, *42*, 428.

(12) Wheatley, P. S.; McKinlay, A. C.; Morris, R. E.; Antoine Gédéon, P. M.; Florence, B. In *Stud. Surf. Sci. Catal.*; Elsevier: 2008; Vol. Volume 174, Part 1, p 441.

(13) Férey, G.; Mellot-Draznieks, C.; Serre, C.; Millange, F.; Dutour, J.; Surble, S.; Margiolaki, I. *Science* **2005**, *309*, 2040.

(14) Lebedev, O. I.; Millange, F.; Serre, C.; Van Tendeloo, G.; Férey, G. *Chem. Mater.* **2005**, *17*, 6525.

(15) Horcajada, P.; Surble, S.; Serre, C.; Hong, D. Y.; Seo, Y. K.; Chang, J. S.; Greneche, J. M.; Margiolaki, I.; Férey, G. *Chem. Commun.* **2007**, 2820.

(16) Latroche, M.; Surblé, S.; Serre, C.; Mellot-Draznieks, C.; Llewellyn, P. L.; Lee, J.-H.; Chang, J.-S.; Jhung, S. H.; Férey, G. *Angew. Chem., Int. Ed.* **2006**, *45*, 8227.

(17) Llewellyn, P. L.; Bourrelly, S.; Serre, C.; Vimont, A.; Daturi, M.; Hamon, L.; De Weireld, G.; Chang, J.-S.; Hong, D.-Y.; Kyu Hwang, Y.; Hwa Jhung, S.; Férey, G. *Langmuir* **2008**, *24*, 7245.

(18) Horcajada, P.; Serre, C.; Vallet-Regí, M.; Sebban, M.; Taulelle, F.; Férey, G. *Angew. Chem., Int. Ed.* **2006**, *45*, 5974.

(19) Hwang, Y. K.; Hong, D. Y.; Chang, J. S.; Jhung, S. H.; Seo, Y. K.; Kim, J.; Vimont, A.; Daturi, M.; Serre, C.; Férey, G. *Angew. Chem., Int. Ed.* **2008**, *47*, 4144.

(20) Keefer, L. K. *Annu. Rev. Pharmacol. Toxicol.* **2003**, *43*, 585.

(21) Miller, M. R.; Megson, I. L. *Br. J. Pharmacol.* **2007**, *151*, 305.

(22) Ingleson, M. J.; Heck, R.; Gould, J. A.; Rosseinsky, M. J. *Inorg. Chem.* **2009**, *48*, 9986.

(23) Gil, B.; Adamski, A. *Micropor. Mesopor. Mater.* **2010**, *127*, 82.

(24) Starokon, E. V.; Dubkov, K. A.; Pirutko, L. V.; Panov, G. I. *Top. Catal.* **2003**, *23*, 137.

(25) Blasin-Aubé, V.; Marie, O.; Saussey, J.; Plesniar, A.; Daturi, M.; Nguyen, N.; Hamon, C.; Mihaylov, M.; Ivanova, E.; Hadjiivanov, K. *J. Phys. Chem. C* **2009**, *113*, 8387.

(26) Hadjiivanov, K. I. *Catal. Rev. - Sci. Eng.* **2000**, *42*, 71

(27) Ford, P. C.; Lorkovic, I. M. *Chem. Rev.* **2002**, *102*, 993.

6 Other MOFs for NO storage and delivery

6.1 Introduction

The majority of this thesis thus far has focused on the M-CPO-27 series of materials and iron-based MIL frameworks. However, other MOFs were also synthesised and characterised using NO adsorption and release measurements. All the MOFs were chosen as a comparison with either M-CPO-27 or another MOF already investigated for NO storage and release. The MOFs chosen were Ni succinate, Ni STA-12 and finally Mn and Cu BTT.

6.2 Aims of chapter 6

The overall aim in chapter 6 was to show the NO adsorption and release results obtained from different MOFs and compare them with those already reported. It was also an opportunity to compare different metal centres to see if any effect on the storage and release of NO from different MOFs was observed. Ni succinate and Mn, Cu BTT MOFs were synthesised and the sample of Ni STA-12 was very kindly donated from the Wright group at the University of St Andrews.

6.3 Ni succinate

Paul Forster and Anthony Cheetham synthesised the Ni succinate MOF in 2002[1], and there are numerous different MOF structures utilising different metals with succinic acid as the organic linker[2-5]. Indeed, high-throughput analysis has shown that reaction conditions play a decisive role in the framework produced from the same

metal and succinic acid[6] reactants. The Ni succinate that Forster and Cheetham produced was the first porous succinate structure and also the first hybrid to display full 3D metal-oxygen-metal connectivity. The structure of Ni succinate can be seen in figure 6.1. It shows a framework similar to the honeycomb of M-CPO-27. This Ni succinate material also contains coordinatively unsaturated metal sites (CUS) when fully activated, and should therefore provide an interesting comparison with the M-CPO-27 series of structures.

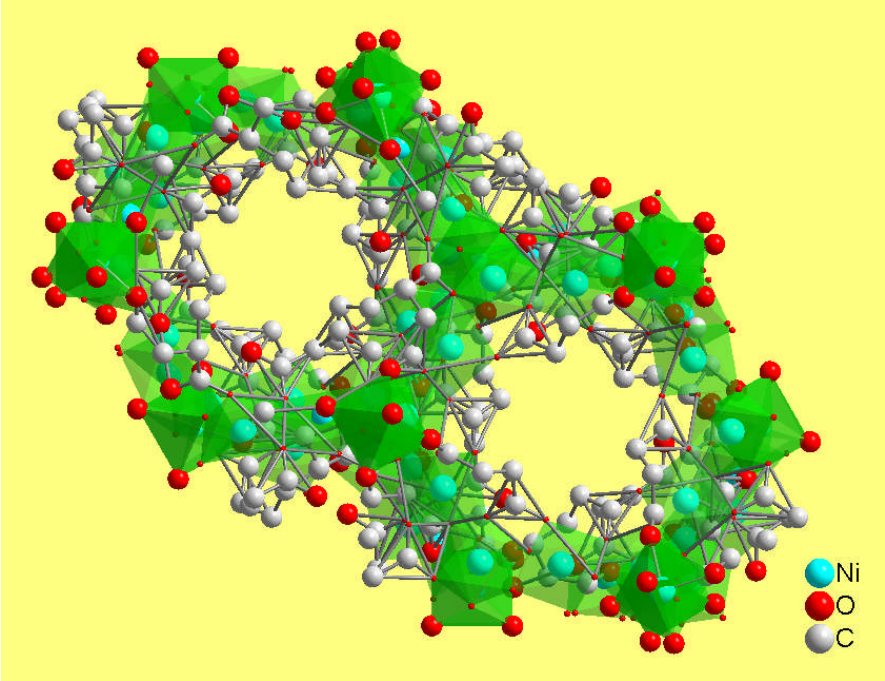

Figure 6.1 A portion of the Ni succinate structure, viewed down the c-axis. Hydrogen atoms are removed for clarity.

Using the method described in the literature[1], Ni succinate was successfully synthesised using Ni acetate and succinic acid mixed in water in the ratio 1:2:50. The mixture was then placed in autoclaves for 3 days at 150°C. Following synthesis, characterisation methods were employed to confirm that the powder obtained was indeed Ni succinate. Comparing both the experimental and theoretical powder

patterns it can be seen that the pattern produced matches very closely with the theoretical one (figure 6.2).

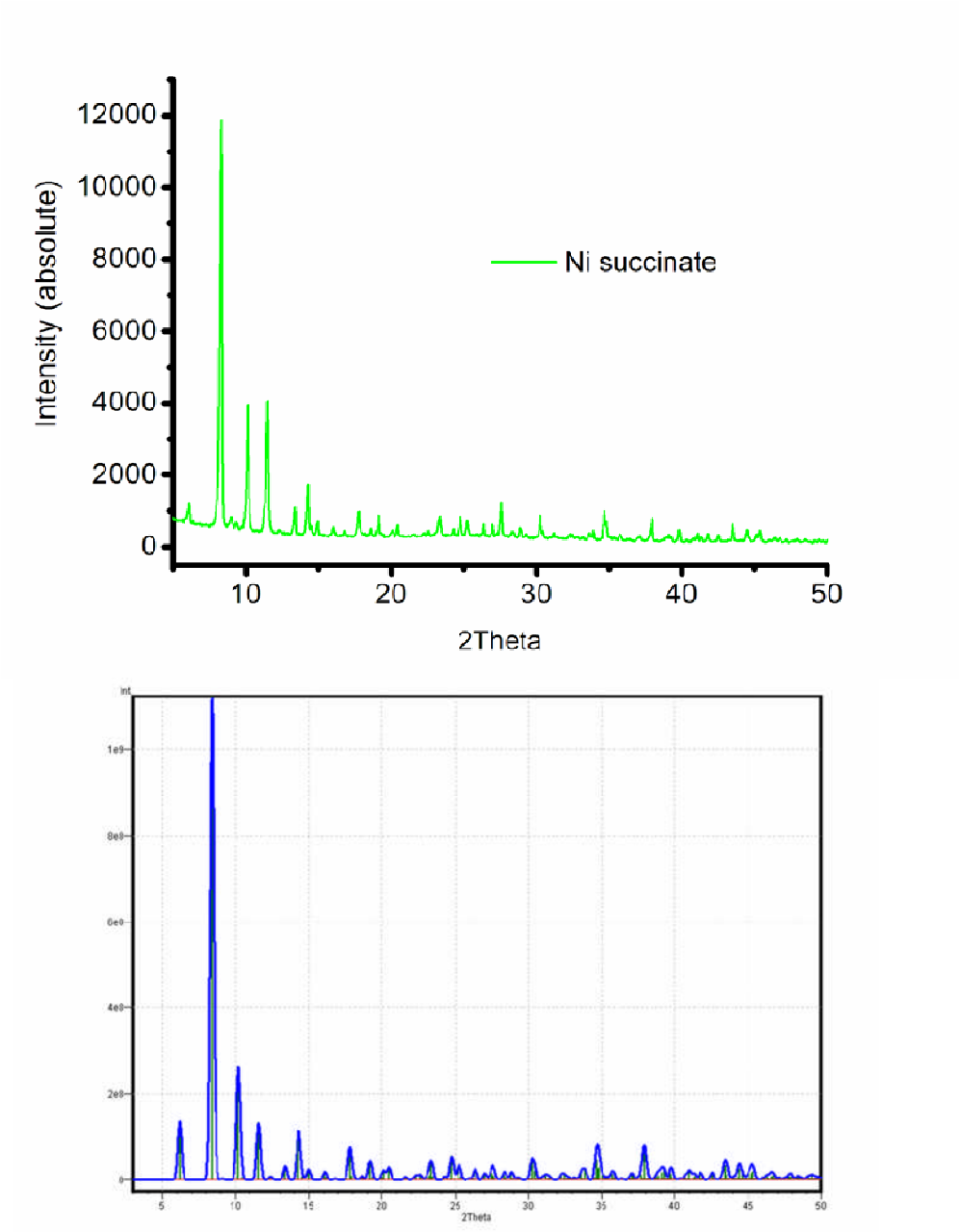

Figure 6.2 Experimental powder XRD pattern of Ni succinate (top) and theoretical powder pattern of Ni succinate produced with Diamond 3.0 software (bottom).

XRD analysis was then followed by TGA measurements. The graph obtained can be seen below (figure 6.3). This closely matches the literature, and two distinct mass losses are obtained. The first gradual mass loss between 50 and 250°C corresponds to both the coordinated and uncoordinated water molecules being removed (~6%). The second loss occurs at ~300°C and corresponds to pyrolysis of the succinic acid and destruction of the framework (~50%).

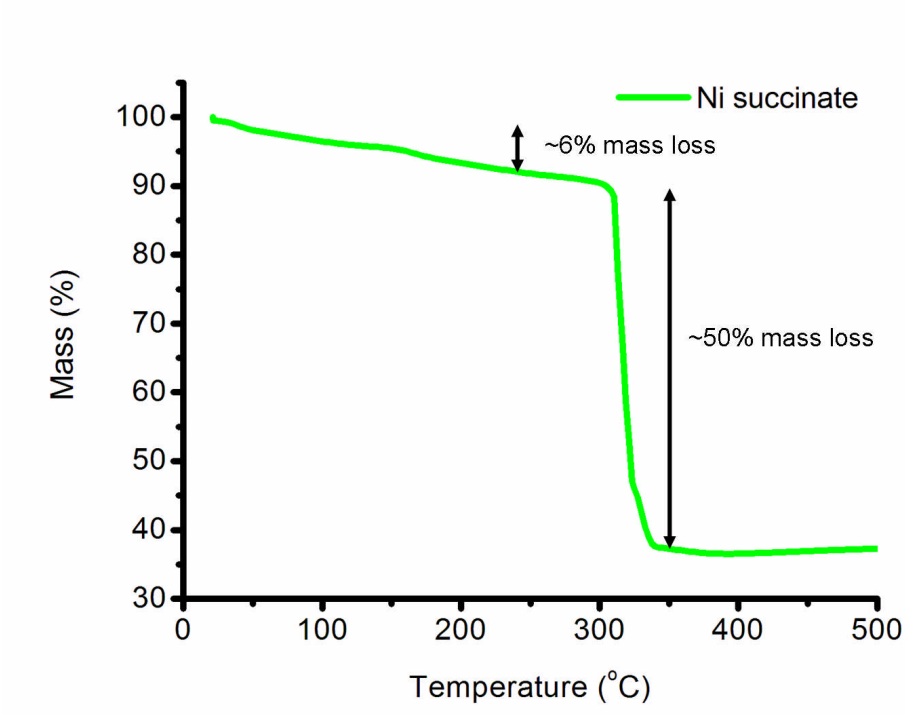

Figure 6.3 An experimental TGA curve performed under air atmosphere of Ni succinate showing the two distinct mass losses.

The results from both the XRD and TGA confirm that the required Ni succinate phase has been obtained. Following dehydration procedures (240°C under vacuum) the Ni succinate was exposed to NO for both adsorption and release measurements. One key observation is that the Ni succinate samples change colour when activated, from blue-green to a much lighter green. This is one of the indicators of CUSs being

present in the structure. NO adsorption measurements on the framework were then carried out. The NO adsorption/desorption isotherm can be observed in figure 6.4.

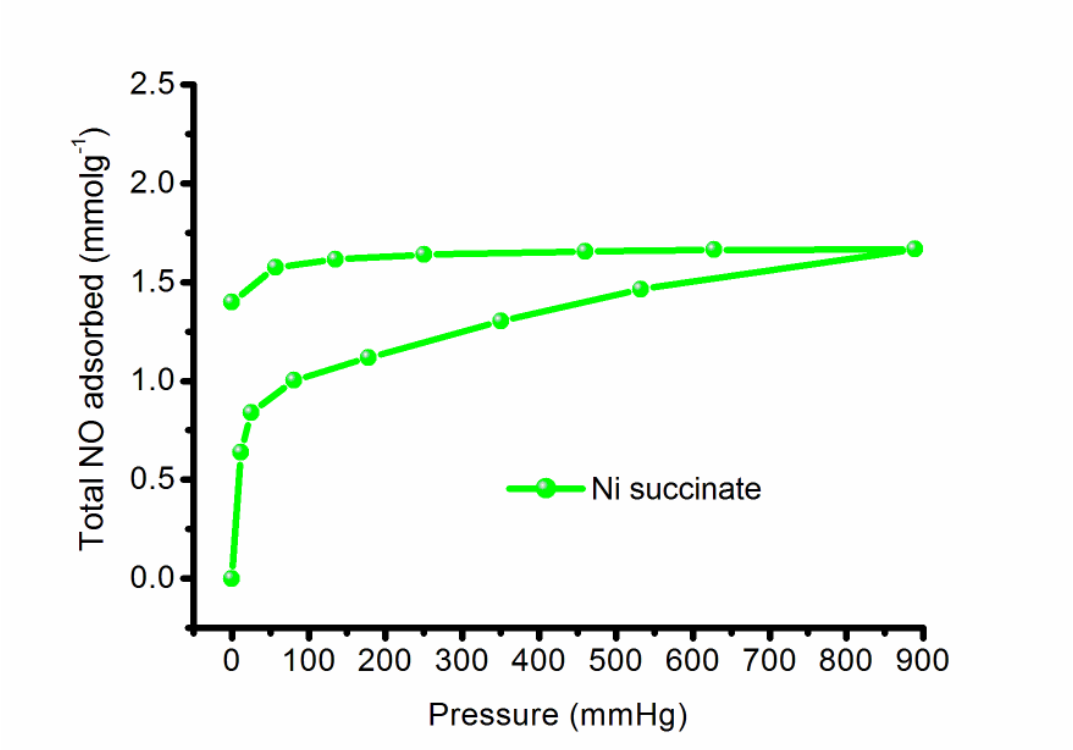

Figure 6.4 NO adsorption isotherm carried out at 298K for Ni succinate.

As can be seen both the total NO adsorbed and the amount of NO chemisorbed are much lower compared with the Ni CPO-27 structure. However this is not surprising as the pores in Ni succinate are congested with methylene groups from the succinic acid and so there is much less space available in the structure for NO to occupy. The theoretical chemisorption of NO for Ni succinate is 1.75 $mmolg^{-1}$ based on 1 NO per metal atom. The actual amount irreversibly adsorbed experimentally is 1.4 $mmolg^{-1}$, which is very close to the theoretical adsorption. This implies that there may be some CUSs that are not fully unsaturated or that there may be some pore blockage which does not allow NO into the pores as they are only ~4Å wide and NO has a kinetic diameter of 3.1Å. Measurement of NO release from 4 samples showed an average

release of ~1.1 mmolg^{-1} of NO and the samples released biologically significant amounts of NO for about 12 hours. The graphs of release measurements can be seen below in figure 6.5.

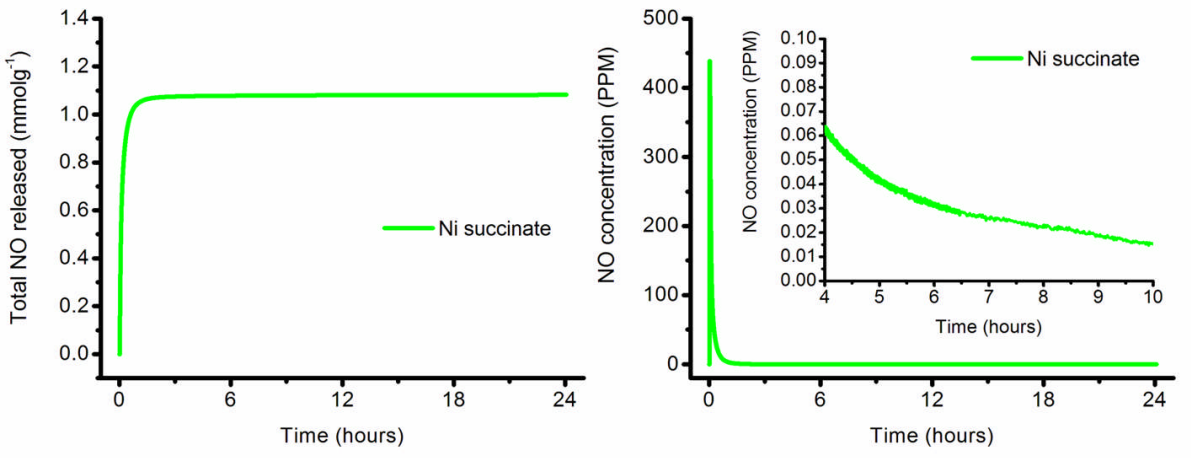

Figure 6.5 Total NO release and concentration measurements for Ni succinate over 24 hours.

As illustrated, the total NO released is almost the same as the amount initially adsorbed. In fact, the framework releases 78.5% of its store which is much higher than most other frameworks investigated. This is a significant result as it shows that both Ni CPO-27 and Ni succinate release almost the same amount of NO as they adsorb. This implies that Ni metal has a good affinity for NO, which is then easily replaced with water when exposed to moisture.

6.4 Ni STA-12

The vast majority of MOFs which have shown promise for gas storage and release have used dicarboxylic acids as the organic linker. There has, however, been an increase in research into alternative linkers for use in MOFs. One of the most heavily researched alternative linker types is phosphonates[7]. The Wright group based at the University of St Andrews have focused their efforts on synthesising MOFs using phosphonate linkers[8-9]. They successfully created large pore metal phosphonate structures in 2006 utilising two different phosphonate linkers[8], *N,N'*–piperazinebis(methylenephosphonic acid) and *N,N'*-2-methylpiperazinebis(methylenephosphonic acid). Reactions of *N,N'*–piperazinebis(methylenephosphonic acid) with nickel, cobalt and iron resulted in the formation of a MOF known as STA-12 (St Andrews porous material-12), the structure of which can be seen in figure 6.6. Ni STA-12 has the molecular formula $Ni_2L{\cdot}8H_2O$ where L= $O_3PCH_2NC_4H_8NCH_2PO_3$. The structure consists of inorganic chains of edge-sharing NiO_5N octahedra and the resulting structure looks very similar to that of Ni CPO-27. Indeed Ni STA-12 has CUSs upon activation of the framework in a similar manner to that of Ni CPO-27, however as phosphonates show higher thermal stability, Ni STA-12 is stable to a higher temperature by about 100°C. The cobalt and iron versions of STA-12 are less thermally robust and indeed the iron analogue collapses during dehydration[8]. However Ni STA-12 differs from Ni CPO-27 in that during activation its structure changes. When initially removing the uncoordinated (physisorbed) water molecules it retains its hexagonal honeycomb structure. However, after treatment at 373K all the coordinated water molecules are

removed and the structure shifts to a triclinic space group (P-1) and changes to an elliptical shape rather than the hexagonal shape observed initially[9] (see figure 6.6).

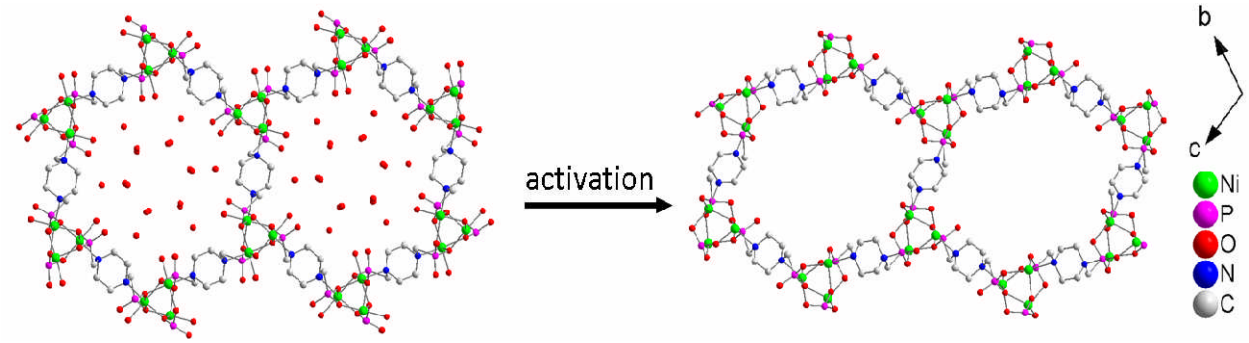

Figure 6.6 A diagram of the structure of Ni STA-12 viewed down the a-axis before and after activation. As can be seen the structure changes during activation.

Ni STA-12 was chosen for NO adsorption measurements as it should provide a useful comparison with Ni CPO-27 and Ni succinate. Ni STA-12 had also already shown to be of significant interest in the storage of fuel related gases[9]. It has a very similar structure visually to Ni CPO-27 and contains unsaturated Ni^{2+} sites when activated, and as such was expected to show good adsorption and release of NO. A sample of Ni STA-12 was very kindly donated by the Wright group to allow NO experiments to be performed on this phosphonate-based MOF. Following activation at 150°C, the NO adsorption measurements were carried out. The NO adsorption curve can be seen in figure 6.7.

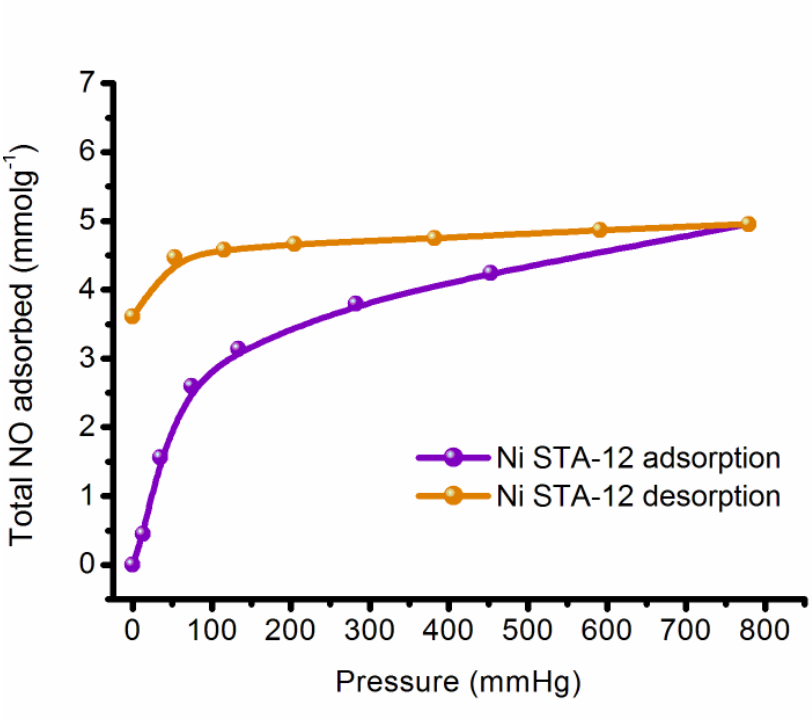

Figure 6.7 NO adsorption isotherm for Ni STA-12 carried out at 298K.

As can be observed, a large amount of NO is adsorbed by Ni STA-12. This is not unexpected as there should be the same number of CUSs per gram as for Ni CPO-27 and the structures are relatively similar. The theoretical adsorption of NO in Ni STA-12 is 5.2 $mmolg^{-1}$, assuming one NO per available Ni^{2+} site. It adsorbs 5 $mmolg^{-1}$ and when exposed to vacuum, retains about 3.5 $mmolg^{-1}$, which is an indicator of chemisorption. It is clear that the huge initial uptake of NO seen in Ni CPO-27 is not observed in the Ni STA-12 structure.

Release experiments were also carried out on Ni STA-12. The same activation procedure was applied (150°C under vacuum) and samples of Ni STA-12 were exposed to 2 atm of NO. The release curves that Ni STA-12 displayed can be seen in figure 6.8.

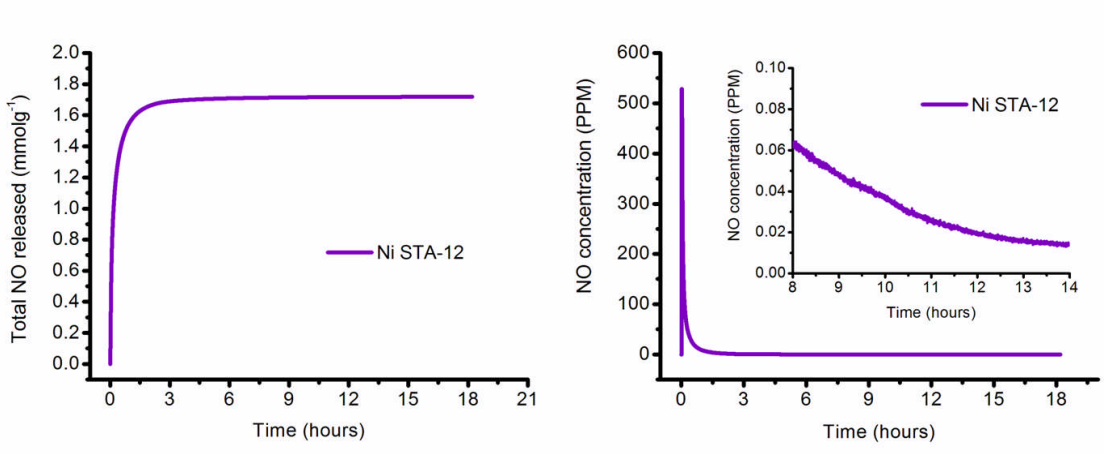

Figure 6.8 NO release curves for Ni STA-12.

From figure 6.8 it can be seen that Ni STA-12 does not release its entire store of NO, however it does release ~1.7 mmolg^{-1} which is about 50% of the total NO initially adsorbed. It is also still releasing biologically significant quantities of NO after 14 hours. These results confirm that Ni is very good at binding and releasing NO in all three of the structures investigated (Ni CPO-27, Ni succinate and Ni STA-12).

6.5 Mn and Cu BTT

Another alternative ligand which has been used for the creation of MOFs is the polytetrazolate-based ligand known as 1,3,5-tris(tetrazol-5-yl)benzene (BTT). This ligand was used in the preparation of two isostructural frameworks which show CUSs upon desolvation and display high hydrogen uptakes[10-11]. In 2006 Jeffrey Long's group produced a microporous MOF which contained unsaturated Mn^{2+} sites after activation[11]. This activated MOF adsorbs a large amount of hydrogen and through neutron scattering experiments it was shown that the hydrogen binds at the exposed metal site. A Cu based isostructural analogue was also successfully synthesised. Hydrogen storage measurements were also carried out on this version[10] and it displayed an uptake of 5.7 wt% at 90 bar, which is slightly lower than the Mn version which shows an uptake of 6.9 wt% at 90 bar.

The chemical formula for both Mn and Cu versions of this MOF is $[M(DMF)_6]_3[(M_4Cl)_3(BTT)_8(H_2O)_{12}]_2.42DMF.11H_2O.20CH_3OH$ where H_3BTT = 1,3,5– tris(tetrazol-5-yl)benzene). The MOF's structure is cubic, in which $[M_4Cl]^{7+}$ square planer units are linked via BTT^{3-} ligands to form an anionic 3D framework (see figure 6.9). A sodalite[12] type cage structure is formed. Within this framework water ligands occupy the sixth coordination site on each M^{2+}. These water groups can be removed under activation to allow access to the unsaturated Mn and Cu sites. This framework is synthesised using DMF and therefore has to be solvent-exchanged with methanol prior to activation to allow full activation and access to the unsaturated metal sites. The structure shows a remarkable similarity to that of HKUST-1 on which NO measurements have already been carried out[13].

Surface area measurements carried out on these frameworks show large BET N_2 isotherms. The Mn version (when activated) displays a calculated BET surface of 2100 m^2g^{-1} and the Cu version 1710 m^2g^{-1}. This discrepancy is due to shorter bond lengths shown in the Cu version which contracts the unit cell parameters[10].

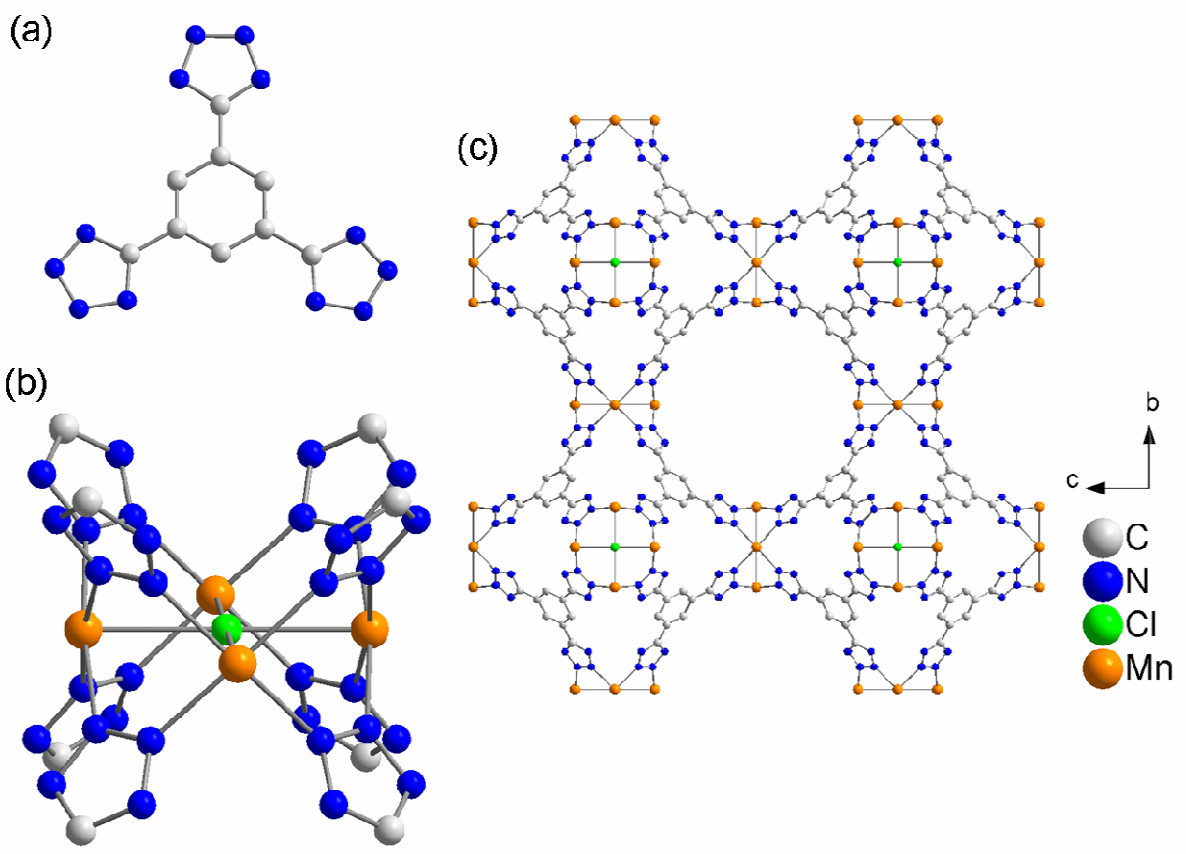

Figure 6.9 (a) The tritopic ligand H_3BTT. (b) The square-planer Mn_4Cl surrounded by 8 tetrazolate rings (c) A portion of the activated MOF's cubic structure shown down the a-axis. Hydrogen atoms and solvent molecules are omitted for clarity.

6.5.1 Synthesis of Mn and Cu BTT

Both versions of this MOF were synthesised. Initially the BTT ligand had to be synthesised as it cannot be purchased through commercial vendors. Using the methods described in the literature[11,14] firstly 1,3,5-tricarbamoylbenzene then 1,3,5-tricycanobenzene were synthesised, followed by 1,3,5-tris(2*H*-tetrazol-5yl)benzene hydrochloride. Finally using the prepared linker the MOF structure could be formed.

6.5.1.1 Synthesis of 1,3,5-tricarbamoylbenzene

Following the procedure in the literature[14], benzene-1,3,5-tricarbonyl trichloride was added to concentrated ammonia solution. Once the vigorous exothermic reaction had subsided a white precipitate formed which was then stirred for 2 hours at room temperature. The solid was filtered, and washed with ethanol and diethyl ether before being dried overnight in an oven at 110°C. This product was then used to form 1,3,5-tricyanobenzene. 1,3,5-tricarbomoylbenzene is insoluble in all common solvents so was used as prepared.

6.5.1.2 Synthesis of 1,3,5-tricyanobenzene[14]

A calculated amount of 1,3,5-tricarbamoylbenzene was added to DMF. Thionyl chloride was added to the suspension over 1 hour while maintaining a temperature of 60°C. After the addition of the thionyl chloride, stirring at 60°C was maintained for a further 6 hours in which time complete dissolution occurred. Pouring the solution into dilute hydrochloric acid (HCl) to decompose unreacted $SOCl_2$ resulted in a dense white precipitate. The solid was filtered and washed with water until neutral to pH paper and then dried at 110°C overnight. Crystallisation from a mixture of

acetone and ethanol resulted in the product being formed as colourless needles. The ^{1}H NMR of the product was carried out in deuterated dimethyl sulfoxide (DMSO) and compared with the literature. The resulting spectrum can be seen in figure 6.10. NMR [$(CD_3)_2SO$]: ^{1}H δ 8.80 (s, 3H, o-C_6H_3).

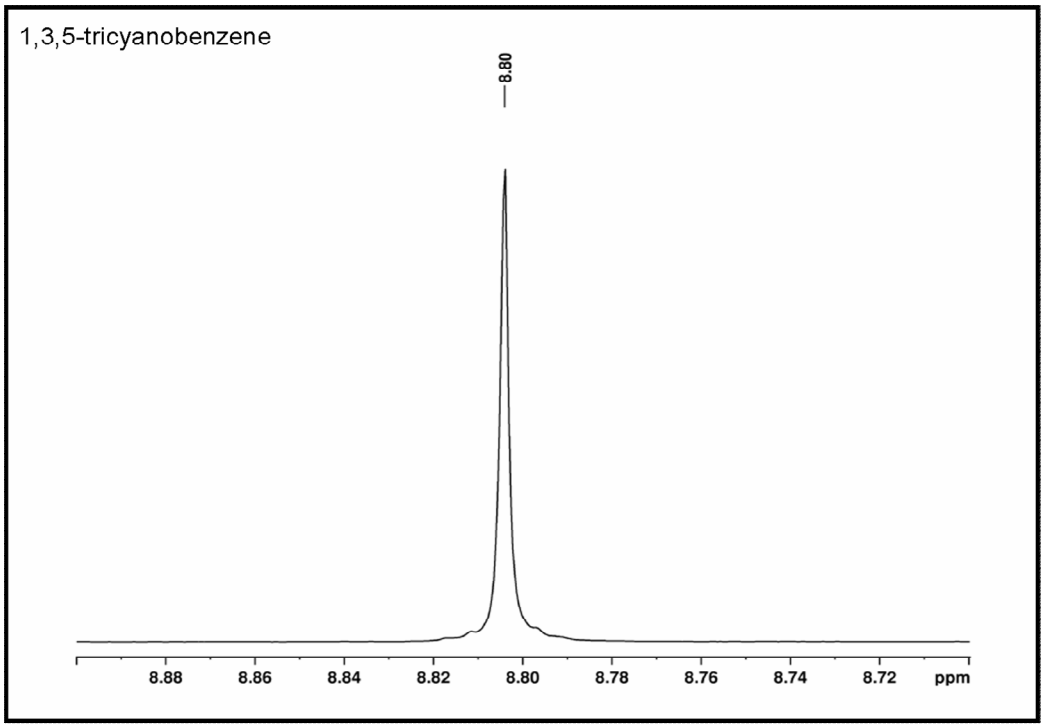

Figure 6.10 ^{1}H NMR spectrum of 1,3,5-tricyanobenzene.

6.5.1.3 1,3,5-tris(2*H*-tetrazol-5-yl)benzene hydrochloride[11]

A mixture of 1,3,5-tricyanobenzene, sodium azide and triethylamine hydrochloride in 150 ml of toluene and 30 ml methanol was heated to reflux in a 500ml round-bottomed flask for 3 days. After cooling to room temperature 100 ml of aqueous sodium hydroxide (NaOH 1 $molL^{-1}$) was added and the mixture was stirred for 30 minutes. The aqueous layer was then treated with 100 ml dilute HCl until a white precipitate formed, and this was then filtered and dried before being dissolved in 1M NaOH. The resulting clear colourless solution was titrated with ~75 ml of 1M HCl until the pH was 4-5. The resulting white precipitate was washed with water, methanol and acetone to yield the final product[11]. Again the ^{1}H NMR spectrum was collected using DMSO and the spectrum can be seen in figure 6.11. NMR [$(CD_3)_2SO$]: ^{1}H, δ 8.85 (s, 3H, o-C_6H_3). A ^{13}C spectrum was also obtained and the spectrum is in shown in figure 6.12. NMR [$(CD_3)_2SO$]: ^{13}C, 125.72 (*o*-C of C_6H_3), 129.13 (*ipso*-C of C_6H_3) and 157.11 (C of tetrazol).

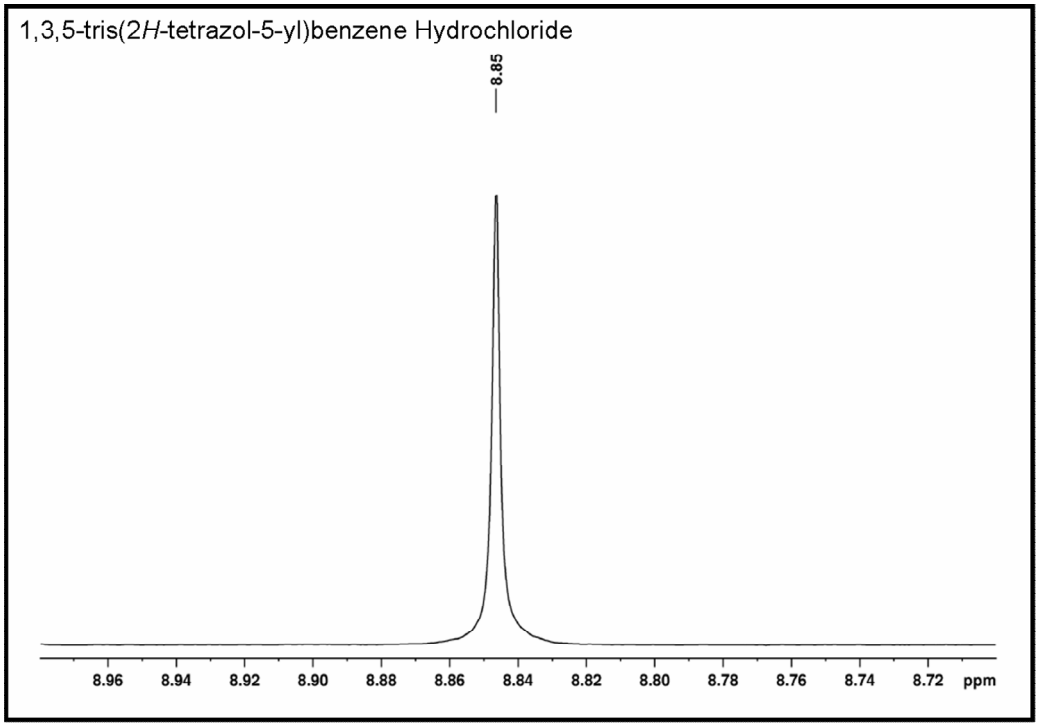

Figure 6.11 ^{1}H NMR spectrum of 1,3,5-tris(2*H*-tetrazol-5-yl)benzene hydrochloride.

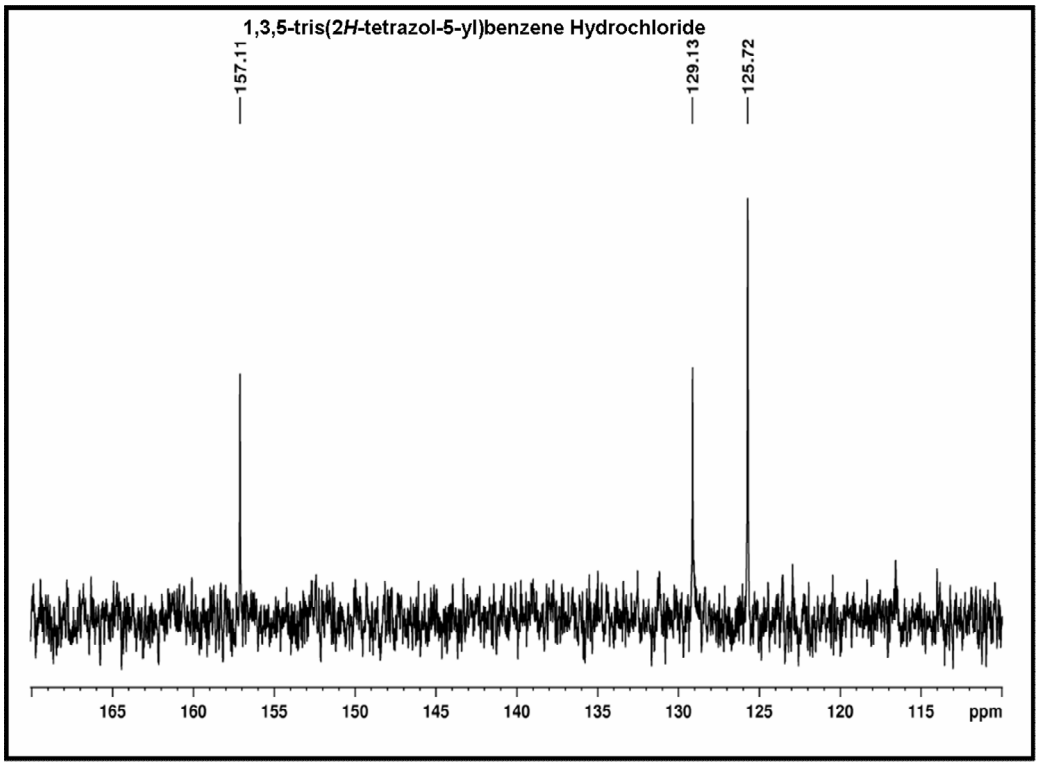

Figure 6.12 ^{13}C NMR spectrum of 1,3,5-tris(2*H*-tetrazol-5-yl)benzene hydrochloride.

6.5.1.4 Synthesis of the framework

Both versions of the framework were synthesised in a similar manner. A metal salt solution of Mn or Cu chloride was dissolved in methanol and added to a solution of $H_3BTT.2HCl.H_2O.CH_3OH$ dissolved in DMF in the Teflon liner of an autoclave. The pH of the slurry was adjusted to ~3 using 1M HCl. The mixture was then capped and placed in the metal autoclave before being sealed. The Mn version was heated at 70°C and the Cu analogue was synthesised at 60°C, both for 24 hours before filtering the resulting powder and washing with DMF and methanol.

6.5.2 Characterisation of Mn and Cu BTT

Following successful synthesis, powder XRD was employed to characterise the synthesised Mn and Cu BTT structures. It should be noted at this point that both Mn and Cu BTT are extremely hygroscopic. This meant that XRD measurements were only taken over short times, rather than using overnight runs. Both Mn and Cu BTT were run on the Phillips diffractometer for 90 minutes to prevent degradation of the powder samples. The powder XRD patterns for Mn and Cu BTT can be seen in figure 6.13 along with the theoretical pattern produced for Mn BTT from the cif file using the Diamond 3.0 software. As can be seen the patterns match each other and the theoretical pattern well, although some degradation occurs due to air exposure.

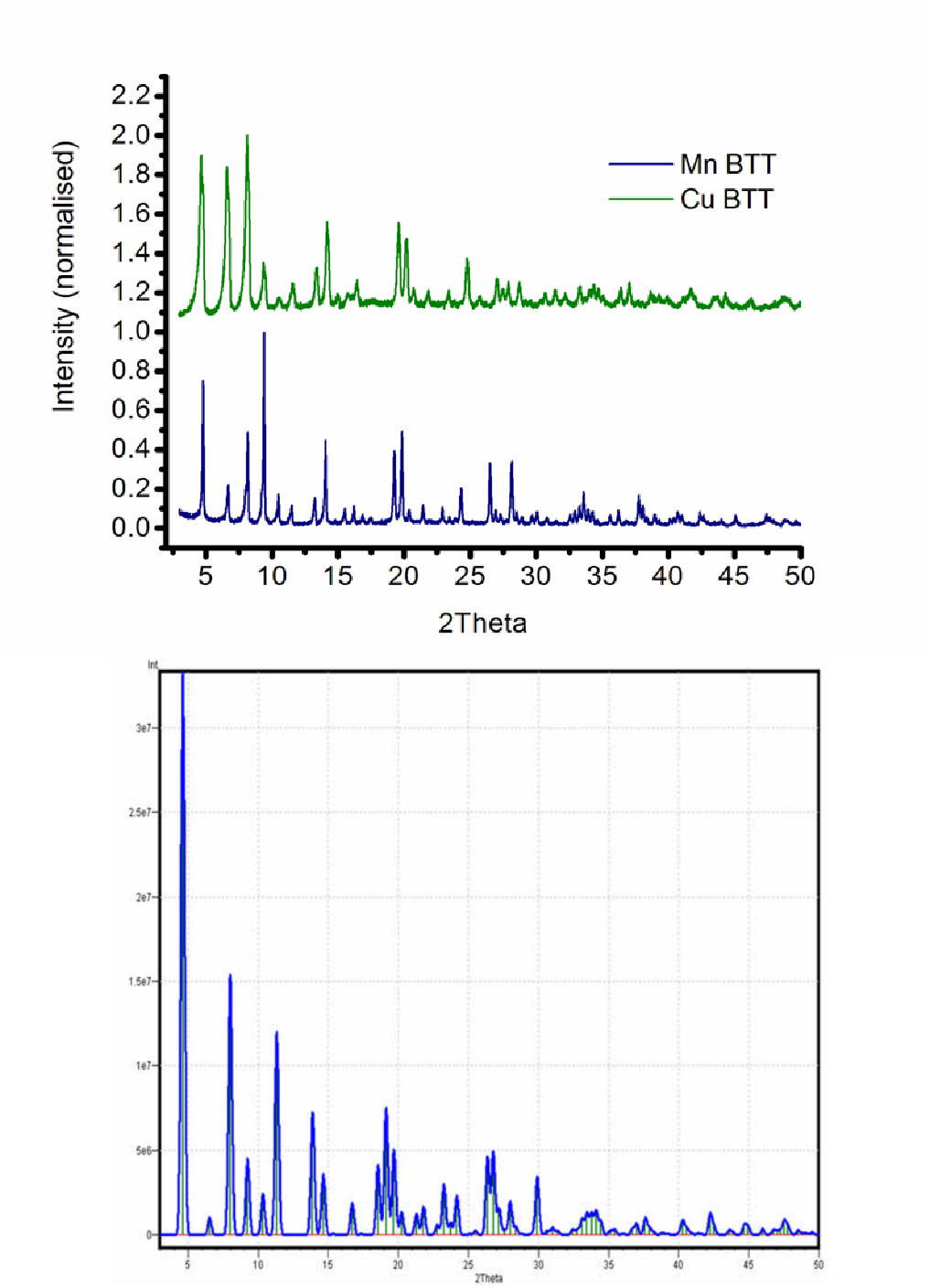

Figure 6.13 The top graph shows the experimental powder XRD patterns of both Mn and Cu BTT. The bottom graph illustrates the theoretical XRD pattern for Mn BTT generated using the Diamond 3.0 software package.

6.5.3 NO adsorption and release results for Mn and Cu BTT

Due to the hygroscopic nature of these MOFs, obtaining accurate NO adsorption and release measurements was difficult. Indeed, following failed attempts to solvent exchange these materials with methanol without exposure to air, it was expected that the NO adsorption and release results would be poor. Unfortunately, NO adsorption measurements could not be made on a solvent exchanged sample due to the degradation shown by the samples during the solvent exchange procedures.

Nevertheless NO adsorption and release measurements were taken for both versions of this MOF prior to solvent exchange and the results are detailed below.

The NO adsorption graph for both the Mn and Cu versions of this MOF can be seen in figure 6.14. As explained earlier, these curves are for the samples that have not been solvent exchanged and therefore will most likely contain DMF solvent molecules even after activation has been carried out. The activation conditions used were identical for each version (150°C under vacuum).

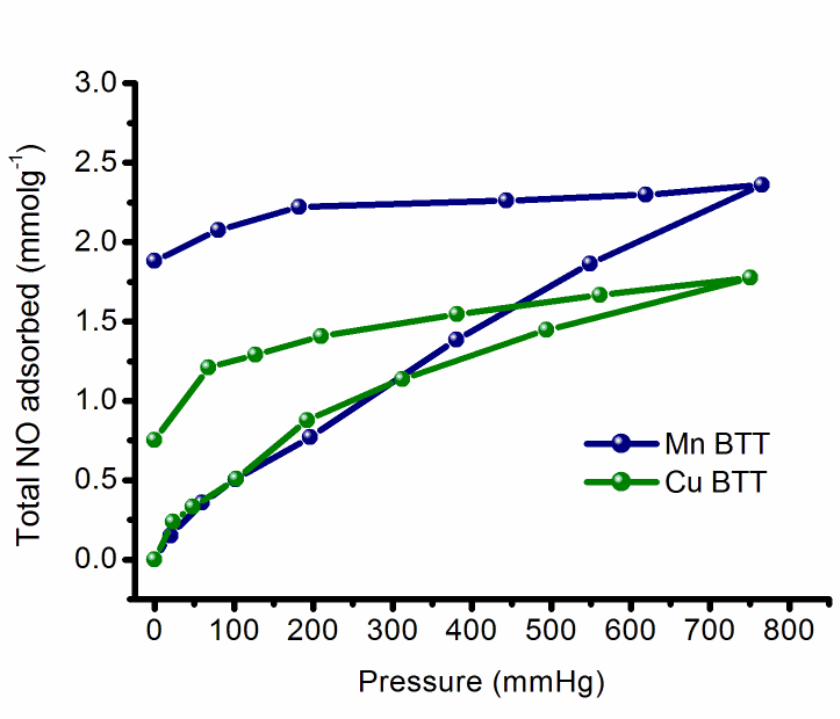

Figure 6.14 NO adsorption curve for Mn and Cu BTT, with solvent molecules possibly still present, carried out at 298K.

As can be seen, the Mn version adsorbs more NO compared with the Cu version. This was not unexpected as results carried out on both frameworks for hydrogen adsorption showed that the Mn version performed better and indeed the Mn version shows a higher surface area[10-11]. The total amount of NO adsorbed is low compared with many other frameworks investigated in this thesis for NO storage. This can be explained by the lack of available metal sites due to guest DMF molecules still present in the pores. In the literature the surface area almost doubled in the Mn version (1100 to 2100 m^2g^{-1}) when the framework was solvent exchanged and then activated. It also means that there are less CUSs available for the NO to bind to as there are still DMF molecules present in the pores.

Following this, partially evacuated samples were loaded with NO and placed in the sample holder of the NO analyser to quantify the amount of NO released. The results can be seen in the curves below.

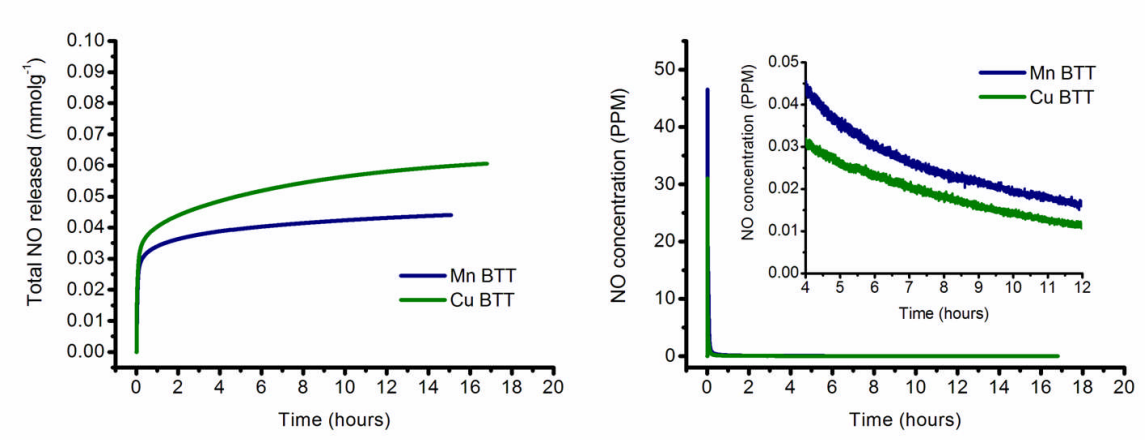

Figure 6.15 NO release curves for the solvent filled samples of Mn and Cu BTT.

As illustrated in figure 6.15 there is very little NO released from the frameworks. This is not surprising as if the NO was inserted into the pores the solvent molecules would probably block the path for water molecules to diffuse into the pores in order to replace the NO molecules at the metal sites.

A sample of each framework which had been solvent-exchanged and sealed under argon was very kindly donated by the Long group in the U.S.A for comparison in NO storage and release. NO release results were possible by loading the samples into sealable vials and then into an air-tight schlenk tube using a glovebox under argon atmosphere. The samples were then activated in the normal manner before NO release results were obtained. The results can be seen below.

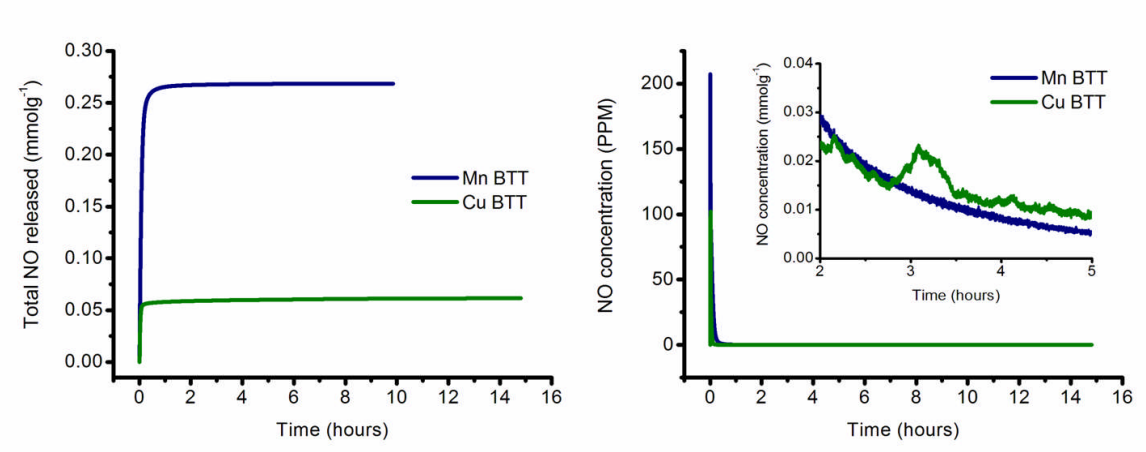

Figure 6.16 NO release from the M BTT solvent exchanged samples from the USA.

As can be seen the amount of NO released from the Mn version of this framework increases dramatically from ~0.04 mmolg^{-1} to ~0.27 mmolg^{-1}. There is no significant improvement noted in the Cu sample. However as was observed for HKUST-1, Cu based MOFs do not seem to release the NO after it is bound to the metal during the adsorption process. HKUST-1 showed similar behaviour, as it adsorbed ~3 mmolg^{-1} but only released 2μmog^{-1} of NO. As the two frameworks are relatively similar in structure, it is not surprising that the NO release from Cu BTT is very poor.

6.6 Summary of chapter 6

It has been shown that Ni metal provides an excellent environment for NO to bind to and be released from. Both Ni STA-12 and Ni succinate MOFs show good adsorption and release of NO, although not as high as Ni CPO-27. Cu based MOFs have once again been shown to release very minimal amounts of NO as evidenced by Cu BTT. Mn BTT shows good NO adsorption and releases about 15% of the NO chemisorbed. This value is higher than the corresponding Mn CPO-27 which only released 5% of the total NO initially chemisorbed. All these MOFs still display higher NO adsorption compared with the best zeolites. Overall, the MOFs studied in this chapter show good potential for the storage and release of NO.

6.7 References

(1) Forster, P. M.; Cheetham, A. K. *Angew. Chem., Int. Ed.* **2002**, *41*, 457.

(2) Livage, C.; Egger, C.; Férey, G. *Chem. Mater.* **1999**, *11*, 1546.

(3) Livage, C.; Egger, C.; Férey, G. *Chem. Mater.* **2001**, *13*, 410.

(4) Livage C., E. C., Nogues M., Férey G. *J. Mater. Chem.* **1998**, 2743

(5) Long, L.-S.; Chen, X.-M.; Tong, M.-L.; Sun, Z.-G.; Ren, Y.-P.; Huang, R.B.; Zheng, L.-S. *J. Chem. Soc., Dalton Trans.* **2001**, 2888.

(6) Forster, P. M.; Burbank, A. R.; O'Sullivan, M. C.; Guillou, N.; Livage, C.; Férey, G.; Stock, N.; Cheetham, A. K. *Solid State Sci.* **2005**, *7*, 1549.

(7) Shimizu, G. K. H.; Vaidhyanathan, R.; Taylor, J. M. *Chem. Soc. Rev.* **2009**, *38*, 1430.

(8) Groves, J. A.; Miller, S. R.; Warrender, S. J.; Mellot-Draznieks, C.; Lightfoot, P.; Wright, P. A. *Chem. Commun.* **2006**, 3305.

(9) Miller, S. R.; Pearce, G. M.; Wright, P. A.; Bonino, F.; Chavan, S.; Bordiga, S.; Margiolaki, I.; Guillou, N.; Férey, G.; Bourrelly, S.; Llewellyn, P. L. *J. Am. Chem. Soc.* **2008**, *130*, 15967.

(10) Dinca, M.; Han, Won S.; Liu, Y.; Dailly, A.; Brown, Craig M.; Long, J. R. *Angew. Chem., Int. Ed.* **2007**, *46*, 1419.

(11) Dinca, M.; Dailly, A.; Liu, Y.; Brown, C. M.; Neumann, D. A.; Long, J. R. *J. Am. Chem. Soc.* **2006**, *128*, 16876.

(12) Wells, A. F. **1977**, *Three dimensional nets and polyhedra* Wiley New York.

(13) Xiao, B.; Wheatley, P. S.; Zhao, X. B.; Fletcher, A. J.; Fox, S.; Rossi, A. G.; Megson, I. L.; Bordiga, S.; Regli, L.; Thomas, K. M.; Morris, R. E. *J. Am. Chem. Soc.* **2007**, *129*, 1203.

(14) Hill, M., Mahon, M.F., Molloy, K.C. *J. Chem. Soc., Dalton Trans.* **1996**, 1857

7 Formulation of MOFs for medicinal applications

7.1 Introduction

Arising from the exceptional performance shown by MOFs in their ability to store and controllably release NO, it is of interest to investigate the wide range of possible therapies utilising MOFs in the area of medicine. MOFs have potential for both *in vitro* and *in vivo* applications. Obviously the easiest applications to test for and investigate are those using NO as a wound healing therapy due to the topological nature of such treatment. This chapter therefore focuses on initial topological or dermatological investigations. In addition to this, the adsorption and delivery of drugs or pharmaceuticals is of significant interest as an application for MOFs. Therefore, initial investigations using MOFs to store antibiotics for medicinal purposes have also been undertaken.

7.2 Aims of chapter 7

The main aim in chapter 7 is to show the initial progress which has been made towards implementing NO releasing MOFs in different formulations. There are many potential methods of presenting NO-loaded MOFs in formulations and as such many of the possibilities have been tested to see if the amount of NO released can be controlled for the application required. The overall goal is to establish formulations of MOFs to deliver their store of NO in a suitable manner. For example, in the form of a bandage, or through a topically applied cream.

7.3 In vitro applications

Due to the significant role of NO in wound healing[1], one of the main aims for any NO-releasing MOF would be its use as a therapy in accelerating wound healing times. This has been shown to occur in patients with diabetic wounds (wounds which have very long repair times and are extremely susceptible to infection). It has also been demonstrated to be useful in healing second degree burns in mice[2]. In fact several healing therapies have already been developed for delivering NO into a wound[3-4]. However, some of these have had detrimental effects to the skin[5]. Our method, employed here would only release pure NO and therefore not harm the skin. In addition to this, because NO would be delivered directly onto the site required, it will only be local and not systematic effects that would be observed. As all the samples of MOFs synthesised are produced in powdered form, a suitable method for storing powders has to be found so that they can be used in a practical formulation which can be commercially sold in a patient friendly manner. As such numerous different applications were tested for practicality and the ability to release the stored NO.

7.3.1 Porous paper bags

The first method of delivery attempted was to show that a porous paper bag containing NO-loaded MOF powder would release the same amount of NO as the powder by itself. This was to illustrate the possibility of storing and releasing NO from a “bandage”. A similar product known as QuikClot which utilises zeolites in a bandage is currently available[6]. To test this, a number of porous papers, tea filters and teabags were investigated. The teabags were emptied of their contents before

being replaced with MOF sample and sealed using a heat sealer. The bags were activated and loaded with NO, before being stored in vials. Figure 7.1 shows a NO-loaded MOF bag. It was required that the bags be stored in vials to ensure that air exposure to the sample was minimal.

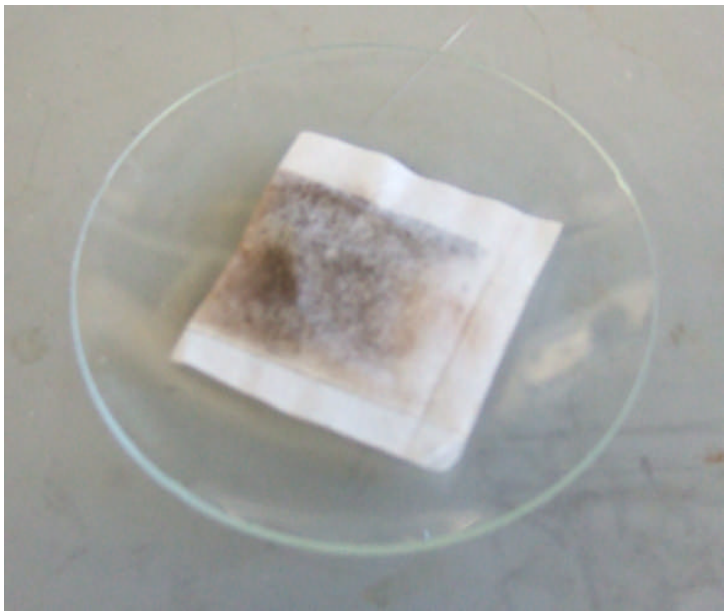

Figure 7.1 An NO-loaded MOF bag.

The MOF chosen for this investigation was the Ni CPO-27 framework which displayed exceptional NO storage and delivery properties as shown in chapter 4. When being used for *in vitro* applications the toxicity of the nickel is of no concern, however many people have allergies to Ni metal and that would preclude certain patients using this formulation. Following the production of NO-loaded MOF bags, the NO release measurements were carried out and can be seen in figure 7.2. Initial measurements from the Ni CPO-27 loaded bag yielded the expected 7 $mmolg^{-1}$, which is equivalent to the amount released by the powdered samples. However this amount of NO was released over almost 3 days compared with the release time of 1

day observed for the powder by itself. This is an excellent result as it allows the amount of NO to be controllably released over a few days as opposed to only an initial burst of NO.

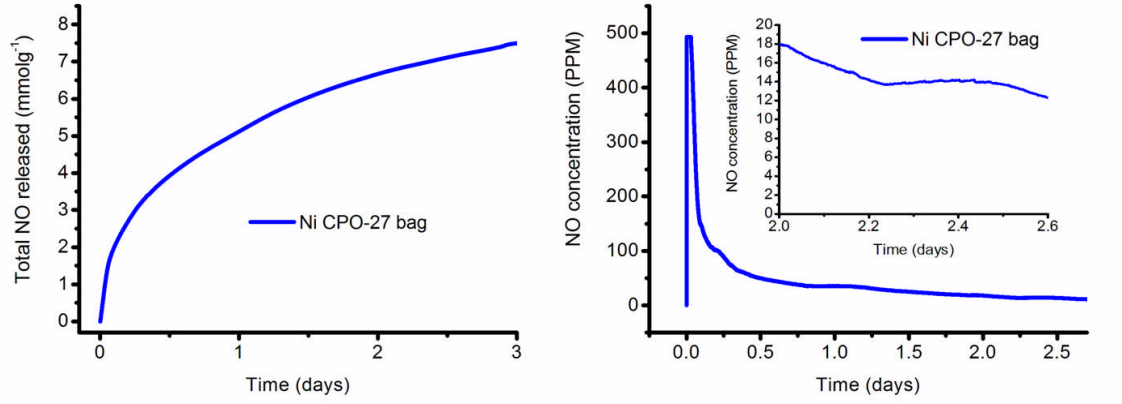

Figure 7.2 NO release profiles for a Ni CPO-27 loaded bag.

The release results suggested that there was no detrimental effect arising from the use of porous paper. Another key requirement for any NO-releasing application is the ability to be stored for lengthy time periods. Initial storage using a vacuum sealer yielded results whereby the total amount of NO released decreased week by week (figure 7.3). As can be seen, initial release from a Ni CPO-27 bag showed the expected ~7 $mmolg^{-1}$ of NO release. However subsequent release profiles show a reduction which was attributed to the vacuum bag used not being perfectly gas tight. Following this, air-tight glass sample vials were used to store the ready-made bags and this resulted in no reduction in the total amount of NO being released from Ni CPO-27 bags (figure 7.4). The slight differences in total NO released arise from calculating the mass of MOF used in the experiment by weighing porous bag by difference. This causes small errors in the mass of the MOF used, leading to very slight differences in the graphs. This proves that the storage of these bags is very

important to their successful practical application. The technology of using gas tight foil packaging already exists and is in use in the aforementioned QuikClot products, and it could easily be implemented for storing NO releasing bandages based on the porous materials.

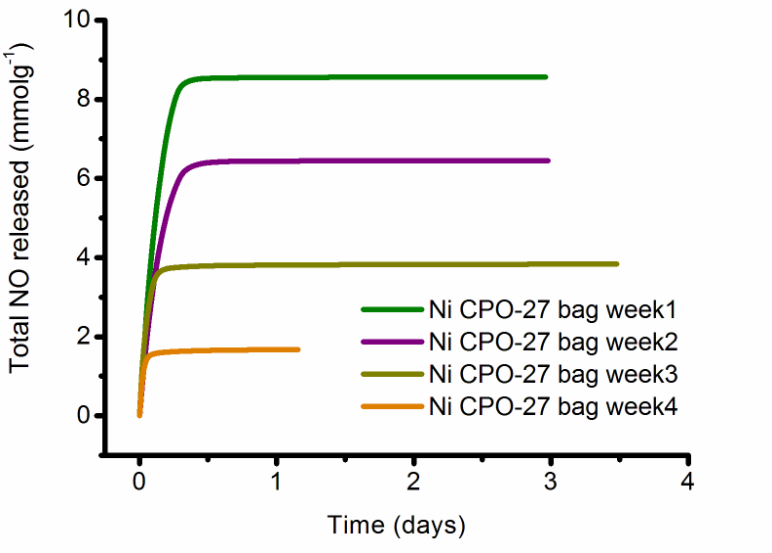

Figure 7.3 Storage of MOF bags under vacuum leads to a decrease of NO released over weeks.

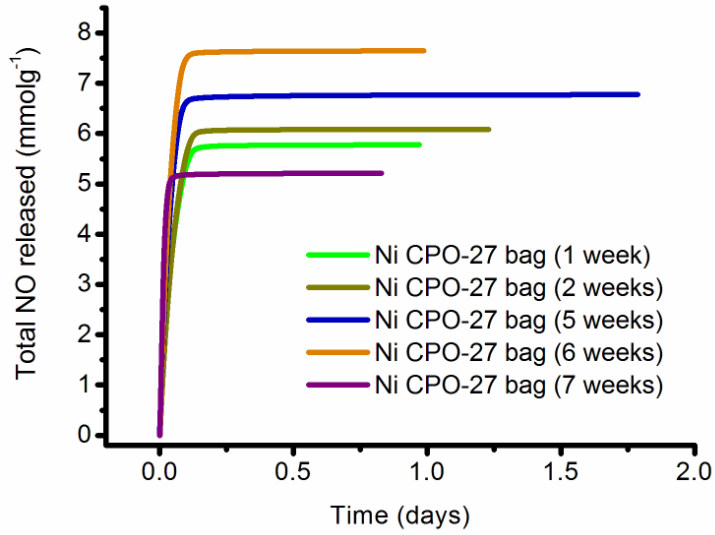

Figure 7.4 NO release profiles for bags, showing that there is no loss of NO released when stored in air-tight vials.

Overall it has been shown that it is possible to store and release NO from MOFs in a porous paper bag with no detrimental effect to the total NO available for release being observed. It has also been demonstrated that it is possible to store these "bandages" for long periods of time without any loss of total NO releasable.

7.3.2 NO releasing creams

One of the most heavily researched areas in NO releasing formulations is the use of a NO releasing cream[7]. A prime example uses an acidified nitrate cream[4], where sodium nitrate and citric acid are combined leading to NO being released. Unfortunately one of the major side-effects of this treatment is that it burns the skin[5]. Another method which is currently being investigated and that would be similar to the use of MOFs in creams is NO-releasing zeolites in creams. Research is currently ongoing for this application, and it has been shown that zeolites display no unwanted side effects when placed into a cream formulation[5].

A variety of different creams were initially tested. Water based, paraffin based and wax based creams were all used. The reason for this was to provide an insight into the release of NO from a cream which promotes the replacement of NO with water (aqua based cream) and compare it with a cream that should prevent that reaction happening too quickly (paraffin based cream). This should delay the total release of NO from the MOF. If this delay in NO release was possible, then a cream of this sort could last a number of days or weeks as opposed to the number of hours shown in the powder release experiments. The experiment was set up in the following manner. A calculated amount of each cream was placed into a sealable vial. An amount of pre

NO-loaded MOF was added and the two were then mixed before being sealed with a vial cap fitted with a septum. The flowing "wet N_2" line was then fed into the vial using a needle and the output was fed through a different needle to the analyser. Several different frameworks were investigated, Cr MIL-100 and Cr MIL-101 together with Ni and Co CPO-27. Figure 7.5 shows the release curves for Cr MIL-101 and Cr MIL-100 with the three different creams. A sample size of 10 wt% MOF was used in the cream mixtures.

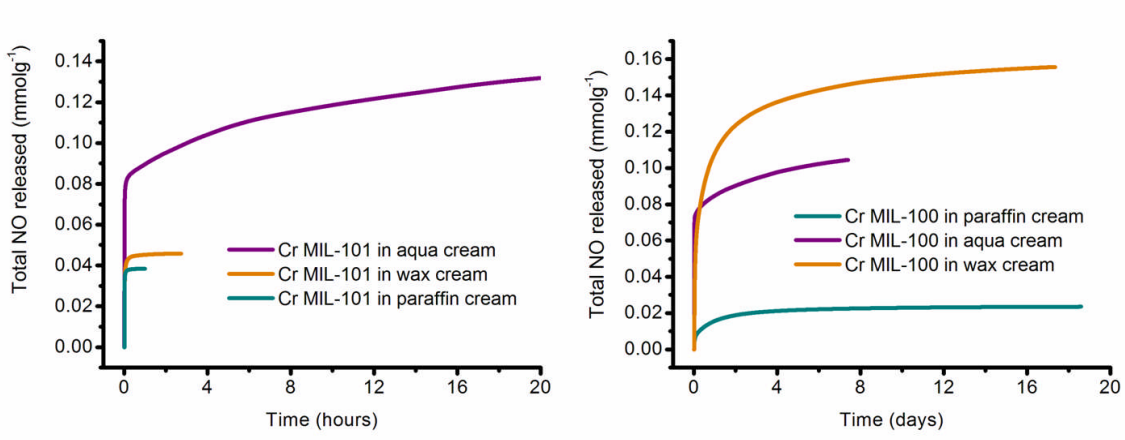

Figure 7.5 NO release results from the Cr MIL frameworks when mixed with the various different creams.

As can be seen, the amounts of NO released from the Cr MIL-101 structure are about half of the amount the powder releases by itself. The same result is observed with the Cr MIL-100 structure. The cream that allows the smallest amount of NO to be released is the paraffin based cream. This is not unexpected as the paraffin stops moisture entering into the MOF and therefore the NO is not being substituted for the water molecules in the "wet N_2" gas. This is a result that could be useful as it should prolong the release of NO. However, the paraffin cream does not allow any moisture

in at all and so does not have the desired effect. The aqua based cream shows potential, as although it releases its NO quite quickly, it might find use as an antibacterial delivery agent as these require an initial burst of NO[8] which also promotes wound healing.

Co and Ni CPO-27 were also investigated using the three different creams and the results can be seen below.

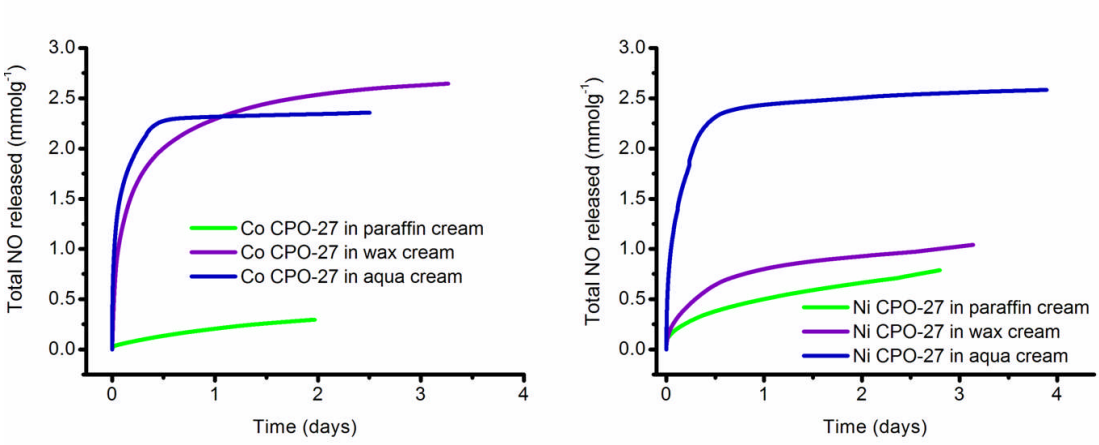

Figure 7.6 NO release graphs for the Ni and Co CPO-27 frameworks in the three different creams.

Once again, the paraffin based cream inhibits the release of NO from the mixture and shows the poorest release of NO. The aqua based cream shows good release of NO from the CPO-27 structures over 4 days, which is a much improved and more promising result. The wax cream appears to produce unpredictable results as in some release curves it shows good release, but in others it displays poor performance. One reason for this could be the fact that the release measurements are dependent on the mixing of the NO-loaded MOF with the pre-weighed cream in a vial. If the mixing is inadequate then the release measurements will either follow the powder release

profile closely or show no release at all. At the same time, as soon as the NO-loaded MOF powder comes into contact with both air and cream, it starts to release its gaseous content. So the mixing stage is crucial, as too long spent mixing and the cream mixture will show poor release, but too little mixing results in the powder release pattern being repeated. Much more work is required to achieve an optimal formulation of cream that will both inhibit and help release NO from a framework. Indeed even mixing different quantities of these creams in a specific ratio could result in the desired controlled release of NO. An example could be the use of 50% of the paraffin cream with 50% of the aqua based cream.

7.3.3 NO releasing hydrocolloids

The final formulation that has been initially investigated is the possible utilisation of a NO-releasing hydrocolloid. Hydrocolloids are among some of the most widely used dressings in medicine. They utilise gel forming agents and, when combined with a polymer to produce a waterproof film or wafer, form a gel when applied to a wound. The combination of a polymer and NO-loaded MOF together with a binder such as cellulose could be a promising combination for use as a wound healing antibacterial dressing. The hydrocolloids made in the laboratory used 10% cellulose, 50% poly-isobutanol (PIB) and 40% NO-loaded MOF material. Heating the PIB to ~80°C allows it to become flexible. The cellulose and the NO-loaded MOF are then added and mixed together under an inert atmosphere resulting in the production of a hydrocolloid with the ability to release NO over several days. For this study Ni CPO-27 was chosen as the MOF to be used. In figure 7.7 a picture of the hydrocolloid formed in the laboratory can be seen. Chemiluminescence measurements of NO

release were taken from the hydrocolloid and the resulting curves are illustrated in figure 7.8.

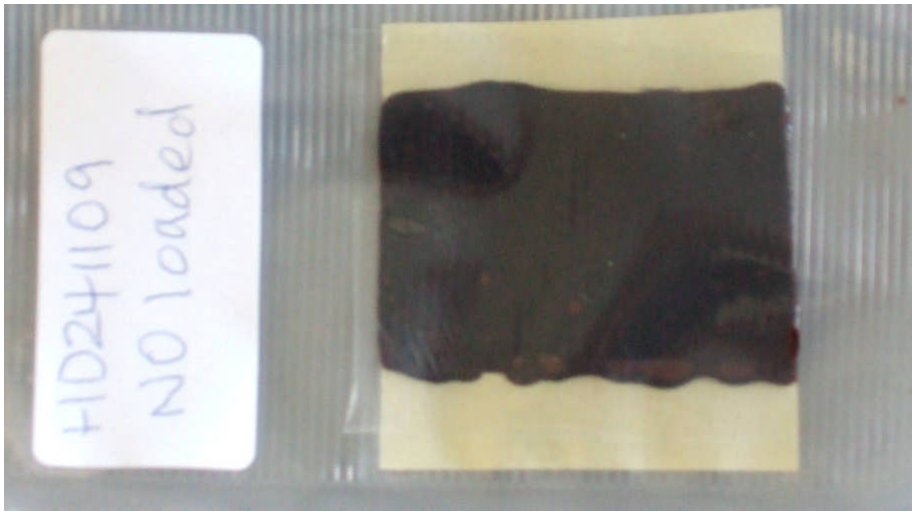

Figure 7.7 Photograph of a NO-loaded hydrocolloid.

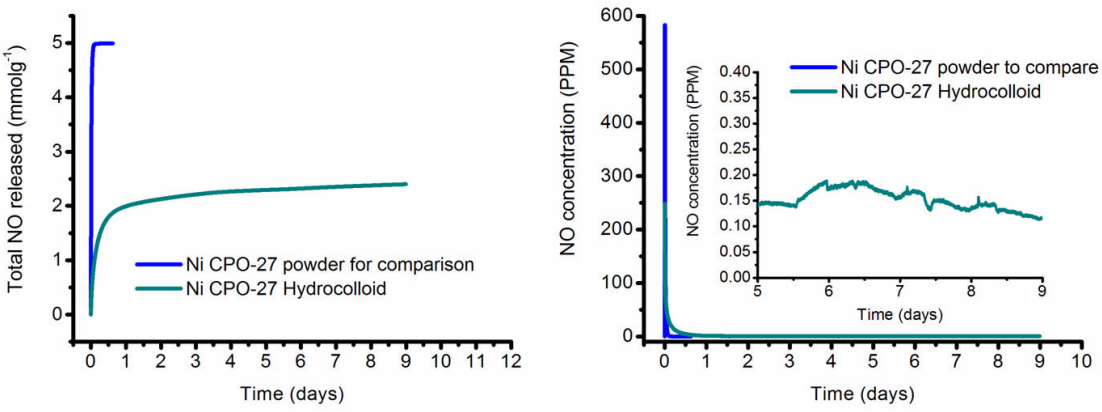

Figure 7.8 NO release curves for the hydrocolloid shown against a powder sample for comparison.

These initial results show major potential as, although releasing ~2.5 $mmolg^{-1}$ (about half of the amount released by the powder used for comparison) it released this store over almost 10 days, which is extremely significant. Further to this, the amount of NO released is much higher than that which is released by powdered zeolites[9-12] and therefore merits further investigation. For a hydrocolloid to be useful it must demonstrate that it will not leach out the toxic metal contained within the MOF structure. To investigate this, atomic adsorption measurements were carried out to calculate the amount of nickel leaching out of the prepared hydrocolloid. A pellet of Ni CPO-27 was used as a comparison. The two samples were placed into PBS (phosphate buffered saline) solution and kept at 37°C (simulating body temperature) using a water circulator over several days. Measurements were taken to calculate the total amount of nickel contained in the solution. Figure 7.9 shows the results for both. As can be seen the hydrocolloid retains the Ni from the MOF significantly better than the pellet sample of Ni CPO-27. This result confirms expectations that when mixed with PIB the MOF will not decompose and leach out as much nickel as the MOF by itself, due to the polymeric nature of PIB.

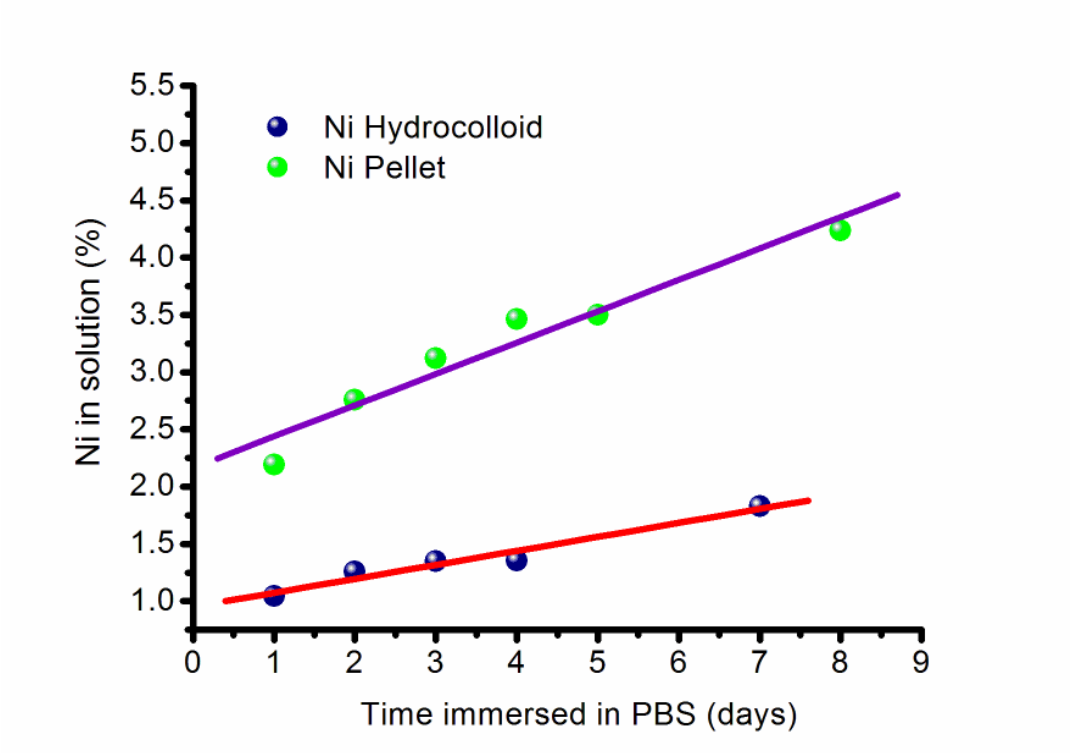

Figure 7.9 Atomic adsorption measurements carried out on a prepared hydrocolloid and a Ni CPO-27 pellet for comparison.

7.4 Testing NO release in PBS solution

The only possible initial testing which could be conducted relative to "in the body" applications is to see how stable the frameworks are in simulated body fluid and to monitor the amount of NO that is released from NO-loaded materials when placed in a phosphate-buffered saline (PBS pH 7.4) solution. The flowing "wet N_2" gas is only representative of scarce water conditions, such as those situations using NO topologically applied to skin. Using PBS is the best way to simulate physiological conditions similar to those encountered in the body. The testing for stability in simulated body fluid has already been carried out[13] and it showed that the amount of metal ions leaching out was minimal and the framework would have certainly

delivered its entire store of NO before dissolving in the solution. The NO release measurements were carried out on a variety of frameworks. The M-CPO-27 series and a variety of MIL frameworks were investigated and the results are reported below. The experiment was set-up in a similar manner to the cream investigations, using sealable vials and needle-fed gas lines. In this case the NO-loaded MOF was placed into the vial along with a miniature stirring bar. The septum lid was then placed on top, prior to injecting PBS through the septum into the vial, before connecting the appropriate needles to the analyser and supply of "wet N_2".

Studies were carried out using the M-CPO-27 series using M= Co, Ni and Zn metals. Zinc was chosen as it has no toxicological complications unlike the Co and Ni analogues. However, the zinc version does not release the same significant amount of NO which the Co and Ni frameworks liberate. Therefore Co and Ni CPO-27 were also investigated to see if they still release their remarkable store of NO in a PBS solution. The release results for the three frameworks can be seen in figure 7.10.

Initial release results using the NO-loaded powder show only a total NO release of 0.4 $mmolg^{-1}$ when the PBS is injected. Follow-up experiments used pellets constructed from 10 wt% of polytetrafluoroethylene (Teflon) combined with the MOF. This resulted in much better total NO release measurements (3.5 $mmolg^{-1}$). It is noticeable that the half life of NO delivery is reduced from several hours under flowing gas conditions, to only ~10 minutes when exposed to the PBS solution. The lack of NO released from the powder samples can be rationalised by the NO being liberated so quickly that the analyser cannot detect it. The detector only measures

NO concentrations up to ~500 PPM. Most samples of M-CPO-27 when initially inserted will register over this value but will quickly fall below the limit for detection. When the Co or Ni CPO-27 powder is exposed to the PBS, it rises above the detector limit and eventually returns below the limit. However, when over the limit, it may be releasing much greater amounts of NO very quickly and therefore could be releasing the expected amounts of 5-6 $mmolg^{-1}$ without being registered. The decrease in total NO liberated from the pellet samples could be attributed to the Teflon blocking some of the pores when it is combined with the MOF in the pellet press. The ability of these MOFs to release their entire store seems to be retained even when placed into a buffer solution. Both versions of Zn CPO-27 show very minimal release of NO, in fact only about one-fifth of the amount which the powder itself releases. However, even the small amount released could still be of biological significance as the release takes place over 30 hours and in a controlled manner.

Of most interest, however, were the iron based carboxylates of MIL-88 and MIL-100 due to studies showing that iron carboxylates pose no health risk[14]. Fe MIL-88-A, B, B-2OH and B-NO_2 were all run in the analyser and exposed to PBS buffer solution. The results for Fe MIL-88-B were extremely poor as it only released 0.016 $mmolg^{-1}$ of NO. Furthermore the results for Fe MIL-88-B-NO_2 were inconsistent with large variances from one experiment to the next. The results for Fe MIL-88-A and Fe MIL-88-B-2OH are shown in figure 7.11 below. The Fe MIL-88-A sample shows a significant increase in the amount of NO liberated compared with the powder run under flowing “wet gas” conditions. This can be explained as studies have shown that under PBS conditions Fe MIL-88-A decomposes, this would therefore liberate

much more NO as the structure is collapsing. The Fe MIL-88-B-2OH also shows improved NO release under PBS buffer conditions compared with the scarce water conditions reported earlier. Fe MIL-100 was also tested although this experiment was carried out using distilled water. The MIL-100 with injected water shows a lower total release. However, it is encouraging that the release lasts longer than the powder itself under flowing "wet gas" conditions (see concentration curve of figure 7.12). These results show potential and merit further research for possible *in vivo* applications using NO delivery therapies from MOFs.

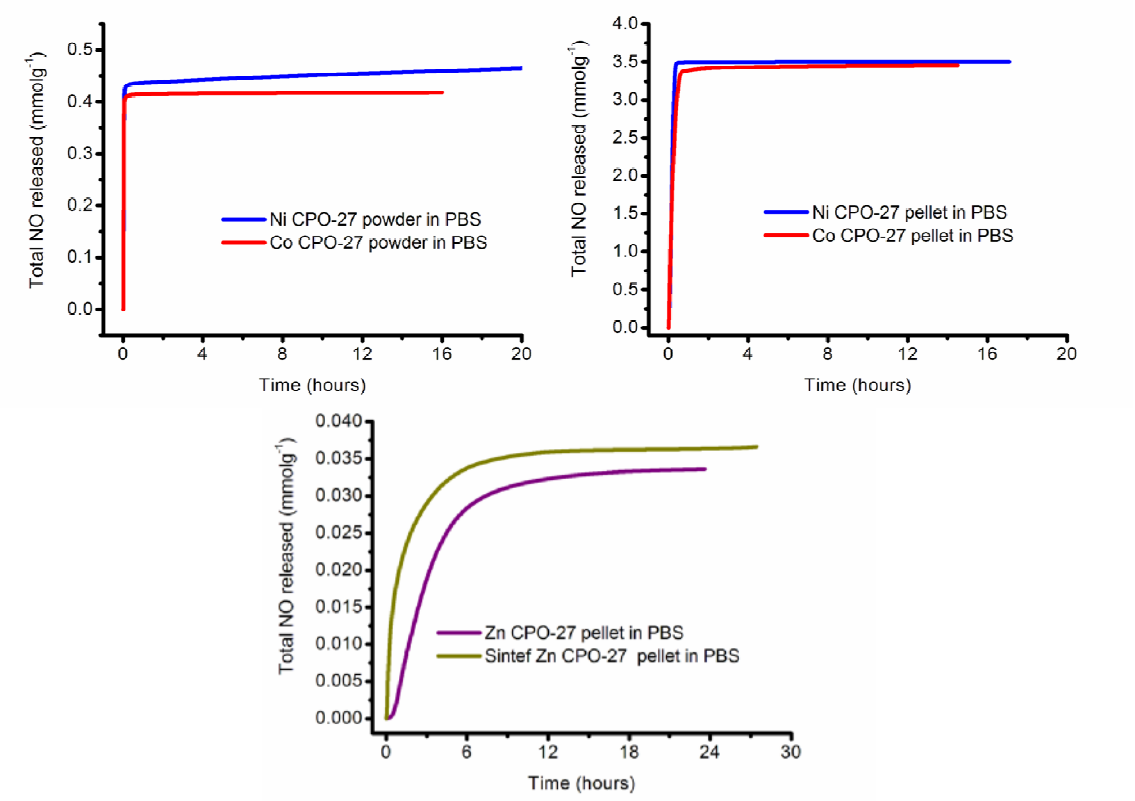

Figure 7.10 Top left, the NO release curve for powdered samples of Ni and Co CPO-27 in PBS buffer solution. Top right, a ten-fold increase in NO release observed using pellets of the same MOFs. Bottom centre, shows the release curve for both versions of Zn CPO-27.

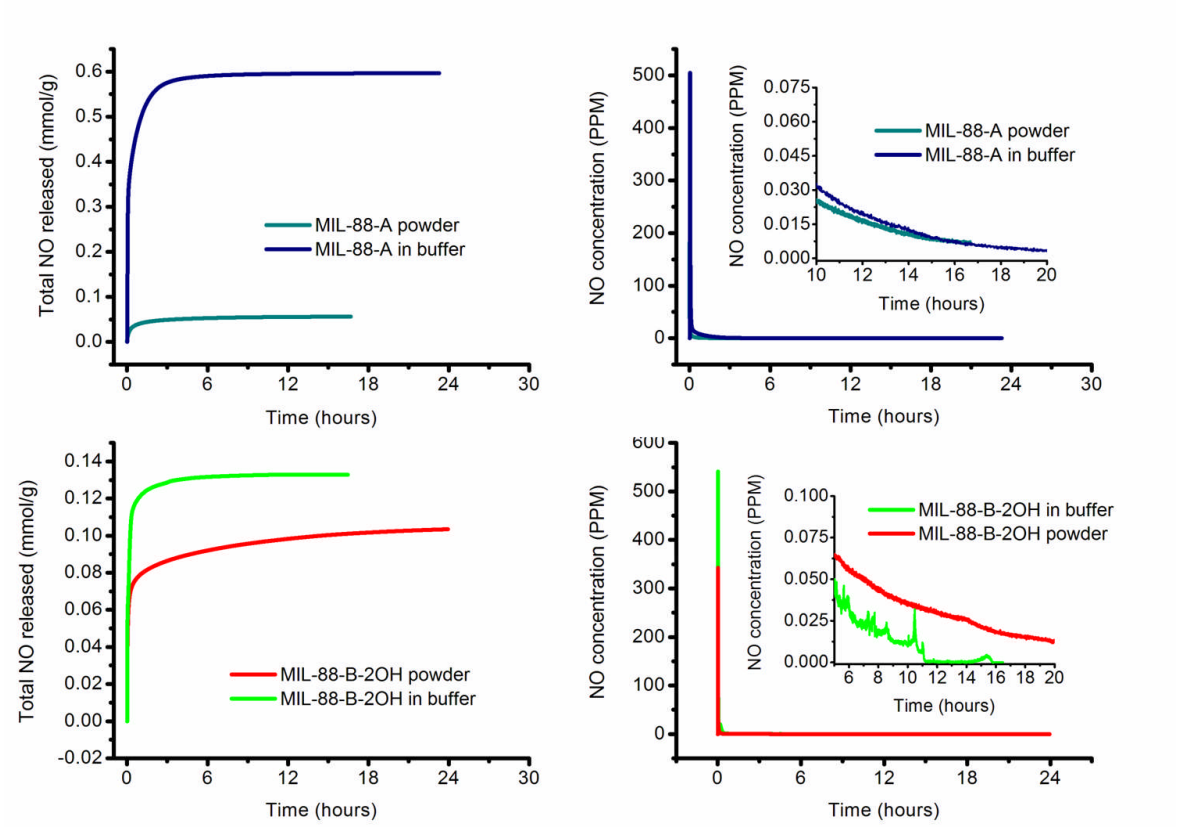

Figure 7.11 NO deliveries from Fe MIL-88-A and Fe MIL-88-B-2OH under PBS buffer conditions.

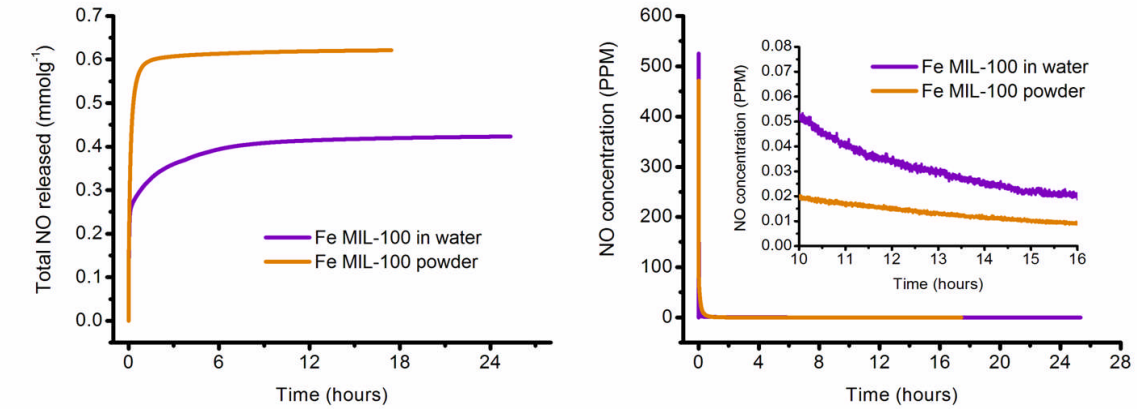

Figure 7.12 NO release curves for Fe MIL-100 under flowing wet gas (powder) and under aqua conditions (in water).

7.5 Preliminary biological investigations of NO-releasing MOFs

As has been shown above, MOFs can release their store of NO under PBS conditions which mimic the body's own physiological environment. It is important however that, when released, this store of NO promotes a relevant tissue response. As has been shown already, NO-loaded MOFs can completely inhibit the formation of platelet aggregation in blood[20]. To see the effect of an NO-loaded MOF on tissue, an initial biological experiment was carried out[21]. The impact of a pressed pellet of Ni CPO-27 (5 mg) on pre-contracted pig coronary arteries *in vitro* was investigated (figure 7.13). Placement of pellets a distance of 2 mm from the vessel in the 10 mL organ bath resulted in rapid 100% relaxation of the vessel. The pellet could be seen to generate bubbles of gas for ~10 minutes of submersion, although the relaxation remained maximal for longer than 1 hour. In some experiments (figure 7.13), the pellet was removed from the bath after 10 minutes and the relaxation was seen to gradually recover. Parallel control experiments with NO-free Ni CPO-27 MOFs failed to cause relaxation and did not generate bubbles on submersion, indicating that NO release from the loaded MOF is responsible for the relaxing effect.

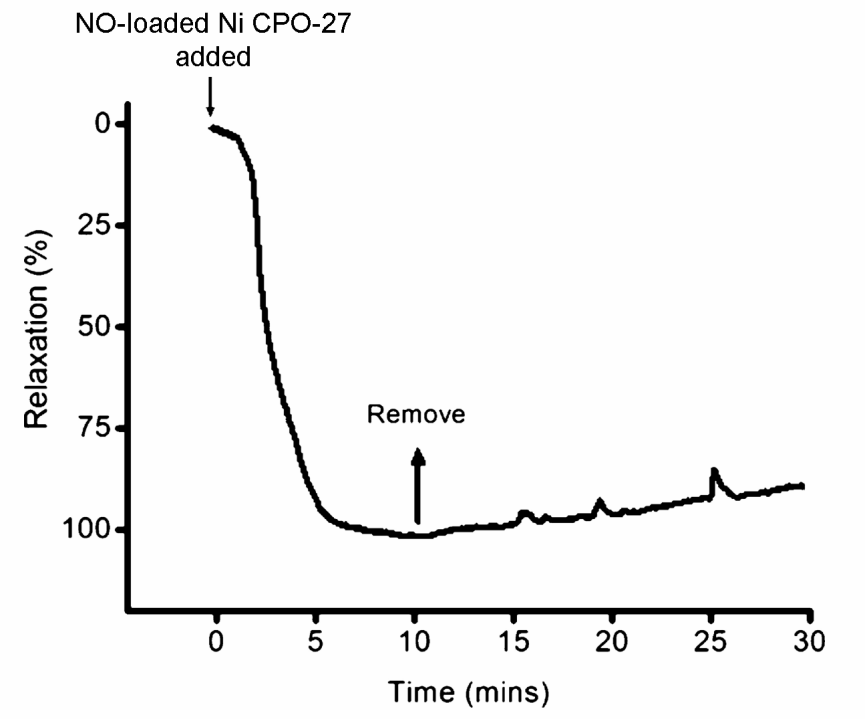

Figure 7.13. Representative trace showing the vasodilatory effect of NO-loaded Ni CPO-27 in a pre-contracted porcine coronary artery. A pellet (~5 mg) of NO-loaded Ni CPO-27 was placed in the organ bath (10 mL) and removed as indicated. Within 4 minutes of the addition of the pellet, 100% relaxation was achieved, and the relaxation slowly recovered upon pellet removal. In experiments where the pellet was left in the bath, recovery was not seen for up to 1 hour after pellet addition.

7.6 Antibiotic loading in Ni CPO-27

As mentioned in the introductory chapter, one of the applications that has been targeted by chemists interested in biological therapies has been the adsorption storage and delivery of pharmaceuticals[14-16]. So far the Férey group has led the way in this niche field of MOFs. They have demonstrated that it is possible to store large amounts of ibuprofen in MIL-101[16], deliver ibuprofen from MIL-53 over an extremely long time period[15] and most recently they have demonstrated the ability of MOFs to store and release significant amounts of both anti-AIDS and anti-cancer drugs[14]. Using this work as a basis the storage of antibiotics was attempted using Ni CPO-27. The adsorption of ibuprofen (figure 7.14) was also attempted to compare and contrast with the amounts stored in MILs 101,100 and 53.

Ibuprofen is a well known pharmaceutical and is commonly used as an anti-inflammatory drug[17]. It was introduced into the UK in 1967 and the USA in 1974 and is classed as a non-steroidal anti-inflammatory drug (NSAID). It also has analgesic effects which are attributed to its anti-inflammatory nature. Metronidazole (figure 7.14) is an antibiotic[18-19] which is used to treat a variety of both gram-positive and gram-negative bacteria. It is notably used to treat Clostridium difficile (*C. diff*) a gram positive bacteria which is most commonly found in hospitals and nursing homes which causes severe intestinal infection. Due to the small size and functional groups of metronidazole, it should be readily adsorbed in Ni CPO-27.

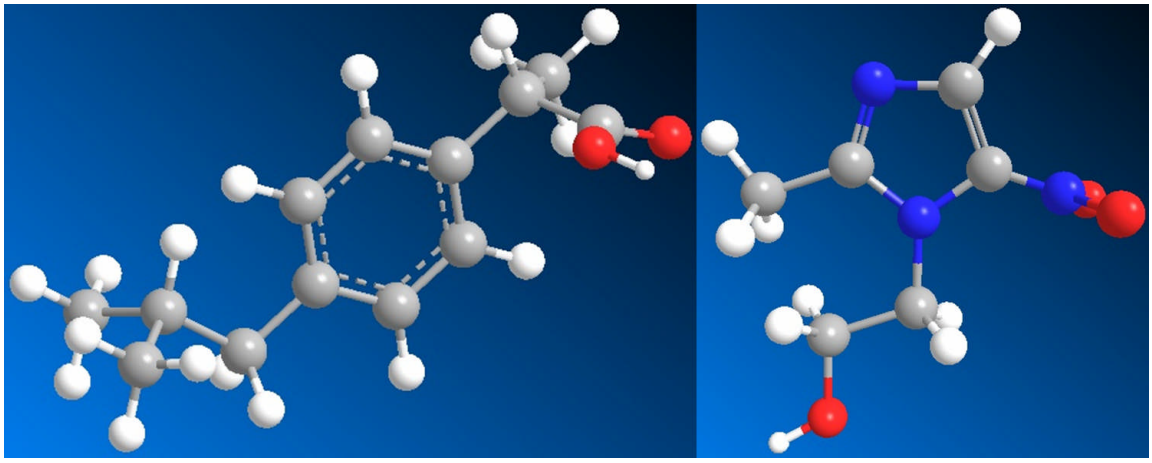

Figure 7.14 Drugs stored within Ni CPO-27. Ibuprofen (left) and metronidazole (right) Carbon atoms shown as grey, oxygen as red, hydrogen as white and nitrogen as blue.

The ability to load drugs into Ni CPO-27 in combination with NO would lead to the possibility of double functionality which would be extremely useful as a formulation. For example, a bandage containing a MOF loaded with both NO and metronidazole could be used to ensure that no infection occurs while the wound is being repaired with the NO.

Testing of 1:2, 1:3 and 1:4 ratios of MOF:drug were used. A calculated amount of Ni CPO-27 was activated and stored using the procedure described earlier. Ibuprofen and metronidazole were added in calculated amounts to sample vials. To the sample vial 10ml of solvent was added (dried hexane for ibuprofen and dried methanol for metronidazole). Once the drug had fully dissolved in the solvent the dehydrated MOF sample was added to the sample vial and the mixture was left stirring for 3 days. Using a variety of characterisation methods it was shown that the drugs had indeed been adsorbed inside the pores of Ni CPO-27.

7.6.1 Ibuprofen loading of Ni CPO-27

As explained earlier, samples of dehydrated MOF were exposed to a stirring solution containing dissolved ibuprofen in hexane for 3 days. The resulting powder was centrifuged and dried. Accurate weighing measurements before and after the adsorption process led to estimates of how much ibuprofen had been adsorbed by the Ni CPO-27.

There was no noticeable difference in the adsorption amounts shown between the different ratios of MOF:ibuprofen. The average amount of ibuprofen adsorbed using this method was observed to be 0.3973g of ibuprofen and hexane per gram of activated MOF. This means that if the ibuprofen was interacting with the CUSs, then 30% of the metal sites available are being bound to the drug molecule. However this value could be inaccurate as there is residual hexane still present in the framework.

To further investigate the adsorption of ibuprofen in Ni CPO-27, CHN elemental analysis was used. Following immersion in the hexane solution containing ibuprofen, it was expected that some residual hexane may still be present in the pores. This was removed using an activation temperature of 100°C under vacuum. The formula of the dehydrated structure is $Ni_2(C_8H_2O_6)$, which has the following composition; C = 30.85% and H = 0.64%. For comparison the hydrated Ni CPO-27 structure has the following formula and expected and calculated composition $M_2(C_8H_2O_6)(H_2O)_2.8H_2O$. Expected C = 19.56%, H = 4.48% and calculated C = 20.09%, H = 4.02%. The percentages for the ibuprofen loaded structure were shown to be C = 38.84% and H = 3.84%. This indicates that ibuprofen has indeed been

adsorbed into the pores of Ni CPO-27. Using the calculated amounts of C and H it can be estimated that the formula for the ibuprofen loaded Ni CPO-27 is $Ni_2(C_8H_2O_6).0.35(C_{13}H_{18}O_2)$, thus indicating an adsorption of 0.232g ibuprofen per gram of activated MOF.

The final method used to estimate the amount of ibuprofen incorporated into Ni CPO-27 was TGA. The graph comparing the two samples can be seen in figure 7.15.

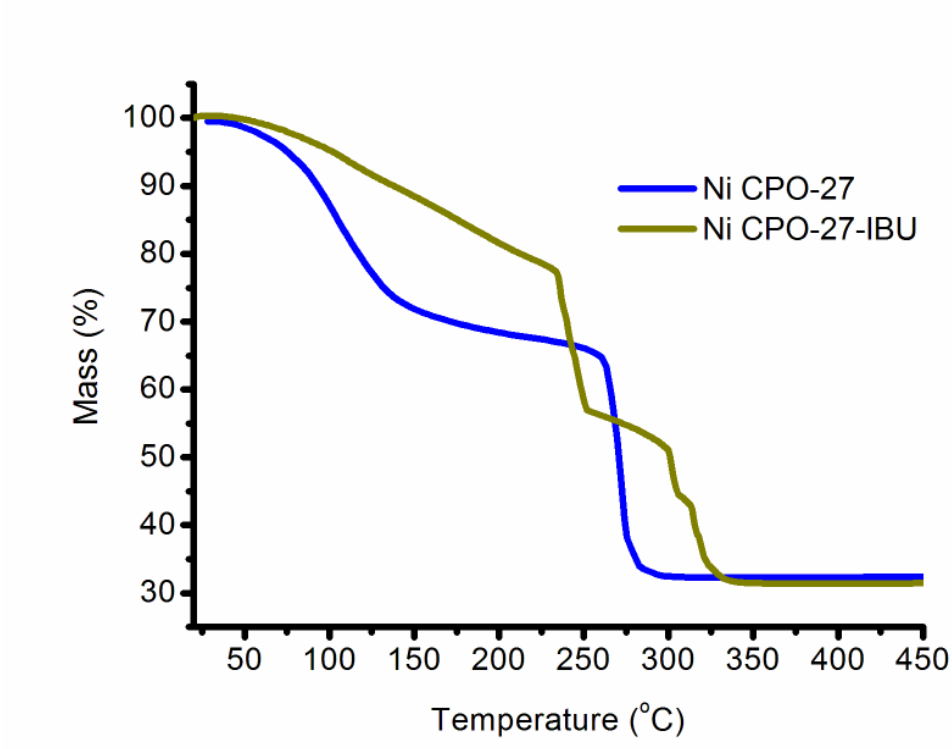

Figure 7.15 TGA curves of Ni CPO-27 and Ni CPO-27-IBU.

Clearly ibuprofen has been adsorbed as the TGA profile has changed considerably. Using TGA as an estimate of ibuprofen content gives an adsorption of 0.2007g ibuprofen per gram of activated MOF. This is taken from the loss of mass in the region between 230 and 250°C. However TGA is not ideal for estimation of an

organic molecule in a MOF as some of the ibuprofen may remain trapped within the pores until the structure completely collapses.

Overall the results for the different characterisation methods for estimations of ibuprofen content are as follows;

Estimation of Ibuprofen content (g IBU/g activated MOF)			
MOF	Mass changes	Elemental analysis	TGA
Ni CPO-27-IBU	0.397	0.232	0.201

Figure 7.16 Table showing estimates of ibuprofen adsorption by Ni CPO-27.

As can be seen the TGA and the elemental analysis result match closely. The amount of ibuprofen adsorbed into Ni CPO-27 when estimated from accurate weighing is most likely to be inaccurate due to the presence of residual solvent. Indeed a close look at the TGA curve shows that ~22% of the mass is lost before the MOF releases the ibuprofen. If the mass changes value is decreased by 22% this results in an estimation of ibuprofen content of 0.3g IBU per gram activated MOF. With the other MOFs studied for ibuprofen storage the most accurate method was shown to be elemental analysis[15-16]. The amount of ibuprofen actually adsorbed is comparable with that adsorbed by MIL-53[15]. The amount adsorbed by MIL-100 and MIL-101 was in fact much higher. However, this is to be expected as they contain much larger cages and pore sizes compared with Ni CPO-27. MIL-101 has pore sizes of 29Å and

34Å wide compared with only 11Å wide for Ni CPO-27. Added to this, an ibuprofen molecule is ~10Å wide by ~5Å in height.

The testing carried out so far has not totally proved that the ibuprofen is actually in the pores of the MOF, although it does show that something has been adsorbed. To show that ibuprofen has indeed been adsorbed into the Ni CPO-27 pores, infrared spectroscopy (IR) was undertaken for samples of Ni CPO-27, ibuprofen and the ibuprofen loaded Ni CPO-27 (Ni CPO-27-IBU). The results can be seen in figure 7.17. The IR spectra show that ibuprofen has indeed been incorporated into Ni CPO-27. Particularly with the huge increase in intensity of the υAr(C-H) bands at 3050 cm^{-1} are due to the aromatic groups of the ibuprofen. Slight increases in the υ (C=O) and υ (C-H) at 2600 cm^{-1} and 1725 cm^{-1} are also characteristic of incorporation of the drug into Ni CPO-27. These observations were also made for the previous MOFs studied for ibuprofen storage[15-16].

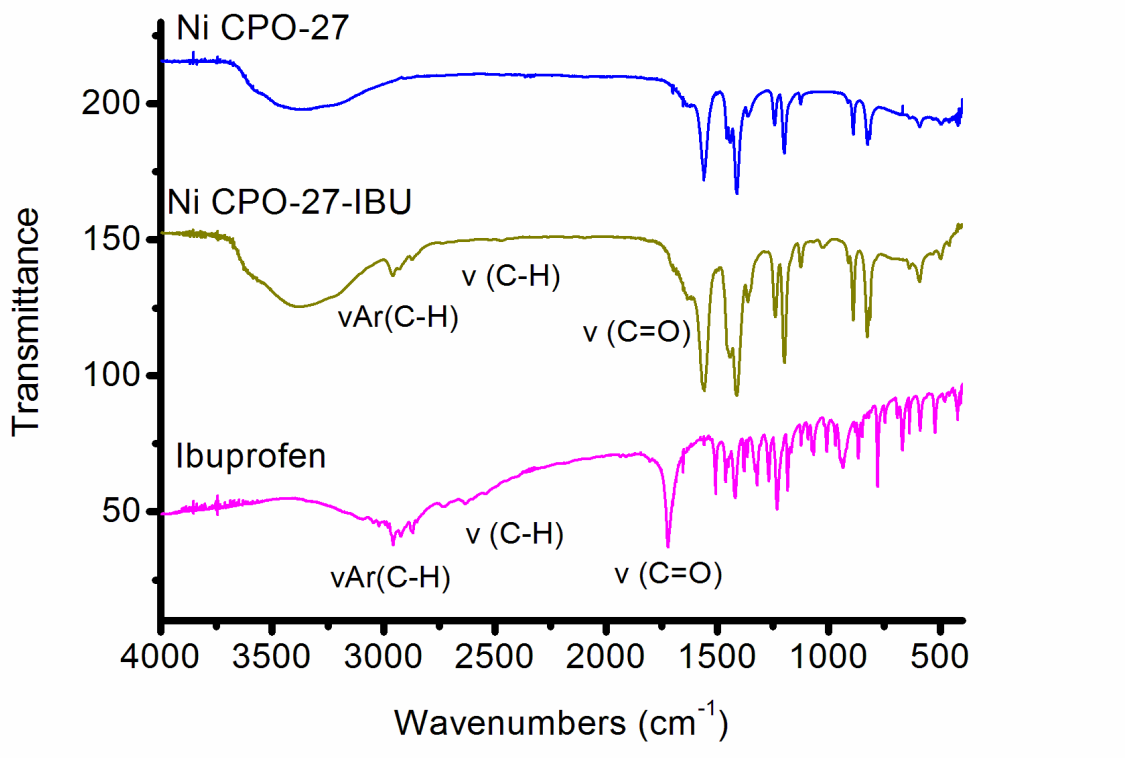

Figure 7.17 IR graphs for Ni CPO-27 (blue), Ni CPO-27-IBU (dark yellow) and ibuprofen (magenta). As can be seen the ibuprofen loaded Ni CPO-27 displays many of the peaks seen in the ibuprofen sample indicating incorporation of the drug into the pores of the framework.

7.6.2 Metronidazole loading in Ni CPO-27

A similar adsorption method was used to introduce metronidazole into Ni CPO-27. However, in this case methanol was used as the solvent as metronidazole does not dissolve in hexane. Following careful calculations and exposure of dehydrated MOF samples to pre-dissolved metronidazole, characterisation methods were used to quantify the amount of metronidazole incorporated by Ni CPO-27.

Using accurate weighing of the MOF before and after impregnation yielded an average uptake of 0.436g of metronidazole per gram of activated MOF. However, as explained earlier, this method is very unreliable due to the large error present in weighing individual samples and due to residual solvent. Especially in this case as methanol is a much less volatile solvent compared with hexane. Indeed it is also possible that some methanol may still reside in the pores of Ni CPO-27. However, it does give an indication that metronidazole has indeed been adsorbed.

The next characterisation method utilised was CHN elemental analysis, using the calculated and expected ratios of both the hydrated and activated samples of Ni CPO-27 as a comparison. The results obtained were as follows: C = 31.98%, H = 3.66% and N = 3.46%. This result shows clearly that metronidazole has been adsorbed as metronidazole contains 3 nitrogen atoms per molecule, whereas Ni CPO-27 does not contain any nitrogen atoms. Calculating the amount of metronidazole present using these ratios gives a formula of $Ni_2(C_8H_2O_6).0.3(C_6H_9N_3O_3)$. This results in an estimation of 0.165g of metronidazole for 1g of activated MOF.

The final characterisation method was TGA. A sample of metronidazole-loaded Ni CPO-27 (Ni CPO-27-METRO) was run and the graph produced is shown in figure 7.18.

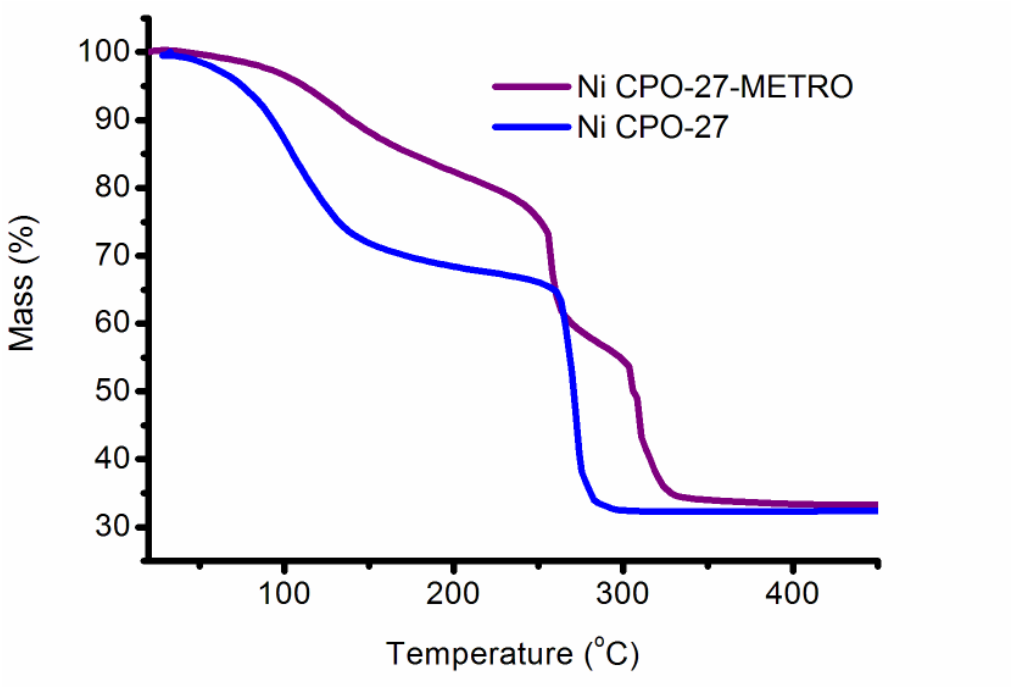

Figure 7.18 TGA curves of Ni-CPO-27 and Ni CPO-27-METRO.

It is much more difficult to observe at exactly which point the metronidazole is released from the framework. However, attempts to remove the excess methanol and retain the metronidazole showed that at 100°C under vacuum all the metronidazole is released. This would indicate that the metronidazole is released in the TGA curve between 100 and 170°C, which indicates a mass loss of 11.337%. This gives an estimate of metronidazole adsorption of 0.11337g of metronidazole per gram of activated Ni CPO-27. As with the TGA for the ibuprofen-loaded material, this value underestimates the actual value as some of the drug may remain trapped in the pores until the structure collapses at 250°C.

The overall results can be seen in figure 7.19. Once again the most reliable estimate of metronidazole content of Ni CPO-27 is given by the elemental analysis.

Estimation of Metronidazole content (g METRO/g activated MOF)			
MOF	Mass changes	Elemental analysis	TGA
Ni CPO-27-METRO	0.436	0.165	0.113

Figure 7.19 Table showing the estimated adsorption values of metronidazole in Ni CPO-27.

Again the estimation of metronidazole content using mass changes and accurate weighing is inaccurate due to solvent content. Unfortunately the solvent is released at the same time as the drug. This also means that the TGA estimation is inaccurate for this reason as well as residual metronidazole content.

Finally IR measurements were taken to show that the metronidazole had indeed been adsorbed into the pores. Figure 7.20 shows the IR spectra for the dehydrated Ni CPO-27, the metronidazole-loaded Ni CPO-27 and the metronidazole by itself.

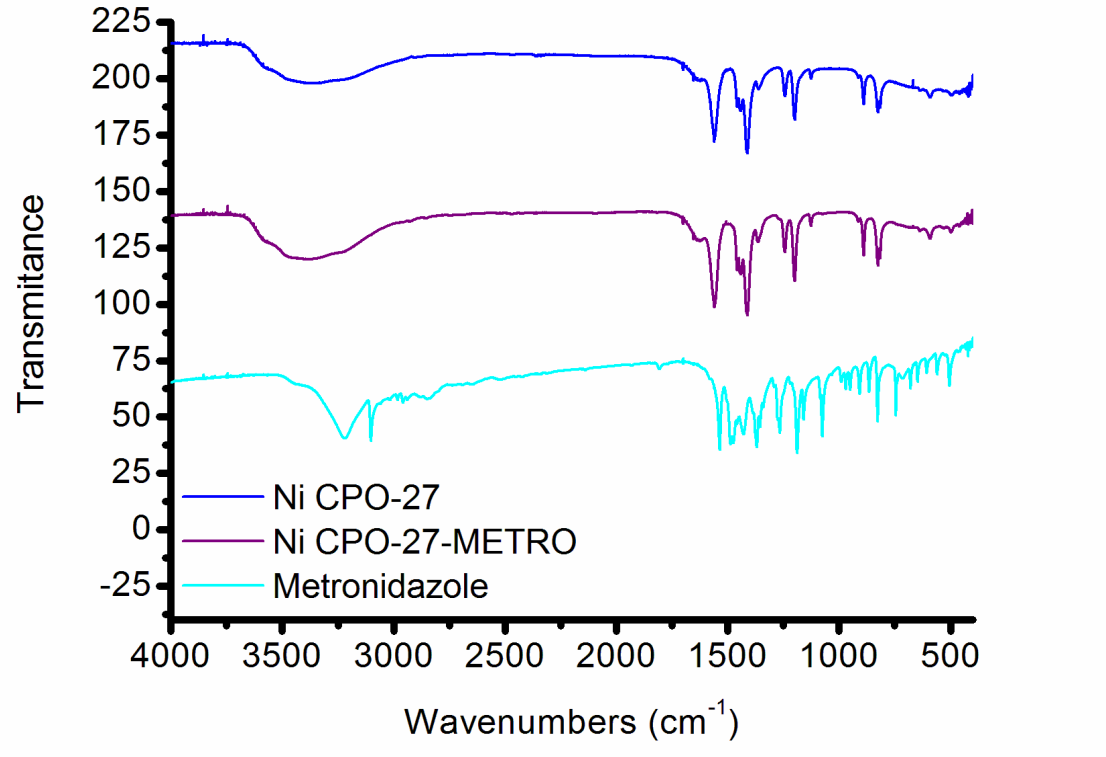

Figure 7.20 IR spectra for the three samples.

As shown above it is very hard to see peaks present in the Ni CPO-27-METRO sample which are representative of metronidazole. Unfortunately, many of the most obvious peaks in the metronidazole overlap with peaks already present in the Ni CPO-27. For example the imidazole ring peak of metronidazole is observed at 800 cm^{-1}. The most obvious peak which is missing from the Ni CPO-27-METRO sample is the υ(C-H) from the imidazole ring at 3100 cm^{-1}. Clearly the IR result is inconclusive and further characterisation would be necessary such as solid state NMR to prove that metronidazole had indeed been adsorbed.

7.6.3 NO adsorption in ibuprofen-loaded Ni CPO-27

As mentioned earlier, the storage of both NO and drugs within MOFs would provide potential for double functionality. To this end initial NO adsorption experiments were carried out on a sample of ibuprofen-loaded Ni CPO-27 to see if it was possible to store any NO within the framework as well as the already stored anti-inflammatory. Activation of the sample was carried out at 80°C to avoid removing the ibuprofen. The NO adsorption graph can be seen in figure 7.21. It illustrates that it is indeed possible to store both NO and ibuprofen within the same framework. The sample irreversibly stores ~3.3 $mmolg^{-1}$ of NO which is a strong indicator that the NO is binding to the CUSs available as the ibuprofen would be expected to interact with the linker.

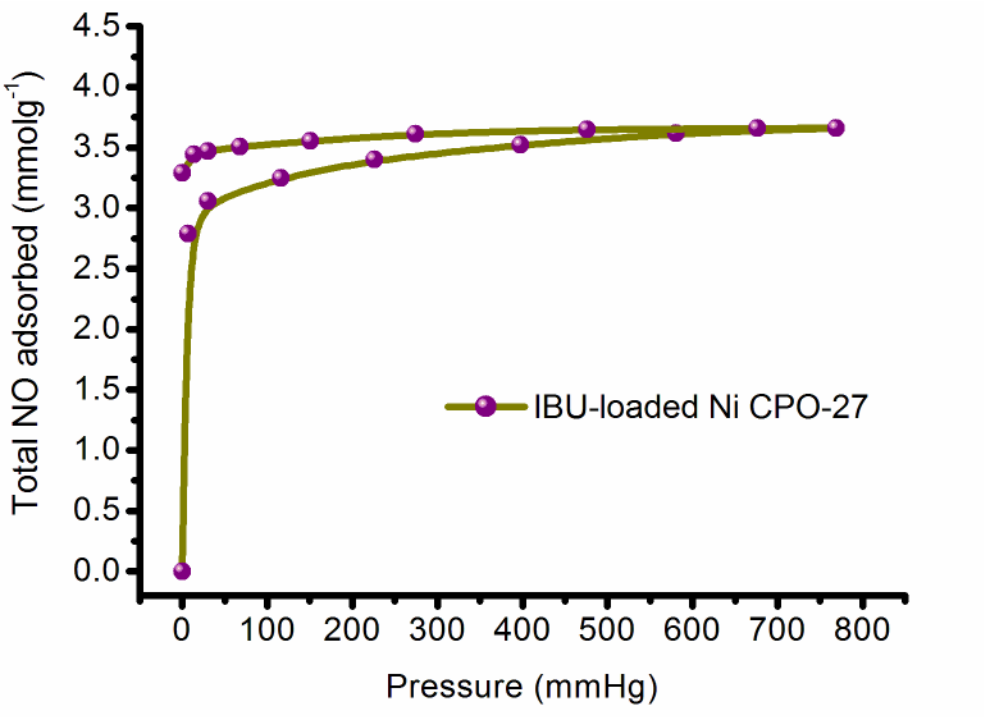

Figure 7.21 Experimental NO adsorption isotherm of ibuprofen-loaded Ni CPO-27 carried out at 298K.

A significant result is that the first point in the adsorption curve which is responsible for the vast majority of the NO stored in both Ni CPO-27 and ibuprofen loaded Ni CPO-27 takes significantly longer to reach equilibrium in the ibuprofen loaded sample compared with the bare framework. Figure 7.22 displays the adsorption of NO over time. It is clear from this graph that the ibuprofen delays the NO from accessing the pores and in particular the CUSs.

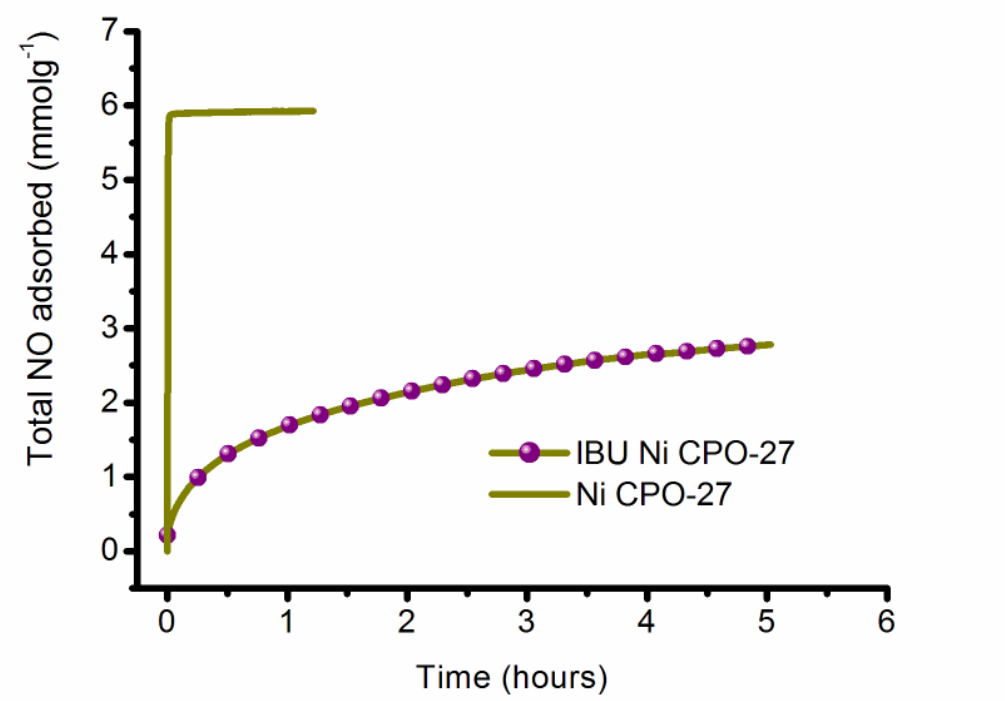

Figure 7.22 A graph showing the difference in time for equilibrium to occur for the first NO adsorption point between the ibuprofen-loaded Ni CPO-27 and the bare framework Ni CPO-27.

This result shows major potential for further research to be conducted in this area. If it takes a long time for the NO to enter into the pores and attach to the vacant metal site perhaps the NO release curve will display a longer release time.

7.6 Summary of chapter 7

In summary it has been shown in this chapter that MOFs present significant potential for medicinal applications. A wide variety of applications could be available for NO-loaded MOFs. The major drawbacks with regard to the use of MOFs as delivery agents of biologically significant gases (such as NO) and drugs is the dermatological testing required using humans and the study of possible toxicity of the MOFs, which are both necessary before any commercial application can be fully realised. Nevertheless, these initial tests show that MOFs are of significant interest for use in many medicinal applications. Testing has been carried out using porous paper bags and it has been shown that porous paper does not cause any detrimental value to the total NO available from MOFs. Initial studies using different cream formulations have been attempted and have shown mixed results. Further investigation into the optimal formulation for the release of NO from a cream is required. More promising are the results from NO-loaded MOF based hydrocolloids which illustrate very good release of NO and initially demonstrate good stability in PBS when stored at body temperatures (37°C). Initial biological experiments of NO-containing MOFs have shown great promise for NO-releasing formulations. A porcine artery is shown to completely relax when exposed to NO-loaded Ni CPO-27 and only contracts once the NO-loaded MOF is either removed or has completely released its entire store of NO. Finally, initial studies into the storing of pharmaceuticals have shown that it is possible to store both anti-inflammatory and antibiotic drugs within MOFs. There is tremendous potential for the use of MOFs as drug delivery agents and much more research needs to be carried out into this particular area of MOF research.

7.7 References

(1) Maria, B. W.; Adrian, B. *Am. J. Surg.* **2002**, *183*, 406.

(2) Zhu, H.; Wei, X.; Bian, K.; Murad, F. *J. Burn Care Res.* **2008**, *29*, 804.

(3) Martinez, L. R.; Han, G.; Chacko, M.; Mihu, M. R.; Jacobson, M.; Gialanella, P.; Friedman, A. J.; Nosanchuk, J. D.; Friedman, J. M. *J. Invest. Dermatol.* **2009**, *129*, 2463.

(4) Weller, R.; Finnen, M. J. *Nitric Oxide* **2006**, *15*, 395.

(5) Mowbray, M.; Tan, X.; Wheatley, P. S.; Morris, R. E.; Weller, R. B. *J. Invest. Dermatol.* **2007**, *128*, 352.

(6) http://www.z-medica.com/quikclot/index.asp.

(7) Weller, R. *Clin. Sci.* **2003**, *105*, 533.

(8) Weller, R.; Price, R. J.; Ormerod, A. D.; Benjamin, N.; Leifert, C. *J. Appl. Microbiol.* **2001**, *90*, 648.

(9) Fox, S.; Wilkinson, T. S.; Wheatley, P. S.; Xiao, B.; Morris, R. E.; Sutherland, A.; Simpson, A. J.; Barlow, P. G.; Butler, A. R.; Megson, I. L.; Rossi, A. G. *Acta Biomater.* **2010**, *doi:10.1016/j.actbio.2009.10.038*

(10) Wheatley, P. S.; Butler, A. R.; Crane, M. S.; Fox, S.; Xiao, B.; Rossi, A. G.; Megson, I. L.; Morris, R. E. *J. Am. Chem. Soc.* **2006**, *128*, 502.

(11) Wheatley, P. S.; Butler, A. R.; Crane, M. S.; Rossi, A. G.; Megson, I. L.; Morris, R. E. *Molecular Sieves: From Basic Research to Industrial Applications, Pts a and B* **2005**, *158*, 2033.

(12) Wheatley, P. S.; McKinlay, A. C.; Morris, R. E.; Antoine Gédéon, P. M.; Florence, B. In *Stud. Surf. Sci. Catal.*; Elsevier: 2008; Vol. Volume 174, Part 1, p 441.

(13) Hinks, N. J.; McKinlay, A. C.; Xiao, B.; Wheatley, P. S.; Morris, R. E. *Micropor. Mesopor. Mater.* **2010**, *doi:10.1016/j.micromeso.2009.04.031*

(14) Horcajada, P.; Chalati, T.; Serre, C.; Gillet, B.; Sebrie, C.; Baati, T.; Eubank, J. F.; Heurtaux, D.; Clayette, P.; Kreuz, C.; Chang, J.-S.; Hwang, Y. K.; Marsaud, V.; Bories, P.-N.; Cynober, L.; Gil, S.; Férey, G.; Couvreur, P.; Gref, R. *Nat. Mater.* **2010**, *9*, 172.

(15) Horcajada, P.; Serre, C.; Maurin, G.; Ramsahye, N. A.; Balas, F.; Vallet-Regi, M.; Sebban, M.; Taulelle, F.; Férey, G. *J. Am. Chem. Soc.* **2008**, *130*, 6774.

(16) Horcajada, P.; Serre, C.; Vallet-Regí, M.; Sebban, M.; Taulelle, F.; Férey, G. *Angew. Chem., Int. Ed.* **2006**, *45*, 5974.

(17) Kantor, T. G. *Ann. Intern. Med.* **1979**, *91*, 877.

(18) Brogden, R. N.; Heel, R. C.; Speight, T. M.; Avery, G. S. *Drugs* **1978**, *16*, 387.

(19) Freeman, C. D.; Klutman, N. E.; Lamp, K. C. *Drugs* **1997**, *54*, 679.

(20) Xiao, B.; Wheatley, P. S.; Zhao, X. B.; Fletcher, A. J.; Fox, S.; Rossi, A. G.; Megson, I. L.; Bordiga, S.; Regli, L.; Thomas, K. M.; Morris, R. E. *J. Am. Chem. Soc.* **2007**, *129*, 1203.

(21) McKinlay, A. C.; Xiao, B.; Wragg, D. S.; Wheatley, P. S.; Megson, I. L.; Morris, R. E. *J. Am. Chem. Soc.* **2008**, *130*, 10440.

8 Conclusions and Further Work

8.1 Conclusions

The overall aim of this project was to investigate MOFs which contained open metal sites when activated and examine if they could store and controllably release biologically significant quantities of NO. There are many conclusions that can be drawn from the work carried out in this thesis. However, most importantly, it has been shown that MOFs can be used to store and release significant amounts of NO for medical applications. However, the performance of the different MOFs studied varies considerably.

It has been shown that nickel based frameworks (Ni CPO-27, Ni succinate and Ni STA-12) in particular show a remarkable ability not only to store large quantities of NO but also controllably release the majority, if not all of its store resulting in an almost perfect gas storage and release material. So far only one cobalt framework has been investigated (Co CPO-27) but it has also shown almost perfect storage and releaseability of NO. Other analogues of M-CPO-27 (Zn, Mg and Mn) exhibit very good adsorption, but poor release by comparison. This behaviour is also noted in the Fe based frameworks investigated (Fe MIL-88s). Further to this, the results gained from Cu based MOFs show good adsorption but extremely poor release. A table detailing the various NO adsorption and release totals investigated in this thesis can be seen in figure 8.1. While the number of frameworks studied is small, it is striking from figure 8.1 that the nickel and cobalt-based MOFs release considerably more NO

than all the others. The question arises – is there something particularly suitable about these metals?

<table>
<tr><th>MOF</th><th>Theoretical NO ads ($mmolg^{-1}$)</th><th>Total amount of NO adsorbed ($mmolg^{-1}$)</th><th>Actual NO chemisorbed ($mmolg^{-1}$)</th><th>NO released ($mmolg^{-1}$)</th><th>% of NO chemisorbed which is released</th></tr>
<tr><td>Co CPO-27</td><td>6.412</td><td>6.507</td><td>5</td><td>7</td><td>140.00%</td></tr>
<tr><td>Ni CPO-27</td><td>6.423</td><td>7.211</td><td>5.91</td><td>6.64</td><td>112.35%</td></tr>
<tr><td>Sintef Zn CPO-27</td><td>6.158</td><td>3.645</td><td>2.57</td><td>0.127</td><td>4.94%</td></tr>
<tr><td>Zn CPO-27</td><td>6.158</td><td>5.636</td><td>4.71</td><td>0.181</td><td>3.84%</td></tr>
<tr><td>RT Zn CPO-27</td><td>6.158</td><td>8.024</td><td>7.35</td><td>0.152</td><td>2.07%</td></tr>
<tr><td>Sintef Mg CPO-27</td><td>8.243</td><td>8.267</td><td>8.05</td><td>0.305</td><td>3.79%</td></tr>
<tr><td>Mg CPO-27</td><td>8.243</td><td>5.152</td><td>4.73</td><td>0.175</td><td>3.70%</td></tr>
<tr><td>Mn CPO-27</td><td>6.581</td><td>3.226</td><td>2.93</td><td>0.15</td><td>5.12%</td></tr>
<tr><td>Cr MIL-101</td><td rowspan="5">Depends on how many CUSs are available or amine-grafted on the trimer</td><td>4.13</td><td>1.75</td><td>0.3</td><td>17.14%</td></tr>
<tr><td>Cr MIL-101 MEDA</td><td>2.49</td><td>1.8</td><td>0.013</td><td>0.722%</td></tr>
<tr><td>Fe MIL-100</td><td>2.67</td><td>1.81</td><td>0.365</td><td>20.17%</td></tr>
<tr><td>Fe MIL-100 (250°C)</td><td>4.64</td><td>3.34</td><td>0.6</td><td>17.96%</td></tr>
<tr><td>Fe MIL-100 carbazide</td><td>3.92</td><td>2.35</td><td>0.12</td><td>5.11%</td></tr>
<tr><td>Ni succinate</td><td>1.75</td><td>1.67</td><td>1.4</td><td>1.08</td><td>77.14%</td></tr>
<tr><td>Ni STA-12</td><td>5.163</td><td>4.95</td><td>3.61</td><td>1.72</td><td>47.60%</td></tr>
<tr><td>Mn BTT</td><td>3.72</td><td colspan="2" rowspan="2">Not carried out when solvent exchanged</td><td>0.27</td><td rowspan="2">N/A</td></tr>
<tr><td>Cu BTT</td><td>3.74</td><td>0.062</td></tr>
</table>

Figure 8.1 A table containing all the NO adsorption and release data for the MOFs investigated in this thesis.

It was noted in chapter 4 that the two materials which performed the best over the whole NO adsorption-release cycle were also the two easiest to activate. The theory presented was that the mechanism of the release reaction probably involved a transition state that was structurally similar to the dehydrated material. Given that the other two nickel compounds studied in this thesis also show good NO release, can this be explained by looking at the basic chemistry of Ni?

Undergraduate chemistry texts suggest that $18e^-$ complexes of transition elements are the most stable. Simple counting of electrons would therefore suggest that the 5 coordinate dehydrated present in activated Ni CPO-27 should be relatively stable as it contains a total of $18e^-$ (see figure 8.2). Therefore one would expect any reaction where the transition state has a similar structure to the dehydrated phase to proceed relatively well. This may partly explain why all the nickel materials perform well in these studies. Additionally it partly explains why the cobalt analogue of CPO-27 also performs well and potentially why the manganese version performs poorly too. These changes are the most likely explanation as the coordination environment is constrained and so other possible environments that could be observed in the solution state are not seen in the solid. The simple electron counting method is not particularly applicable to a d^{10} ion like Zn^{2+}, but there is clearly no gain in stability for the uncoordinated ion.

All of the iron-based MOFs studied in this thesis display reasonable uptakes of NO but poor overall release - the question is why?

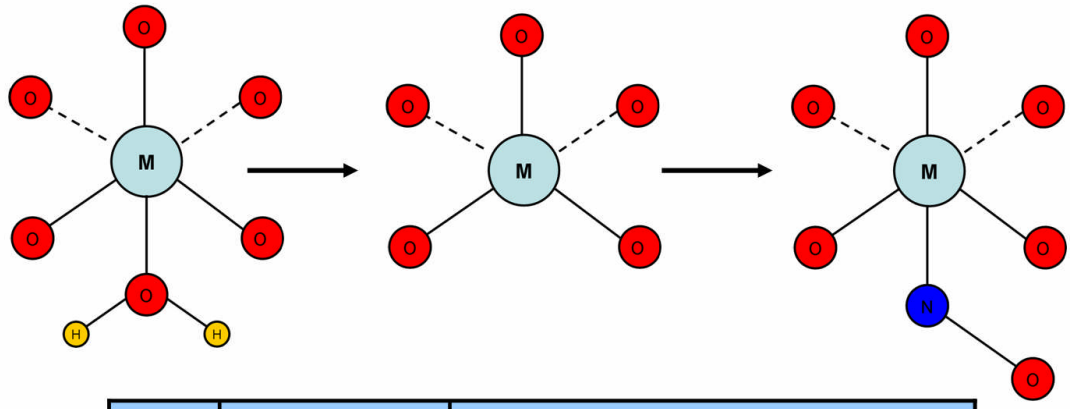

Metal	d configuration	Total number of electrons		
		hydrated	dehydrated	NO-loaded
Ni	d^8	20	18	19
Co	d^7	19	17	18
Fe	d^6	18	16	17
Mn	d^5	17	15	16
Zn	d^{10}	22	20	21

Figure 8.2 A diagram showing the dehydration and NO loading mechanism combined with a table showing the total number of electrons in the complex (assuming one electron donated from the bent NO molecule)

The case of iron is more complex as there is the possibility of redox chemistry at the metal. This was seen in chapter 5 where, when activated, a "self-reduction" hydrolysis reaction occurs in iron zeolites, which leads to a majority of Fe^{2+} and some unchanged Fe^{3+}. This "self-reduction" reaction is likely to be present in the MIL MOFs studied in this thesis and indeed a majority of Fe^{2+} is observed when the material studied is activated (see in-situ IR on Fe MIL-100 chapter 5). This complication makes any straightforward theories based on simple electron counting even less likely to provide the complete answer.

However, looking at iron in terms of the 18 rule, it can be seen that Fe^{2+} has 6 d electrons and combined with the 12 electrons from the surrounding oxygen atoms, gives a total of 18 e^- (from figure 8.2). It can be deduced from this that there is no extra stability from crystal field stabilisation energy (CFSE) to help the dehydrated state as the most favourable state is the hydrated structure. Following NO adsorption the iron complex has a total of 17 e^-, which is probably more stable than the dehydrated complex and therefore it is unlikely to go back to the dehydrated state and replace the NO for a water molecule. A similar case is also observed for Mn where the hydrated structure has 17 e^- and the dehydrated structure only has 15 e^-. Therefore, when the activated material is exposed to NO, it appears to irreversibly bind to the metal. The in-situ IR also showed that when NO-loaded materials are exposed to water, the vast majority of NO stays bound or is involved in the possible formation of N_2O. This is explained by the NO-loaded complex structure being relatively more stable compared with the intermediate "dehydrated structure" that would be evoked if the water were indeed to replace the NO.

However the 18e^- doesn't necessarily apply in this situation as it more properly applies to classical metal complexes, although it might give an insight as to why certain metals perform better in the activation-storage-delivery cycle for NO. Another key factor which would strongly influence the ability of MOFs to release bound NO, is the way in which the NO has bound to the metal. NO can bind in two ways to transition metals, either linearly or in a bent fashion. As was shown in chapter 4, the Co and Ni versions of M-CPO-27 bind NO in a bent manner. This means that there is no π backbonding and therefore the bond will be weaker

compared to the linearly bound NO which will form π bonds with the metal centre. This weaker bond is important as it allows the water to replace the NO in the mechanism described at the end of chapter 4. A diagram showing the two possible binding modes is shown below.

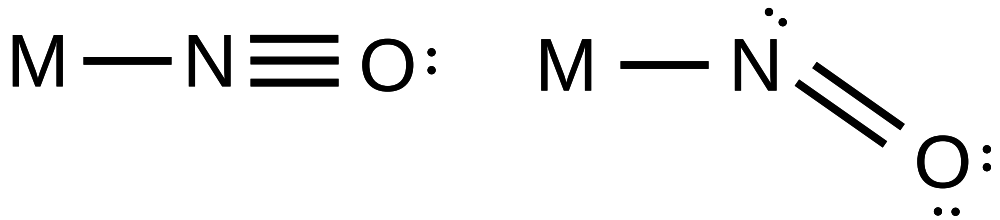

Figure 8.3 Two possible binding modes for NO with transition metals.

If the manganese, zinc and magnesium versions were to bind NO in a linear way then this might explain why good adsorption of NO is seen but poor release. The linear bond is much stronger and therefore it will be much harder for the water to replace the NO. It might also be the same for the Fe MIL compounds investigated. Further powder X-ray diffraction studies of the NO-loaded materials (Mn, Zn, Mg CPO-27 and Fe MILs) using a synchrotron source should show if the NO binds to the metals in a linear or a bent fashion or a combination of both leading to poor release values for NO.

As mentioned before, the iron atom situation is made more complicated by the "self-reduction" reaction that takes place in zeolites and could be occurring in the MIL materials too. The reduction of Fe^{3+} to Fe^{2+} is never 100% successful so even after extensive thermal treatments under vacuum some residual Fe^{3+} will remain. This will bind the NO, but very weakly as described in chapter 5. However the Fe^{2+} seems to

strongly bind NO even when exposed to water, indicating that the amount of NO which can be recovered from an NO-loaded MOF will be less than the expected total. Also in chapter 5 it was shown that when exposed to water, N_2O is produced meaning that the situation is made more complex due to the interactions taking place between different iron environments. It is for this reason that Fe-based zeolites have been heavily investigated for use as deNOX catalysts for use in car exhausts where NO is reduced to N_2 in the presence of water at elevated temperatures[1].

The case of Cu based MOFs, is separate as it forms completely different structures, many of which contain Cu-Cu dimers. However, it is not difficult to imagine that a similar situation could be observed in these structures. Indeed Cu, has also been heavily researched for its redox properties and its use as a deNOX catalyst[2]. Cu^{2+} readily reduces to Cu^{+} under similar "self-reduction" (hydrolysis) conditions to iron and therefore this could be an added complication for MOFs storing NO as the Cu^{2+} could be reduced and therefore irreversibly bind to the NO. This is evident from the extremely small amounts of NO released from the two Cu MOFs investigated so far. This explanation, combined with the theory put forward in chapter 4 and the in-situ IR studies conducted on Fe MIL-100 in chapter 5, is a potential explanation as to why certain metals show greater affinity for NO compared with others.

Further conclusions can be drawn regarding the formulations of MOFs for medicinal applications. The total NO released from differing formulations is still remarkable and merits further research. It has been shown that the delivery of NO from MOFs in a variety of different formulations is possible and that there can be advantages to

utilising different delivery methods for different applications. For example, utilising a hydrocolloid it is possible to deliver very significant quantities of NO for up to 10 days, whereas using porous bags or bandages this time can be reduced to a number of hours. NO-loaded MOF formulations can therefore be tailor-made to the desired application and this is a huge advantage for commercialisation. It has also been initially demonstrated that it is possible to produce MOFs with double functionality as both pharmaceutical products and NO can be stored in MOFs at the same time.

This thesis has shown the enormous potential that MOFs have as gas storage materials, in particularly with regard to the storage of the biologically significant gas NO. It can be concluded that MOFs range from being exceptional to poor in their behaviour towards NO, which as mentioned previously gives a wide range of delivery rates and amounts. For example Ni CPO-27 delivers 7 $mmolg^{-1}$ of NO[3] and this is 7000 times as much as HKUST-1[4]. This means that MOFs can be tailored towards different applications depending on the amount of NO required and over what time period. Much more research needs to be carried out regarding the formulation and the toxicology of these materials before bringing any products to market, however there is great potential has been shown for the use of MOFs in the delivery of NO for many applications.

8.2 Further Work

In this thesis great promise has been shown for the use of MOFs as delivery vehicles of biologically significant molecules, in particular, the wound healing gas NO. Initial studies concerning the use of MOFs in storing pharmaceuticals have also been presented.

However there are several investigations which still need to be carried out to fully understand the chemical processes occurring inside the pores of MOFs during the activation, storage and controlled release of gas and possibly other drugs as well.

The first and most logical investigation should be the synthesis and full characterisation (including NO storage and release isotherms) of Fe CPO-27 which has been published recently[5]. Not only would the NO storage and release results be of interest as a comparison with the other analogues of the M-CPO-27 series, but comparison with the Fe based MIL structures would be of significant interest too. It would also help to confirm the theory put forward in the Conclusions section. In Fe CPO-27 there would be no redox chemistry present as the iron complex is fully Fe^{2+} and therefore eliminates any redox complication. A direct comparison can therefore be made with the Ni and Co versions.

Secondly, it is of significant interest to understand the reasons why the release of NO from Zn, Mg and Mn CPO-27 is poor in comparison with the Ni and Co versions. If the reasons for this poor release can be understood, then possibly a method can be found to increase the delivery of NO and therefore these much less toxic analogues

could also find potential uses in formulations. In-situ IR experiments would be helpful in understanding which reactions are occurring at the metal and to see if the NO is staying bound to the metal despite the presence of water. Calorimetric experiments would also be useful as they should give strong indicators about the relative strength of the metal-NO bond.

Further alternative synthesis of such frameworks should be carried out to see if they can possibly be successfully synthesised using cheaper methods. HKUST-1 has been successfully synthesised using an electrochemical process which also gives the optimised surface area for this MOF[6]. If it is possible to synthesise versions of the M-CPO-27 series then it might be feasible to increase the NO storage and release from the Zn, Mg and Mn versions. Alternatively if it were possible to synthesise the Ni and Co structures at room temperature, like the Zn version[7], then this would help cut costs for the industrial production of these MOFs, if they are to be used in formulations for applications.

There are also a number of improvements which could be made to make these experiments much more accurate. The first of which would be the calculation of total adsorption of NO volumetrically and use this to calculate surface areas of activated MOFs. At the moment all calculations are made gravimetrically and are subject to mass changes which makes the calculations much more inaccurate than if NO isotherms were calculated volumetrically utilising a similar apparatus as that used for N_2 adsorption.

It would also be an improvement if the activation conditions used in the loading of MOF samples for release experiments matched those in the NO adsorption experiments. The NO adsorption utilises a diffusion pump which allows high vacuums to be generated, this currently is not used in the loading mechanism. It would not be too difficult to match the conditions exactly, therefore achieving more accurate release results.

However the investigations that need be carried out in the immediate future are dermatological and biological experiments to see if the MOFs that store NO are acceptable as NO delivery agents. Testing has been carried out using NO-loaded zeolites and has been shown to be extremely effective against a number of different bacteria and also non-destructive to the skin when placed in cream[8-9]. The zinc version of M-CPO-27 would also be of significant interest as bare zinc zeolites show anti-bacterial properties and suppress the growth of further bacteria. Therefore the NO-loaded Zn CPO-27 could also have double functionality against bacteria in a similar way to Zn zeolite-A. Similar experiments using M-CPO-27 or MIL MOFs need to be carried out and also need to show advantageous results for MOFs to continue to be considered of use as NO delivery agents.

8.3 References

(1) Feng, X.; Keith Hall, W. *J. Catal.* **1997**, *166*, 368.

(2) Sato, S.; Yu-u, Y.; Yahiro, H.; Mizuno, N.; Iwamoto, M. *Applied Catalysis* **1991**, *70*, L1.

(3) McKinlay, A. C.; Xiao, B.; Wragg, D. S.; Wheatley, P. S.; Megson, I. L.; Morris, R. E. *J. Am. Chem. Soc.* **2008**, *130*, 10440.

(4) Xiao, B.; Wheatley, P. S.; Zhao, X. B.; Fletcher, A. J.; Fox, S.; Rossi, A. G.; Megson, I. L.; Bordiga, S.; Regli, L.; Thomas, K. M.; Morris, R. E. *J. Am. Chem. Soc.* **2007**, *129*, 1203.

(5) Bhattacharjee, S.; Choi, J.-S.; Yang, S.-T.; Choi, S. B.; Kim, J.; Ahn, W.-S. *J. Nanosci. Nanotechnol.* **2010**, *10*, 135.

(6) Mueller, U.; Schubert, M.; Teich, F.; Puetter, H.; Schierle-Arndt, K.; Pastre, J. *J. Mater. Chem.* **2006**, *16*, 626.

(7) Tranchemontagne, D. J.; Hunt, J. R.; Yaghi, O. M. *Tetrahedron* **2008**, *64*, 8553.

(8) Fox, S.; Wilkinson, T. S.; Wheatley, P. S.; Xiao, B.; Morris, R. E.; Sutherland, A.; Simpson, A. J.; Barlow, P. G.; Butler, A. R.; Megson, I. L.; Rossi, A. G. *Acta Biomater.* **2010**, *6*, 1515.

(9) Mowbray, M.; Tan, X.; Wheatley, P. S.; Morris, R. E.; Weller, R. B. *J. Invest. Dermatol.* **2007**, *128*, 352.